Spurenanalytik und Authentizitätsuntersuchungen – Eine Herausforderung an die moderne Analytik

DISSERTATION

Zur Erlangung des Doktorgrades der Naturwissenschaften
(Dr. rer. nat.)

der

Naturwissenschaftlichen Fakultät II
Chemie, Physik, Mathematik

der Martin-Luther-Universität
Halle-Wittenberg

vorgelegt von

Frau Theresa Schmidt

Gutachter:

1. Prof. Dr. René Csuk (Martin-Luther-Universität Halle-Wittenberg)
2. Prof. Dr. Ester Simoes B Ferreira (Technische Hochschule Köln)

Verteidigt am 10.12.2024, Halle (Saale)

Vorwort

Die vorliegende wissenschaftliche Arbeit wurde von Juli 2019 bis Mai 2023 am Institut für Chemie (Bereich Organische Chemie) der Martin-Luther-Universität Halle-Wittenberg im Arbeitskreis von Herrn Prof. Dr. René Csuk angefertigt.

Die Arbeit wurde von der Deutschen Forschungsgemeinschaft unterstützt (DFG, Projektnummer 425225219, PI Dr. A.E. Kramell).

Die Dissertation wurde in kumulativer Form verfasst und die experimentellen Daten, die Einzelergebnisse sowie deren Diskussion sind bereits in international anerkannten Fachzeitschriften publiziert worden. Die veröffentlichten Beiträge bzw. Manuskripte sind zudem im Anhang aufgeführt.

Danksagung

Einen besonderen Dank möchte ich an dieser Stelle meinem Doktorvater Herrn Prof. Dr. René Csuk aussprechen. Der stets gute Zuspruch, sowie das entgegengebrachte Vertrauen und der gewährte Freiraum zur Verwirklichung eigener Ideen während der Bearbeitung waren von unschätzbarem Wert und haben maßgeblich zum Gelingen dieser Arbeit beigetragen. Auch für die vielen wertvollen Ratschläge und die unermüdliche Unterstützung in jeglichen Situationen auf diesem Weg möchte ich mich bedanken.

Ein weiterer Dank gilt der gesamten Arbeitsgruppe und allen ehemaligen Mitgliedern, welche durch stetige Hilfsbereitschaft und Zusammenarbeit, viele interessante Gespräche und vielfältige Ratschläge zum Gelingen dieser Arbeit beigetragen haben. Ein großer Dank gilt dabei Jenny Werner, ohne deren Hilfe die Vielzahl an Vorbereitungen der Messungen und Einwaagen bei weitem nicht so schnell möglich gewesen wären. Ein besonders von Herzen kommendes Dankeschön richtet sich hierbei zudem an Olli, Toni, Niels, Julia und Marie, die durch ihre fröhliche Art und die sehr unterhaltsamen Mittags- und Kaffeepausen eine unvergessliche Doktorandenzeit ermöglicht haben.

Ein herzlicher Dank geht an Frau Dr. Annemarie Kramell für die zahlreichen Ratschläge und die fortwährende Unterstützung während der Bearbeitung dieser Arbeit. Auch an alle Studenten, die ich während ihrer Abschlussarbeiten betreuen durfte und die durch ihre direkte oder indirekte Hilfe einen großen Beitrag zum Gelingen dieser Arbeit beigetragen haben, möchte ich ein Wort des Dankes richten.

Des Weiteren möchte ich mich bei allen bedanken, die durch einzelne Messungen zur Ergänzung der vorliegenden Datensätze beigetragen haben.

Ein großes Dankeschön richtet sich an all meine Freunde, die mich während der gesamten Zeit sowohl seelisch als auch moralisch unterstützt haben und in den richtigen Momenten stets für Ablenkung gesorgt haben, wodurch auch die Zeit außerhalb des Labors unvergesslich geworden ist.

Abschließend möchte ich meiner Familie und meinem Freund Christoph für den liebevollen Rückhalt, jedes aufbauende Wort, die bedingungslose Unterstützung und das entgegengebrachte Verständnis in all den Jahren von Herzen unendlich danken.

Inhaltsverzeichnis

Abkürzungsverzeichnis

100LC/SC	long chain/short chain ratio
^{14}C-Datierung	Radiokohlenstoffdatierung
ACN	Acetonitril
AD	im Jahre des Herrn (lateinisch: Anno Domini)
Ala	Alanin
AM	*Antheraea mylitta* Drury
APCI	Atmospheric Pressure Chemical Ionization
ASAP	Atmospheric solids analysis probe
Asx	Summe Asparaginsäure & Asparagin
AtA	*Atlas attacus* Guérin-Méneville
ATR	Abgeschwächte Totalreflexion
BC	vor Christus (englisch: Before Christ)
BM	*Bombyx mori* L.
BtMG	Betäubungsmittelgesetz
C_{18}	Octadecyl-Phase (Umkehrphase)
CBD	Cannabidiol
CBN	Cannabinol
DAD	Diodenarray-Detektor
DC	Dünnschichtchromatographie (englisch: Thin-layer Chromatographie; TLC)
DESI	Desorption Electrospray Ionization
DMF	N,N-Dimethylformamid
ECD	Elektroneneinfangdetektor
EDTA	Ethylendiamintetraacetat
ESI	Electrospray Ionization
et *al.*	lateinisch: und andere
FID	Flammenionisationsdetektor
FT	Fourier-Transformation
GC	Gaschromatographie
GLC	Gas-Flüssig-Chromatographie (englisch: gas liquid chromatography)
Glx	Summe Glutaminsäure & Glutamin
GSC	Gas-Feststoff-Chromatographie (englisch: gas solid chromatography)
HCl	Salzsäure
HPLC	High Performance Liquid Chromatography
HPTLC	Hochleistungsdünnschichtchromatographie (englisch: High Performance Thin-layer chromatography)
IR	Infrarot-Spektroskopie

L.	botanisches Autorenkürzel Carl von Linné
LC	Liquid Chromatography
LMJ-SSP	Liquid Microjunction Surface Sampling Probe
LOD	Nachweisgrenze (englisch: Limit of detection)
LOQ	Bestimmungsgrenze (englisch: limit of quantitation)
m/z	Masse-Ladungs-Verhältnis
MALDI	Matrix-Assisted Laser Desorption/Ionization
MeOH	Methanol
MS	Massenspektrometrie
MS/MS	Tandem-Massenspektrometrie
NMR	Nuclear Magnetic Resonanz
OM	Optische Mikroskopie
PCA	Hauptkomponentenanalyse (englisch: Prinicipal Component Analysis)
PCF	Propylchlorofrormat
Phe	Phenylalanin
ppb	parts per billion (10^{-9})
ppt	parts per trillion (10^{-12})
REM	Rasterelektronenmikroskopie (englisch: scanning electron microscope; SEM)
R_f	Retentionsfaktor (englisch: ratio of fronts)
RP	Umkehrphase (englisch: Reverse Phase)
Ser	Serin
SIMS	Sekundärionen-Massenspektrometrie
SPE	Festphasenextraktion (englisch: solid phase extraction)
TLC	Thin-layer Chromatographie
TOF	Time-of-Flight Mass Spectrometer
UV	Ultraviolett
v. Chr.	vor Christus
v/v	Volumen-Volumen-Verhältnis
Val	Valin
Vis	Sichtbar (englisch: visible)
WLD	Wärmeleitfähigkeitsdetektor
Δ^8-THC	(-)-trans-Δ^8-Tetrahydrocannabinol
Δ^9-THC	(-)-*trans*-Δ^9-Tetrahydrocannabinol
Δ^9-THCA	(-)-*trans*-Δ^9-Tetrahydrocannabinolsäure
λ	Wellenlänge (griechisch: Lambda)

1. Einleitung

„Analytische Chemie ist eine Wissenschaft am Rande des Nichts.“, so lautet ein Aphorismus von Hans-Jürgen Quadbeck-Seeger (*1939)[1], welcher die Herausforderung und Bedeutung dieser Disziplin für die Erforschung von Vergangenheit und Gegenwart unterstreicht. Wenn man den genauen Wortlaut betrachtet, muss man feststellen, dass diese Aussage nicht korrekt ist, da die analytische Chemie eine entscheidende Rolle in vielen wissenschaftlichen Disziplinen spielt. Dennoch kann ein Fünkchen Wahrheit darin erkannt werden, da die analytische Chemie, speziell die Spurenanalytik, oft vor der Herausforderung steht nur wenig Probenmaterial zur Verfügung zu haben oder nur kleinste Mengen an Analyten nachweisen zu müssen. Dies erfordert hochsensible und selektive analytische Methoden sowie eine sorgfältige Probenvorbereitung, um sicherzustellen, dass keine Verunreinigungen das Ergebnis beeinflussen. Zudem ist die Auswahl der geeigneten Analysemethode von verschiedenen Faktoren abhängig, wie zum Beispiel der Art des Analyten, der Matrix der Probe, dem geforderten Nachweisniveau und den verfügbaren Ressourcen. Zwar erlauben es die heutigen technologischen Fortschritte bereits Spuren von Analyten im Bereich von ppb bzw. ppt nachzuweisen, jedoch müssen diese Nachweisgrenzen, durch die sich stets verändernde Studien- und Gesetzeslage, häufig auch angepasst und verbessert werden, weshalb bei der Entwicklung analytischer Methoden kein Stillstand eintreten wird.[2-6]

Durch die Identifizierung und Quantifizierung von unterschiedlichsten Verbindungen in verschiedenen Proben ermöglicht es die analytische Chemie wichtige Erkenntnisse in Bereichen von Umweltschutz, Lebensmittelindustrie, Gesundheitsschutz, Forensik, Materialwissenschaften und Kulturwissenschaften zu generieren.[7] Bereits im 18. Jahrhundert wurden erste Untersuchungen von archäologischen Funden und Artefakten dokumentiert.[7-9] Die in der Archäometrie eingesetzte analytische Chemie stellt in der heutigen Zeit daher ein wichtiges Teilgebiet der kulturgeschichtlichen Forschung dar. Durch die Analyse von Materialien wie Keramik, Metallen, Textilien oder anderen organischen Substanzen können Forscher wichtige Erkenntnisse über die Herkunft, Herstellungstechniken und Verwendungszwecke dieser Objekte gewinnen. Zudem kann dazu beigetragen werden, das kulturelle Erbe zu bewahren, da durch minimalinvasive Analyse von archäologischen Funden und Artefakten, historische Objekte erhalten, restauriert und besser verstanden werden können.[10, 11] Ein wichtiger Punkt hierbei ist auch die Datierungsmethode, wie z.B. die Radiokarbondatierung, um das Alter von archäologischen Funden zu bestimmen und wodurch ermöglicht wird Zeitlinien zu erstellen, historische Ereignisse genauer zu datieren und so die Erforschung vergangener Zivilisationen voranzubringen. [12, 13]

Ein weiterer wichtiger Anwendungsbereich der analytischen Chemie ist die Authentizitätsuntersuchung. Authentizität ist ein Konzept, welches heutzutage in nahezu allen Bereichen des Lebens Auswirkungen hat, seien es Konsumgüter, Kunst, Tourismus oder zwischenmenschliche Interaktionen, dennoch ist es schwierig eine eindeutige Definition in der Literatur dafür zu finden. Im Allgemeinen wird Authentizität als Konzept angesehen, welches darauf abzielt die Dimensionen der Wahrheit oder Verifizierung zu erfassen, wobei auch häufig

Begriffe wie Glaubwürdigkeit, Zuverlässigkeit, Sicherheit und Echtheit verwendet werden.[14, 15] Hierbei können analytische Methoden eingesetzt werden, um die Echtheit bzw. Unverfälschtheit von Kunstwerken, historischen Artefakten oder auch Lebensmitteln zu überprüfen. Durch die Analyse von bspw. Materialzusammensetzungen, Isotopenverhältnissen oder chemischen Signaturen kann festgestellt werden, ob ein Objekt oder Produkt authentisch ist oder ob es sich um eine Fälschung handelt. In den vergangenen Jahren hat vor allem die Produktauthentizität und die damit verbundene Untersuchung von Verfälschungen in der Lebensmittelindustrie enorm an Bedeutung gewonnen.[16-19] Das Bewusstsein der Verbraucher für Qualität und Sicherheit sowie der Regionalität von Lebensmittel ist stark gewachsen. Jedoch sind auch die Kosten für die Produktion von Konsumgütern gestiegen, weshalb eine der häufigsten Verfälschungen der Ersatz mit einem billigeren lebensmittelfremden Stoff ist, wodurch eine bessere Qualität vorgetäuscht bzw. das jeweilige Produkt gestreckt werden soll. Neben dem gesundheitlichen Verbraucherschutz ist die Sicherstellung, dass authentische Produkte die gesetzlichen Anforderungen in der Beschaffenheit und Kennzeichnung erfüllen, das höchste Gut in der heutigen Lebensmittelüberwachung. Bei der Erfüllung dieser Aufgabe spielt die analytische Chemie eine zentrale Rolle und auch hier ist es wichtig stets neue instrumentelle Methoden zu entwickeln, welche zur Lösung der unterschiedlichsten Problemstellungen herangezogen werden können.[16, 17, 20, 21]

Insgesamt zeigt sich, dass die analytische Chemie einen entscheidenden Beitrag zur Erhaltung unseres kulturellen Erbes, zur Sicherheit unserer Gesellschaft und der Gesundheit leistet. Ihre Bedeutung wird auch in Zukunft weiter zunehmen, da sie hilfreich dabei ist, die Geheimnisse der Vergangenheit zu entschlüsseln und die Herausforderungen der Gegenwart zu bewältigen.

2. Zielstellung

Im Rahmen der vorliegenden Arbeit wurde das Ziel verfolgt, mit Hilfe verschiedener massenspektrometrischer und gaschromatographischer Methoden, wie z.B. HPTLC-MS, GC-FID und GC-MS zu zeigen, wie wertvoll die (Weiter)entwicklung instrumenteller analytischer Methoden ist und wie diese Analytik einen Beitrag leisten kann, das Wissen um die Vergangenheit zu vertiefen, aber auch zur Beantwortung aktuell relevanter Fragestellungen herangezogen werden kann. Des Weiteren sollte auch verdeutlicht werden, welche Herausforderungen bei der Entwicklung und Etablierung analytischer Methoden innerhalb der Spurenanalytik und Authentizitätsuntersuchung zu bewältigen sind. In diesem Zusammenhang wurden verschiedene Materialien unterschiedlichen Ursprungs wie Sedimentproben und Seidenfilamente, aber auch Pflanzenharze und -öle untersucht. Jede der zu untersuchenden Proben wurde unter einer anderen Fragestellung bearbeitet.

Mit Hilfe von dünnschichtchromatographischen Methoden, gekoppelt mit massenspektrometrischer Analyse sollte die teilweise sehr zeitaufwendige Probenaufbereitung einiger Materialen, wie Sedimentproben oder Pflanzenöle und -harze vereinfacht werden. Des Weiteren ermöglicht es diese Variante der Analytik eine Vielzahl an Proben zeitgleich aufzutrennen, wodurch ein Hochdurchsatz-Screening erfolgen kann. Ziel war es eine schnelle und vielseitig auf unterschiedliche Probenmatrices einsetzbare Analytik zu generieren, um auch mit wenig Aufwand repräsentative Ergebnisse zu gewinnen. Diese könnten nachfolgend für die Beantwortung von z.B. archäometrischen Fragestellungen aber auch aktuell präsenter Problematiken hilfreich sein. Ein aktuelles Bespiel ist dabei *Cannabis sativa* L.. Die Pflanze spielt in der heutigen Zeit eine große Rolle, vor allem durch ihre berauschende Wirkung und die aktuell immer wieder aufkommende Diskussion bezüglich der Wirkung auf den Menschen. Auch die Einführung vieler neuartiger Produkte wie das Cannabidiol-Öl (CBD) weckt vor allem hinsichtlich der Inhaltsstoffe großes analytische Interesse. Daher sollten im Zuge der vorliegenden Arbeit verschiedene CBD-Öle hinsichtlich ihrer Cannabinoidzusammensetzung untersucht werden. Aber auch die historische Bedeutung dieser Pflanze wird dabei wieder mehr in den Vordergrund gerückt. In diesem Kontext wurden in der vorliegenden Arbeit Sedimentproben vom Badhanital-See im Himalaya auf den Gehalt von Cannabinol (CBN), ein Abbauprodukt vom psychoaktiven Δ^9-Tetrahydrocannabinol (Δ^9-THC), untersucht. Dabei sollte ermittelt werden, ob in diesem See vor tausenden von Jahren die Verarbeitung von *Cannabis sativa* L., z.B. zur Textilproduktion, stattgefunden hat.

In Hinblick auf historische Textilverarbeitung, sollte des Weiteren untersucht werden, ob mit Hilfe mikroskopischer, gaschromatographischer und spektroskopischer Methoden die Unterscheidung verschiedener Seidenarten möglich gemacht werden kann, wodurch vor allem auch bei historischen Funden die Möglichkeiten zur Bestimmung der biologischen Herkunft und Einordung der verwendeten Fasern erweitert werden soll. Die weiterführende Materialanalyse soll bereits vorangegangene Analysen bestätigen und somit die weitere Authentizitätsuntersuchung der Proben gewährleisten. Daher sollte eine Analysenstrategie entwickelt werden, mit Hilfe derer das Fibroinprotein verschiedener Seidenspinnerarten charakterisiert

und ein Vergleich der Seidenfilamente ermöglicht wird. In diesem Zusammenhang wurde die einzigartige Aminosäurezusammensetzung, sowie weitere Strukturmerkmale des Fibroins, einer Auswahl an verschiedenen Seidenarten bestimmt. Dabei wurde zunächst eine Reihe von rezenten Materialen auf deren spezifische Aminosäurezusammensetzung untersucht. Des Weiteren wurde bei ausgewählten historischen Seidentextilien überprüft, ob es Hinweise auf den Einsatz von nicht entbasteter Seide gibt. In diesem Kontext wurden verschiedene Entbastungmethoden, historische als auch aktuell angewandte Varianten, getestet. Außerdem sollte der Einfluss historisch verwendeter Färbe- und Beizmethoden auf die Bestimmung der Aminosäurezusammensetzung untersucht werden, weshalb eine Auswahl an Färbe- und Beiztechniken an der zuvor entbasteten Seide angewendet wurde. Mittels der Untersuchung des Verhältnisses von D- zu L-Enantiomeren der Aminosäuren, wurde dies weiterführend untersucht. Im Zuge dessen wurden die Racemisierungsraten verschiedener Entbastungsmethoden bestimmt. Anschließend wurde die entwickelte Methode auf verschiedene historische Textilfunde angewandt. Neben der gaschromatographischen Untersuchung mittels GC-FID oder GC-MS kamen hierbei ebenfalls mikroskopische und spektroskopische Methoden (ATR-FTIR-Spektroskopie) zum Einsatz, um die Identifizierung der Textilfasern zu unterstützen.

3. Theoretischer Teil

3.1. Analytische Chemie- Definition und Geschichte

Definiert wird die analytische Chemie als die eigenständige chemische Teildisziplin, welche geeignete Methoden und Werkzeuge entwickelt und bereitstellt, um Informationen über die Zusammensetzung und Struktur der Materie zu gewinnen. Es werden verschiedene Techniken verwendet, wodurch aus den gemessenen chemischen Signalen, meist spezifische Wechselwirkungen zwischen der Materie und Energie, Informationen und neues Wissen generiert wird und dies in bereits vorhandenes Wissen eingeordnet werden kann.[7, 22]

Bereits vor 2500 Jahre wurde sich darum bemüht die Zusammensetzung von Materialen, vorwiegend von Metallen als wichtigsten Werkstoff des Altertums, zu verstehen und zu untersuchen. Auch wenn hierbei vergleichsweise primitivere und weniger umfangreiche Untersuchungen durchgeführt wurden, zeugt dies schon von Streben nach einer angemessenen Qualität und Authentizität.[23, 24] Da verschiedene Metallobjekte aus Gold oder Silber wie Münzen, Waffen oder Skulpturen seit Jahrhunderten Bestandteil kulturhistorischer Geschichte und chemischer Untersuchungen sind, ist es nicht verwunderlich, dass die Untersuchung dieser Objekte als eine der ältesten analytischen Kenntnisse beschrieben wird. Der Chemiehistoriker *Ferenc Szabadváry* beschreibt in seiner „Geschichte der Analytik“ (1966), dass das Verfahren der Goldprüfung, die sogenannte Kupellation, welche als quantitative Methode auf der Gewichtsbestimmung durch Schmelzen im Ofen basiert, bereits im Alten Testament der Bibel an mehreren Stellen Erwähnung fand.[7, 25] Auch in einigen Keilschriften, welche auf die Zeit Mesopotamiens (ca. 1500 v. Chr.) datiert werden, wurden bereits Hinweise auf ein Verfahren zur Reinigung von Gold und Silber gefunden, welches zur Prüfung dieser Zahlungsmittel eingesetzt wurde und Fälschungen aufdecken sollte.[23] Dies zeigt, dass schon sehr früh Methoden zur Reinheitsprüfung entstanden sind, wie z.B. der Nachweis von Eisen(II)-sulfat in Grünspan mit Gallapfelsaft, welche später auch Grundlage für analytische Nachweise waren.[7, 23]

Das Erkenntniswachstum von analytischer Chemie und der produzierenden Chemie standen bereits in den vergangenen Jahrhunderten in Zusammenhang, schließlich war es stets von großer Bedeutung die Stoffe zunächst zu untersuchen, bevor entsprechende Gesetzmäßigkeiten gefunden werden konnten.[25] Mit der Entwicklung der Hüttenindustrie und der damit verbundenen Analyse der Erze erlebte unter anderem die analytische Chemie im Phlogistonzeitalter einen Aufschwung.[26] Mit der sogenannten chemischen Revolution im 18. Jahrhundert begann dann die moderne Chemie wie man sie heute kennt, die analytische Chemie wurde jedoch erst im 19. Jahrhundert als eigenständiges Wissenschaftsgebiet anerkannt und die ersten physikalischen Methoden, wie die Spektralanalyse (Bunsen und Kirchhoff, 1859)[27], wurden entwickelt.[7, 28] Die Zeit um den Zweiten Weltkrieg brachte bei der analytischen Chemie einen Wandel zu vermehrt instrumentellen Methoden. Ab den 1950er Jahren nahmen die technologischen Entwicklungen Fahrt auf und es wurden unter anderem IR-, GC- und HPLC-Geräte entwickelt und bereits bestehende analytische Geräte, wie das MS, weiter optimiert.[28] Mit diesen technischen Verbesserungen erlebte die instrumentelle Analytik

auch durch die Senkung von Nachweisgrenzen und Verkürzungen von Analysenzeiten durch bspw. Automatisierung, einen Aufschwung. Die Spurenanalytik erlebte hierbei ebenfalls einen enormen Popularitätsgewinn, da diese zur Datengewinnung bezüglich der Qualität von Luft, Wasser und Lebensmitteln, aber auch von Arzneimitteln genutzt wurde und auch heutzutage weiterhin eine große Rolle dabei spielt.[3, 7]

Die heutige analytische Chemie ist durch eine schnelle Entwicklung in der Gerätetechnologie, durch unterschiedlich komplexe Matrices und durch sich immer ausweitende Aufgabenstellungen aus den verschiedensten Bereichen der technischen Wissenschaften, Natur- und Kulturwissenschaften wie z.B. Archäologie oder Kunstgeschichte, geprägt.[7] Ein weiteres bedeutendes Feld in der analytischen Chemie stellt die Untersuchung und Analytik biologischer Systeme dar, wie z.B. die Struktur und Funktion von Proteinen, aber auch deren Wechselwirkung mit anderen Molekülen.[28] Daher stellt die analytische Chemie in der heutigen Zeit, insbesondere die spurenanalytische Untersuchung, ein wissenschaftliches Instrument dar, welches der Gesellschaft, der Umwelt, den Geisteswissenschaften und der Politik dient, wobei mittlerweile ein sich kontinuierlich erweiterndes Wissen entstanden ist und dieses zur Klärung vieler verschiedener Fragestellungen beiträgt.[7, 28] Trotz aller Fortschritte und des Wissensgewinns der letzten Jahrzehnte befindet sich der analytische Chemiker in einem nach wie vor nicht enden wollenden Kampf, bei dem es keinen endgültigen Sieg geben kann, auch wenn es auf dem Weg dorthin viele herausragende Erfolge und Triumphe geben wird. Dies beschreibt das stete Streben nach Antworten und dem methodisch angestrebten Perfektionismus, welcher die analytische Chemie sowohl heute als auch schon 1974 wo *H.M.N.H. Irving* dies beim Jubiläum anlässlich des hundertjährigen Bestehens der analytischen Chemie beschrieb, sehr passend.[29]

3.2. Einblick in die Instrumentelle Analytik

In der Instrumentellen Analytik macht die Massenspektrometrie einen Großteil aller Methoden aus. Daneben kommen auch häufig Chromatographische Methoden, wie die Gaschromatographie oder Flüssigkeitschromatographie, zum Einsatz. Demgegenüber existieren aber ebenfalls zahlreiche spektroskopische und optische Methoden, wie FTIR-Spektroskopie, UV/Vis- und Fluoreszenzspektroskopie, Polarimetrie oder auch mikroskopische Untersuchungen. Im folgenden Abschnitt werden die in dieser Arbeit verwendeten Methoden näher betrachtet.

3.2.1. Massenspektrometrie

Die Massenspektrometrie ist bereits seit über hundert Jahren ein fester Bestandteil analytischer Methoden. Die ersten Errungenschaften, welche Jahre später zur Entwicklung des uns bekannten Massenspektrometers führten, waren der Nachweis des Elektrons und die Messung dessen Verhältnis von Ladung zu Masse durch *Joseph J. Thomson* im Jahr 1897. Damit legte er den Grundstein für die heutige Massenspektrometrie. Im vergangenen Jahrhundert erfolgte eine enorme Weiterentwicklung der ersten Kenntnisse der Massenspektrometrie, welche heutzutage zu einem idealen Werkzeug für die Charakterisierung vieler Materialen geworden ist und zur Analyse von nahezu jeder Art von Substanz angewendet wird, egal ob anorganischer, organischer, biologischer oder synthetischer Natur.[30]

Bei der Massenspektrometrie handelt es sich um eine hochentwickelte Methode der instrumentellen Analytik, welche in einer Vielzahl verschiedener Gebiete, wie der Chemie, Biochemie, Pharmazie, Geowissenschaften oder Physik, Anwendung findet. Das breite Anwendungsspektrum der Massenspektrometrie führt dazu, dass sie neben der Analyse von Element- und Isotopenverhältnissen auch eine große Rolle bei der Strukturaufklärung unbekannter Substanzen oder bei der Analyse bekannter Substanzen aus Umwelt und Forensik spielt.[31, 32] Mit der hohen Sensitivität und Selektivität dieser Methode findet die Massenspektrometrie auch in der Spurenanalytik, unter anderem auch im Bereich der Archäometrie, vermehrt Anwendung.[33-36] Auch bei Authentizitäts- und Qualitätsfragen kann diese genutzt werden, um kleinste Mengen an Verunreinigungen zu detektieren und somit bei der Qualitätskontrolle von bspw. Arzneimitteln oder Lebensmitteln angewandt werden.[37-39] Mit der Massenspektrometrie wird es ermöglicht die Masse, genauer gesagt das Masse-zu-Ladungsverhältnis (*m/z*), von Atomen, Molekülen und allen anderen Teilchen, welche in Lösung oder der Gasphase daraus gebildet werden, zu bestimmen. Dafür müssen die Analyten jedoch als ionisierte Moleküle in der Gasphase vorliegen, egal ob als positiv oder negativ geladenes Ion.[31] Die Ionisierung kann auf unterschiedliche Weise erfolgen. Dabei kann zwischen einer harten und weichen Ionisierung unterschieden werden. Bei der weichen Ionisierung wird dem Molekül nur so viel Energie zugeführt, wie zur Ionenbildung nötig ist und das Molekül bleibt erhalten. Bei der harten Ionisierung hingegen wird mit einem Energieüberschuss gearbeitet, was dazu führt, dass im Massenspektrum Fragment-Ionen des

Moleküls zu finden sind.[40] Mit der Entwicklung von sanften Ionisationsmethoden in den 1980er Jahren, wie z.B. Elektrospray-Ionisation (ESI) oder Matrixunterstützte Laser-Desorption/Ionisation (MALDI), konnte das Anwendungsspektrum der Massenspektrometrie auch auf Biomoleküle, wie z.B. Proteine, erweitert werden.[41] Aufgrund der Vielfalt massenspektrometrischer Techniken gibt es für fast jede Verbindung eine oder mehrere spezielle Methoden, mit denen diese charakterisiert werden kann. Häufig handelt es sich dabei um Kopplungen verschiedener analytischer Methoden, wie HPLC-MS, GC-MS, LC-MS/MS, oder spezielle hochauflösende Analysenmethoden, wie MALDI-TOF-MS, TOF-SIMS, DESI-MS, wobei oft eine chromatographische Trennung vorgelagert ist.[33-37, 42-44]

In den vergangenen Jahren haben die ambienten Ionisationsmethoden, wie DESI oder ASAP, stark an Bedeutung gewonnen und werde seitdem vermehrt auf unterschiedliche Probenmaterialen angewandt. Hierbei wird eine direkte Untersuchung, ohne oder mit sehr geringer Vorbereitung des Probenmaterials, unter Atmosphärendruck ermöglicht.[45-47] Eine weitere Methode, die ebenfalls in den letzten Jahren an Bedeutung gewonnen hat und bereits auf eine Vielzahl verschiedene Analyten angewandt wurde, ist die (HP)TLC-MS Kopplung.[48-52] Hierbei wird die seit jeher im Labor für chromatographische Trennung genutzte Dünnschicht-chromatographie mit der Massenspektrometrie gekoppelt. Die Technik der Liquid Microjunction Surface Sampling Probe (LMJ-SSP) wird hierbei angewandt, um die aufgetrennten Spots auf der (HP)TLC-Platte einzeln untersuchen zu können (siehe Abbildung ***1***). Der Analyt wird dabei mittels kontinuierlichen Lösungsmittelstroms aus der Oberfläche der (HP)TLC-Platte extrahiert, im gelösten Zustand zur Ionenquelle transportiert und nachfolgend mittels ESI- oder APCI-Technik ionisiert.[53, 54]

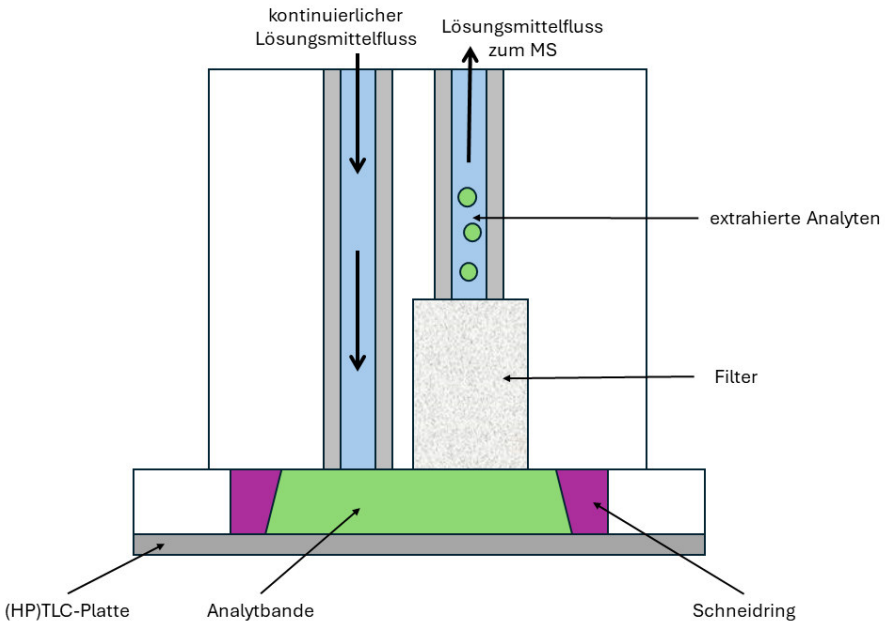

Abbildung 1: Schematische Darstellung der, bei der Untersuchung der Analytbanden mittels (HP)TLC-MS-Kopplung, eingesetzten LMJ-SSP-Extraktionstechnik durch das Plate Express® von Advion.

Dies ermöglicht es den zeitaufwendigen Schritt der Probenvorbereitung zu reduzieren und auch über unbekannte Spots Informationen zu erhalten, was eine Identifizierung erleichtern

kann. Zudem können bei Anwendung dieser Methodik durch kürzere Analysenzeiten auch die Lösungsmittelverbräuche gesenkt werden.[48-50, 54-59]

All dies zeigt, dass, obwohl die Massenspektrometrie nur eine Methodik darstellt, sie in Kombination mit neuen Techniken und verschiedenen chromatographischen Methoden, ein sehr wichtiges Werkzeug bei der Identifizierung und Quantifizierung, sowie der Strukturaufklärung ist und damit eine unverzichtbare Methode darstellt.

3.2.2. Gaschromatographie

Neben der Massenspektrometrie erfolgt ein Großteil aller analytischen Untersuchungen mittels chromatographischer Methoden. Dazu zählen die Flüssigkeitschromatographie (z.B. HPLC oder DC) sowie die Gaschromatographie.[40, 60] In der vorliegenden Arbeit spielt die HPLC jedoch keine wesentliche Rolle, weshalb im Folgenden auf diese Methode nicht näher eingegangen wird.

Die Methode der Gaschromatographie wurde in den 1950er Jahren entwickelt und eine der wichtigsten, am weitesten verbreitete und am häufigsten genutzte Technik der modernen Chemie, welche zur Trennung und Identifizierung unterschiedlicher chemischer Verbindungen genutzt werden kann.[61] Die Erfindung der Gaschromatographie wird häufig mit den Namen des Nobelpreisträgers *Archer J.P. Martin* sowie seiner Kollegen *Richard L. M. Synge* und *Anthony T. James* in Verbindung gebracht. Ihre Arbeiten rund um die Flüssig-Gas-Verteilungschromatographie bilden die Grundlage für die Entwicklung der Gaschromatographie.[62] Obwohl das Jahr 1952 als das Geburtsjahr der Gaschromatographie angesehen wurde, gab es vorher bereits zahlreiche Forschungsarbeiten zu dieser Methode, jedoch hauptsächlich in ihrer Gas-Feststoff-Version.[63] In der Zeit der Entwicklung dieser Methode wurden bessere analytische Kontrollen in der petrochemischen Industrie erforderlich, weshalb sich die Gaschromatographie schnell etabliert hat und bis heute für die Analyse fast aller Arten von organischen Verbindungen eingesetzt wird, auch solche, die in ihrem ursprünglichen Zustand nicht flüchtig sind, aber in flüchtige Derivate umgewandelt werden können.[62]

Während des Trennvorgangs verteilen sich die Bestandteile eines Probengemisches zwischen der stationären und mobilen Phase. Je nach Beschaffenheit der stationären Phase kann die Gaschromatographie in die Gas-Feststoff-Chromatographie (GSC), bei der die stationäre Phase ein Feststoff ist, und die weitaus verbreitetere Gas-Flüssig-Chromatographie (GLC), die eine Flüssigkeit als stationäre Phase verwendet, unterteilt werden. Bei einer gaschromatographischen Trennung wird die Probe am Anfang der chromatographischen Säule verdampft und anschließend von der mobilen Gasphase (d. h. dem Trägergas) durch die Säule zum Detektor transportiert. Die Trennung der verschiedenen Komponenten erfolgt dabei auf Grundlage ihrer Flüchtigkeit, wobei bei polaren stationären Phasen zusätzliche Wechselwirkungen, wie z.B. Dipolwechselwirkungen, die Trennung beeinflussen können.[40, 62] Im Laufe der Entwicklung der Gaschromatographie wurden eine Vielzahl von Detektoren untersucht und eingesetzt, um die aufgetrennten Verbindungen zu detektieren. Neben Detektoren, die lediglich die Anwesenheit von Analytmolekülen am Säulenausgang anzeigen können [z.B.

Flammenionisationsdetektor (FID), Wärmeleitfähigkeitsdetektor (WLD), Elektroneneinfangdetektor (ECD)], gibt es auch Detektoren, die Informationen über die Identität der Analyten liefern sollen (z.B. MS, FTIR). Obwohl jeder dieser Detektoren unterschiedliche Empfindlichkeiten aufweist, sind diese dennoch weitverbreitet und für verschiedenste Fragestellungen von großer Bedeutung, zumal es keine idealen Detektoren gibt und die Verwendung eines Detektors für jede Fragestellung neu bewertet werden muss.[64] In den letzten Jahren hat vor allem die Bedeutung der GC-MS Kopplung an Bedeutung gewonnen, da hierbei sehr niedrige Nachweisgrenzen ermöglicht werden und es nicht zwangsläufig nötig ist alle in der Probe vorhandenen Komponenten auftrennen zu müssen.[62]

Generell hat die kontinuierliche Weiterentwicklung der Gaschromatographie dazu beigetragen, dass sie heute zu den wichtigsten analytischen Techniken gehört und einen bedeutenden Beitrag zur Forschung und Entwicklung in verschiedenen Bereichen leistet. Die Gaschromatographie findet bei verschiedensten Problematiken, unter anderem auch in der Spurenanalytik, Authentizitätsuntersuchung und Archäometrie, Anwendung.[37, 65-67] In der Umweltanalytik erfolgt die Identifizierung und Quantifizierung von Schadstoffen wie z.B. Pestiziden, Schwermetallen oder anderen organischen Verbindungen in Boden-, Wasser- und Luftproben oftmals mittels GC-Methoden[68], aber auch in der Lebensmittelanalytik (Bestimmung der Zusammensetzung des Lebensmittels, Konzentration von Zusatzstoffen oder Rückständen wie Pestiziden)[69] oder der pharmazeutischen Analytik (Reinheitsprüfungen von Medikamenten, Identifizierung von Verunreinigungen, Konzentrationsbestimmung von Wirkstoffen)[70, 71] wird die gaschromatographische Methodik häufig angewandt. Besonders bei der Analyse von organischen Komponenten während der Untersuchung von kulturhistorischen Gütern findet die Methode der GC-MS große Anwendung (z.B. bei Kunst und Malereien).[72-75] Den größten Nutzen bringt die GC-MS-Methode jedoch, wenn sie als ergänzende Technik eingesetzt wird, die sich auf andere Analysemethoden stützt und mit ihnen zusammenwirkt, um Informationen über das erforschte Material zu generieren.[74]

Zusammenfassend kann festgehalten werden, dass die Gaschromatographie vor allem durch ihre hohe Auflösung und Empfindlichkeit bei zahlreichen Analysen von komplexen Gemischen eine Auftrennung ermöglicht und somit eine wichtige Rolle bei der Identifizierung sowie Quantifizierung von Molekülen spielt und somit einen entscheidenden Beitrag in vielen Bereichen der Wissenschaft und Industrie leistet.

3.2.3. Spektroskopische und optische Methoden

Bei der Identifizierung bzw. des qualitativen Nachweises von verschiedenen Molekülen stellen die chromatographischen Methoden eine teilweise weniger effektive Variante dar. Methoden wie die IR- oder NMR-Spektroskopie dagegen liefern eindeutigere Ergebnisse, wenn es um eine Strukturaufklärung geht.[40, 76, 77] Oftmals sind daher Kombinationen verschiedener Methoden, wie die IR-Spektroskopie mit einer (gas)chromatographischen Methode (z.B. GC-FID, GC-MS, HPLC) von Vorteil, um den größten Informationsgewinn zu garantieren. Der Bereich der Spektroskopie oder auch der Einsatz von optischen Methoden bei der Untersuchung sowie

Identifizierung und Charakterisierung von verschiedensten Materialen, spielen daher ebenfalls eine große Rolle in der analytischen Chemie und tragen zur Klärung verschiedener Fragestellungen bei.[18, 19, 78-81]

Eins der ältesten Verfahren in der Materialcharakterisierung ist die Licht- oder optische Mikroskopie. Bereits im 19. Jahrhundert wurde die Mikroskopie eingesetzt, um mikrostrukturelle Untersuchungen bei verschiedenen Materialen durchzuführen. Mit der Entwicklung neuer Methoden und hochauflösender Geräte, wie bspw. dem Rasterelektronen-mikroskop (REM), dem Polarisationsmikroskop oder dem Fluoreszenzmikroskop, hat sich das Repertoire dieser Methodik seit jeher stark erweitert.[82-84] Besonders im Bereich der Charakterisierung von Fasern bzw. Textilien findet die Mikroskopie häufig Anwendung, da häufig schon anhand ihrer Form eine erste Identifizierung erfolgen kann.[85, 86] Auch bei der morphologischen Unterscheidung von Seidenfilamenten kann die Mikroskopie herangezogen werden (siehe Abbildung 2).[87, 88] Mit Hilfe der Mikroskopie können Oberflächenstrukturen sowie die Form und Größe von Materialien analysiert werden, wodurch Informationen über deren Beschaffenheit, Rauheit und Homogenität erhalten werden können.

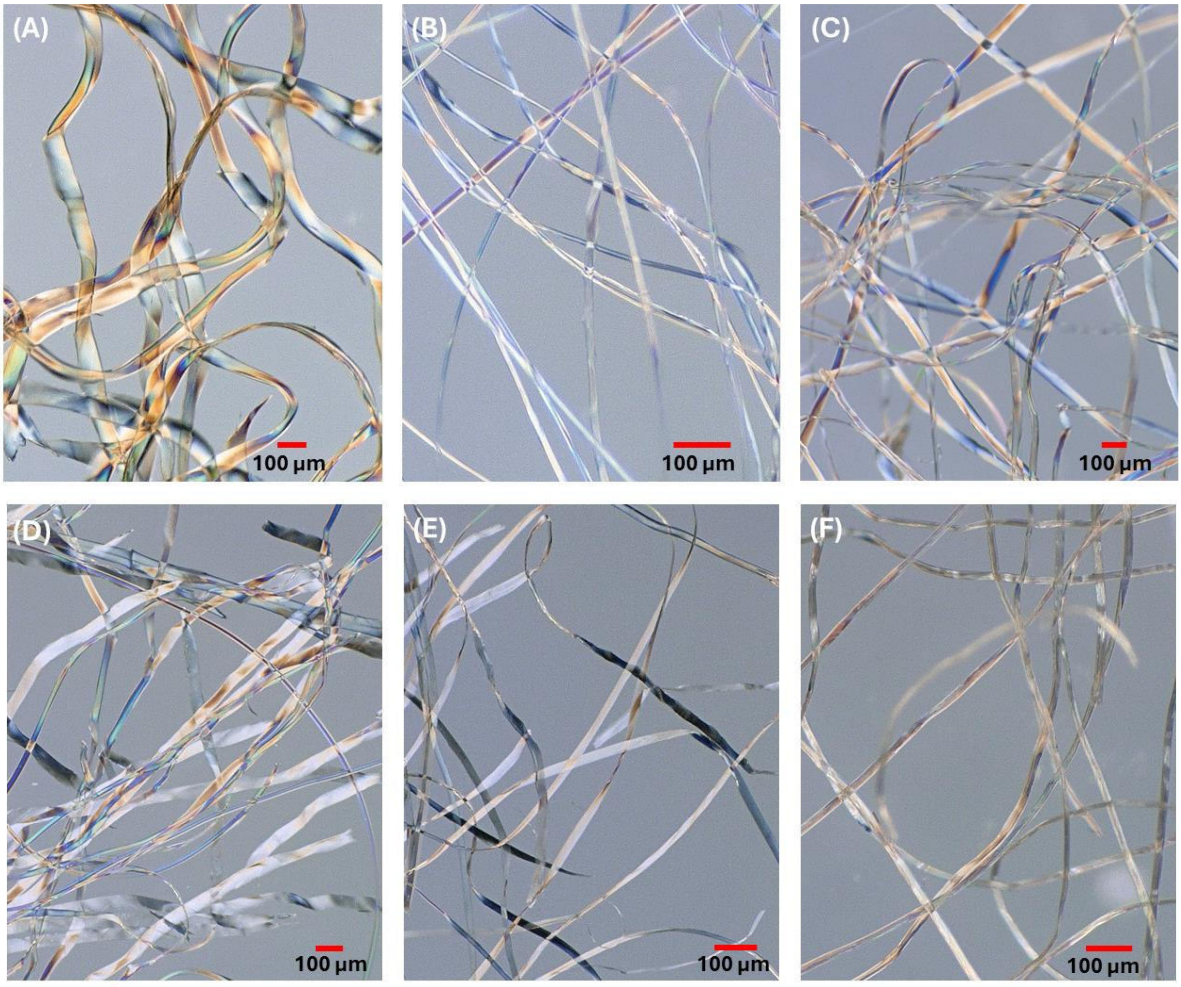

Abbildung 2: Darstellung mikroskopischer Bilder, welche die unterschiedlichen Morphologien verschiedener entbasteter Seidenfilamente aufzeigt. (A) *Caligula cachara* Moore, (B) *Bombyx mori* L., (C) *Antheraea mylitta* Drury, (D) *Saturnia pavonia* L. England, (E) *Samia canningii* Hutton, (F) *Attacus atlas* L.

Mit Hilfe der spektroskopischen Methoden, wie der IR-Spektroskopie, können z.B. bereits gewonnene Informationen detaillierter untersucht werden und somit weitere Daten gesammelt werden, welche zur Identifizierung der Probe beitragen. Bei der IR-Spektroskopie handelt es sich um ein physikalisches Analyseverfahren, welches die Absorption von Infrarotstrahlung durch chemische Bindungen in einem Material über einen bestimmten Wellenlängenbereich misst. Durch die Umwandlung der absorbierten Strahlung in Energie werden die Atome in einem Molekül zum Schwingen angeregt und das resultierende Spektrum zeigt anschließend die charakteristischen Peaks, die verschiedenen Schwingungsmodi der Atome im Molekül zugeordnet werden können. Die Art und Weise, wie die Atome schwingen, hängt von ihrer chemischen Umgebung ab, was es ermöglicht, Rückschlüsse auf enthaltene funktionelle Gruppen und damit die Struktur des Moleküls zu ziehen.[40, 89-92] Seit der ersten Experimente von *Sir William Herschel* im frühen 19. Jahrhundert (Untersuchung der Energieverteilung im Sonnenspektrum), welche für die Entwicklung der IR-Spektroskopie von grundlegender Bedeutung waren, haben die stetigen technologischen Fortschritte es ermöglicht, daraus eine vielseitige und weitverbreitete Analysentechnik zu enwickeln.[93] Mit der Einführung der Fourier-Transform-Infrarot (FT-IR)-Spektroskopie Anfang der 1970er wurde eine schnellere Datenaufnahme, sowie eine höhere Empfindlichkeit ermöglicht. Hierbei wir die gemessene Infrarotstrahlung durch ein Interferometer geleitet, wobei die Intensität des Lichtes in einem Interferogramm detektiert wird. Mit Hilfe der Fourier-Transformation werden die Daten nachfolgend in die spezifischen Absorptionswerte eines Moleküls über den gesamten Wellenlängenbereich berechnet und im Spektrum als Funktion der Wellenlänge dargestellt.[40, 94, 95] Auch die Anwendung der abgeschwächten Totalreflexions-Fourier-Transformations-Infrarotspektroskopie (ATR-FTIR-Spektroskopie) hat dazu beigetragen, Probleme und Einschränkungen der klassischen Transmissionsmethoden zu überwinden. So erlaubt die ATR-FTIR-spektroskopische Methodik auch den Zugang zu den Schwingungsfrequenzen der Oberfläche ohne das untersuchte Material zu beschädigen oder eine aufwendige Probenvorbereitung durchzuführen, weshalb diese häufig bei der Untersuchung historischer Proben (z.B. Lacke, Knochen, Seide, Leder)[96-99] eingesetzt wird.[95, 100] Auch zur Charakterisierung von Fasermatrices kann die ATR-FTIR-Spektroskopie herangezogen werden, wobei diese erste Informationen für eine Klassifizierung einzelner Fasern, verwendeter Farbstoffe oder andere anhaftender Farbstoffe bzw. Moleküle liefert.[101-106]

Abschließend kann festgehalten werden, dass sowohl die spektroskopischen als auch die mikroskopischen Untersuchungen einen wichtigen Beitrag zur Identifizierung von Materialen liefern und die Ergebnisse vorangegangener oder anschließender Analysen bestärken können. Vor allem bei archäometrischen Fragestellungen kommen diese Methoden vermehrt zum Einsatz, da es sich hierbei oftmals um zerstörungsfreie bzw. minimalinvasive Methoden handelt und somit das wertvolle Probenmaterial von historischen Proben weitestgehend erhalten bleibt.[107, 108]

4. Diskussion der Ergebnisse

Im folgenden Abschnitt dieser Dissertation sollen die erzielten Forschungsergebnisse der einzelnen zugrundeliegenden Publikationen zusammenfassend erläutert und diskutiert werden, sowie gezeigt werden, welchen Beitrag diese zur modernen Analytik, sowie zur Klärung von Fragestellungen mit historischem Kontext liefern können. Im Allgemeinen können die Ergebnisse der vorliegenden Arbeit in zwei größere Abschnitte unterteilt werden. Zum einen wurde die Methode der Massenspektrometrie gekoppelt mit der Dünnschichtchromatographie als Möglichkeit einer Hochdurchsatz-Screening Methode auf verschiedene Materialen angewandt und zum anderen erfolgten gaschromatographische Untersuchungen der Aminosäurezusammensetzung verschiedener Seidenkokons, sowie die Untersuchung entbasteter Seidenproben.

4.1. Identifizierung und Quantifizierung von CBN in Sedimentproben mittels HPTLC-MS (P1)

Ein recht aktuelles Thema, welches immer wieder in den Schlagzeilen zu finden ist und Bestandteil zahlreicher Publikationen ist, sind die Cannabinoide.[109-113] Die recht kontroverse Diskussion rund um diese Thematik führt zu zahlreichen neuen Untersuchungsergebnissen,[114] aber weckt auch das Interesse an der Verwendung dieser Pflanze in der Vergangenheit, weshalb auch hier die (Weiter)entwicklung analytischer Methoden von Interesse ist, welche die unterschiedlichen Anforderungen der Probenmatrices gewachsen sind.

Im Rahmen von interdisziplinären Untersuchungen eines Bohrkerns aus einem See im Badhani-Tal in Indien (Garhwal, Himalaya) sollte eine HPTLC-ESI-MS Methode zum Nachweis von CBN in den Sedimentproben entwickelt werden. Die zentrale Frage war, ob es möglich ist, das CBN – ein Abbauprodukt des psychoaktiven Δ^9-THC – in diesen Sedimentproben nachzuweisen. Die Freie Universität Berlin hatte bereits mit Hilfe von ^{14}C-Datierung die untersuchten Sedimentproben auf ein Alter von bis zu 4500 Jahren datiert. Des Weiteren wurden bei Pollenanalysen des Bohrkerns in einigen Pollenzonen eine erhöhte Konzentration an Pollen aus der Familie der *Cannabaceae* nachgewiesen. Die Erkenntnisse über das so erhaltene Pollenprofil (siehe Demske *et al.*)[115] sollten mit Hilfe dieser Methode erweitert werden. In früheren Untersuchungen verschiedener Sediment von europäischen Seen wurde die Anwesenheit von Pollen des Cannabis Typs bzw. Humulus/Cannabis Typs, welcher auch bei den untersuchten Proben aus dem Badhani-Tal gefunden wurden, als Indikator für die historische Fasergewinnung aus Hanf interpretiert.[116-122] Die Untersuchung von Lavrieux *et al.*[118] zeigte bereits, dass eine Korrelation zwischen in Sedimenten gefundenen Pollen und einem Nachweis von CBN in den entsprechenden Sedimenten besteht und das CBN daher als eine Art Biomarker für die Fasergewinnung aus Hanfpflanzen in dem untersuchten Gewässer genutzt werden kann. In frühen Zeiten wurde der Prozess des Rottens oftmals in flachen Gewässern durchgeführt, wobei die Freisetzung von Bastfasern aus gebündelten Hanfstängeln durch mikrobielle Prozesse erleichtert wurde.[123-126] Während dieses Prozesses gelangen neben

verschiedenen Pflanzenmaterialen, wie Stängel, Blätter oder Pollen, aber unteranderem auch die in der Pflanze metabolisierten Phytocannabinoide, welche einzigartig für die Cannabis Spezies sind,[127] in die Gewässer. Unter Lagerungs- bzw. Alterungsbedingungen, welche in zahlreichen Studien nachempfunden wurden, kommt es zum Abbau der in Cannabis enthaltenen psychoaktiven Substanzen – zurück bleibt das Cannabinol.[128-132] Eine detailliertere Beschreibung dieser Abbaumechanismen kann ebenfalls in der Publikation eingesehen werden.

Ziel der entwickelten HPTLC-ESI-MS Methode war es daher den Gehalt an CBN in den Sedimenten mit positiven Pollenbefund zu bestimmen und somit, bei der Rekonstruktion der Vergangenheit, zu weiterem Erkenntnisgewinn beizutragen und einen Hinweis auf eine mögliche Fasergewinnung aus Hanf an diesem See zu liefern. So sollen weitere Erkenntnisse über mögliche Anbaugebiete und die Nutzung von Hanf in früheren Zeiten gesammelt werden und damit die historische Verbreitung und Verwendung von Cannabis besser nachvollzogen werden.

Bisherige in der Literatur beschriebene Studien zum Nachweis von CBN in historischen Proben basieren meist auf HPLC-Methoden und GC-MS/FID.[109, 118, 128, 129, 132-136] Jedoch ist dabei oft die Derivatisierung des Analyten nötig und um diesen zeitintensiven Schritt zu vermeiden, wurde mit HPTLC-ESI-MS eine Methode entwickelt, welche diesen Schritt umgeht. Zudem wurden in der Literatur bisher nur wenige (HP)TLC Methoden in Zusammenhang mit der Analyse von Cannabinoiden beschrieben.[51] Die Verwendung einer entsprechenden MS-Kopplung ermöglicht hierbei eine recht schnelle Untersuchung. Da es sich bei den Sedimentproben aber um eine sehr komplexe Matrix handelt, war zunächst eine Extraktion des Probenmaterials und anschließend eine Auftrennung des Probenextraktes mittels Dünnschichtchromatographie notwendig. Zudem ermöglicht die gewählte HPTLC-ESI-MS Methode, neben der recht kurzen Analysenzeit, auch mehrere Proben in kurzer Zeit parallel zu untersuchen und so ein Hochdurchsatz-Screening.[57] Dies ist bei der Untersuchung von Bohrkernen von besonderem Interesse, da hier zumeist eine hohe Probenanzahl analysiert wird.

Zur Entwicklung einer validen HPTLC-ESI-MS Methode wurden zunächst die stationäre und mobile Phase optimiert. Bei der stationären Phase wurden verschieden modifizierte Kieselgelplatten getestet, wobei die HPTLC-Platte auf Kieselgelbasis zu sehr reproduzierbaren Ergebnissen bei sehr geringer Nachweisgrenze geführt hat (LOD: 6.4 ng CBN/HPTLC Bande; LOQ: 20.7 ng CBN/HPTLC Bande). Die HPTLC Platte ist mit einem optimierten Kieselgel 60 ausgestattet und weist eine deutlich kleinere Teilchengröße als bei der klassischen TLC-Platte auf. Dadurch wird eine höhere Packungsdichte und eine glattere Oberfläche ermöglicht. Es wird die Probendiffusion reduziert, was zu kompakten Banden oder Spots führt. Durch eine höhere Reinheit des Plattenmaterials ist zudem der Background deutlich geringer. Darüber hinaus erhöhen die geringere Partikelgröße und die dünnere Schicht die Nachweisempfindlichkeit und die Analysegeschwindigkeit erheblich. [57, 137] Die sehr schmalen Banden waren bei der Kopplung mit dem Massenspektrometer von großer Bedeutung, da der Extraktionskopf nur eine begrenze Fläche erfassen kann und dadurch nur ein sehr punktueller Bereich erfasst werden kann.

Bei der mobilen Phase wurde zunächst mit für Cannabinoiden literaturbekannten Laufmittelgemischen gearbeitet, wobei dort eine Vielzahl an Varianten existiert.[138-141] Zur Trennung vom untersuchten CBN und der sichtbaren und/oder UV-aktiven Matrix, wurde eine Auswahl dieser Laufmittel getestet. Im Zuge dessen wurde auch die Zusammensetzung dieser Laufmittel variiert, um so den Abstand von den Analyt- und Matrixspots möglichst groß zu halten. Dadurch wurden Interferenzen mit Matrixbestandteilen vermieden und die schmale Erscheinungsform der Banden gewahrt. Nach einer Vielzahl an Variationen wurde mit einer Mischung aus *n*-Heptan/Diethylether (90:10 v/v) eine zufriedenstellende Trennung von Analyt und Matrix erreicht. Anschließend konnte unter Einbeziehung von verschieden konzentrierten Standardlösungen und der Nullproben (Sedimentproben, bei denen keine Pollen des Cannabis Typ detektiert wurden) eine HPTLC-ESI-MS Messmethode zur Bestimmung der CBN-Gehalte in den Sedimentproben entwickelt werden. Für detaillierte Beschreibungen zur Methodenentwicklung kann in der Publikation Einsicht genommen werden.

Die direkte Aufbringung und anschließende Analyse eines Extraktes der Sedimentproben auf die HPTLC-Platte erwies sich als sehr schwierig bis unmöglich. Bei dieser Variante wurde eine sehr große Menge an interferierenden Matrixbestandteilen auf die Kieselgelplatte aufgebracht. Dadurch wurde diese überladen und ein eindeutige Spotentwicklung bzw. Auftrennung des Gemisches war nicht möglich. Es wurde ein weiterer Extraktions- bzw. Probenreinigungsschritt eingeführt. Dafür wurden verschiedene Kombinationen aus Extraktion des CBN aus den Sedimentproben und weiterer Auftrennung des Extraktes ausgetestet. Die Kombination aus Extraktion im Ultraschallbad mit Methanol/*n*-Hexan (9:1 v/v) und zwei hintereinander durchgeführte SPE-Schritte führten zu einer guten Abtrennung der störenden Matrix. Der Verlust an CBN konnte dabei sehr gering gehalten werden, was sich in einer Widerfindung über die gesamte Methode von durchschnittlich 73 % widerspiegelt. Auch die relative Standardabweichung der Methodenpräzision mit 4.1 % weist auf eine gute Wiederholbarkeit und Reproduzierbarkeit der Ergebnisse hin. Das Vorgehen und die generierten Daten zur Validierung können in der Publikation eingesehen werden.

Nach der erfolgreichen Validierung der entwickelten HPTLC-ESI-MS Methode wurden die vorliegenden Sedimentproben auf den Gehalt von CBN untersucht. Entsprechend der vorher bestimmten Pollenzonen[115] konnten zunächst die Nullproben verifiziert werden, da bei diesen weder mit postchromatographischen Detektionsmethoden noch bei Messungen mittels HPTLC-ESI-MS CBN detektiert werden konnte. Bei der anschließenden Untersuchung der Realproben konnten CBN-Gehalte zwischen 99.2 und 486.5 ng CBN/g Sediment detektiert werden. Die erhaltenen Daten korrelierten dabei mit den Pollenfunden, wobei der höchste Gehalt an Pollen des Typs Humulus/Cannabis mit der Sedimentprobe mit dem höchsten detektierten CBN-Gehalt übereinstimmt.

Dass Proben von Sediment- bzw. Bohrkernen relevante Informationen beinhalten und herangezogen werden, um detaillierte Informationen über den Einfluss verschiedener Faktoren und Ereignisse, wie z.B. der menschlichen Einwirkung auf die Natur zu sammeln, ist seit vielen Jahren bekannt. Dazu gibt es in der Literatur viele verschiedene Ausführungen[142-152], am präsentesten dabei sind zurzeit wohl die Veröffentlichungen über den Lake Crawford in

Kanada, welcher eine große Rolle bei Diskussionen über den Beginn eines neuen Erdzeitalters, das Anthropozän, spielt.[153-155] Von daher war es nicht verwunderlich, dass mit der Detektion von CBN in den Sedimentproben auch diese Daten die These von Demske et al.[115], dass in der Zeit von 480 BC bis 1050 AD ein erhöhtes Aufkommen an Cannabispollen auf das Rotten von Hanfpflanzen im Badhani-Tal zurückzuführen sein könnte, bestärkt werden konnte.

Zusammenfassend kann festgehalten werden, dass die in der vorliegenden Arbeit entwickelte HPTLC-ESI-MS-Methode dazu beitragen kann solche komplexen Probenmatrices aufzutrennen und das in diesem Fall in Spuren vorhandene CBN selektiv zu detektieren. Dennoch sollten in zukünftigen Studien weitere Bohrkerne verschiedener Seen dieser Region auf das Vorhandensein von CBN untersucht und diese Daten mit den Ergebnissen von Pollenanalysen abgeglichen werden. Des Weiteren können historische Dokumente, welche die Hanfverarbeitung in der Region in der jeweiligen Zeit belegen, herangezogen werden, um die experimentellen Daten zu belegen.

4.2. Identifizierung und Quantifizierung von CBD, Δ^9-THC und CBN in CBD-Ölen mittels HPTLC-MS (P2)

Nachdem die HPTLC-Methode sehr gut geeignet war, um Spuren von CBN in den untersuchten Sedimentproben nachzuweisen, stellte sich die Frage, ob die Methode auch eine hilfreiche Ergänzung für das analytische Repertoire für sehr aktuelle Probenmatrices darstellen könnte. Die CBD-Öle erlebten in den letzten Jahren einen Aufschwung und wurden sehr populär, weshalb in der vorliegenden Arbeit eine Auswahl an verschiedenen Ölen (verschiedene Hersteller und Konzentrationen) untersucht wurde. Obwohl den CBD-Ölen viele positive Eigenschaften nachgesagt werden, handelt es sich hierbei um ein recht kontroverses Thema, da die Wirkmechanismen noch sehr unerforscht sind.[156-158] Zudem gibt es immer wieder Meldungen, dass diese Öle eine falsche Deklaration der enthaltenen Inhaltstoffe aufweisen.[159, 160] Besonders kritisch ist dies in Bezug auf das psychoaktive Δ^9-THC zu betrachten.[156, 161] In Übereinstimmung mit der europäischen Rechtsprechung und dem Betäubungsmittelgesetz (BtMG), darf der Gehalt an Δ^9-THC die 0.2 % bzw. seit Januar 2023 die 0.3 % (angegeben als Summe von Δ^9-THC und Δ^9-THCA) nicht überschreiten.[162-164] Beim CBD ist die Gesetzeslage etwas schwieriger. Bisher gibt es keine eindeutige Regelung diesbezüglich, da die Studienlage zu dieser Substanz noch nicht ausreichend ist, um eine eindeutige Beurteilung vornehmen zu können. In der EU unterliegen Produkte mit zugesetztem CBD, wie es bei den CBD-Ölen oft der Fall ist, der Novel-Food-Verordnung und bedürfen einer separaten Zulassung, welche nur erteilt wird, wenn diese Produkte keine gesundheitlichen Risiken bürgen.[165-167] Diese unklare Gesetzgebung macht deutlich, wie wichtig es ist über etablierte und validierte Methoden zur Bestimmung von verschiedenen Cannabinoiden in CBD-Ölen zu verfügen, um sowohl den Gehalt an Cannabinoiden zu bestimmen als auch über die Authentizität der Produkte entscheiden zu können.

Zur Identifizierung von Molekülen in komplexen Matrices werden häufig die Molekülmassen herangezogen, jedoch besteht bei den untersuchten Cannabinoiden die Besonderheit, dass

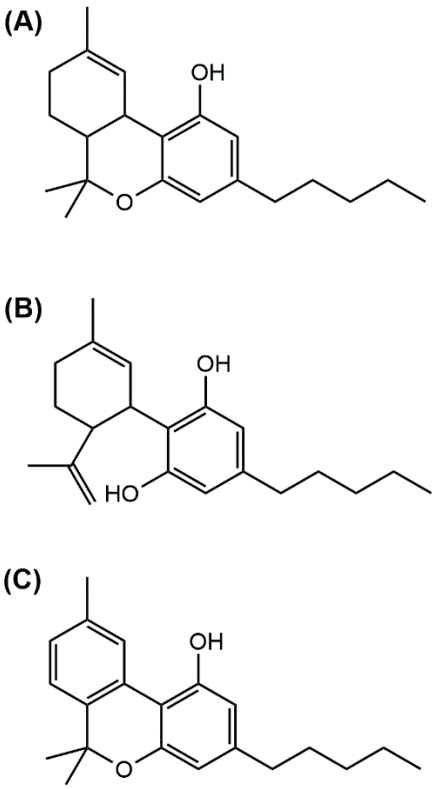

Abbildung 3: Darstellung der Struktur der untersuchten Cannabinoide.
(A) Δ^9-THC, (B) CBD, (C) CBN

CBD und Δ^9-THC die gleiche elementare Zusammensetzung aufweisen, wodurch eine Unterscheidung der beiden Derivate, rein auf die Masse bezogen, unmöglich ist. In Verbindung mit einer chromatographischen Auftrennung der Cannabinoidderivate sollte die Identifizierung und Quantifizierung der Cannabinoide CBD, CBN und Δ^9-THC ermöglicht werden. Bei der Optimierung der HPTLC-ESI-MS Methode zur Untersuchung von CBD-Ölen war es daher wichtig die Trennung und Detektion der einzelnen Cannabinoide zu berücksichtigen. Mit dem in der ersten Publikation verwendeten Laufmittel für die Bestimmung von CBN in Sedimentproben (*n*-Heptan/Diethylether, 90:10 v/v)[168] konnte keine Trennung von CBD, CBN und Δ^9-THC erreicht werden, weshalb hierbei weitere in der Literatur für die Auftrennung von Cannabinoiden bekannte Laufmittelgemische ausgetestet wurden.[58, 138, 141, 169] Daraufhin konnte mit *n*-Hexan/Diethylether (80:20 v/v) als Laufmittel eine komplette Trennung der einzelnen untersuchten Cannabinoid-Derivate CBN, CBD und Δ^9-THC erreicht werden. Eine weitere Herausforderung war die Detektion, da nur das CBN auf der HPTLC-Platte unter UV-Licht (λ = 254 nm) detektierbar war. Sowohl CBD als auch Δ^9-THC konnten über den auf der HPTLC-Platte integrierten Fluoreszenzindikator (λ_{max} = 254 nm) nicht detektiert werden. Daraufhin wurden die UV-Spektren der untersuchten Cannabinoide untersucht und es konnte entsprechend in der Literatur beschriebener Daten[170] festgestellt werden, dass obwohl CBN, CBD und Δ^9-THC jeweils ein Absorptionsmaximum um λ = 280 nm aufweisen, der Extinktionskoeffizient von CBN fünfzehnfach höher ist, als von den anderen beiden Cannabinoiden. Auch bei der Wellenlänge von λ = 254 nm weist CBN einen deutlich höheren Absorptionskoeffizienten auf, weshalb die Detektion mittels UV-Licht möglich ist. Die entsprechenden Absorptionsspektren und die entsprechenden Extinktionskoeffizienten können in der Publikation eingesehen werden. Die Cannabinoide CBD und Δ^9-THC würden entsprechend dieser Messungen erst bei sehr hohen auf der HPTLC-Platte aufgebrachten Konzentrationen (> 120 ng/Bande) mittels UV-Licht bei λ = 254 nm detektierbar sein. Aus diesem Grund wurde das in der Literatur für Cannabinoide als selektives Detektionsreagenz beschriebene FBS als postchromatographische Detektionsmöglichkeit verwendet.[51, 141, 170-172] Dies kam bereits in der oben angeführten Publikation (siehe 4.1 bzw. Anhang – Publikation P1) bei der Bestimmung von CBN zum Einsatz und ermöglichte eine sensitive Detektion der CBN-Spots. Im Anschluss dessen, konnten mittels HPTLC-ESI-MS für jedes untersuchte Cannabinoid eine zufriedenstellende Nachweis- und Bestimmungsgrenzen ermittelt werden (genaue Angaben sind der Publikation P2 zu entnehmen).

Auch bei der Untersuchung der CBD-Öle galt es eine Überladung der HPTLC-Platte zu vermeiden. Neben der Tatsache, dass ölige Proben schlecht und nur sehr unpräzise auf eine

DC-Platte hätten aufgetragen werden können und die sehr hohe Konzentration an enthaltenem CBD für eine Überladung und daraus resultierend zu keiner Separierung bzw. Überlappung der Analytbanden geführt hätte, musste eine Verdünnung der Öle stattfinden. Eine für die DC-Platte passende Konzentration konnte durch eine Verdünnung der CBD-Ölprobe auf 1g/L mit Hexan erreicht werden. Im Zuge der Validierung erfolgte die Bestimmung der Nachweis- (LOD) und Bestimmungsgrenze (LOQ) der untersuchten Cannabinoide. Diese verdeutlichen, dass auch für die im CBD-Öl zumeist weniger konzentriert vorliegenden Cannabinoide CBN und Δ^9-THC ab einem Gehalt von 3.6 ng CBN/HPTLC Bande bzw. 7.0 ng Δ^9-THC/HPTLC Bande die Identifizierung sowie auch eine Quantifizierung ab einem Gehalt von 16.6 ng CBN/HPTLC Bande bzw. 29.3 ng Δ^9-THC/HPTLC Bande möglich ist. Ein positiver Effekt dieser niedrigen Konzentration war es, dass dadurch keinerlei Matrixeinfluss beobachtet werden konnte, da störende Matrixbestandteile durch die Verdünnung keinerlei Einfluss mehr hatten und jegliche auf der DC-Platte ersichtliche Interferenz unterbunden wurde. Dies führte dazu, dass kein weiterer Schritt zur Aufreinigung der Probe, wie z.B. eine SPE-Säule benötigt wurde. Da die handelsüblichen CBD-Öle oft auf Basis verschiedener Speiseöle hergestellt werden und um den verschiedenen Anforderungen der Öle gerecht zu werden, wurden verschiedene Speiseöle als Referenz in dieser Methode ausgetestet, unter anderem Sonnenblumenöl, Olivenöl und Hanfsamenöl. Die Validierung der Methode erfolgte für alle Referenzöle gesondert. Mit einer durchschnittlichen Wiederfindung aller bestimmten Cannabinoide von 89.6 % wird deutlich, dass während dieser Methode trotz der recht hohen Verdünnung sehr reproduzierbare und verlässliche Ergebnisse erzielt werden können. Auch die Methodenpräzision (CBN 6.8 %, CBD 4.3 % und Δ^9-THC 7.1 %) bestätigt die Reproduzierbarkeit der Messungen dieser Methode. Die detaillierten Ergebnisse der Validierung dieser HPTLC-Methode können in der Publikation nachgelesen werden. Im Allgemeinen kann diese für die Untersuchung von CBD-Ölen modifizierte HPTLC-ESI-MS Methode als eine sehr effektive und schnelle Methode angesehen werden, um einen Überblick über den Cannabinoidgehalt, zunächst der drei am häufigsten betrachteten Cannabinoide, zu erhalten. Dies kann ein großer Vorteil sein, wenn viele verschiedene Öle parallel untersucht werden.

Um die Anwendbarkeit und Reproduzierbarkeit der Methode zu überprüfen wurden insgesamt 15 handelsübliche Öle analysiert (eine genaue Auflistung der Ergebnisse ist in der Publikation zu finden). Für den Großteil der untersuchten Proben konnte eine Übereinstimmung des auf der Verpackung deklarierten CBD-Gehaltes festgestellt werden. So lagen Abweichungen zwischen bestimmten und deklarierten Werten, bei 0.1 bis max. 0.6 %. Dennoch gab es bei einigen Proben sowohl beim CBD-Gehalt als auch beim Gehalt der anderen bestimmten Cannabinoide etwas schwerwiegendere Abweichungen. Ein Öl, welches mit einem Gehalt von 33 % CBD deklariert war, stach dabei besonders hervor, da bei der Analyse dieser Probe kein Cannabinoid nachgewiesen werden konnte, und der Gehalt an CBD hier sogar unter der Nachweisgrenze lag. Auf Grund der rechtlichen Vorgaben war die Bestimmung des Δ^9-THC Gehaltes der Proben besonders interessant. Bei dem Großteil der untersuchten Öle konnte auch kein Δ^9-THC, welches über der LOQ lag nachgewiesen werden. Allerdings konnte bei zwei Ölen ein erhöhter Gehalt an Δ^9-THC von bis zu 1.3 % nachgewiesen werden. Nachdem durch die vollständige Auftrennung von CBD und Δ^9-THC während der dünnschichtchromato-

graphischen Entwicklung ausgeschlossen werden konnte, dass es sich hierbei um eine Kontamination durch den hohen Anteil an CBD (bis 11.3 %) handelt, kann vermutet werden, dass dieser hohe Eintrag durch das Extraktionsverfahren zur Herstellung des CBD-Öls erfolgt ist. Allerdings ist eine weiterführende Einordnung schwierig, da keine weiteren Angaben zum Extraktionsverfahren gemacht wurden. Diese Ergebnisse sollten in weiterführenden Untersuchungen verifiziert werden.

Dass die Methode eine gute Variante darstellt um die Cannabinoidzusammensetzung schnell und einfach einordnen zu können, zeigt auch ein Vergleich der in der vorliegenden Arbeit entwickelten Methode mit einer in einem Handelslabor angefertigten Analyse eines der untersuchten Öle (siehe Tabelle 1). Dieses war mit einem CBD-Gehalt von 10 % deklariert. Bei den hierbei dargestellten Daten handelt es sich um unveröffentlichte Daten, welche aber eine hervorragende Ergänzung zu der vorliegenden Publikation darstellen. Die vom Handelslabor eingesetzte Methode zur Bestimmung des Cannabinoidgehaltes ist allerdings nicht genau bekannt, lediglich, dass es sich um eine HPLC-Methode handelt.

Tabelle 1: Angabe des jeweils ermittelten CBD, CBN und Δ^9-THC Gehaltes, des durch das Handelslabor analysierten CBD-Öls im Vergleich zum Ergebnis ermittelt mittels HPTLC-ESI-MS.

Cannabinoid	HPTLC-ESI-MS	Externe Analyse
CBD	10.2 %	8.9 %
CBN	<LOD	<LOD
Δ^9-THC*	<LOQ	0.005 %

*Bestimmung des Δ^9-THC-Gehaltes erfolgte ohne Einbeziehung des Gehaltes der THCA.

Hierbei wird deutlich, dass sich die Ergebnisse bezüglich des Δ^9-THC-Gehaltes und der CBN-Konzentration nicht merklich unterscheiden und lediglich der CBD-Gehalt bei der externen Analyse etwas niedriger bestimmt wurde, als bei der HPLTC-ESI-MS Methode. Dennoch können diese Ergebnisse als vergleichbare Daten angesehen werden. Um hierbei aber detailliertere Aussagen treffen zu können, sollte das Probenspektrum ausgeweitet werden und mehrere Methoden verglichen werden. Zudem wären auch Gehaltsuntersuchungen weiterer Bestandteile, wie das Δ^8-THC interessant, welches nach neusten Studien eine ähnliche Pharmakokinetik und -dynamik wie das Δ^9-THC aufweist und damit ebenfalls als psychoaktive Substanz behandelt werden sollte.[173-176] Eine Anpassung der entwickelten Methode war dafür bisher nicht erfolgreich, da hierbei die Problematik besteht die einzelnen THC-Isomere aufzutrennen. Dies soll Gegenstand zukünftiger Untersuchungen sein.

Zusammenfassend lässt sich festhalten, dass mit der beschriebenen Methode eine einfache und schnelle Methode zur Bestimmung des CBD-Gehaltes in CBD-Ölen ermöglicht wird. Somit ist es möglich eine erste Einschätzung der Cannabinoidzusammensetzung der Öle vorzunehmen. Dennoch sollten weitere Optimierungen bei der Untersuchung der Öle vorgenommen werden, da die Cannabinoidanalytik ein Feld ist, welches stetig neue Erkenntnisse generiert und sich in einem stetigem Wandel befindet.

4.3. Bestimmung von chemotaxonomischen Markern in Pflanzenharzen mittels (HP)TLC-MS (P3)

Die erfolgreiche Anpassung der für die Untersuchung der Sedimentprobe auf CBN entwickelten HPTLC-ESI-MS Methode auf eine ölige Matrix zeigt, dass diese Art der chromatographisch-instrumentellen Analytik für die Untersuchung verschiedener Zielanalyte bzw. Matrices angepasst werden kann, weshalb die Betrachtung weiterer Anwendungsgebiete ein vielversprechendes Unterfangen darstellte. In der Literatur sind in den letzten Jahren bereits zahlreiche verschiedene Anwendungsgebiete beschrieben worden – darunter die Bestimmung von Fettsäuren im Gelée Royal[177], der phenolischen Bestandteile in Propolis[178] , der Bestandteile von Pflanzenextrakten[179, 180] oder des Alkaloidgehaltes in Kräutern.[181] Dabei fällt auf, dass es sich bei den untersuchten Materialien oft um Proben natürlichen Ursprungs handelt und die (HP)TLC-MS Methode häufig verwendet wird einen Überblick über die Inhaltsstoffe zu erlangen bzw. Proben vergleichend zu untersuchen. Ein großes Feld, welches die analytische Chemie viele Jahre vor eine große Herausforderung gestellt hat sind die Pflanzenharze.[182, 183] Bei den Pflanzenharzen handelt es sich um Stoffwechselnebenprodukte pflanzlichen Gewebes, die seit Jahrtausenden für unterschiedliche Zwecke verwendet werden, z.B. als Klebstoffe, Hydrophobierungsmittel, Beschichtungs- und Dichtungsmittel oder zur Herstellung von Duft- und Aromastoffen und Arzneimitteln.[184] Auch im historischen Kontext waren Harze bei der Herstellung von bspw. Ölfarben, Firnessen, Siegel- und Holzlacken von großer Bedeutung. [183, 185] Als Hauptbestandteil sind in diesen Pflanzenharzen Terpenoide zu finden.[186] Beispiele häufig verwendeter Harze sind Weihrauch, Myrrhe und Dammar. Es gibt aber auch eine weitere wichtige Gruppe der Harze, welche als Hauptbestandteil phenolische Strukturelemente, wie aromatische Ester, Alkohole und Carbonsäuren, aufweist.[183, 186, 187]

Bisher bekannte Methoden dieser Harzcharakterisierung basieren häufig auf gaschromatographischen oder hochleistungsflüssigkeitschromatographischen (HPLC) Methoden, welche oft mit einer zeitaufwendigen Probenvorbereitung, -derivatisierung und -analyse verbunden sind.[188-193] In der Publikation von Salomé-Abarca *et al.* wurde bereits der Einsatz von HPTLC bei der Untersuchung von Pflanzenharzen als wertvoll und als mit einer GC-MS-Methode vergleichbar beschrieben, da dadurch eine Vielzahl verschiedener Proben gleichzeitig betrachtet werden kann. Auch die unkomplizierte (präparative) Auftrennung zur Gewinnung von Informationen über unbekannte Verbindungen wurde hervorgehoben.[192] Aus diesem Grund sollte eine einfache und schnelle sowie spezifische (HP)TLC-MS Methode etabliert werden, welche die Identifizierung von Triterpenoiden und phenolischen Verbindungen in verschiedenen Pflanzenharzen ermöglicht und so eine einfache Unterscheidung der untersuchten Harze hinsichtlich ihrer botanischen Herkunft gewährleistet.

Zu Beginn wurden, wie schon bei den Cannabinoiden beschrieben, Messungen der einzelnen Referenzsubstanzen durchgeführt, um die charakteristischen Signale und entstehende Fragmentionen zuordnen zu können. Dabei stellte sich heraus, dass die triterpenoiden Substanzen im positiven APCI-Modus die beste Signalintensität aufweisen, wohingegen sich der negative Modus für den Nachweis von phenolischen Strukturen eignet. Da im ESI-Modus

nur sehr wenige substanzspezifische Signale detektiert werden konnten, wurden alle folgenden Messungen mittels APCI durchgeführt. Eine Übersicht der charakteristischen (Fragment)Ionen ist in der Publikation notiert.

Obwohl dadurch für jede Substanz charakteristische Ionen ermittelt werden konnten, konnte bei einer direkten Injektion der Extrakte und Messung mittels APCI-MS keine genaue Unterscheidung der Pflanzenharze erfolgen. Bei den Triterpenen handelt es sich häufig um isomere Verbindungen, die sich zwar in ihren funktionellen Gruppen unterscheiden, aber häufig ähnliche (Fragment)Ionen aufweisen, weshalb eine Zuordnung der gemessenen Molekül- bzw. Fragmentionenpeaks ohne vorherige chromatographische Auftrennung des Substanzgemisches schwierig ist. Dennoch erwies sich eine Direktinfundierung der methanolischen Extrakte als hilfreich, um eine erste Einschätzung über die enthaltenen Verbindungen treffen zu können und das weitere Vorgehen zu definieren.

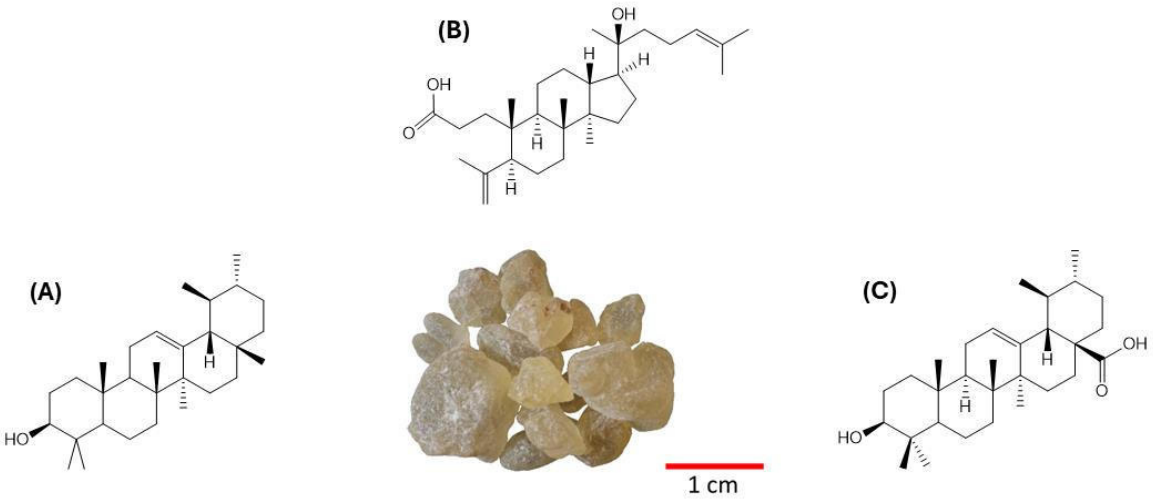

Abbildung 4: Dammarharz und dessen herangezogene Referenzsubstanzen (A) *α*-Amyrin, (B) Dammarenolsäure, (C) Ursolsäure.

Die Vielzahl an verschiedenen Bestandteilen und die unterschiedliche Zusammensetzung stellten eine Herausforderung bei der Auswahl von stationärer und mobiler Phase dar. Trotz zahlreicher Variationen verschiedener DC-Platten und Laufmittel, war es nicht möglich, eine Methode für alle untersuchten Harze zu bestimmen. Letztendlich konnte für die triterpenhaltigen Harze mittels RP-C_{18} (HP)TLC-Platten eine zufriedenstellende Trennung erreicht werden, wobei jedoch zwischen den Harzen unterschieden werden musste. Für die Extrakte von Dammar (Abbildung 4) und Mastix (Abbildung 6) wurde mit Acetonitril/ Wasser (95:5 v/v) ein anderes Laufmittelgemisch verwendet als für die Weihrauchextrakte, für welche mit einem Gemisch aus Methanol/Wasser (7:1 v/v) eine optimale Trennung erreicht werden konnte. Auch die Auftrennung des Benzoextraktes (Abbildung 5), ein Harz mit phenolischen Markersubstanzen (z.B. Zimtsäure, Benzoesäure), erfolgte mit einem anderen chromatographischen System. Hier wurde auf Normalphase DC-Platten in Kombination mit einem Laufmittelgemisch aus 2%iger Essigsäurelösung in *n*-Hexan/Ethylacetat versetzt (5:1 v/v) zurückgegriffen. Die entsprechenden R_f-Werte können der Publikation entnommen werden.

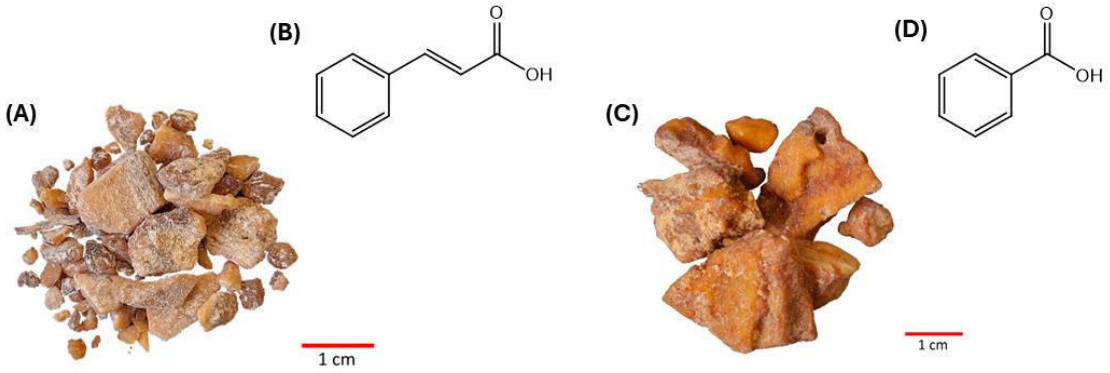

Abbildung 5: (A) Sumatra-Benzoeharz und dessen herangezogene Referenzsubstanz *trans*-Zimtsäure (B); (C) Siam-Benzoeharz und dessen herangezogene Referenzsubstanz Benzoesäure (D).

Eine weitere Herausforderung triterpenoider Substanzen ist, dass diese oftmals nicht bei λ = 254 nm oder 366 nm mit den Standard-UV-Lampen detektierbar sind. Eine postchromatographische Detektion war daher notwendig, weshalb verschiedenste Sprühreagenzien, wie das Cerium-Molybdän- oder das Vanillin-Schwefelsäure-Reagenz als Detektionsreagenz getestet wurden. Keines der verwendeten Sprühreagenzien führte zu zufriedenstellenden Ergebnissen. Eine in der Literatur von Noller et al.[194] als spezifische Farbreaktion von terpenoiden Sapogeninen beschriebene Reaktion mit Thionylchlorid und Zinnchlorid wurde daraufhin erstmals als Sprühreagenz eingesetzt (Reagenz A). Nach einigen Optimierungen der Zusammensetzung gelang es für nahezu alle in dieser Arbeit untersuchten Substanzen einen unterschiedlichen Farbverlauf der aufgetrennten Spots festzuhalten, da die angefärbten Spots innerhalb weniger Minuten die Farbe verändert haben. Da diese Veränderung spezifisch für die jeweiligen Analyten auftrat, konnte somit eine für jeden Analyten charakteristische Farbfolge ermittelt werden und zur Identifizierung der aufgetrennten Harzextrakte herangezogen werden. Eine Übersicht der einzelnen Farbverläufe ist der Publikation zu entnehmen. Dabei fällt auf, dass bei dieser Auflistung die phenolischen Substanzen Benzoesäure und Zimtsäure fehlen. Diese beiden Analyten konnten mit diesem Anfärbereagenz nicht detektiert werden, jedoch stellt dies kein Problem dar, da es sich bei diesen Verbindungen um UV-aktive Strukturen handelt und diese bei einer Wellenlänge von λ = 254 nm auf den DC-Platten detektierbar sind.

Die damit als charakteristisch eingestuften Auftrennungsmuster und R_f-Werte, die nach der chromatographischen Entwicklung der Extraktbestandteile erhalten wurden, sowie die mit der postchromatographischen Detektion mit Reagenz A beobachteten Farbfolge, können neben den mittels APCI-MS gemessenen (Fragment)Ionen zur Charakterisierung der Harze hinsichtlich ihrer botanischen Herkunft eingesetzt werden.

Zur Evaluation der Robustheit und Reproduzierbarkeit, der in dieser Arbeit optimierten (HP)TLC-APCI-MS Methode, wurde für eine Auswahl an untersuchten Referenzsubstanzen (z.B. Acetyl-11-keto-*β*-boswelliasäure, Lupeol, Moronsäure, Benzoesäure) herangezogen. Dabei wurde darauf geachtet, von jedem Strukturtyp jeweils mindestens einen Vertreter mit einzubeziehen. Dabei konnte die Präzision mit einer relativen Standardabweichung von 0.8 % bis 10.4 % bestimmt werden. Auch die Nachweisgrenze, welche für die verschiedenen

Substanzen in einem Bereich zwischen 2 bis 20 ng/Bande bestimmt werden konnte, zeigt eine zufriedenstellende Validität für die entwickelte Methode. Die detaillierten Datensätze sind in der Publikation zu finden.

Die entwickelte (HP)TLC-APCI-MS Methode wurde anschließend zur Untersuchung von 20 verschiedenen Harzextrakten herangezogen. Diese wurden von verschiedenen Händlern bezogen, wobei ebenfalls darauf geachtet wurde, unterschiedliche Varietäten einer Pflanzenharzklasse vertreten zu haben. Mit Hilfe der oben beschriebenen Methode war es nun möglich anhand der R_f-Werte, der unterschiedlichen Farbverläufe bei Umsetzung mit Reagenz A und der detektierten charakteristischen (Fragment)Ionen die untersuchten Harze zu identifizieren und zu unterscheiden.

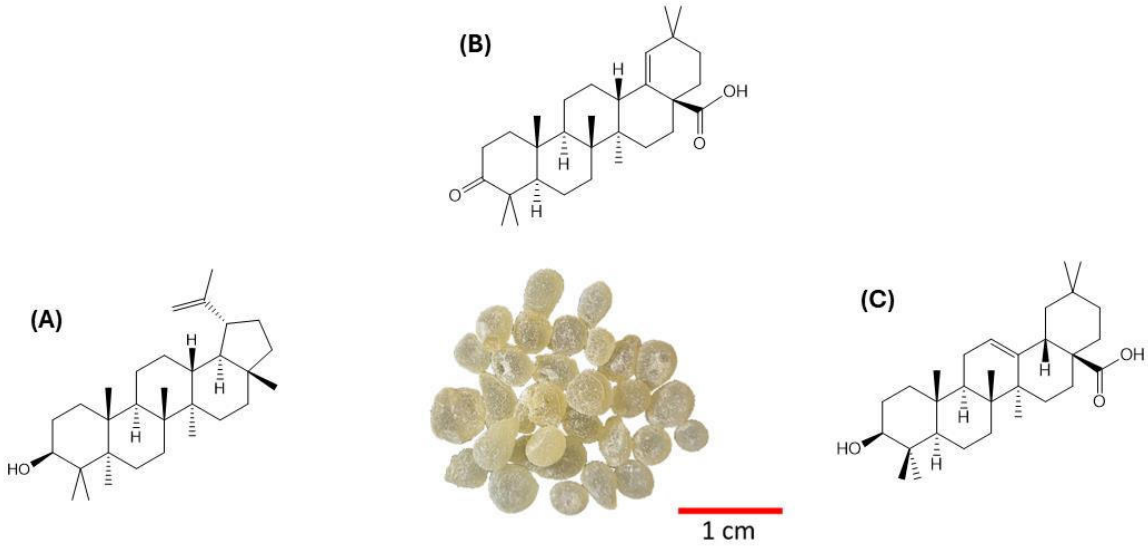

Abbildung 6: Mastixharz und dessen herangezogene Referenzsubstanzen (A) Lupeol, (B) Moronsäure, (C) Oleanolsäure.

Zudem wurde ein methanolischer Extrakt eines natürlich gealterten Mastixlacks untersucht, welcher etwa ein Jahr in einem dünnen Film, aufgetragen auf einer Holzplatte, vorlag. Zunächst erfolgte die Vermessung des Extraktes mittels APCI-MS-Direktinfundierung. Hierbei konnten Übereinstimmungen mit den vorher untersuchten Mastixharzproben festgestellt werden. Daher wurde die chromatographische Auftrennung mittels RP-C_{18}-HPTLC-Platten und Acetonitril/Wasser (95:5 v/v) als mobile Phase durchgeführt. Auch hierbei konnte eine Ähnlichkeit des Auftrennungsmusters sowie der entstehenden Farbverläufe bei der postchromatographischen Detektion mit Reagenz A nicht bestritten werden. In Verbindung mit der anschließend durchgeführten HPTLC-APCI-MS Messung, wobei die für Mastixharz charakteristischen Markersubstanzen nachgewiesen werden konnten, war eine eindeutige Identifizierung des Mastixharzes möglich. Dies soll in künftigen Studien ausgeweitet und auch auf Lacke mit unbekannter Zusammensetzung übertragen werden.

Zusammenfassend kann festgehalten werden, dass eine Identifizierung von triterpenoiden und phenolischen Markersubstanzen, die eine Unterscheidung von Pflanzenharzen ermöglichen, durch die entwickelte (HP)TLC-APCI-MS-Methode und die spezifischen

postchromatographischen Nachweisreaktionen mit Reagenz A, für alle getesteten Naturharzextrakte erfolgreich durchgeführt werden konnte. Auch handelt es sich hierbei um eine einfache, schnelle, kostengünstige sowie empfindliche und spezifische Methode für das Screening von Harzen und Lacken auf Harzbasis ist. Zudem kann diese Methodik erste Hinweise auf den botanischen Ursprung der untersuchten Harze und Lacke liefern. Die Untersuchung einer großen Anzahl von Proben, welche gleichzeitig analysiert werden können, bildet auch bei dieser Variante der DC-MS-Kopplung einen großen Vorteil gegenüber anderen analytischen Methoden. Eine Erweiterung der Referenzsubstanzen und untersuchten Harze, sowie die Möglichkeit diese Methode auch zur Quantifizierung einsetzen zu können ist späteren Studien vorbehalten.

4.4. Charakterisierung von *Saturniidae* und *Bombyx mori* L. Seiden mit Hilfe verschiedener mikroskopischer, spektroskopischer und chromatographischer Methoden (P4)

Seide stellt eine der exklusivsten und luxuriösesten Fasern der Welt dar und wird bereits seit tausenden von Jahren für die Textilherstellung verwendet.[195] In den letzten Jahrzehnten hat die Seide besonders auf Grund ihrer bemerkenswerten mechanischen Eigenschaften besonderes Interesse geweckt.[196-199] In der Literatur gibt es bereits viele Studien, welche sich mit der morphologischen Struktur sowie den mechanischen Eigenschaften und der Unterscheidung verschiedener Seidenarten beschäftigen.[87, 88, 199-202] Obwohl Seide einiger Seidenspinner, wie z.B. *Bombyx mori* L. (BM), *Antheraea mylitta* Drury (AM), *Antheraea pernyi* Guérin-Méneville oder *Samia cynthia* Drury (siehe Abbildung 7) bereits detailliert betrachtet wurden[199, 203-209], gibt es immer noch viele Seidenarten, die nur wenig untersucht wurden, weshalb eine Unterscheidung dieser erschwert ist. Neben dem Voranbringen der Aufklärung der Proteinstruktur und dem Verständnis wie die mechanischen Eigenschaften zu Stande kommen, könnte es auch im Hinblick auf mögliche Fragestellungen bezüglich der Herkunft einer Seidenprobe hilfreich sein, die Untersuchung verschiedener Seidenarten voranzutreiben. In diesem Teil der vorliegenden Arbeit wurde sich daher mit der Charakterisierung von einer Auswahl an verschiedenen Seidenspinnerarten beschäftigt.

In der Literatur sind bereits verschiedene Analysemöglichkeiten bekannt, um die Zucht- und Wildseide voneinander zu unterscheiden.[106, 195, 209-215] Dabei fällt auf, dass unter anderem viele proteomische Ansätze verfolgt werden. Auch die Untersuchung der Aminosäurezusammensetzung wurde in der Literatur zur Unterscheidung von Zucht- und Wildseide bereits angewandt und erwies sich als sehr hilfreich.[196, 209, 216-218] Im Zuge der vorliegenden Arbeit soll die Untersuchung der relativen Aminosäurezusammensetzung verschiedener Seidenproben zur weiteren Charakterisierung von Wild- und Zuchtseidenproduzenten herangezogen werden. Der Fokus lag dabei auf Seidenproduzenten, welche im historischen Kontext bei der Textilherstellung Anwendung fanden. Dies soll anschließend in weiterführenden Untersuchungen betrachtet werden (siehe 4.5 bzw. Anhang – Publikation P5).

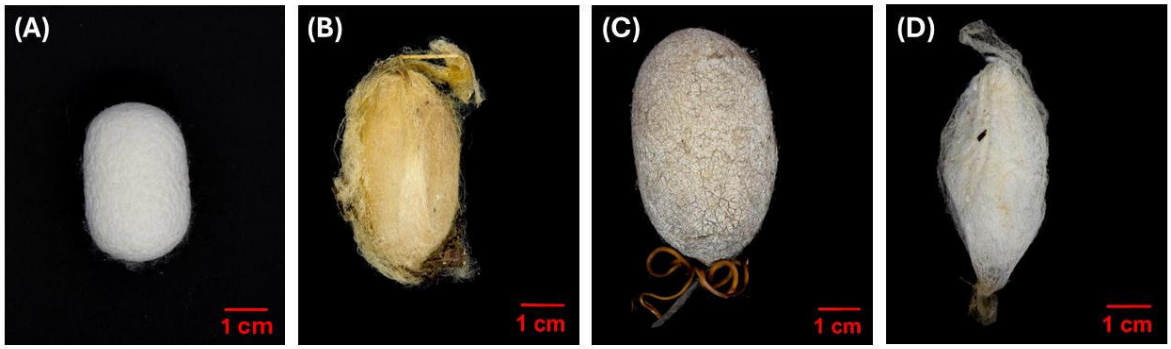

Abbildung 7: Darstellung einiger Seidenkokons (eine detaillierte Übersicht der untersuchten Seidenkokons ist im Supplementary material vom Publikation P4 zu finden). (A) *Bombyx mori* L., (B) *Antheraea pernyi* Guérin-Méneville, (C) Antheraea mylitta Drury, (D) *Samia cynthia* Drury.

Zunächst wurde eine Charakterisierung der untersuchten Seidenarten anhand der Morphologie und Struktur der Kokons bzw. der Seidenfilamente vorgenommen. Dies erfolgte mit Hilfe mikroskopischer und spektroskopischer (ATR-FTIR-Spektroskopie) Untersuchungen. Im Zuge dessen erfolgte eine Identifizierung charakteristische IR-Banden, welche im weiteren Verlauf der Untersuchungen zur Differenzierung herangezogen wurden. Zudem konnten die ATR-FTIR-spektroskopischen Daten auch im Hinblick auf die Identifizierung und Quantifizierung von sekundären Strukturelementen, wie β-Faltblatt, oder α-Helix, aber auch anderen an der Kokonoberfläche vorhandenen Substanzen, wie z.B. Calciumoxalat, Tanninen oder anderen phenolischen Strukturen, genutzt werden. In der Literatur sind dazu bereits verschiedene Studien veröffentlicht und an verschiedenen Seidenarten angewandt worden, weshalb diese Banden als Referenz für die in der Arbeit erzielten Daten herangezogen wurden.[106, 215, 219-222] Die auf diese Weise erhaltenen detaillierten Informationen über die Sekundärstruktur der untersuchten entbasteten Seidenproben sind in der Publikation einzusehen. Im Allgemeinen konnte aber über diese Daten eine Differenzierung zwischen Seide der Gattung *Bombyx* und der Seiden der Familie *Saturniidae* ermöglicht werden.

Neben der mikroskopischen und spektroskopischen Charakterisierung der Seidenfilamente, erfolgte die Untersuchung der Aminosäurezusammensetzung der einzelnen Seidenarten mittels GC-FID. In der Literatur sind bereits einige gaschromatographische Methoden für die Bestimmung von Aminosäuren in verschiedensten Matrices bekannt, wobei in den letzten Jahren vor allem die Chloroformate als Derivatisierungsreagenz an Bedeutung gewonnen haben.[223-228] In Anlehnung an die beschriebenen Messbedingungen wurde eine für die Untersuchung der Seidenproben modifizierte GC-FID Methode entwickelt und erfolgreich validiert, mit Hilfe derer eine Identifizierung und Quantifizierung von 15 Aminosäuren möglich war. Die Derivatisierung der Aminosäuren erfolgte mittels Propylchloroformat (PCF).

In vorherigen Studien konnte bereits bewiesen werden, dass es einen Unterschied in der Aminosäurezusammensetzung des Fibroins bei verschiedenen Seidenproduzenten gibt.[229, 230] Das hierbei zur Untersuchung herangezogene Fibroin ist ein filamentöses Protein, welches im gesponnenen Zustand im Kokon als Doppelstrangfilament vorliegt (siehe Abbildung 8), wobei

die beiden Fibroinfilamente durch das Protein Sericin als „Klebstoff“ zusammengehalten werden.[229, 231-233] Das wasserlösliche Sericin war bereits Gegenstand zahlreicher Studien, wobei sowohl die Struktur als auch die Zusammensetzung untersucht wurden und das Sericin daher in dieser Studie eine untergeordnete Rolle spielt. [233-237] Im Verlauf der Methodenentwicklung wurden verschiedene Varianten zur Trennung von Sericin und Fibroin getestet. Dieser Prozess wird als Entbastung bezeichnet. In der Literatur wurden bereits zahlreiche Entbastungsmethoden beschrieben, z.B. unter alkalischen bzw. sauren Bedingungen. Aber auch Enzyme oder Ananassaft werden zur Entbastung genutzt. [238-246] Letzteres ist ein seit Jahrhunderten verwendeter Ansatz zur Entbastung von Seide. Oftmals wird dabei zwischen der Entbastung von BM-Seide und Wildseide [z.B. AM, *Attacus atlas* (AtA)] unterschieden, da für die Entbastung von Wildseide auf Grund ihrer morphologischen Merkmale häufig harschere Bedingungen benötigt werden.[209, 242] Um einen guten Vergleich verschiedener moderner, aber auch historischer Methoden zu erhalten, wurden neun in der Literatur beschriebene Entbastungsvarianten getestet. Diese wurden dabei in Konzentration der eingesetzten Reagenzien, Dauer der Behandlung bzw. Temperatur des Wasserbades variiert. Die Effektivität der jeweiligen Entbastungsmethode wurde neben dem Massenverlust auch mittels mikroskopischer und spektroskopischer Untersuchungen (ATR-FTIR-Spektroskopie) kontrolliert. Eine detaillierte Beschreibung des Vorgehens ist in der Publikation einzusehen. Bei BM ist der Sericin-Anteil bereits aus früheren Studien bekannt und beträgt ca. 20-30 %[232, 234, 247, 248], daher kann mit Hilfe des Massenverlustes während der Entbastung eine Einschätzung der Effektivität der angewandten Methode vorgenommen werden.[245, 249] Auch mittels ATR-FTIR-spektroskopischer Messungen konnten die entsprechenden Sericin- bzw. Fibroinbanden und deren Intensität kontrolliert werden, welche als Indikator für die Entbastungseffizienz dienen können.[106, 238, 250, 251] Bei den mikroskopischen Untersuchungen kann zudem überprüft werden, ob die Filamente als Einzel- oder Doppelstrang vorliegen. Des Weiteren kann die Oberfläche der Filamente begutachtet und eine Einschätzung der Oberflächenbeschaffenheit vorgenommen werden. Eine raue und brüchige Oberfläche weist auf sehr harsche Bedingungen hin, wie es beim Einsatz von z.B. einer 10%igen Ethylendiaminlösung der Fall war. Die Kombination der Methoden ermöglicht eine hervorragende erste Einschätzung der Entbastungsmethode bevor eine Untersuchung der Aminosäurezusammensetzung erfolgte.

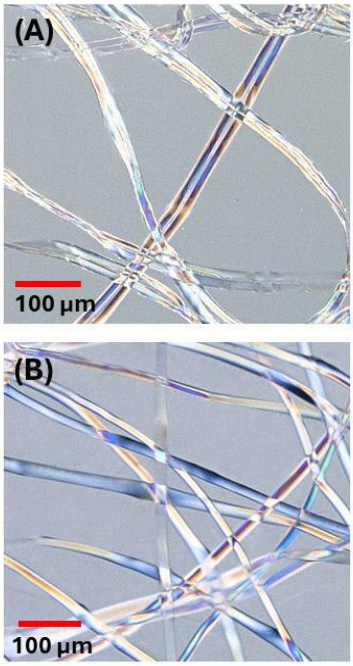

Abbildung 8: (A) BM vorliegend als Doppelstrangfilament, entbastet mit Citronensäure [1g/L; 120 min]; (B) BM vorliegend als Einzelstrangfilament, entbastet mit 0.1 % Na_2CO_3 und 2.5 % Ethylendiamin [60 min].

Die Bestimmung der Aminosäurezusammensetzung erfolgte vergleichend an entbasteten Seidenproben und unentbasteten Kokons als Referenz. Zunächst fand eine Hydrolyse der Proteine statt, um eine Bestimmung der Aminosäuren möglich zu machen. Dies erfolgte über einen Zeitraum von 24 h bei 110 °C mit einer 6 N HCl-Lösung. Die erhaltenen Hydrolysate wurden anschließend zur Trockene gebracht und in einem definierten Volumen aufgenommen.

Ein Aliquot dieser Lösung wurde daraufhin zur Derivatisierung eingesetzt. Nach der Derivatisierung konnte eine Vermessung der Lösung mittels GC-FID erfolgen. Das genaue Vorgehen ist in der Publikation beschrieben. Auf diese Weise wurde unteranderem die Aminosäurezusammensetzung der entbasteten Kokons von BM, als auch verschiedener Wildseidenkokons bestimmt.

Auf Grundlage der erhaltenen Aminosäurezusammensetzungen der entbasteten Kokons konnte, in Kombination mit den jeweiligen IR-spektroskopischen Daten und mikroskopischen Bildern, die erste Einschätzung der Entbastungsmethode verifiziert werden. Die zunächst nur auf BM angewandten Entbastungsvarianten wurden anschließend auf die Wildseiden übertragen. Für erste detailliertere Untersuchungen diesbezüglich wurden als Vertreter der Wildseiden AM Kokons, als sehr kompakte und harte Kokons, sowie AtA Kokons, als weiche und papieren wirkende Kokons, ausgewählt. Im Verlauf der Untersuchungen erwies sich eine Kombination aus Natriumcarbonat-Lösung (Na_2CO_3) und Ethylendiamin als optimal, um alle betrachteten Kokons, unabhängig ob Wild- oder Zuchtseide, entbasten zu können. Bei der Entbastung der unterschiedlichen Wildseidenkokons musste lediglich die Dauer der angepasst bzw. variiert werden. Dies kann sehr gut mittels mikroskopischer Untersuchungen sowie ATR-FTIR-spektroskopischer Messungen überprüft und eingeschätzt werden.

In der vorliegenden Studie wurden neben Seide von BM, auch Seidenproben verschiedener Gattungen der *Saturniidae*-Familie untersucht. Es wurde hierbei die chemische Zusammensetzung der verschiedenen Seiden vergleichend betrachtet, wobei sowohl die Aminosäurezusammensetzung als auch die IR-spektroskopische und mikroskopischen Daten zur Beurteilung herangezogen wurden. Obwohl keine direkten Zusammenhänge zwischen der Aminosäurezusammensetzung und der biologischen Klassifizierung des Fibroins festgestellt werden konnte, war es möglich Ähnlichkeiten in der Aminosäurezusammensetzung und den sich daraus ergebenden Strukturindizes innerhalb einer Gattung aufzuzeigen. Im Gegensatz dazu konnten zwischen den einzelnen Gattungen Unterschiede in der Aminosäurezusammensetzung festgestellt werden. Diese Ergebnisse stehen im Einklang mit bereits veröffentlichten Studien von Lucas *et al.* zur Unterscheidung von Seidenfibroinen.[252] Es wurde auch eine PCA durchgeführt, wobei hier beachtet werden muss, dass es sich lediglich um einen kleinen Datenpool handelt und die Ergebnisse durch Erweiterung des Datenpools in weiterführenden Studien verifiziert werden sollten. Dennoch wurde ersichtlich, dass es beispielsweise signifikante Unterschiede zwischen *Antheraea*-, *Saturnia*- und *Bombyx*-Seiden gibt. Eine Erweiterung des Datenspektrums und die Ausweitung der beschriebenen Untersuchungen auf weitere Seidenproduzenten ist zukünftigen Studien vorbehalten.

4.5. Studien zur Aminosäureracemisierung von Seiden mittels chiraler GC-MS (P5)

Artefakte jeglicher Art besitzen als Zeitzeugnisse der Vergangenheit einen kulturgeschichtlichen Wert. Ein besonders informationsreiches Gebiet, welches in den letzten Jahrzehnten viel Aufmerksamkeit in der naturwissenschaftlichen Welt erhalten hat und in dem viel

Forschung betrieben wird, sind historische Textilien. Obwohl historische Textilien bereits Gegenstand von Untersuchungen vieler verschiedener Kunsthistoriker waren, wurde häufig nur dem Muster und der Farbgebung der untersuchten Textilien Aufmerksamkeit geschenkt, jedoch nur in wenigen Fällen der Herstellungstechnik bzw. der Faser aus dem die Textilien bestehen. Erst im Verlauf des 20. Jahrhunderts wurden Untersuchungen zu gewebetechnischen Gesichtspunkten und zur chemischen Zusammensetzung der verwendeten Garne oder Fasern zum festen Bestandteil von archäometrischen Untersuchungen. Dadurch können sowohl Einordnungen zur biologischen Herkunft der Fasern ermöglicht werden als auch Einblicke über die handwerklichen Geschicke oder über mögliche Handelswege der Vergangenheit, wie z.B. der Seidenstraße, gesammelt werden.[253-255]

In der Literatur sind bereits viele Untersuchungen verschiedenster historischer Textilmaterialien zu finden, wobei die Seide einen großen Teil ausmacht.[254, 256-261] Viele der heutzutage verwendeten Methoden basieren auf bildgebenden und sehr minimalinvasiven Methoden, um die oft sehr seltenen und fragilen Fundstücke nahezu unbeschädigt lassen zu können. So kann bereits mit Hilfe spektroskopischer und optischer Methoden ein Einblick in die physikalische und chemische Beschaffenheit einer Faser bzw. einer historischen Probe erfolgen und es ermöglichen, diese entsprechend ihrer Herkunft zu charakterisieren. Dabei kann unterschieden werden, ob eine Faser tierischen oder pflanzlichen Ursprungs ist, ob diese eher einen runden, eckigen oder ovalen Querschnitt aufweist oder ob andere Substanzen, wie z.B. Farbstoffe oder Salze (siehe Abbildung 9), auf der Oberfläche zu detektieren sind.[257, 262, 263] Auch erste Erkenntnisse über den Degradationszustand[218, 248] oder zur Unterscheidung verschiedener Spezies, bspw. ob bei einer Seidenprobe BM Seide oder eine Wildseide wie AM vorliegt, können darüber gewonnen werden.[106, 215, 254, 260] Um einen weitreichenden Blick zu erhalten, benötigt man zu den spektroskopischen und optischen Verfahren auch oftmals weitere instrumentell analytische Methoden, um bspw. die Identität einer Faser eindeutig bestimmen zu können.[264]

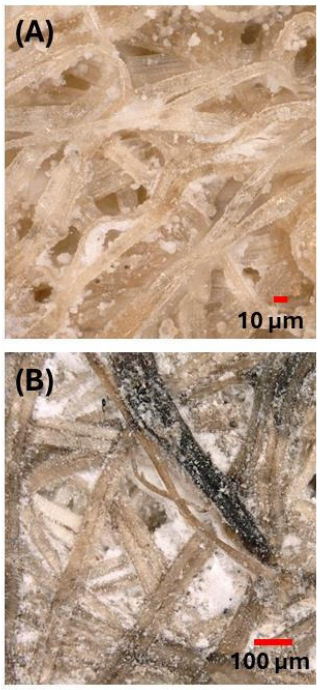

Abbildung 9: Mikroskopische Bilder von Oxalatkristallen an der Kokonoberfläche von (A) Ata und (B) AM.

In der vorangegangenen Publikation[265] und auch in weiteren in der Literatur zu findenden Studien[209, 210, 214, 230, 242, 266, 267] wird deutlich, dass über die Protein bzw. Aminosäurezusammensetzung eine Identifizierung ermöglicht und auch weitere Hinweise bezüglich der Herkunft tierischer Fasern gesammelt werden können. Teilweise werden bei historischen Proben auch Aminosäuren, speziell die Racemisierungsrate dieser, zur Altersbestimmung herangezogen.[217, 268, 269] Hierbei wird die Tatsache genutzt, dass diese in der Natur hauptsächlich als L-Enantiomer vorliegen und verschiedene Faktoren die Racemisierung beeinflussen. Dabei ist es egal ob es sich um Wolle oder Seide handelt, all diese textilen Materialen unterliegen im Laufe der Jahrhunderte einer Alterung und die enthaltenen Aminosäuren einer natürlichen Racemisierung, welche durch verschiedene Faktoren, wie UV-Licht, Mikroorganismen,

pH-Wert oder Metallionen, beeinflusst wird.[270-274] Oftmals wurden die verarbeiteten Fasern auch verschiedenen Prozessen, wie dem Färben und Beizen, unterzogen, was sich auf die Beschaffenheit der Faser auswirken kann.[217, 275]

In der folgenden Publikation wurde daher der Einfluss verschiedener Färbe- und Beizprozesse, sowie verschiedener pH-Werte während des Entbastens auf die Aminosäurezusammensetzung, insbesondere auch im Hinblick auf die Racemisierungsraten der untersuchten Aminosäuren, betrachtet. Alle Versuche und Analysen wurden zunächst an Referenzseiden (BM, AM, AtA), welche sich in ihren morphologischen Merkmalen sowie ihrer chemischen Zusammensetzung und physikalischen Struktur unterscheiden, durchgeführt. Zur Untersuchung der Racemisierungsraten wurde eine chirale GC-MS Methode entwickelt und validiert, welche eine Identifizierung und Quantifizierung von 11 Enantiomerenpaaren in den untersuchten Seidenfilamenten ermöglicht und somit eine Bestimmung der Racemisierungsraten ausgewählter AS ermöglicht.

Um nun den Einfluss verschiedener Färbe- und Beizmethoden untersuchen zu können, wurden die ausgewählten Seidenfilamente mit einer Auswahl historisch relevanter Methoden zur Färbung, wie z.B. mit Indigo oder dem aus der Pflanzenart *Rubia tinctorum* L. gewonnenen roten Farbstoff (bekannt als Krappfärbung) behandelt (siehe Abbildung 10).[276-279] Ein häufiges, vor allem bei roten Farbstoffen eingesetztes Verfahren, um eine dauerhafte und kräftigere Färbung der Fasern hervorzurufen ist das Beizen.[280-282] Ende des 19. Jahrhunderts wurden bei der Verarbeitung von Seide auch verschiedene Metallsalze eingesetzt um den Massenverlust durch das Entbasten auszugleichen und so einen höheren Preis erzielen zu können.[283-285]

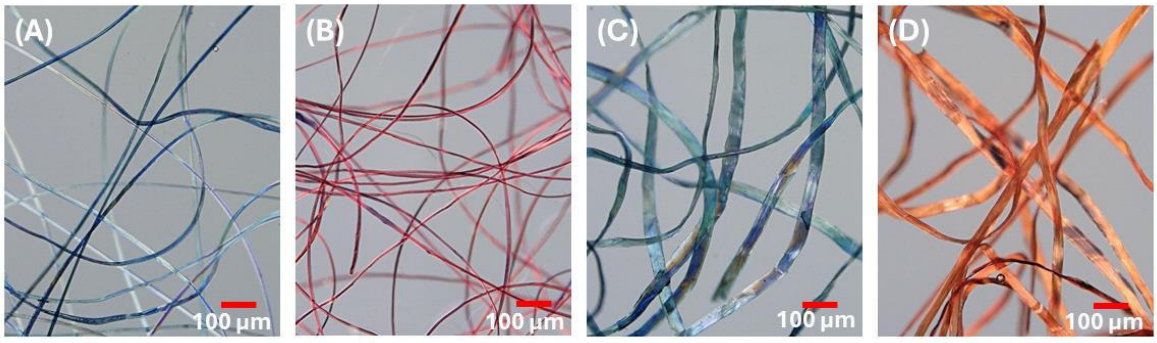

Abbildung 10*:* Mikroskopische Bilder der gefärbten Seidenfilamente; Anwendung der Indigofärbung bei BM (A) und AM (C); Anwendung der Krappfärbung mit vorheriger Behandlung mit Alaun bei BM (B) und AM (D).

Der Einfluss des Beizens auf die Aminosäurezusammensetzung wurde im Zuge der vorliegenden Studie mit einigen ausgewählten Beispielen, z.B. Alaun oder Kupfer(II)- und Eisen(II)-sulfat, ebenfalls betrachtet. Im Zuge dessen wurde darüber hinaus untersucht, ob das häufig an den Seidenkokons der Wildseide anhaftende Calciumoxalat eine Auswirkung auf die Bestimmung der Aminosäurezusammensetzung aufweist.[106] In der Literatur sind bereits verschiedene Aspekte bezüglich der Effekte von Metall-Kationen, wie z.B. Fe^{2+}, Cu^{2+}, Ca^{2+}, Zn^{2+}, beschrieben.[286] Diese können unteranderem starke Komplexe mit den zu untersuchenden Aminosäuren bilden und diese für die anschließende Derivatisierung und Identifizierung unzugänglich werden lassen.[228, 286-288] Auch Degradationsprozesse können unter stark sauren

Bedingungen, wie der auch hier angewandten sauren Hydrolyse mit 6 N HCl, durch Metallionen verstärkt werden.[289]

Mittels der zuvor entwickelten GC-FID-Methode (siehe Schmidt *et al.* 2023)[265] erfolgte zunächst die Bestimmung der Aminosäurezusammensetzung der gefärbten und gebeizten Seidenfilamente. Vergleichend dazu wurde die Aminosäurezusammensetzung der unbehandelten Referenzproben (BM, AM, AtA) herangezogen. Zur Charakterisierung wurden verschiedene strukturelle Merkmale, wie das Verhältnis von Gly/Ala oder das Verhältnis zwischen langen und kurzen Seitenketten des Proteins (100LC/SC) herangezogen.[265, 290] Obwohl ein leichter Anstieg der sauren Aminosäuren zu beobachten war, konnten keine signifikanten Unterschiede zwischen den gefärbten sowie den gebeizten und den unbehandelten Materialen festgestellt werden. Bei der Betrachtung der D-/L-Enantiomere wurden ebenfalls vergleichbare Daten generiert. Hierbei wurde jedoch festgestellt, dass einige Aminosäuren zu einer höheren Racemisierung neigen und deren D-Enantiomer in höheren Mengen detektierbar war. Dazu zählen unter anderem Asx und Ser. Hierbei sollte jedoch bedacht werden, dass diese teilweise auffälligen Aminosäuren thermodynamisch instabilere Aminosäuren darstellen und daher auch eher zur Racemisierung neigen.[272, 291] Des Weiteren befindet sich ein Großteil dieser Aminosäuren in den amorphen Regionen des Fibroins, welche wiederum anfälliger für chirale Umlagerungen sind als Aminosäuren die in der kristallinen Region vorkommen.[275] Obwohl einige Proben eine Erhöhung der D-Aminosäuren zeigten, kann im Allgemeinen davon ausgegangen werden, das das Färben und Beizen keine signifikanten Auswirkungen auf die Aminosäurezusammensetzung der rezenten Seidenfilamente hat.

Um dennoch jeglichen Interferenzen von bspw. Metallionen entgegenzuwirken, sollte ein zusätzlicher Aufreinigungsschritt in die Methode integriert und die Metallionen entfernt werden. Oftmals sind die untersuchten historischen Proben auch nur in sehr geringer Menge vorhanden bzw. sollen im Zuge einer analytischen Untersuchung nur geringfügigen Schaden erleiden, weshalb nur eine geringe Probenmenge entnommen werden kann. In der vorliegenden Arbeit sollte aufgrund dessen nun ermöglicht werden, sowohl den Farbstoff als auch das Seidenfilament zu charakterisieren. Daher sollte der Reinigungsschritt zugleich eine Extraktion vorliegender Farbstoffe ermöglichen und anschließend im Extrakt enthaltene Farbstoffe identifiziert werden. In der Literatur sind bereits verschiedene Wege der Farbstoffextraktion bei unterschiedlichen Probenmatrices dokumentiert.[262, 279, 292-295] Davon wurden zwei vielversprechende Varianten, eine etwas mildere (EDTA/ACN/MeOH) und eine etwas harschere (EDTA/DMF), in der vorliegenden Arbeit auf deren Auswirkung auf die Aminosäurezusammensetzung überprüft. Übereinstimmend mit der Literatur konnten hierbei in Verbindung mit der EDTA-DMF-Methode die Farbstoffe Alizarin und Purpurin, sowie Indigo extrahiert und anschließend mittels HPLC-DAD identifiziert werden. Obwohl bei den anschließend untersuchten historischen Seidenproben keine Farbstoffe detektiert wurden, konnte dieses Vorgehen bei der Untersuchung einer historischen Wollprobe, zur erfolgreichen Identifizierung von Indigo angewandt werden.

Die Einflussnahme beider Extraktionsmethoden auf die Aminosäurezusammensetzung der gebeizten bzw. gefärbten Seidenfilamente wurde mittels GC-FID ermittelt. Hierzu wurden die

mit dem jeweiligen Extraktionsmittel behandelten Seidenproben einer Hydrolyse sowie Derivatisierung mittels PCF unterzogen und anschließend analysiert. Hier konnte weder zwischen den einzelnen Extraktionsmethoden noch zwischen der mit dem jeweiligen Extraktionsmittel behandelten und der unbehandelten Seidenprobe eine signifikante Veränderung der Aminosäurezusammensetzung festgestellt werden. Auch bei der Betrachtung der Racemisierung der Aminosäuren konnte bei Anwendung dieser Extraktionsmittel keine auf die Aminosäurezusammensetzung beeinträchtigende Wirkung festgestellt werden. Vor der Hydrolyse einer untersuchten Seidenprobe wurde daher im weiteren Verlauf stets eine Extraktion aller anhaftender Substanzen (z.B. Farbstoffe, Metallionen, organische Substanzen) durchgeführt.

Die Betrachtung der verschiedenen pH-Werte erfolgte in der vorliegenden Arbeit unter Bezugnahme der Racemisierungsrate der untersuchten Aminosäuren. Hierbei wurden verschiedene alkalische Entbastungsmethoden sowie die harsche Behandlung der Seidenfilamente mit einer Na_2CO_3-Lösung (pH 9, 11, 13) aber auch die saure Hydrolyse der Seidenfilamente mittels chiraler GC-MS-Methode analysiert (nähere Informationen dazu sind in dem Manuskript zu finden). In der Literatur wird beschrieben, dass ein höherer pH-Wert zum Anstieg der Racemisierungsraten, besonders bei Asx, führt.[217, 275] Auch bei der in dieser Arbeit durchgeführten Studie, konnte bei alkalischen pH-Werten (> 10) ein Anstieg in der Konzentration des D-Asx festgestellt werden, welcher bei einem pH-Wert von 13 zu einem D-/L-Verhältnis von nahezu 100 % führte. In diesem Zuge konnte auch bei weiteren Aminosäuren (z.B. Ser, Glx, Phe) ein Anstieg des Anteils der D-Enantiomere festgestellt werden. Im Einklang mit den Erkenntnissen aus ATR-FTIR-spektroskopischen und GC-FID-Messungen[265] konnten, trotz geringfügiger Anstiege der D-Enantiomerenkonzentration weniger Aminosäuren (z.B. Ala, Val, Ser, Glx), jedoch keine systematischen Erhöhungen der D-/L-Verhältnisse bei der zuvor etablierten Entbastungsmethode (0.1 % Na_2CO_3 und 2.5 % Ethylendiamin, siehe 4.4 bzw. Anhang – Publikation P4) festgestellt werden. Übereinstimmend mit Moini *et al.*[296] konnte bei der Hydrolyse der Seidenfilamente mit 6 N HCl bei 110 °C für 24 h nur ein leichter Anstieg der D-Aminosäurenkonzentration festgestellt werden. Im Zuge dessen wurde auch eine mikrowellenassistierte Variante der Hydrolyse getestet. Jedoch führte diese, trotz vollständiger Hydrolyse in weniger als einer Stunde, zu einer nahezu vollständigen Umwandlung der L-Aminosäuren in ihre entsprechenden D-Enantiomere.

Die entwickelte chirale GC-MS Methode samt vorangehendem Extraktionsschritt wurde anschließend auf historische Seidenproben angewandt. Die untersuchten Textilproben stammen von den archäologischen Fundstätten Niya und Yanghai in der Region Xinjiang in China. In dieser Region wurden zahlreiche gut erhaltene und vollständig bekleidete mumifizierte menschliche Überreste, sowie viele Artefakte und Accessoires des täglichen Lebens gefunden. Diese sind Bestandteil zahlreicher Studien.[254, 257, 260, 261, 297-300] Mittels OM, SEM, ATR-FTIR-Spektroskopie und verschiedener HPLC-Methoden wurden bereits in einer dieser vorangegangenen Studien ausführliche Untersuchungen der in dieser Arbeit verwendeten Proben zur Oberflächenbeschaffenheit sowie zur Detektion von Farbstoffen detailliert beschrieben und diskutiert.[257, 263] Die mit Hilfe der spektroskopischen Unter-

suchungen erlangten Erkenntnisse, sollten nun mittels der GC-MS Methode erweitert bzw. bekräftigt werden. Die untersuchten Proben konnten so zweifelsfrei, als Seide der Gattung *Bombyx* identifiziert werden, wobei verschiedene Hinweise (wie z.B. ein erhöhter Ser-Gehalt) darauf hindeuten, dass bei den historischen Textilproben sowohl kurze, evtl. nicht vollständig entbastete Seidenfilamente als auch lange entbastete Filamente zur Textilherstellung verwendet wurden. Besonders die Probe 03SAYM376:13-1 (Abbildung 11) fiel dabei auf, da diese mit den versponnenen Seidenfilamenten eine untypische Verarbeitungsform der Seide aufwies.

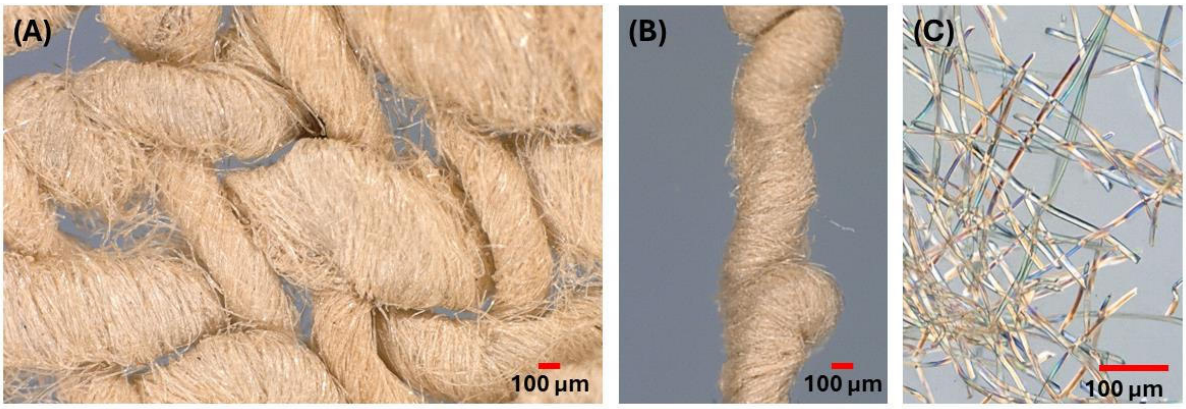

Abbildung 11: Mikroskopische Bilder der Probe 03SAYM376:13-1, (A) Verarbeitungsmuster des Textilstückes, (B) versponnene Seidenfilamente der Textilprobe, (C) Vergrößerung einzelner kurzer Seidenfilamente.

Auch wurden eher kurze Seidenfilamente zur Herstellung dieses Textils verwendet, was darauf hindeutet, dass zur Herstellung dieses Kleidungsstückes Kokons von bereits geschlüpften Faltern verwendet wurde. Zudem konnten charakteristische Banden des Sericins (1400 und 1070 cm^{-1}) im ATR-FTIR-Spektrum detektiert werden. Im Vergleich zu den weiteren untersuchten historischen Proben konnten diese Peaks eindeutig identifiziert werden, was auf einen höheren Sericin-Gehalt dieser Probe hindeutet. Daher kann auch der Einsatz der sogenannten Bourette-Seide, wo defekte Kokons und Abfälle aus der Entbastung der Kokons verwendet werden und somit oftmals ein erhöhter Sericingehalt beobachtet wird, in diesem Zusammenhang nicht ausgeschlossen werden.[301]

Zusammenfassend kann festgehalten werden, dass es gelungen ist eine selektive Methodik zu entwickeln, die es ermöglicht Textilfasern anhand deren Aminosäurezusammensetzung zu charakterisieren. Durch die Untersuchung einer historischen Wollprobe konnte zudem die Selektivität der entwickelten Methodik bekräftigt werden, da diese eindeutig von der Aminosäurezusammensetzung der Seidenproben zu unterscheiden ist.

5. Zusammenfassung und Ausblick

Bei der analytischen Chemie gilt es oftmals bestimmte Analyten nachzuweisen, wobei sich die Möglichkeiten der Untersuchungen stetig weiterentwickeln, während die Anforderungen an die Ergebnisse bzw. die Analysenmethoden stets höher werden.[302-304] Im Rahmen der vorliegenden Arbeit wurden nun verschiedene instrumentell-analytische Methoden hinsichtlich differenzierter Fragestellungen entwickelt und validiert. Bei der Untersuchung verschiedener Proben, wie Sedimentproben, pflanzliche Harze, Seidenkokons und historische Seidentextilien, mussten verschiedene Aspekte während der Methodenentwicklung beachtet und dementsprechend optimiert werden. Es kamen unter anderem verschiedene Aufreinigungs- und Extraktionsschritte zum Einsatz, welche besonders bei der zielgerichteten Bestimmung der verschiedenen Analyten dazu beitrugen, interferierende Moleküle abzutrennen, wie es bspw. bei der Bestimmung des CBN in Sedimentproben der Fall war. Zudem konnten so an den Proben anhaftenden Substanzen bzw. Farbstoffe extrahiert und die Extrakte anschließend für weitere Untersuchungen, wie der Identifizierung von Farbstoffen bei Textilfasern, herangezogen werden.

Mit Hilfe der dünnschichtchromatographisch gekoppelten Massenspektrometrie gelang es eine Methode für ein Hochdurchsatzscreening mit geringem Probenvorbereitungsaufwand zu etablieren und auf verschiedene Materialien anzuwenden. Durch den Einsatz der Dünnschichtchromatographie konnten sowohl interferierende Probenbestandteile als auch parallel zu analysierende Analyten, wie z.B. die Cannabinoide Δ^9-THC, CBD und CBN, ab- bzw. aufgetrennt werden, welche anschließend mittels MS vermessen werden konnten. Mit Hilfe dieser Methode wurden ebenfalls kommerziell erhältliche CBD-Öle untersucht, wobei eine oftmals unzureichende Deklaration bezüglich des angegebenen CBD-Gehaltes festgestellt wurde. Aber auch eine schnelle Identifizierung verschiedener pflanzlicher Triterpenharze wurde durch eine (HP)TLC-MS-Methode ermöglicht. Dies könnte in weiterführenden Studien ein vielversprechender Ansatz sein, um harzbasierte Lacke historischer Kulturgüter hinsichtlich ihres botanischen Ursprungs zu untersuchen und die eingesetzten Harze zu identifizieren. Auch erlaubt die (HP)TLC-MS-Methode das parallele Aufbringen einer Vielzahl von Proben, wodurch eine schnelle und vergleichende Untersuchung ermöglicht wird.

In den letzten Jahrzehnten ist die analytische Chemie auch zu einem wichtigen Bestandteil geworden, um das Verständnis und die Erhaltung von kulturellem Erbe zu unterstützen.[10, 305, 306] Oftmals werden die Anforderungen an die analytische Methodik hierbei komplexer oder man muss mit sehr wenig Material auskommen und dies möglichst unbeschadet belassen, da Probenmaterial nur in begrenzten Mengen zur Verfügung stehen. Daher war ein Ziel dieser Arbeit, welches bei den verschiedenen Methoden und untersuchten Materialen nicht aus den Augen verloren wurde, dass die jeweilige Methode geeignet ist, um historische Materialen zu untersuchen und so zur Klärung historischer Fragestellungen beitragen zu können. In der vorliegenden Arbeit erfolgten dementsprechend auch Untersuchungen verschiedener historischer Proben. Bei der Untersuchung der Sedimentproben konnte etwa, entsprechend vorangegangener Pollenuntersuchung, die Anwesenheit von CBN, welches ein Abbauprodukt

von Δ^9-THC darstellt, bestätigt werden. Dieser Fund des für Hanfpflanzen spezifischen Cannabinoids bekräftigt die Annahme, dass der Badanital-See im Himalaya, dem Ursprung der untersuchten Proben, in früheren Zeiten zur Fasergewinnung aus Hanfpflanzen gedient hat. Des Weiteren wurden historische Textilien untersucht, wobei diese anhand ihrer Aminosäurezusammensetzung als Seide identifiziert werden konnten. Dabei wurden unteranderem verschiedene Prozesse (z.B. das Färben und Beizen), die die Aminosäurezusammensetzung beeinflussen können untersucht. Die dabei entwickelte chirale GC-MS-Methode konnte dabei zu einem erweiterten Verständnis des Einflusses der Verarbeitungsschritte auf die D/L-Verhältnisse der Aminosäuren beitragen. In einer weiteren Studie wurde die Unterscheidung verschiedener Seidenproduzenten thematisiert, die als mögliche Seidenlieferanten in früheren Zeiten gedient haben könnten. Trotz morphologischer und chemischer Unterschiede konnte keine eindeutige Differenzierung einzelner Seidenproduzenten vorgenommen werden. Zum aktuellen Zeitpunkt können lediglich hohe Gemeinsamkeiten struktureller und chemischer Merkmale innerhalb einer Gattung bestimmt werden, wodurch jedoch eine Unterscheidung der untersuchten Gattungen *Antheraea*, *Saturnia* und *Bombyx* ermöglicht wird. Durch eine Erweiterung der Daten und das Heranziehen weiterer Identifizierungskriterien in zukünftigen Studien, könnte es über eine PCA ermöglicht werden, historische Seidenproben weiterführend zu klassifizieren.

Zusammenfassend kann gesagt werden, dass obwohl eine Vielzahl an Methoden entwickelt, optimiert und an verschiedenen Probenmaterialen angewandt wurde, sich stets neue Möglichkeiten für weiterführende Untersuchungen ergeben und der Wunsch nach Wissenserweiterung nicht versiegt. Nichtsdestotrotz konnte gezeigt werden, dass instrumentell-analytische Methoden für eine Vielzahl an unterschiedlichen Fragestellungen ein hilfreiches Werkzeug sind und es ermöglichen gesicherte Aussagen zu generieren. Auch ist es durch die Untersuchung historischer Proben möglich ein Fenster in die Vergangenheit zu öffnen und so vergangene Zivilisationen besser verstehen zu lernen.

6. Literaturverzeichnis

[1] Beyer, D. T.; *Analytische Chemie - ein Definition als Aphorismus*. Analytik News - Das Online-Labormagazin, **2017**. https://analytik.news/blog/2017/23.html (Zugriff: 01.03.2024).

[2] Namieśnik, J.; Trace Analysis — Challenges and Problems. *Crit. Rev. Anal. Chem.* **2002**, *32* (4), 271-300.

[3] Baranowska, I.; *Handbook of trace analysis: Fundamentals and Applications*; Springer International Publishing AG: Basel, **2016**.

[4] Tölg, G.; Problems and trends in extreme trace analysis for the elements. *Anal. Chim. Acta* **1993**, *283* (1), 3-18.

[5] Stoney, D. A.; Stoney, P. L.; Critical review of forensic trace evidence analysis and the need for a new approach. *Forensic Sci. Int.* **2015**, *251*, 159-170.

[6] Fischer, K.; Fries, E.; Körner, W.; Schmalz, C.; Zwiener, C.; New developments in the trace analysis of organic water pollutants. *Appl. Microbiol. Biotechnol.* **2012**, *94* (1), 11-28.

[7] Schwedt, G.; Schmidt, T. C.; Schmitz, O. J.; *Analytische chemie: Grundlagen, Methoden und Praxis*; Wiley-VCH: Weinheim, **2016**.

[8] Riederer, J.; Zur Geschichte der Anwendung der chemischen Analyse in der Archäologie. *Ber. Wiss.gesch.* **1988**, *11* (2), 125-126.

[9] Riederer, J.; Analytische Methoden in der kulturgeschichtlichen Forschung. In *Analytiker-Taschenbuch*, Fresenius, W., Günzler, H., Huber, W., Lüderwald, I., Tölg, G., Wisser, H. Eds.; Springer Berlin Heidelberg, **1985**; pp 3-32.

[10] Nigra, B. T.; Faull, K. F.; Barnard, H.; Analytical Chemistry in Archaeological Research. *Anal. Chem.* **2015**, *87* (1), 3-18.

[11] Trojanowicz, M.; Modern chemical analysis in archaeometry. *Anal. Bioanal. Chem.* **2008**, *391* (3), 915-918.

[12] Bronk Ramsey, C.; Radiocarbon Dating: Revolutions in Understanding. *Archaeometry* **2008**, *50* (2), 249-275.

[13] Martini, M.; Sibilia, E.; Radiation in archaeometry: archaeological dating. *Radiat. Phys. Chem.* **2001**, *61* (3), 241-246.

[14] Newman, G. E.; Smith, R. K.; Kinds of Authenticity. *Philos. Compass* **2016**, *11* (10), 609-618.

[15] Ulrich, A.; *Authentizität*. **2013**. https://doi.org/10.1515/hwro.10.authentizitaet (Zugriff: 01.03.2024).

[16] Karoui, R.; *Chemical Analysis of Food* Academic Press Amsterdam, **2020**.

[17] Wadood, S. A.; Boli, G.; Xiaowen, Z.; Hussain, I.; Yimin, W.; Recent development in the application of analytical techniques for the traceability and authenticity of food of plant origin. *Microchem. J.* **2020**, *152*, 104295.

[18] Kharbach, M.; Alaoui Mansouri, M.; Taabouz, M.; Yu, H.; Current Application of Advancing Spectroscopy Techniques in Food Analysis: Data Handling with Chemometric Approaches. *Foods* **2023**, *12* (14), 2753.

[19] Boyaci, I. H.; Temiz, H. T.; Geniş, H. E.; Soykut, E. A.; Yazgan, N. N.; Güven, B.; Uysal, R. S.; Bozkurt, A. G.; İlaslan, K.; Torun, O.; Dispersive and FT-Raman spectroscopic methods in food analysis. *RSC Adv.* **2015**, *5* (70), 56606-56624.

[20] Medina, S.; Perestrelo, R.; Silva, P.; Pereira, J. A. M.; Câmara, J. S.; Current trends and recent advances on food authenticity technologies and chemometric approaches. *Trends Food Sci. Technol.* **2019**, *85*, 163-176.

[21] Danezis, G. P.; Tsagkaris, A. S.; Camin, F.; Brusic, V.; Georgiou, C. A.; Food authentication: Techniques, trends & emerging approaches. *TrAC, Trends Anal. Chem.* **2016**, *85*, 123-132.

[22] Cammann, K.; Analytical Chemistry — today's definition and interpretation. *Fresenius J. Anal. Chem.* **1992**, *343* (11), 812-813.
[23] Volke, K.; Zu den Anfängen der Analytischen Chemie: Wider Fälscher und Betrüger. *Chem. Unserer Zeit* **2004**, *38* (4), 268-275.
[24] Ballschmiter, K. Woraus besteht ein Stoff? Vergangenheit und Gegenwart einer Fragestellung. Mitteilungen, Gesellschaft Deutscher Chemiker/Fachgruppe Geschichte der Chemie: Frankfurt/Main, 1993; Vol. Bd. 9.
[25] Szabadváry, F.; *Geschichte der analytischen Chemie* Vieweg-Verlag: Braunschweig, **1966**.
[26] Szabadváry, F.; Kurze Geschichte der analytischen Chemie. *Period. Polytech. Chem. Eng.* **1958**, *2* (1), 49-57.
[27] Nesterov-Müller, A.; Erfolgreicher Grenzgang. *Phys. Unserer Zeit* **2016**, *47* (5), 233-237.
[28] Karayannis, M. I.; Efstathiou, C. E.; Significant steps in the evolution of analytical chemistry—Is the today's analytical chemistry only chemistry? *Talanta* **2012**, *102*, 7-15.
[29] Irving, H.; Centenary lecture. One hundred years of development in Analytical Chemistry. *Analyst* **1974**, *99* (1185), 787-801.
[30] Griffiths, I. W.; J. J. Thomson — the Centenary of His Discovery of the Electron and of His Invention of Mass Spectrometry. *Rapid Commun. Mass Spectrom.* **1997**, *11* (1), 2-16.
[31] Gross, J. H.; *Massenspektrometrie*; Springer Spektrum Berlin: Heidelberg, **2019**.
[32] Gross, J. H.; Einleitung. In *Massenspektrometrie: Ein Lehrbuch*, Gross, J. H. Ed.; Springer Berlin: Heidelberg, **2013**; pp 1-22.
[33] Colombini, M. P.; Andreotti, A.; Bonaduce, I.; Modugno, F.; Ribechini, E.; Analytical Strategies for Characterizing Organic Paint Media Using Gas Chromatography/Mass Spectrometry. *Acc. Chem. Res.* **2010**, *43* (6), 715-727.
[34] Rosenberg, E.; Characterisation of historical organic dyestuffs by liquid chromatography–mass spectrometry. *Anal. Bioanal. Chem.* **2008**, *391* (1), 33-57.
[35] Sandström, E.; Vettorazzo, C.; Mackay, C. L.; Troalen, L. G.; Hulme, A. N.; Development and Application of Desorption Electrospray Ionization Mass Spectrometry for Historical Dye Analysis. *Anal. Chem.* **2023**, *95* (11), 4846-4854.
[36] Puchalska, M.; Połeć-Pawlak, K.; Zadrożna, I.; Hryszko, H.; Jarosz, M.; Identification of indigoid dyes in natural organic pigments used in historical art objects by high-performance liquid chromatography coupled to electrospray ionization mass spectrometry. *J. Mass Spectrom.* **2004**, *39* (12), 1441-1449.
[37] Howes, M.-J. R.; Simmonds, M. S. J.; Kite, G. C.; Evaluation of the quality of sandalwood essential oils by gas chromatography–mass spectrometry. *J. Chromatogr. A* **2004**, *1028* (2), 307-312.
[38] Ehling, S.; Cole, S.; Analysis of Organic Acids in Fruit Juices by Liquid Chromatography–Mass Spectrometry: An Enhanced Tool for Authenticity Testing. *J. Agric. Food Chem.* **2011**, *59* (6), 2229-2234.
[39] Møller, J. K.; Catharino, R. R.; Eberlin, M. N.; Electrospray ionization mass spectrometry fingerprinting of whisky: immediate proof of origin and authenticity. *Analyst* **2005**, *130* (6), 890-897.
[40] Hug, H.; *Instrumentelle Analytik: Theorie und Praxis*; Verlag Europa-Lehrmittel Nourney, Vollmer: Haan-Gruiten, **2011**.
[41] Meyer, H. E.; Fröhlich, T.; Nordhoff, E.; Kuhlmann, K.; Massenspektrometrie. In *Bioanalytik*, Kurreck, J., Engels, J. W., Lottspeich, F. Eds.; Springer Berlin Heidelberg, **2022**; pp 359-414.
[42] Boleda, M. R.; Galceran, M. T.; Ventura, F.; Trace determination of cannabinoids and opiates in wastewater and surface waters by ultra-performance liquid chromatography–tandem mass spectrometry. *J. Chromatogr. A* **2007**, *1175* (1), 38-48.

[43] Bouvier, C.; Van Nuffel, S.; Walter, P.; Brunelle, A.; Time-of-flight secondary ion mass spectrometry imaging in cultural heritage: A focus on old paintings. *J. Mass Spectrom.* **2022**, *57* (1), e4803.
[44] Kuckova, S.; Cejnar, P.; Santrucek, J.; Hynek, R.; Characterization of proteins in cultural heritage using MALDI–TOF and LC–MS/MS mass spectrometric techniques. *Phys. Sci. Rev.* **2019**, *4* (5).
[45] Laskin, J.; Lanekoff, I.; Ambient Mass Spectrometry Imaging Using Direct Liquid Extraction Techniques. *Anal. Chem.* **2016**, *88* (1), 52-73.
[46] Chen, H.; Gamez, G.; Zenobi, R.; What can we learn from ambient ionization techniques? *J. Am. Soc. Mass Spectrom.* **2009**, *20* (11), 1947-1963.
[47] Monge, M. E.; Fernández, F. M.; *Ambient ionization mass spectrometry*; Royal Scociety of Chemistry: London, **2014**.
[48] Jug, U.; Glavnik, V.; Kranjc, E.; Vovk, I.; HPTLC–densitometric and HPTLC–MS methods for analysis of flavonoids. *J. Liq. Chromatogr. Relat. Technol.* **2018**, *41* (6), 329-341.
[49] Shrikrishna Madhukar, N.; Vinayak S, M.; A novel digitally optimized rapid quantification of carcinogenic aryl azo amines from various food matrices by HPTLC-MS. *J. Liq. Chromatogr. Relat. Technol.* **2020**, *43* (13-14), 445-454.
[50] Rani, R.; Medhe, S.; Srivastava, M.; HPTLC–MS based method development and validation for the detection of adulterants in spices. *J. Food Meas. Charact.* **2015**, *9* (2), 186-194.
[51] Fischedick, J. T.; Glas, R.; Hazekamp, A.; Verpoorte, R.; A qualitative and quantitative HPTLC densitometry method for the analysis of cannabinoids in Cannabis sativa L. *Phytochem. Anal.* **2009**, *20* (5), 421-426.
[52] He, F.; He, Y.; Zheng, X.; Wang, R.; Lu, J.; Dai, Z.; Ma, S.; Screening of Chemical Dyes in Traditional Chinese Medicine by HPTLC-MS. *J. AOAC Int.* **2019**, *101* (3), 686-694.
[53] Simon, D.; Oleschuk, R.; The liquid micro junction-surface sampling probe (LMJ-SSP); a versatile ambient mass spectrometry interface. *Analyst* **2021**, *146* (21), 6365-6378.
[54] Van Berkel, G. J.; Kertesz, V.; King, R. C.; High-Throughput Mode Liquid Microjunction Surface Sampling Probe. *Anal. Chem.* **2009**, *81* (16), 7096-7101.
[55] Bhole, R. P.; Tamboli, F. R.; Development and Validation of Stability Indicating HPTLC-MS Method for Estimation of Empagliflozin in Pharmaceutical Dosage Form. *Anal. Chem. Lett.* **2018**, *8* (2), 244-256.
[56] Kasote, D.; Ahmad, A.; Chen, W.; Combrinck, S.; Viljoen, A.; HPTLC-MS as an efficient hyphenated technique for the rapid identification of antimicrobial compounds from propolis. *Phytochem. Lett.* **2015**, *11*, 326-331.
[57] Rani, S.; Rahman, K.; Younis, P. M.; Akhtar, O.; HPTLC: An Emerging Technique in Herbal Medicine. *J. Herb. Med.* **2015**, *4* (2), 25-37.
[58] Sharma, P.; Bharath, M. S.; Murthy, P.; Qualitative high performance thin layer chromatography (HPTLC) analysis of cannabinoids in urine samples of Cannabis abusers. *Indian J. Med. Res.* **2010**, *132* (2), 201-208.
[59] Cheng, S.-C.; Huang, M.-Z.; Shiea, J.; Thin layer chromatography/mass spectrometry. *J. Chromatogr. A* **2011**, *1218* (19), 2700-2711.
[60] Stock, R.; Rice, C. B. F.; *Chromatographic methods*; Chapman and Hall: Salisbury, **1974**.
[61] Bartle, K. D.; Myers, P.; History of gas chromatography. *TrAC, Trends Anal. Chem.* **2002**, *21* (9), 547-557.
[62] Piantanida, A. G.; Barron, A. R.; Principles of gas chromatography. *OpenStax CNX* **2014**.
[63] Kolomnikov, I. G.; Efremov, A. M.; Tikhomirova, T. I.; Sorokina, N. M.; Zolotov, Y. A.; Early stages in the history of gas chromatography. *J. Chromatogr. A* **2018**, *1537*, 109-117.

[64] Skoog, D. A.; Leary, J. J.; Gaschromatographie (GC). In *Instrumentelle Analytik: Grundlagen — Geräte — Anwendungen*, Skoog, D. A., Leary, J. J. Eds.; Springer Berlin Heidelberg, **1996**; pp 650-674.

[65] Al-Rubaye, A. F.; Hameed, I. H.; Kadhim, M. J.; A review: uses of gas chromatography-mass spectrometry (GC-MS) technique for analysis of bioactive natural compounds of some plants. *Int. J. Toxicol. Pharmacol. Res.* **2017**, *9* (1), 81-85.

[66] Reber, E. A.; Gas chromatography-mass spectrometry (GC-MS): applications in archaeology. In *Encyclopedia of Global Archaeology*, Springer: New York, **2020**; pp 4441-4457.

[67] Pastor, K.; Ačanski, M.; Vujić, D.; Gas chromatography in food authentication. In *Gas Chromatography-Derivatization, Sample Preparation, Application*, IntechOpen: London, **2019**; p 109.

[68] Santos, F. J.; Galceran, M. T.; The application of gas chromatography to environmental analysis. *TrAC, Trends Anal. Chem.* **2002**, *21* (9), 672-685.

[69] Lehotay, S. J.; Hajšlová, J.; Application of gas chromatography in food analysis. *TrAC, Trends Anal. Chem.* **2002**, *21* (9), 686-697.

[70] Bristow, T.; Harrison, M.; Sims, M.; The application of gas chromatography/atmospheric pressure chemical ionisation time-of-flight mass spectrometry to impurity identification in Pharmaceutical Development. *Rapid Commun. Mass Spectrom.* **2010**, *24* (11), 1673-1681.

[71] Fliszar, K.; Wiggins, J. M.; Pignoli, C. M.; Martin, G. P.; Li, Z.; Analysis of organic volatile impurities in pharmaceutical excipients by static headspace capillary gas chromatography. *J. Chromatogr. A* **2004**, *1027* (1), 83-91.

[72] Bonaduce, I.; Ribechini, E.; Modugno, F.; Colombini, M. P.; Analytical Approaches Based on Gas Chromatography Mass Spectrometry (GC/MS) to Study Organic Materials in Artworks and Archaeological Objects. In *Analytical Chemistry for Cultural Heritage*, Mazzeo, R. Ed.; Springer International Publishing: Basel, **2017**; pp 291-327.

[73] Andreotti, A.; Izzo, F. C.; Bonaduce, I.; Archaeometric Study of the Mural Paintings by Saturnino Gatti and Workshop in the Church of San Panfilo, Tornimparte (AQ): The Study of Organic Materials in Original and Restored Areas. *Appl. Sci.* **2023**, *13* (12), 7153.

[74] Sutherland, K.; Gas chromatography/mass spectrometry techniques for the characterisation of organic materials in works of art. *Phys. Sci. Rev.* **2019**, *4* (6).

[75] Poulin, J.; A New Methodology for the Characterisation of Natural Dyes on Museum Objects Using Gas Chromatography–Mass Spectrometry. *Stud. Conserv.* **2018**, *63* (1), 36-61.

[76] Elyashberg, M.; Identification and structure elucidation by NMR spectroscopy. *TrAC, Trends Anal. Chem.* **2015**, *69*, 88-97.

[77] Breitmaier, E.; *Structure elucidation by NMR in organic chemistry: a practical guide*; John Wiley & Sons Ltd.: Chichester, **2002**.

[78] Nivens, D. A.; Padgett, C. W.; Chase, J. M.; Verges, K. J.; Jamieson, D. S.; Art, Meet Chemistry; Chemistry, Meet Art: Case Studies, Current Literature, and Instrumental Methods Combined To Create a Hands-On Experience for Nonmajors and Instrumental Analysis Students. *J. Chem. Educ.* **2010**, *87* (10), 1089-1093.

[79] Pelton, J. T.; McLean, L. R.; Spectroscopic Methods for Analysis of Protein Secondary Structure. *Anal. Biochem.* **2000**, *277* (2), 167-176.

[80] Kolev, T.; Spiteller, M.; Koleva, B.; Spectroscopic and structural elucidation of amino acid derivatives and small peptides: experimental and theoretical tools. *J. Amino Acids* **2010**, *38* (1), 45-50.

[81] Degano, I.; Ribechini, E.; Modugno, F.; Colombini, M. P.; Analytical Methods for the Characterization of Organic Dyes in Artworks and in Historical Textiles. *Appl. Spectrosc. Rev.* **2009**, *44* (5), 363-410.

[82] Abd Mutalib, M.; Rahman, M. A.; Othman, M. H. D.; Ismail, A. F.; Jaafar, J.; Chapter 9 - Scanning Electron Microscopy (SEM) and Energy-Dispersive X-Ray (EDX) Spectroscopy. In *Membrane Characterization*, Hilal, N., Ismail, A. F., Matsuura, T., Oatley-Radcliffe, D. Eds.; Elsevier: Amsterdam, **2017**; pp 161-179.

[83] Leng, Y.; *Materials characterization: introduction to microscopic and spectroscopic methods*; Wiley-VCH: Weinheim, **2013**.

[84] Zhao, C.; Zhang, Y.; Wang, C.-C.; Hou, M.; Li, A.; Recent progress in instrumental techniques for architectural heritage materials. *Herit. Sci.* **2019**, *7* (1), 36.

[85] Bergfjord, C.; Holst, B.; A procedure for identifying textile bast fibres using microscopy: Flax, nettle/ramie, hemp and jute. *Ultramicroscopy* **2010**, *110* (9), 1192-1197.

[86] Haugan, E.; Holst, B.; Determining the fibrillar orientation of bast fibres with polarized light microscopy: the modified Herzog test (red plate test) explained. *J. Microsc.* **2013**, *252* (2), 159-168.

[87] Chen, F.; Porter, D.; Vollrath, F.; Morphology and structure of silkworm cocoons. *Mater. Sci. Eng. C* **2012**, *32* (4), 772-778.

[88] Chen, F.; Porter, D.; Vollrath, F.; Structure and physical properties of silkworm cocoons. *J. R. Soc. Interface.* **2012**, *9* (74), 2299-2308.

[89] Derrick, M. R.; Stulik, D.; Landry, J. M.; *Infrared spectroscopy in conservation science*; Getty Publications: Los Angeles, **2000**.

[90] Nawrocka, A.; Lamorska, J.; Determination of food quality by using spectroscopic methods. In *Advances in agrophysical research*, IntechOpen: London, **2013**.

[91] Alpert, N. L.; Keiser, W. E.; Szymanski, H. A.; *IR: theory and practice of infrared spectroscopy*; Springer Science & Business Media: New York, **2012**.

[92] Thompson, J. M.; *Infrared spectroscopy*; Pan Stanford Publishing Pte. Ldt.: Singapore, **2018**.

[93] Günzler, H.; Gremlich, H.-U.; *IR-Spektroskopie: Eine Einführung*; Wiley-VCH Weinheim, **2012**.

[94] Mohamed, M. A.; Jaafar, J.; Ismail, A. F.; Othman, M. H. D.; Rahman, M. A.; Chapter 1 - Fourier Transform Infrared (FTIR) Spectroscopy. In *Membrane Characterization*, Hilal, N., Ismail, A. F., Matsuura, T., Oatley-Radcliffe, D. Eds.; Elsevier: Amsterdam, **2017**; pp 3-29.

[95] Blum, M.-M.; John, H.; Historical perspective and modern applications of Attenuated Total Reflectance – Fourier Transform Infrared Spectroscopy (ATR-FTIR). *Drug Test. Anal.* **2012**, *4* (3-4), 298-302.

[96] Cortea, I. M.; Cristache, R.; Sandu, I.; Characterization of historical violin varnishes using ATR-FTIR spectroscopy. *Rom. Rep. Phys* **2016**, *68* (2), 615-622.

[97] Geminiani, L.; Campione, F. P.; Corti, C.; Giussani, B.; Gorla, G.; Luraschi, M.; Recchia, S.; Rampazzi, L.; Historical silks: a novel method to evaluate their condition with ATR-FTIR spectroscopy and Principal Component Analysis. *J. Cult. Herit.* **2024**, *67*, 9-22.

[98] Falcão, L.; Araújo, M. E. M.; Application of ATR–FTIR spectroscopy to the analysis of tannins in historic leathers: The case study of the upholstery from the 19th century Portuguese Royal Train. *Vib. Spectrosc.* **2014**, *74*, 98-103.

[99] Bayarı, S. H.; Özdemir, K.; Sen, E. H.; Araujo-Andrade, C.; Erdal, Y. S.; Application of ATR-FTIR spectroscopy and chemometrics for the discrimination of human bone remains from different archaeological sites in Turkey. *Spectrochim. Acta A* **2020**, *237*, 118311.

[100] Liu, G.-L.; Kazarian, S. G.; Recent advances and applications to cultural heritage using ATR-FTIR spectroscopy and ATR-FTIR spectroscopic imaging. *Analyst* **2022**, *147* (9), 1777-1797.

[101] Peets, P.; Leito, I.; Pelt, J.; Vahur, S.; Identification and classification of textile fibres using ATR-FT-IR spectroscopy with chemometric methods. *Spectrochim. Acta A* **2017**, *173*, 175-181.
[102] Garside, P.; Wyeth, P.; Identification of Cellulosic Fibres by FTIR Spectroscopy - Differentiation of flax and hemp by polarizied ART-FTIR *Stud. Conserv.* **2006**, *51* (3), 205-211.
[103] Geminiani, L.; Campione, F. P.; Corti, C.; Luraschi, M.; Motella, S.; Recchia, S.; Rampazzi, L.; Differentiating between Natural and Modified Cellulosic Fibres Using ATR-FTIR Spectroscopy. *Heritage* **2022**, *5* (4), 4114-4139.
[104] Baran, A.; Fiedler, A.; Schulz, H.; Baranska, M.; In situ Raman and IR spectroscopic analysis of indigo dye. *Anal. Methods* **2010**, *2* (9), 1372-1376.
[105] Kavkler, K.; Gunde-Cimerman, N.; Zalar, P.; Demšar, A.; FTIR spectroscopy of biodegraded historical textiles. *Polym. Degrad. Stab.* **2011**, *96* (4), 574-580.
[106] Boulet-Audet, M.; Vollrath, F.; Holland, C.; Identification and classification of silks using infrared spectroscopy. *J. Exp. Biol.* **2015**, *218* (19), 3138-3149.
[107] Adriaens, A.; Non-destructive analysis and testing of museum objects: An overview of 5 years of research. *Spectrochim. Acta B* **2005**, *60* (12), 1503-1516.
[108] Janssens, K.; Van Grieken, R.; *Non-destructive micro analysis of cultural heritage materials*; Elsevier: Amsterdam, **2004**.
[109] Citti, C.; Braghiroli, D.; Vandelli, M. A.; Cannazza, G.; Pharmaceutical and biomedical analysis of cannabinoids: A critical review. *J. Pharm. Biomed. Anal.* **2018**, *147*, 565-579.
[110] Radwan, M. M.; Wanas, A. S.; Chandra, S.; ElSohly, M. A.; Natural Cannabinoids of Cannabis and Methods of Analysis. In *Cannabis sativa L. - Botany and Biotechnology*, Chandra, S., Lata, H., ElSohly, M. A. Eds.; Springer International Publishing AG: Basel, **2017**; pp 161-182.
[111] Whiting, P. F.; Wolff, R. F.; Deshpande, S.; Di Nisio, M.; Duffy, S.; Hernandez, A. V.; Keurentjes, J. C.; Lang, S.; Misso, K.; Ryder, S.; et al.; Cannabinoids for Medical Use: A Systematic Review and Meta-analysis. *JAMA* **2015**, *313* (24), 2456-2473.
[112] Haney, M.; Hill, M. N.; Cannabis and Cannabinoids: From Synapse to Society. *Neuropsychopharmacol.* **2018**, *43* (1), 1-3.
[113] Pisanti, S.; Bifulco, M.; Modern History of Medical Cannabis: From Widespread Use to Prohibitionism and Back. *Trends Pharmacol. Sci.* **2017**, *38* (3), 195-198.
[114] Pourseyed Lazarjani, M.; Torres, S.; Hooker, T.; Fowlie, C.; Young, O.; Seyfoddin, A.; Methods for quantification of cannabinoids: a narrative review. *J. Cannabis Res.* **2020**, *2* (1), 35.
[115] Demske, D.; Tarasov, P. E.; Leipe, C.; Kotlia, B. S.; Joshi, L. M.; Long, T.; Record of vegetation, climate change, human impact and retting of hemp in Garhwal Himalaya (India) during the past 4600 years. *Holocene* **2016**, *26* (10), 1661-1675.
[116] Edwards, K. J.; Whittington, G.; Palynological evidence for the growing of Cannabis sativa L.(hemp) in medieval and historical Scotland. *Trans. Inst. Br. Geogr.* **1990**, 60-69.
[117] Edwards, K. J.; Whittington, G.; Male and female plant selection in the cultivation of hemp, and variations in fossil Cannabis pollen representation. *Holocene* **1992**, *2* (1), 85-87.
[118] Lavrieux, M.; Jacob, J.; Disnar, J.-R.; Bréheret, J.-G.; Le Milbeau, C.; Miras, Y.; Andrieu-Ponel, V.; Sedimentary cannabinol tracks the history of hemp retting. *Geology* **2013**, *41* (7), 751-754.
[119] Kittel, P.; Muzolf, B.; Płóciennik, M.; Elias, S.; Brooks, S. J.; Lutyńska, M.; Pawłowski, D.; Stachowicz-Rybka, R.; Wacnik, A.; Okupny, D.; A multi-proxy reconstruction from Lutomiersk–Koziówki, Central Poland, in the context of early modern hemp and flax processing. *J. Archaeol. Sci.* **2014**, *50*, 318-337.

[120] Mercuri, A. M.; Accorsi, C. A.; Bandini Mazzanti, M.; The long history of Cannabis and its cultivation by the Romans in central Italy, shown by pollen records from Lago Albano and Lago di Nemi. *Veg. Hist. Archaeobot.* **2002**, *11*, 263-276.
[121] Schofield, J. E.; Waller, M.; A pollen analytical record for hemp retting from Dungeness Foreland, UK. *J. Archaeol. Sci.* **2005**, *32* (5), 715-726.
[122] Rull, V.; Vegas-Vilarrúbia, T.; Preliminary report on a mid-19th century Cannabis pollen peak in NE Spain: historical context and potential chronological significance. *Holocene* **2014**, *24* (10), 1378-1383.
[123] Clarke, R. C.; Traditional cannabis cultivation in Darchula District, Nepal—seed, resin and textiles. *J. Ind. Hemp* **2007**, *12* (2), 19-42.
[124] Dörfler, W.; Die Geschichte des Hanfanbaus in Mitteleuropa aufgrund palynologischer Untersuchungen und von Großrestnachweisen. *Praehist. Z.* **1990**, *65* (1), 218-244.
[125] French, C.; Moore, P.; Deforestation, Cannabis cultivation and Schwingmoor formation at Cors Llyn (Llyn Mire), Central Wales. *New Phytol.* **1986**, *102* (3), 469-482.
[126] Brown, D. T.; *Cannabis: the genus cannabis*; Harwood academic publishers: Amsterdam, **1998**.
[127] Russo, E. B.; History of cannabis and its preparations in saga, science, and sobriquet. *Chem. Biodiversity* **2007**, *4* (8), 1614-1648.
[128] Trofin, I. G.; Dabija, G.; Filipescu, L.; Long - term Storage and Cannabis Oil Stability. *Rev. Chim.- Bucharest* **2012**, *63* (3), 293-297.
[129] Trofin, I. G.; Vlad, C. C.; Dabija, G.; Filipescu, L.; Voda, M. A.; Influence of Storage Conditions on the Chemical Potency of Herbal Cannabis. *Rev. Chim.- Bucharest* **2011**, *62* (6), 639-645.
[130] Pacifici, R.; Marchei, E.; Salvatore, F.; Guandalini, L.; Busardò, F. P.; Pichini, S.; Evaluation of cannabinoids concentration and stability in standardized preparations of cannabis tea and cannabis oil by ultra-high performance liquid chromatography tandem mass spectrometry. *Clin. Chem. Lab. Med.* **2017**, *55* (10), 1555-1563.
[131] Trofin, I. G.; Dabija, G.; Vaireanu, D. I.; Filipescu, L.; The influence of long-term storage conditions on the stability of cannabinoids derived from cannabis resin. *Rev. Chim.-Bucharest* **2012**, *63* (4), 422-427.
[132] Harvey, D. J.; Stability of cannabinoids in dried samples of cannabis dating from around 1896-1905. *J Ethnopharmacol* **1990**, *28* (1), 117-128.
[133] Lindholst, C.; Long term stability of cannabis resin and cannabis extracts. *Aust. J. Forensic Sci.* **2010**, *42* (3), 181-190.
[134] Leghissa, A.; Hildenbrand, Z. L.; Schug, K. A.; A review of methods for the chemical characterization of cannabis natural products. *J. Sep. Sci.* **2018**, *41* (1), 398-415.
[135] Vozella, V.; Zibardi, C.; Ahmed, F.; Piomelli, D.; Fast and sensitive quantification of Δ9-tetrahydrocannabinol and its main oxidative metabolites by liquid chromatography/tandem mass spectrometry. *Cannabis Cannabinoid Res.* **2019**, *4* (2), 110-123.
[136] Mandrioli, M.; Tura, M.; Scotti, S.; Gallina Toschi, T.; Fast Detection of 10 Cannabinoids by RP-HPLC-UV Method in Cannabis sativa L. *Molecules* **2019**, *24* (11).
[137] Rabel, F.; Sherma, J.; New TLC/HPTLC commercially prepared and laboratory prepared plates: A review. *J. Liq. Chromatogr. Relat. Technol.* **2016**, *39* (8), 385-393.
[138] Watanabe, K.; Yamaori, S.; Funahashi, T.; Kimura, T.; Yamamoto, I.; 8-Hydroxycannabinol: a new metabolite of cannabinol formed by human hepatic microsomes. *Forensic Toxicol.* **2006**, *24* (2), 80-82.
[139] Kitpipit, T.; Methods for the Detection of Cannabis trace in cooked food.
[140] Drugs, U. N. O. o.; *Recommended methods for the identification and analysis of cannabis and cannabis products: manual for use by National Drug Testing Laboratories*; United Nations Publications: **2009**.

[141] *Identification and quantification of different cannabinoids in Cannabis sativa*. CAMAG, **2017**. https://www.camag.com/en/tlc_hptlc/camag_laboratory/methods.cfm?ao=-1 (Zugriff: 03.04.2019).
[142] Eisenhauer, A.; Spielhagen, R. F.; Frank, M.; Hentzschel, G.; Mangini, A.; Kubik, P. W.; Dittrich-Hannen, B.; Billen, T.; 10Be records of sediment cores from high northern latitudes: Implications for environmental and climatic changes. *Earth Planet. Sci. Lett.* **1994**, *124* (1), 171-184.
[143] Arz, H. W.; Pätzold, J.; Wefer, G.; Climatic changes during the last deglaciation recorded in sediment cores from the northeastern Brazilian Continental Margin. *Geo-Mar. Lett.* **1999**, *19* (3), 209-218.
[144] Karabanov, E. B.; Prokopenko, A. A.; Williams, D. F.; Khursevich, G. K.; A new record of Holocene climate change from the bottom sediments of Lake Baikal. *Palaeogeogr. Palaeoclimatol. Palaeoecol.* **2000**, *156* (3), 211-224.
[145] Cheshire, H.; Thurow, J.; Nederbragt, A. J.; Late Quaternary climate change record from two long sediment cores from Guaymas Basin, Gulf of California. *J. Quat. Sci.* **2005**, *20* (5), 457-469.
[146] McMinn, A.; Heijnisj, H.; Harle, K.; McOrist, G.; Late-Holocene climatic change recorded in sediment cores from Ellis Fjord, eastern Antarctica. *Holocene* **2001**, *11* (3), 291-300.
[147] Barber, K.; Battarbee, R.; Brooks, S.; Eglinton, G.; Haworth, E.; Oldfield, F.; Stevenson, A.; Thompson, R.; Appleby, P.; Austin, W.; Proxy records of climate change in the UK over the last two millennia: documented change and sedimentary records from lakes and bogs. *J. Geol. Soc.* **1999**, *156* (2), 369-380.
[148] Hebbeln, D.; Lamy, F.; Wefer, G.; High-Resolution Marine Record of Climatic Change in Mid-latitude Chile during the Last 28,000 Years Based on Terrigenous Sediment Parameters. *Quat. Res.* **1999**, *51* (1), 83-93.
[149] Kotlia, B.; Joshi, L.; Late Holocene climatic changes in garhwal Himalaya. *Curr. Sci.* **2013**, 911-919.
[150] Lavrieux, M.; Jacob, J.; LeMilbeau, C.; Zocatelli, R.; Masuda, K.; Bréheret, J.-G.; Disnar, J.-R.; Occurrence of triterpenyl acetates in soil and their potential as chemotaxonomical markers of Asteraceae. *Organic Geochemistry* **2011**, *42* (11), 1315-1323.
[151] Dearing, J. A.; Climate-human-environment interactions: resolving our past. *Clim. Past* **2006**, *2* (2), 187-203.
[152] Lavrieux, M.; Disnar, J.-R.; Chapron, E.; Bréheret, J.-G.; Jacob, J.; Miras, Y.; Reyss, J.-L.; Andrieu-Ponel, V.; Arnaud, F.; 6700 yr sedimentary record of climatic and anthropogenic signals in Lake Aydat (French Massif Central). *Holocene* **2013**, *23* (9), 1317-1328.
[153] McCarthy, F. M.; Patterson, R. T.; Head, M. J.; Riddick, N. L.; Cumming, B. F.; Hamilton, P. B.; Pisaric, M. F.; Gushulak, A. C.; Leavitt, P. R.; Lafond, K. M.; et al.; The varved succession of Crawford Lake, Milton, Ontario, Canada as a candidate Global boundary Stratotype Section and Point for the Anthropocene series. *Anthropocene Rev* **2023**, *10* (1), 146-176.
[154] Waters, C. N.; Turner, S. D.; Zalasiewicz, J.; Head, M. J.; Candidate sites and other reference sections for the Global boundary Stratotype Section and Point of the Anthropocene series. *Anthr. Rev.* **2023**, *10* (1), 3-24.
[155] Gushulak, C. A.; Marshall, M.; Cumming, B. F.; Llew-Williams, B.; Timothy Patterson, R.; McCarthy, F. M.; Siliceous algae response to the “Great Acceleration” of the mid-20th century in Crawford Lake (Ontario, Canada): A potential candidate for the Anthropocene GSSP. *Anthr. Rev.* **2022**, *9* (3), 571-590.
[156] Hazekamp, A.; The Trouble with CBD Oil. *Med. Cannabis Cannabinoids* **2018**, *1* (1), 65-72.

[157] Peng, J.; Fan, M.; An, C.; Ni, F.; Huang, W.; Luo, J.; A narrative review of molecular mechanism and therapeutic effect of cannabidiol (CBD). *Basic Clin. Pharmacol. Toxicol.* **2022**, *130* (4), 439-456.
[158] Freeman, A. M.; Petrilli, K.; Lees, R.; Hindocha, C.; Mokrysz, C.; Curran, H. V.; Saunders, R.; Freeman, T. P.; How does cannabidiol (CBD) influence the acute effects of delta-9-tetrahydrocannabinol (THC) in humans? A systematic review. *Neurosci. Biobehav. Rev.* **2019**, *107*, 696-712.
[159] Johnson, E.; Kilgore, M.; Babalonis, S.; Label accuracy of unregulated cannabidiol (CBD) products: measured concentration vs. label claim. *J. Cannabis Res.* **2022**, *4* (1), 28.
[160] Fernández, N.; Carreras, L. J.; Larcher, R. A.; Ridolfi, A. S.; Quiroga, P. N.; Quantification of cannabinoids in Cannabis oil using GC/MS: Method development, validation, and application to commercially available preparations in Argentina. *Planta Med. Int. Open* **2020**, *7* (02), e81-e87.
[161] Schweikle, S.; Golombek, P.; Sproll, C.; Walch, S. G.; Lachenmeier, D. W.; The Challenge of Risk Assessment of Tetrahydrocannabinol (THC) in Cannabidiol (CBD) Oils and Food Supplements: An Approach for Deriving Maximum Limits. *Challenges* **2022**, *13* (2), 32.
[162] Commission Regulation (EU) 2022/1393 of 11 August 2022; amending Regulation (EC) No 1881/2006 as regards maximum levels of delta-9-tetrahydrocannabinol (Δ9-THC) in hemp seeds and products derived therefrom. *Official Journal of the European Union*; **2022**.
[163] Commission notice clarifying the applicable legislation to the conditions for import of hemp and hemp seeds under Article 189 of Regulation (EU) No 1308/2013 of the European Parliament and the Council (C/2023/1365). **2023**.
[164] Bundesgesetzblatt - Teil I - zur Regelung einzelner dem Schutz der finanziellen Interessen der Union dienender Bestimmungen im Rahmen der Gemeinsamen Agrarpolitik, zur Änderung des Betäubungsmittelgesetzes sowie zur Aufhebung weiterer Vorschriften. **2023**.
[165] Lachenmeier, D. W.; Walch, S. G.; Evidence for adverse effects of cannabidiol (CBD) products and their non-conformity on the European food market - response to the European Industrial Hemp Association. *F1000Res* **2020**, *9*, 1051.
[166] EFSA Panel on Nutrition, N. F.; Allergens, F.; Turck, D.; Bohn, T.; Castenmiller, J.; De Henauw, S.; Hirsch-Ernst, K. I.; Maciuk, A.; Mangelsdorf, I.; McArdle, H. J.; et al.; Statement on safety of cannabidiol as a novel food: data gaps and uncertainties. *EFSA J.* **2022**, *20* (6), e07322.
[167] Tsvetkova, D.; Peykova, L.; Andonova-Dimitrova, L.; Pencheva, I.; Regulation and control of the use of Cannabis and Cannabidiol in „novel foods". *Pharmacia* **2023**, *70* (4), 1385-1395.
[168] Schmidt, T.; Kramell, A. E.; Oehler, F.; Kluge, R.; Demske, D.; Tarasov, P. E.; Csuk, R.; Identification and quantification of cannabinol as a biomarker for local hemp retting in an ancient sedimentary record by HPTLC-ESI-MS. *Anal. Bioanal. Chem.* **2020**, *412* (11), 2633-2644.
[169] Galand, N.; Ernouf, D.; Montigny, F.; Dollet, J.; Pothier, J.; Separation and Identification of Cannabis Components by Different Planar Chromatography Techniques (TLC, AMD, OPLC). *J. Chromatogr. Sci.* **2004**, *42* (3), 130-134.
[170] Hazekamp, A.; Peltenburg, A.; Verpoorte, R.; Giroud, C.; Chromatographic and Spectroscopic Data of Cannabinoids from Cannabis sativa L. *J. Liq. Chromatogr. Relat. Technol.* **2005**, *28* (15), 2361-2382.
[171] Bladt, S.; *Plant Drug Analysis: A thin layer chromatography atlas*; Springer Verlag Berlin: Heidelberg, **2009**.

[172] Corrigan, D.; Lynch, J.; An investigation of potential staining reagents for the glandular trichomes of Cannabis sativa. *Planta Med.* **1980**, *40* (S 1), 163-169.
[173] Tagen, M.; Klumpers, L. E.; Review of delta-8-tetrahydrocannabinol (Δ8-THC): Comparative pharmacology with Δ9-THC. *Br. J. Pharmacol.* **2022**, *179* (15), 3915-3933.
[174] LoParco, C. R.; Rossheim, M. E.; Walters, S. T.; Zhou, Z.; Olsson, S.; Sussman, S. Y.; Delta-8 tetrahydrocannabinol: a scoping review and commentary. *J. Addict.* **2023**, *118* (6), 1011-1028.
[175] Kruger, J. S.; Kruger, D. J.; Delta-8-THC: Delta-9-THC's nicer younger sibling? *J. Cannabis Res.* **2022**, *4* (1), 4.
[176] Kaczor, E. E.; Greene, K.; Babu, K. M.; Berthold, E. C.; Sharma, A.; Carreiro, S. P.; Commercial Delta-8 THC Products: an Analysis of Content and Labeling. *J. Med. Toxicol.* **2024**, *20* (1), 31-38.
[177] Ibrahim, R. S.; El-Banna, A. A.; Royal jelly fatty acids bioprofiling using TLC-MS and digital image analysis coupled with chemometrics and non-parametric regression for discovering efficient biomarkers against melanoma. *RSC Adv.* **2021**, *11* (31), 18717-18728.
[178] Bertrams, J.; Kunz, N.; Müller, M.; Kammerer, D.; Stintzing, F. C.; Phenolic compounds as marker compounds for botanical origin determination of German propolis samples based on TLC and TLC-MS. *J. Appl. Bot. Food Qual.* **2013**, *86* (1).
[179] Sajewicz, M.; Wojtal, Ł.; Natić, M.; Staszek, D.; Waksmundzka-Hajnos, M.; Kowalska, T.; TLC-MS versus TLC-LC-MS Fingerprints of Herbal Extracts. Part I. Essential Oils. *J. Liq. Chromatogr. Relat. Technol.* **2011**, *34* (10-11), 848-863.
[180] Sajewicz, M.; Staszek, D.; Natić, M.; Wojtal, Ł.; Waksmundzka-Hajnos, M.; Kowalska, T.; TLC-MS versus TLC-LC-MS Fingerprint of Herbal Extracts. Part II. Phenolic acids and flavonoids. *J. Liq. Chromatogr. Relat. Technol.* **2011**, *34* (10-11), 864-887.
[181] Zhang, N.; Wang, M.; Li, Y.; Zhou, M.; Wu, T.; Cheng, Z.; TLC–MS identification of alkaloids in Leonuri Herba and Leonuri Fructus aided by a newly developed universal derivatisation reagent optimised by the response surface method. *Phytochem. Anal.* **2021**, *32* (3), 242-251.
[182] Dieterich, K.; Stock, N.; *Analyse der Harze Balsame und Gummiharze nebst ihrer Chemie und Pharmakognosie: Zum Gebrauch in wissenschaftlichen und technischen Untersuchungslaboratorien unter Berücksichtigung der älteren und neuesten Literatur*; Springer-Verlag: Berlin, **2013**.
[183] Mills, J. S.; White, R.; Natural resins of art and archaeology their sources, chemistry, and identification. *Stud. Conserv.* **1977**, *22* (1), 12-31.
[184] Moyler, D. A.; Clery, R. A.; The aromatic resins: their chemistry and uses. *Spec. Publ. - R. Soc. Chem.* **1997**, *214*, 96-115.
[185] Mills, J.; White, R.; *Organic chemistry of museum objects*; Routledge: Abingdon, **2012**.
[186] Dilworth, L. L.; Riley, C. K.; Stennett, D. K.; Chapter 5 - Plant Constituents: Carbohydrates, Oils, Resins, Balsams, and Plant Hormones. In *Pharmacognosy*, Badal, S., Delgoda, R. Eds.; Academic Press: Boston, **2017**; pp 61-80.
[187] Colombini, M. P.; Modugno, F.; *Organic materials in art and archaeology*; John Wiley & Sons, Ltd: Chichester, **2009**.
[188] Mathe, C.; Culioli, G.; Archier, P.; Vieillescazes, C.; High-performance liquid chromatographic analysis of triterpenoids in commercial frankincense. *Chromatographia* **2004**, *60*, 493-499.
[189] Plante, M.; Bailey, B.; Crafts, C.; Acworth, I. N.; Sensitive HPLC method for triterpenoid analysis using charged aerosol detection with improved resolution. *Thermo Fisher Scientific* **2012**, 2-6.
[190] Burger, P.; Casale, A.; Kerdudo, A.; Michel, T.; Laville, R.; Chagnaud, F.; Fernandez, X.; New insights in the chemical composition of benzoin balsams. *Food Chem.* **2016**, *210*, 613-622.

[191] Hovaneissian, M.; Archier, P.; Mathe, C.; Culioli, G.; Vieillescazes, C.; Analytical investigation of styrax and benzoin balsams by HPLC-PAD-fluorimetry and GC-MS. *Phytochem. Anal.* **2008**, *19* (4), 301-310.
[192] Salomé-Abarca, L. F.; van der Pas, J.; Kim, H. K.; van Uffelen, G. A.; Klinkhamer, P. G.; Choi, Y. H.; Metabolic discrimination of pine resins using multiple analytical platforms. *Phytochemistry* **2018**, *155*, 37-44.
[193] Ganzera, M.; Khan, I. A.; A reversed phase high performance liquid chromatography method for the analysis of boswellic acids in Boswellia serrata. *Planta Med.* **2001**, *67* (08), 778-780.
[194] Noller, C.; Smith, R.; Harris, G.; Walker, J.; Saponins and sapogenins. XX. Some color reactions of triterpenoid sapogenins. *J. Am. Chem. Soc.* **1942**, *64* (12), 3047-3049.
[195] Gong, Y.; Li, L.; Gong, D.; Yin, H.; Zhang, J.; Biomolecular Evidence of Silk from 8,500 Years Ago. *PLOS ONE* **2016**, *11* (12), e0168042.
[196] Nakazawa, Y.; Asakura, T.; High-Resolution 13C CP/MAS NMR Study on Structure and Structural Transition of Antheraea pernyi Silk Fibroin Containing Poly (l-alanine) and Gly-Rich Regions. *Macromolecules* **2002**, *35* (6), 2393-2400.
[197] Senthil Kumar, B.; Ramachandran, T.; Influence of knitting process parameters on the thermal comfort properties of eri silk knitted fabrics. *Fibres Text. East. Eur.* **2018**.
[198] Silva, S. S.; Kundu, B.; Lu, S.; Reis, R. L.; Kundu, S. C.; Chinese Oak Tasar Silkworm Antheraea pernyi Silk Proteins: Current Strategies and Future Perspectives for Biomedical Applications. *Macromol. Biosci.* **2019**, *19* (3), 1800252.
[199] Zhang, J.; Kaur, J.; Rajkhowa, R.; Li, J. L.; Liu, X. Y.; Wang, X. G.; Mechanical properties and structure of silkworm cocoons: A comparative study of Bombyx mori, Antheraea assamensis, Antheraea pernyi and Antheraea mylitta silkworm cocoons. *Mater. Sci. Eng. C* **2013**, *33* (6), 3206-3213.
[200] Zhang, J.; Rajkhowa, R.; Li, J. L.; Liu, X. Y.; Wang, X. G.; Silkworm cocoon as natural material and structure for thermal insulation. *Mater. Des.* **2013**, *49*, 842-849.
[201] Jiang, P.; Liu, H.; Wang, C.; Wu, L.; Huang, J.; Guo, C.; Tensile behavior and morphology of differently degummed silkworm (Bombyx mori) cocoon silk fibres. *Mater. Lett.* **2006**, *60* (7), 919-925.
[202] Zhao, H.-P.; Feng, X.-Q.; Yu, S.-W.; Cui, W.-Z.; Zou, F.-Z.; Mechanical properties of silkworm cocoons. *Polym. J.* **2005**, *46* (21), 9192-9201.
[203] Asakura, T.; Nishimura, A.; Kametani, S.; Kawanishi, S.; Aoki, A.; Suzuki, F.; Kaji, H.; Naito, A.; Refined Crystal Structure of Samia cynthia ricini Silk Fibroin Revealed by Solid-State NMR Investigations. *Biomacromolecules* **2017**, *18* (6), 1965-1974.
[204] Aznar-Cervantes, S. D.; Pagán, A.; Candel, M. J.; Pérez-Rigueiro, J.; Cenis, J. L.; Silkworm Gut Fibres from Silk Glands of Samia cynthia ricini—Potential Use as a Scaffold in Tissue Engineering. *Int. J. Mol. Sci.* **2022**, *23* (7), 3888.
[205] Datta, A.; Ghosh, A. K.; C. Kundu, S.; Purification and characterization of fibroin from the tropical Saturniid silkworm, Antheraea mylitta. *Insect Biochem. Mol. Biol.* **2001**, *31* (10), 1013-1018.
[206] Mazzi, S.; Zulker, E.; Buchicchio, J.; Anderson, B.; Hu, X.; Comparative thermal analysis of Eri, Mori, Muga, and Tussar silk cocoons and fibroin fibers. *J. Therm. Anal. Calorim.* **2014**, *116* (3), 1337-1343.
[207] Reddy, N.; Yang, Y.; Investigation of the Structure and Properties of Silk Fibers Produced by Actias lunas. *J. Polym. Environ.* **2012**, *20* (3), 659-664.
[208] Liu, Y.; Li, Y.; Li, X.; Qin, L.; The origin and dispersal of the domesticated Chinese oak silkworm, Antheraea pernyi, in China: A reconstruction based on ancient texts. *J. Insect Sci.* **2010**, *10* (1).
[209] Sen, K.; Babu K, M.; Studies on Indian silk. I. Macrocharacterization and analysis of amino acid composition. *J. Appl. Polym. Sci.* **2004**, *92* (2), 1080-1097.

[210] Li, L.; Gong, Y.; Yin, H.; Gong, D.; Different Types of Peptide Detected by Mass Spectrometry among Fresh Silk and Archaeological Silk Remains for Distinguishing Modern Contamination. *PLOS ONE* **2015**, *10* (7), e0132827.
[211] Gu, J.; Li, Q.; Chen, B.; Xu, C.; Zheng, H.; Zhou, Y.; Peng, Z.; Hu, Z.; Wang, B.; Species identification of Bombyx mori and Antheraea pernyi silk via immunology and proteomics. *Sci. Rep.* **2019**, *9* (1), 9381.
[212] Li, J.; Ouyang, Y.; Liu, L.; Zhu, C.; Meng, J.; Zheng, H.; Zhou, Y.; Wan, J.; Hu, Z.; Wang, B.; Tailored monoclonal antibody as recognition probe of immunosensor for ultrasensitive detection of silk fibroin and use in the study of archaeological samples. *Biosens. Bioelectron.* **2019**, *145*, 111709.
[213] Lucas, F.; Shaw, J. T. B.; Smith, S. G.; 30—The Chemical Constitution of some Silk Fibroins and its Bearing on their Physical Properties. *J. Text. Inst.* **1955**, *46* (6), T440-T452.
[214] Lee, B.; Pires, E.; Pollard, A. M.; McCullagh, J. S.; Species identification of silks by protein mass spectrometry reveals evidence of wild silk use in antiquity. *Sci. Rep.* **2022**, *12* (1), 4579.
[215] de Palaminy, L.; Daher, C.; Moulherat, C.; Development of a non-destructive methodology using ATR-FTIR and chemometrics to discriminate wild silk species in heritage collections. *Spectrochim. Acta A* **2022**, *270*, 120788.
[216] You, Q.; Li, Q.; Zheng, H.; Hu, Z.; Zhou, Y.; Wang, B.; Discerning silk produced by Bombyx mori from those produced by wild species using an enzyme-linked immunosorbent assay combined with conventional methods. *J. Agric. Food Chem.* **2017**, *65* (35), 7805-7812.
[217] Moini, M.; Rollman, C. M.; Buyid silk and the tale of Bibi Shahrbanu: identification of biomarkers of artificial aging (forgery) of silk. *Anal. Chem.* **2017**, *89* (19), 10158-10161.
[218] Vilaplana, F.; Nilsson, J.; Sommer, D. V. P.; Karlsson, S.; Analytical markers for silk degradation: comparing historic silk and silk artificially aged in different environments. *Anal. Bioanal. Chem.* **2015**, *407* (5), 1433-1449.
[219] Ling, S.; Qi, Z.; Knight, D. P.; Shao, Z.; Chen, X.; Synchrotron FTIR Microspectroscopy of Single Natural Silk Fibers. *Biomacromolecules* **2011**, *12* (9), 3344-3349.
[220] Peng, Z.; Yang, X.; Liu, C.; Dong, Z.; Wang, F.; Wang, X.; Hu, W.; Zhang, X.; Zhao, P.; Xia, Q.; Structural and Mechanical Properties of Silk from Different Instars of Bombyx mori. *Biomacromolecules* **2019**, *20* (3), 1203-1216.
[221] Zhang, X.; Dong, Z.; Guo, K.; Jiang, W.; Wu, X.; Duan, J.; Jing, X.; Xia, Q.; Zhao, P.; Identification and functional study of fhx-L1, a major silk component in Bombyx mori. *Int. J. Biol. Macromol.* **2023**, *232*, 123371.
[222] Guo, C.; Zhang, J.; Jordan, J. S.; Wang, X.; Henning, R. W.; Yarger, J. L.; Structural Comparison of Various Silkworm Silks: An Insight into the Structure–Property Relationship. *Biomacromolecules* **2018**, *19* (3), 906-917.
[223] Dettmer, K.; Stevens, A. P.; Fagerer, S. R.; Kaspar, H.; Oefner, P. J.; Amino acid analysis in physiological samples by GC-MS with propyl chloroformate derivatization and iTRAQ-LC-MS/MS. *Amino Acid Analysis: Methods and Protocols* **2019**, 173-190.
[224] Kaspar, H.; Dettmer, K.; Gronwald, W.; Oefner, P. J.; Automated GC–MS analysis of free amino acids in biological fluids. *J. Chromatogr. B* **2008**, *870* (2), 222-232.
[225] Krumpochova, P.; Bruyneel, B.; Molenaar, D.; Koukou, A.; Wuhrer, M.; Niessen, W.; Giera, M.; Amino acid analysis using chromatography–mass spectrometry: An inter platform comparison study. *J. Pharm. Biomed. Anal.* **2015**, *114*, 398-407.
[226] Zahradníčková, H.; Hušek, P.; Šimek, P.; Hartvich, P.; Maršálek, B.; Holoubek, I.; Determination of D-and L-amino acids produced by cyanobacteria using gas chromatography on Chirasil-Val after derivatization with pentafluoropropyl chloroformate. *Anal. Bioanal. Chem.* **2007**, *388*, 1815-1822.

[227] Waldhier, M. C.; Dettmer, K.; Gruber, M. A.; Oefner, P. J.; Comparison of derivatization and chromatographic methods for GC–MS analysis of amino acid enantiomers in physiological samples. *J. Chromatogr. B* **2010**, *878* (15-16), 1103-1112.
[228] Amelung, W.; Zhang, X.; Determination of amino acid enantiomers in soils. *Soil Biol. Biochem.* **2001**, *33* (4-5), 553-562.
[229] Malay, A. D.; Sato, R.; Yazawa, K.; Watanabe, H.; Ifuku, N.; Masunaga, H.; Hikima, T.; Guan, J.; Mandal, B. B.; Damrongsakkul, S.; et al.; Relationships between physical properties and sequence in silkworm silks. *Sci. Rep.* **2016**, *6* (1), 27573.
[230] Kmet, P.; Kucerova, L.; Sehadova, H.; Chia-hsiang Wu, B.; Wu, Y.-L.; Zurovec, M.; Identification of silk components in the bombycoid moth Andraca theae (Endromidae) reveals three fibroin subunits resembling those of Bombycidae and Sphingidae. *J. Insect Physiol.* **2023**, *147*, 104523.
[231] Pérez-Rigueiro, J.; Viney, C.; Llorca, J.; Elices, M.; Mechanical properties of single-brin silkworm silk. *J. Appl. Polym. Sci.* **2000**, *75* (10), 1270-1277.
[232] Mondal, M.; Trivedy, K.; Nirmal, K. S.; The silk proteins, sericin and fibroin in silkworm, Bombyx mori Linn.,-a review. **2007**.
[233] Guo, K.; Zhang, X.; Zhao, D.; Qin, L.; Jiang, W.; Hu, W.; Liu, X.; Xia, Q.; Dong, Z.; Zhao, P.; Identification and characterization of sericin5 reveals non-cocoon silk sericin components with high β-sheet content and adhesive strength. *Acta Biomater.* **2022**, *150*, 96-110.
[234] Cao, T.-T.; Zhang, Y.-Q.; Processing and characterization of silk sericin from Bombyx mori and its application in biomaterials and biomedicines. *Mater. Sci. Eng. C* **2016**, *61*, 940-952.
[235] Dong, Z.; Guo, K.; Zhang, X.; Zhang, T.; Zhang, Y.; Ma, S.; Chang, H.; Tang, M.; An, L.; Xia, Q.; et al.; Identification of Bombyx mori sericin 4 protein as a new biological adhesive. *Int. J. Biol. Macromol.* **2019**, *132*, 1121-1130.
[236] Kundu, S. C.; Dash, B. C.; Dash, R.; Kaplan, D. L.; Natural protective glue protein, sericin bioengineered by silkworms: Potential for biomedical and biotechnological applications. *Prog. Polym. Sci.* **2008**, *33* (10), 998-1012.
[237] Wang, Y. J.; Zhag, Y. Q.; Three-layered sericins around the silk fibroin fiber from Bombyx mori cocoon and their amino acid composition. *Adv. Mater. Res.* **2011**, *175*, 158-163.
[238] Biswal, B.; Dan, A. K.; Sengupta, A.; Das, M.; Bindhani, B. K.; Das, D.; Parhi, P. K.; Extraction of Silk Fibroin with Several Sericin Removal Processes and its Importance in Tissue Engineering: A Review. *J. Polym. Environ.* **2022**, *30* (6), 2222-2253.
[239] Li, G.; Liu, H.; Li, T.; Wang, J.; Surface modification and functionalization of silk fibroin fibers/fabric toward high performance applications. *Mater. Sci. Eng. C* **2012**, *32* (4), 627-636.
[240] Pervin, A.; Çapar, G.; Toprak, T.; Yener, E.; Sericin removal from silk fibers with eco-friendly alternative methods. *Res. J. Text. Appar.* **2016**, *26* (4), 368-374.
[241] Mahmoodi, N. M.; Arami, M.; Mazaheri, F.; Rahimi, S.; Degradation of sericin (degumming) of Persian silk by ultrasound and enzymes as a cleaner and environmentally friendly process. *J. Clean. Prod.* **2010**, *18* (2), 146-151.
[242] Reddy, N.; Zhao, Y.; Yang, Y.; Structure and properties of cocoons and silk fibers produced by Attacus atlas. *J. Polym. Environ.* **2013**, *21*, 16-23.
[243] Shetty, P.; Madanthyar, B.; Ramasubramanian, S.; Malickal, S.; Ramachandran, L. D.; Udupi, V.; Pineapple: Potential Source of Proteolytic Enzymes for Degumming of Raw Silk. *Modern Concepts & Developments in Agronomy* **2019**, *4*.
[244] Wang, F.; Zhang, Y.-Q.; Effects of alkyl polyglycoside (APG) on Bombyx mori silk degumming and the mechanical properties of silk fibroin fibre. *Mater. Sci. Eng. C* **2017**, *74*, 152-158.

[245] Wang, W.; Pan, Y.; Gong, K.; Zhou, Q.; Zhang, T.; Li, Q.; A comparative study of ultrasonic degumming of silk sericin using citric acid, sodium carbonate and papain. *Color. Technol.* **2019**, *135* (3), 195-201.
[246] Rastogi, S.; Kandasubramanian, B.; Processing trends of silk fibers: Silk degumming, regeneration and physical functionalization. *J. Text. Inst.* **2020**, *111* (12), 1794-1810.
[247] Zhao, Z.-L.; Li, W.-W.; Wang, F.; Zhang, Y.-Q.; Using of hydrated lime water as a novel degumming agent of silk and sericin recycling from wastewater. *J. Clean. Prod.* **2018**, *172*, 2090-2096.
[248] Koperska, M. A.; Pawcenis, D.; Bagniuk, J.; Zaitz, M. M.; Missori, M.; Łojewski, T.; Łojewska, J.; Degradation markers of fibroin in silk through infrared spectroscopy. *Polym. Degrad. Stab.* **2014**, *105*, 185-196.
[249] Feng, Y.; Lin, J.; Niu, L.; Wang, Y.; Cheng, Z.; Sun, X.; Li, M.; High Molecular Weight Silk Fibroin Prepared by Papain Degumming. *Polymers* **2020**, *12* (9), 2105.
[250] Zhang, X.; Wyeth, P.; Using FTIR spectroscopy to detect sericin on historic silk. *Sci. China Chem.* **2010**, *53* (3), 626-631.
[251] Teramoto, H.; Miyazawa, M.; Analysis of structural properties and formation of sericin fiber by infrared spectroscopy. *J. Insect Biotechnol. Sericology* **2003**, *72* (3), 157-162.
[252] Lucas, F.; Shaw, J. T. B.; Smith, S. G.; Comparative studies of fibroins: I. The amino acid composition of various fibroins and its significance in relation to their crystal structure and taxonomy. *J. Mol. Biol.* **1960**, *2* (6), 339-349.
[253] Batigne, R.; Bellinger, L.; The Significance and Technical Analysis of Ancient Textiles as Historical Documents. *Proc. Am. Philos. Soc.* **1953**, *97* (6), 670-680.
[254] Liu, J.; Guo, D.; Zhou, Y.; Wu, Z.; Li, W.; Zhao, F.; Zheng, X.; Identification of ancient textiles from Yingpan, Xinjiang, by multiple analytical techniques. *J. Archaeol. Sci.* **2011**, *38* (7), 1763-1770.
[255] Hood, A. D.; Material Culture and Textiles: An Overview. *Mater. Cult. Rev.* **1990**, *31* (1).
[256] Al-Sharairi, N.; Sandu, I. C. A.; Vasilache, V.; Sandu, I.; Recognition of natural silk fibers, dyes and metal threads of historical Romanian textile fragments using the multi-analytical techniques approach. *Text. Res. J.* **2020**, *90* (15-16), 1671-1688.
[257] Kramell, A. E.; Wertmann, P.; Hosner, D.; Kluge, R.; Oehler, F.; Wunderlich, C.-H.; Tarasov, P. E.; Wagner, M.; Csuk, R.; A multi-analytical techniques based approach to study the colorful clothes and accessories from mummies of Eastern Central Asia. *J. Archaeol. Sci. Rep.* **2016**, *10*, 464-473.
[258] Brzozowska, I.; Bogdanowicz, A.; Szczęsny, P.; Zielenkiewicz, U.; Laudy, A.; Evaluation of bacterial diversity on historical silk velvet textiles from the Museum of King John III's Palace at Wilanów, Poland. *Int. Biodeterior. Biodegrad.* **2018**, *131*, 78-87.
[259] Veit, D.; *Fibers: History, Production, Properties, Market*; Springer International Publishing AG: Basel, **2023**.
[260] Gao, S.; Yao, M.; Narenggaowa; Guo, D.; Li, Y.; Do, K. L.; Liu, J.; Zhao, F.; Identification of fibers and dyes in archaeological textiles from Bazhou, Xinjiang (220-420 CE), and their Silk Road origins. *J. Archaeol. Sci.* **2024**, *164*, 105941.
[261] Wagner, M.; Bo, W.; Tarasov, P.; Westh-Hansen, Sidsel M.; Völling, E.; Heller, J.; The ornamental trousers from Sampula (Xinjiang, China): their origins and biography. *Antiquity* **2009**, *83* (322), 1065-1075.
[262] Gulmini, M.; Idone, A.; Diana, E.; Gastaldi, D.; Vaudan, D.; Aceto, M.; Identification of dyestuffs in historical textiles: Strong and weak points of a non-invasive approach. *Dyes Pigment.* **2013**, *98* (1), 136-145.
[263] Kramell, A.; Li, X.; Csuk, R.; Wagner, M.; Goslar, T.; Tarasov, P. E.; Kreusel, N.; Kluge, R.; Wunderlich, C.-H.; Dyes of late Bronze Age textile clothes and accessories from the Yanghai archaeological site, Turfan, China: Determination of the fibers, color analysis and dating. *Quat. Int.* **2014**, *348*, 214-223.

[264] Degano, I.; Biesaga, M.; Colombini, M. P.; Trojanowicz, M.; Historical and archaeological textiles: An insight on degradation products of wool and silk yarns. *J. Chromatogr. A* **2011**, *1218* (34), 5837-5847.
[265] Schmidt, T.; Puchalla, N.; Schendzielorz, M.; Kramell, A. E.; Degumming and characterization of Bombyx mori and non-mulberry silks from Saturniidae silkworms. *Sci Rep* **2023**, *13* (1), 19504.
[266] Solazzo, C.; Rogers, P. W.; Weber, L.; Beaubien, H. F.; Wilson, J.; Collins, M.; Species identification by peptide mass fingerprinting (PMF) in fibre products preserved by association with copper-alloy artefacts. *J. Archaeol. Sci.* **2014**, *49*, 524-535.
[267] Ge, R.; Cong, L.; Fu, Y.; Wang, B.; Shen, G.; Xu, B.; Hu, M.; Yu, H.; Zhou, J.; Yang, L.; Multi-faceted analysis reveals the characteristics of silk fabrics on a Liao Dynasty DieXie belt. *Herit. Sci.* **2023**, *11* (1), 217.
[268] Csapó, J.; Csapó-Kiss, Z.; Csapó, J.; Use of amino acids and their racemisation for age determination in archaeometry. *TrAC, Trends Anal. Chem.* **1998**, *17* (3), 140-148.
[269] Kalíková, K.; Šlechtová, T.; Tesařová, E.; Enantiomeric Ratio of Amino Acids as a Tool for Determination of Aging and Disease Diagnostics by Chromatographic Measurement. *Separations* **2016**, *3* (4), 30.
[270] Rezić, I.; *Historical textiles and their characterization*; Cambridge Scholars Publishing: Newcastle, **2022**.
[271] Gutarowska, B.; Pietrzak, K.; Machnowski, W.; Milczarek, J. M.; Historical textiles – a review of microbial deterioration analysis and disinfection methods. *Text. Res. J.* **2017**, *87* (19), 2388-2406.
[272] Bada, J.; Racemization of amino acids. In *Chemistry and biochemistry of the amino acids*, Springer: Dordrecht, **1985**; pp 399-414.
[273] Bright, J.; Kaufman, D. S.; Amino acids in lacustrine ostracodes, part III: Effects of pH and taxonomy on racemization and leaching. *Quat. Geochronol.* **2011**, *6* (6), 574-597.
[274] Aguayo, T.; Araya, M. C.; Icaza, T. M.; Campos-Vallette, M.; A vibrational approach for the study of historical weighted and dyed silks. *J. Mol. Struct.* **2014**, *1075*, 471-478.
[275] Shimada, C. M.; McCarthy, B.; Rollman, C. M.; Hare, A.; Ueda, J.; Moini, M.; More Reliable Dating of Japanese Silk Mounting Textiles for Conservation Decisions: Effects of Silk Processing on Silk Surface Morphology and Aspartic Acid Racemization. *Stud. Conserv.* **2023**, 1-16.
[276] Gürses, A.; Açıkyıldız, M.; Güneş, K.; Gürses, M. S.; Historical Development of Colorants. In *Dyes and Pigments*, Springer International Publishing: Basel, **2016**; pp 1-12.
[277] Kramell, A.; Porbeck, F.; Kluge, R.; Wiesner, A.; Csuk, R.; A fast and reliable detection of indigo in historic and prehistoric textile samples. *J. Mass Spectrom.* **2015**, *50* (9), 1039-1043.
[278] Degani, L.; Riedo, C.; Chiantore, O.; Identification of natural indigo in historical textiles by GC–MS. *Anal. Bioanal. Chem.* **2015**, *407* (6), 1695-1704.
[279] Blackburn, R. S.; Natural dyes in madder (Rubia spp.) and their extraction and analysis in historical textiles. *Color. Technol.* **2017**, *133* (6), 449-462.
[280] Bender, M.; Colors for textiles—Ancient and modern. *J. Chem. Educ.* **1947**, *24* (1), 2.
[281] Repon, M. R.; Dev, B.; Rahman, M. A.; Jurkonienė, S.; Haji, A.; Alim, M. A.; Kumpikaitė, E.; Textile dyeing using natural mordants and dyes: a review. *Environ. Chem. Lett.* **2024**.
[282] Manhita, A.; Ferreira, V.; Vargas, H.; Ribeiro, I.; Candeias, A.; Teixeira, D.; Ferreira, T.; Dias, C. B.; Enlightening the influence of mordant, dyeing technique and photodegradation on the colour hue of textiles dyed with madder – A chromatographic and spectrometric approach. *Microchem. J.* **2011**, *98* (1), 82-90.
[283] Garside, P.; Wyeth, P.; Zhang, X.; Understanding the ageing behaviour of nineteenth and twentieth century tin-weighted silks. *Int. J. Conserv. Sci.* **2010**, *33* (2), 179-193.

[284] Hacke, M.; Weighted silk: history, analysis and conservation. *Stud. Conserv.* **2008**, *53* (sup2), 3-15.
[285] Garside, P.; Wyeth, P.; Zhang, X.; The inherent acidic characteristics of silk, Part II–weighted silks. *e-Preservation Science* **2010**, *7* (1), 126-131.
[286] Bonaduce, I.; Cito, M.; Colombini, M. P.; The development of a gas chromatographic–mass spectrometric analytical procedure for the determination of lipids, proteins and resins in the same paint micro-sample avoiding interferences from inorganic media. *J. Chromatogr. A* **2009**, *1216* (32), 5931-5939.
[287] Colombini, M. P.; Modugno, F.; Giacomelli, A.; Two procedures for suppressing interference from inorganic pigments in the analysis by gas chromatography–mass spectrometry of proteinaceous binders in paintings. *J. Chromatogr. A* **1999**, *846* (1), 101-111.
[288] Johnson, A. P.; Pratt, L. M.; Metal-catalyzed degradation and racemization of amino acids in iron sulfate brines under simulated martian surface conditions. *Icarus* **2010**, *207* (1), 124-132.
[289] Colombini, M. P.; Modugno, F.; Characterisation of proteinaceous binders in artistic paintings by chromatographic techniques. *J. Sep. Sci.* **2004**, *27* (3), 147-160.
[290] Freddi, G.; Gotoh, Y.; Mori, T.; Tsutsui, I.; Tsukada, M.; Chemical structure and physical properties of antheraea assama silk. *J. Appl. Polym. Sci.* **1994**, *52* (6), 775-781.
[291] Reischl, R. J.; Lindner, W.; The stereoselective separation of serine containing peptides by zwitterionic ion exchanger type chiral stationary phases and the study of serine racemization mechanisms by isotope exchange and tandem mass spectrometry. *J. Pharm. Biomed. Anal.* **2015**, *116*, 123-130.
[292] Valianou, L.; Karapanagiotis, I.; Chryssoulakis, Y.; Comparison of extraction methods for the analysis of natural dyes in historical textiles by high-performance liquid chromatography. *Anal. Bioanal. Chem.* **2009**, *395* (7), 2175-2189.
[293] Manhita, A.; Ferreira, T.; Candeias, A.; Barrocas Dias, C.; Extracting natural dyes from wool—an evaluation of extraction methods. *Anal. Bioanal. Chem.* **2011**, *400*, 1501-1514.
[294] Claro, A.; Melo, M. J.; de Melo, J. S. S.; van den Berg, K. J.; Burnstock, A.; Montague, M.; Newman, R.; Identification of red colorants in van Gogh paintings and ancient Andean textiles by microspectrofluorimetry. *J. Cult. Herit.* **2010**, *11* (1), 27-34.
[295] Zhang, X.; Laursen, R. A.; Development of mild extraction methods for the analysis of natural dyes in textiles of historical interest using LC-diode array detector-MS. *Anal Chem* **2005**, *77* (7), 2022-2025.
[296] Moini, M.; Klauenberg, K.; Ballard, M.; Dating Silk By Capillary Electrophoresis Mass Spectrometry. *Anal. Chem.* **2011**, *83* (19), 7577-7581.
[297] Beck, U.; Wagner, M.; Li, X.; Durkin-Meisterernst, D.; Tarasov, P. E.; The invention of trousers and its likely affiliation with horseback riding and mobility: A case study of late 2nd millennium BC finds from Turfan in eastern Central Asia. *Quat. Int.* **2014**, *348*, 224-235.
[298] Schröder, O.; Wagner, M.; Wutke, S.; Zhang, Y.; Ma, Y.; Xu, D.; Goslar, T.; Neef, R.; Tarasov, P. E.; Ludwig, A.; Ancient DNA identification of domestic animals used for leather objects in Central Asia during the Bronze Age. *Holocene* **2016**, *26* (10), 1722-1729.
[299] Liu, J.; Mouri, C.; Laursen, R.; Zhao, F.; Zhou, Y.; Li, W.; Characterization of dyes in ancient textiles from Yingpan, Xinjiang. *J. Archaeol. Sci.* **2013**, *40* (12), 4444-4449.
[300] Zhang, X.; Good, I.; Laursen, R.; Characterization of dyestuffs in ancient textiles from Xinjiang. *J. Archaeol. Sci.* **2008**, *35* (4), 1095-1103.
[301] Veit, D.; Silk. In *Fibers: History, Production, Properties, Market*, Veit, D. Ed.; Springer International Publishing AG: Basel, **2022**; pp 351-380.

[302] Rosenberg, E.; Krska, R.; Analytical chemistry in front of the curtain! *Anal. Bioanal. Chem.* **2024**.
[303] Guardia, M. d. l.; An integrated approach of analytical chemistry. *J. Braz. Chem. Soc.* **1999**, *10*, 429-437.
[304] Rains, T. C.; Role of Modern Analytical Chemistry in Material Analyses for Trace Metals. *J. Chin. Chem. Soc.* **1990**, *37* (1), 11-19.
[305] Madariaga, J. M.; Analytical chemistry in the field of cultural heritage. *Anal. Methods* **2015**, *7* (12), 4848-4876.
[306] Doménech-Carbó, M. T.; Osete-Cortina, L.; Another beauty of analytical chemistry: chemical analysis of inorganic pigments of art and archaeological objects. *ChemTexts* **2016**, *2* (3), 14.

Anhang

Publikationen

Die für die vorliegenden Dissertation herangezogenen Publikationen sind nachfolgend aufgelistet:

P1: Identification and quantification of cannabinol as a biomarker for local hemp retting in an ancient sedimentary record by HPTLC-ESI-MS

T. Schmidt, A. E. Kramell, F. Oehler, R. Kluge, D. Demske, P. E. Tarasov, R. Csuk, *Anal. Bioanal. Chem.* **2020***,* 412, 2633–2644.

P2: Separating the true from the false: A rapid HPTLC-ESI-MS method for the determination of cannabinoids in different oils

T. Schmidt, J. Stommel, T. Kohlmann, A. E. Kramell, R. Csuk, *Results Chem.* **2021**, Volume 3, 100234.

P3: TLC and HPTLC-APCI-MS for the rapid discrimination of plant resins frequently used for lacquers and varnishes by artists and conservators

M. Schendzielorz, T. Schmidt, N. Puchalla, R. Csuk, A. E. Kramell, *Phytochem. Anal.* **2024**, 35(1), 64-76.

P4: Degumming and characterization of Bombyx mori and non-mulberry silks from Saturniidae silkworms

T. Schmidt, N. Puchalla, M. Schendzielorz & A. E. Kramell, *Sci. Rep.* **2023**, 13, 19504.

P5: Characterization of recent and historical silks: Effects of silk processing on chemical composition and amino acid racemization

T. Schmidt, J. Koch, N. Puchalla, & A. E. Kramell, *J. Nat. Fibers* **2024**, 21(1).

Publikation P1:

Identification and quantification of cannabinol as a biomarker for local hemp retting in an ancient sedimentary record by HPTLC-ESI-MS

Theresa Schmidt, Annemarie Elisabeth Kramell, Florian Oehler, Ralph Kluge, Dieter Demske, Pavel E Tarasov, René Csuk

Graphical abstract

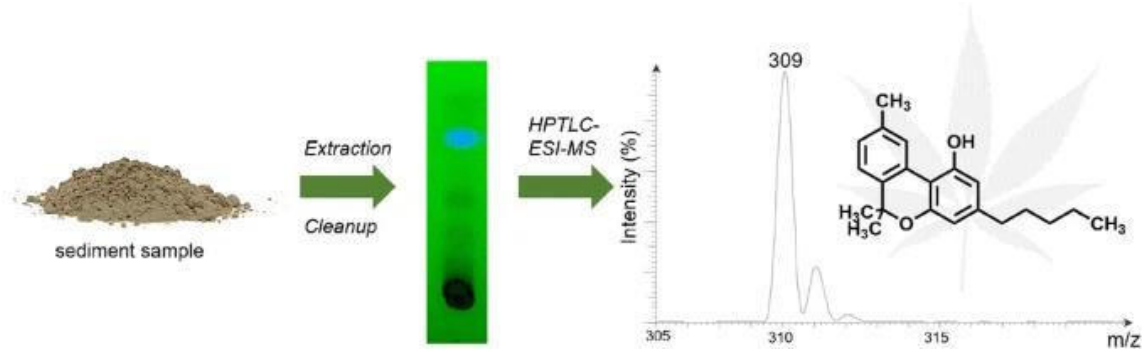

Abstract

Cannabis products have been used in various fields of everyday life for many centuries, and applications in folk medicine and textile production have been well-known for many centuries. For traditional textile production, hemp fibers were extracted from the stems by water retting in stagnant or slow-moving waters. During this procedure, parts of the plant material, among them phytocannabinoids, are released into the water. Cannabinol (CBN) is an important degradation product of the predominant phytocannabinoids found in Cannabis species. Thus, it is an excellent indicator for present as well as ancient hemp water retting. In this study, we developed and validated a simple and fast method for the determination of CBN in sediment samples using high-performance thin-layer chromatography (HPTLC) combined with electrospray ionization mass spectrometry (ESI-MS), thereby testing different extraction and cleanup procedures, as well as various sorbents and solvents for planar chromatography. This method shows a satisfactory overall analytical performance with an average recovery rate of 73 %. Our protocol enabled qualitative and quantitative analyses of CBN in samples of a bottom sediment core, having been obtained from a small lake in Northern India, where intense local retting of hemp was suggested in the past. The analyses showed a maximum CBN content in pollen zone 4 covering a depth range of 262–209 cm, dating from approximately 480 BCE to 1050 CE. These findings correlate with existing records of Cannabis-type pollen. Thus, the method we propose is a helpful tool to track ancient hemp retting activities.

Keywords: HPTLC; Cannabinol; Sediment; Biomarker; Cannabis; Hemp retting

DOI: 10.1007/s00216-020-02492-0

Publikation P2:

Separating the true from the false: A rapid HPTLC-ESI-MS method for the determination of cannabinoids in different oils

Theresa Schmidt, Jacqueline Stommel, Tim Kohlmann, Annemarie E. Kramell, René Csuk

Graphical abstract

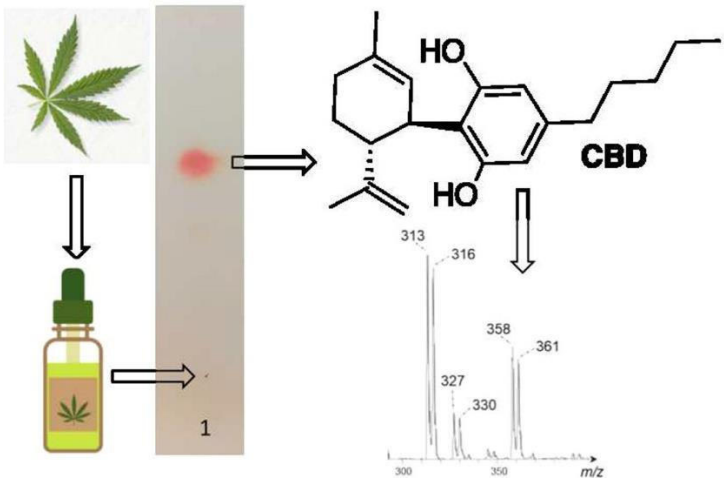

Abstract

Cannabis is one of the oldest cultivated plant, which has been used by humankind for thousands of years due to its biological properties and a wide range of applications. In total, hemp plants contain over 500 different substances while the characteristic components are the cannabinoids. The most important cannabinoids are (-)-Δ^9-trans-tetrahydrocannabinol (Δ^9-THC), cannabidiol (CBD), and cannabinol (CBN – the latter being an oxidation product resulting from Δ^9-THC). In the course of recent years, a paradigm shift has taken place with regard to the use of products and ingredients derived from hemp, especially CBD. Thus, an ever-increasing number of products containing CBD are on the market; this ranges from classic CBD oil to CBD chewing gum and even CBD shampoo. Despite an increasing presence of these products in the market, the regulation of cannabinoids in these products is very inconsistent in different countries, except for Δ^9-THC whose limit is 0.2 % for many products and many countries. The enormous abundance of CBD-containing products calls for the development of new analytical techniques that allow a reliable and quick determination of the main cannabinoids usually found in hemp. This seems all the more necessary since previous examinations of CBD oils often revealed a difference between the declared amount and the actual content of the ingredients. Many methods usually applied to determine cannabinoids are rather time-consuming and associated with high costs. In this study, we developed and validated a sensitive, simple, reliable as well as fast method for the determination of CBN, CBD and Δ^9-THC in commercially available CBD oils using high-performance thin-layer chromatography (HPTLC) combined with electrospray ionization mass spectrometry (ESI-MS). Thus, for this method, a recovery rate of ≥ 90 % was determined. This procedure enables both qualitative and quantitative analyses of CBN, CBD and Δ^9-THC in CBD oils of different matrices such as hempseed oil, olive oil or sunflower oil. Thus, this method is a helpful and fast tool to investigate a broad variety of commercially available CBD oils.

Keywords: CBD oils; Cannabidiol; Tetrahydrocannabinol; Cannabinoids; Cannabis; HPTLC
DOI: 10.1016/j.rechem.2021.100234

Publikation P3:

TLC and HPTLC-APCI-MS for the rapid discrimination of plant resins frequently used for lacquers and varnishes by artists and conservators

Marcel Schendzielorz[a], Theresa Schmidt[a], Nils Puchalla, René Csuk, Annemarie E. Kramell

[a]contributed equally to this work

Introduction

Depending on their terpenoid and phenolic constituents plant resins can be classified as diterpenoid, triterpenoid or phenolic resins; thereby the profile of diterpenes and triterpenes is considered as genus- or even species-specific.

Objectives

We aimed to develop a simple, rapid, inexpensive, sensitive and specific method for the identification of resin-specific triterpenoid and phenolic compounds in plant resins using (HP)TLC [(high-performance) thin-layer chromatography] combined with APCI-MS (atmospheric pressure chemical ionisation mass spectrometry) and post-chromatographic detection reactions.

Methods

Twenty resin samples from different plant species were analysed. Different extraction procedures, post-chromatographic detection reagents as well as various sorbents and solvents for planar chromatography were tested. To evaluate the potential of the optimised (HP)TLC-APCI-MS methods, parameter such as limit of detection (LOD) was determined for selected marker compounds.

Results

Our protocol enabled qualitative analyses of chemotaxonomic molecular markers in natural resins such as dammar, mastic, olibanum and benzoin. For the first time, the application of thionyl chloride-stannic chloride reagent for a specific post-chromatographic detection of triterpenes is reported, sometimes even allowing discrimination between isomers based on their characteristic colour sequences. For triterpene acids, triterpene alcohols and phenolic compounds, detection limits of 2–20 ng/TLC zone and a system precision with a relative standard deviation (RSD) in the range of 3.9 %–7.0 % were achieved by (HP)TLC-APCI-MS. The applicability of the method for the analysis of resin-based varnishes was successfully tested on a mastic-based varnish. Thus, the method we propose is a helpful tool for the discrimination of resins and resin-based varnishes with respect to their botanical origin.

Keywords: benzoin balsam, HPTLC-MS, plant resin, triterpene, varnish

DOI: 10.1002/pca.3273

Publikation P4:

Degumming and characterization of Bombyx mori and non-mulberry silks from Saturniidae silkworms

Theresa Schmidt, Nils Puchalla, Marcel Schendzielorz & Annemarie E. Kramell

Abstract

In this study, cocoons and degummed silk samples of Bombyx mori and twenty Saturniidae species of the genera Actias, Attacus, Argema, Antheraea, Caligula, Callosamia, Cricula, Epiphora, Hyalophora, Loepa, Samia and Saturnia are studied to gain an insight into their morphology, chemical composition and physical structure. For this purpose, silk samples are characterized by optical microscopy and FTIR spectroscopy in attenuated total reflection mode (ATR-FTIR spectroscopy). Furthermore, degummed silk samples are analyzed for their amino acid (AA) composition by GC-FID. In the course of method development, various degumming methods are tested using alkalis, citric acid, enzymes and detergents. A mixture of 0.1 % sodium carbonate and 2.5 % ethylenediamine proves to be an effective agent for degumming Saturniidae and B. mori cocoons. After hydrolysis of the fibroin filaments with 6 N hydrochloric acid and derivatization with propyl chloroformate, fifteen AAs are identified and qualified. This method shows a satisfactory overall analytical performance with an average recovery rate of 95 % at the medium concentration level. The chemical composition of the different silks was considered comparatively. Within a genus, the analyses usually show a high degree of similarity in AA composition and the resulting structural indices, whereas differences are found between genera.

DOI: 10.1038/s41598-023-46474-5

Publikation P5:

Characterization of recent and historical silks: Effects of silk processing on chemical composition and amino acid racemization

Theresa Schmidt, Jacqueline Koch, Nils Puchalla & Annemarie E. Kramell

Abstract

In this work, the influence of dyeing, mordanting and degumming techniques on the amino acid (AA) composition and the AA racemization (AAR) of (non-)mulberry silks is studied by a chiral GC-MS method. The tested dyeing and mordanting procedures as well as a pre-treatment of the silk filaments with EDTA-DMF, which enables a parallel dyestuff analysis by HPLC-DAD, do not cause any significant change in the AA composition. However, an increased proportion of e.g. (D)-Asx can be observed for some of the mordanted BM silks. Increased D/L Asx ratios can also be observed in indigo dyed silks and after an alkaline treatment at 110°C (pH > 9). Furthermore, the GC-MS method was used for the characterization of historical silk samples from finding sites in the Tarim Basin (China). The analysis of these silk fabrics reveals the presence of degraded Bombyx silk with significantly increased D/L Val, D/L Glx and D/L Asx ratios. Including microscopic and spectroscopic investigations, the results of this multi-analytical approach offer insights into the silk processing techniques and raw materials used.

Keywords: Silk; *Bombyx mori*; silk processing; amino acid racemization; chiral GC-MS; historical textiles

DOI: 10.1080/15440478.2024.2361312

Lebenslauf

Persönliche Angaben

Name:	Theresa Schmidt
Staatsangehörigkeit:	deutsch

Bildungsweg

seit Juli 2019	Promotion am Institut für Chemie, Organische Chemie, an der Martin-Luther-Universität Halle-Wittenberg unter der Betreuung von Prof. Dr. René Csuk *Thema der Dissertation: „Spurenanalytik und Authentizitätsuntersuchungen – eine Herausforderung an die moderne Analytik“*
10/14 bis 05/19	Lebensmittelchemie-Studium an der Martin-Luther-Universität Halle-Wittenberg Abschluss: Diplom-Lebensmittelchemikerin *Thema der Diplomarbeit: „Nachweis von Cannabinol in Sedimentproben aus dem Badhani Tal in Indien mittels HPTLC-ESI-MS“*
08/08 bis 07/14	Allgemeine Hochschulreife am Paulus-Praetorius-Gymnasium in Bernau bei Berlin

Berufliche Laufbahn

seit Juni 2023	Chemikerin für die Analytik bei der CREDOXYS GmbH in Dresden
03/20 bis 05/23	Wissenschaftliche Mitarbeiterin am Institut für Chemie der Martin-Luther-Universität Halle-Wittenberg im Fachbereich Organische Chemie im Arbeitskreis von Prof. Dr. R. Csuk (DFG-Projektstelle; Projektleitung: Dr. A. E. Kramell)
07/19 bis 02/20	Wissenschaftliche Hilfskraft am Institut für Chemie der Martin-Luther-Universität Halle-Wittenberg im Fachbereich Organische Chemie im Arbeitskreis von Prof. Dr. R. Csuk

Publikationsliste

Schmidt, T., Koch, J., Puchalla, N., & Kramell, A. E.: Characterization of Recent and Historical Silks: Effects of Silk Processing on Chemical Composition and Amino Acid Racemization. *J. Nat. Fibers* **2024,** 21(1).

Schendzielorz, M., Schmidt, T., Puchalla, N., Csuk, R., & Kramell, A. E.: TLC and HPTLC-APCI-MS for the rapid discrimination of plant resins frequently used for lacquers and varnishes by artists and conservators. *Phytochem. Anal.* **2024,** *35*(1), 64-76.

Schmidt, T., Puchalla, N., Schendzielorz, M., & Kramell, A. E.: Degumming and characterization of Bombyx mori and non-mulberry silks from Saturniidae silkworms. *Sci. Rep*. **2023,** 13(1), 19504.

Kozubek, M., Hoenke, S., Schmidt, T., Ströhl, D., & Csuk, R.: Platanic acid derived amides are more cytotoxic than their corresponding oximes. *Med. Chem. Res*. **2022**, 31(6), 1049-1059.

Kozubek, M., Hoenke, S., Schmidt, T., Deigner, H. P., Al-Harrasi, A., & Csuk, R.: Synthesis and cytotoxicity of betulin and betulinic acid derived 30-oxo-amides. *Steroids* **2022**, 182, 109014.

Heise, N. V., Ströhl, D., Schmidt, T., & Csuk, R.: Stable triterpenoid iminium salts and their activity as inhibitors of butyrylcholinesterase. *J. Mol. Struct*. **2022**, 1249, 131646.

Schmidt, T., Stommel, J., Kohlmann, T., Kramell, A. E., & Csuk, R.: Separating the true from the false: A rapid HPTLC-ESI-MS method for the determination of cannabinoids in different oils. *Results Chem*. **2021**, 3, 100234.

Schmidt, T., Heise, N., Merzweiler, K., Deigner, H. P., Al-Harrasi, A., & Csuk, R. Concise synthesis of both enantiomers of pilocarpine. *Molecules* **2021**, 26(12), 3676.

Schmidt, T., Kramell, A. E., Oehler, F., Kluge, R., Demske, D., Tarasov, P. E., & Csuk, R.: Identification and quantification of cannabinol as a biomarker for local hemp retting in an ancient sedimentary record by HPTLC ESI-MS. *Anal. Bioanal. Chem*. **2020**, *412*, 2633-2644.

Selbstständigkeitserklärung

Hiermit erkläre ich an Eides statt, dass ich die vorliegende Arbeit selbstständig und ohne fremde Hilfe verfasst, keine anderen als die von mir angegebenen Hilfsmittel und Quellen verwendet und die den benutzten Werken wörtlich oder inhaltlich entnommenen Stellen als solche kenntlich gemacht habe. Die Arbeit, weder in gleicher noch in ähnlicher Form, wurde bisher an keiner anderen Universität oder Hochschule vorgelegt.

Halle (Saale), den 02.05.2024 Theresa Schmidt

Angehangene Publikationen

Im nachfolgenden sind die Publikationen P1 – P5 angefügt.

P1

Analytical and Bioanalytical Chemistry (2020) 412:2633–2644
https://doi.org/10.1007/s00216-020-02492-0

RESEARCH PAPER

Identification and quantification of cannabinol as a biomarker for local hemp retting in an ancient sedimentary record by HPTLC-ESI-MS

Theresa Schmidt[1] · Annemarie Elisabeth Kramell[1] · Florian Oehler[2] · Ralph Kluge[1] · Dieter Demske[3] · Pavel E Tarasov[3] · René Csuk[1]

Received: 28 November 2019 / Revised: 22 January 2020 / Accepted: 5 February 2020 / Published online: 14 February 2020

Abstract

Cannabis products have been used in various fields of everyday life for many centuries, and applications in folk medicine and textile production have been well-known for many centuries. For traditional textile production, hemp fibers were extracted from the stems by water retting in stagnant or slow-moving waters. During this procedure, parts of the plant material, among them phytocannabinoids, are released into the water. Cannabinol (CBN) is an important degradation product of the predominant phytocannabinoids found in *Cannabis* species. Thus, it is an excellent indicator for present as well as ancient hemp water retting. In this study, we developed and validated a simple and fast method for the determination of CBN in sediment samples using high-performance thin-layer chromatography (HPTLC) combined with electrospray ionization mass spectrometry (ESI-MS), thereby testing different extraction and cleanup procedures, as well as various sorbents and solvents for planar chromatography. This method shows a satisfactory overall analytical performance with an average recovery rate of 73%. Our protocol enabled qualitative and quantitative analyses of CBN in samples of a bottom sediment core, having been obtained from a small lake in Northern India, where intense local retting of hemp was suggested in the past. The analyses showed a maximum CBN content in pollen zone 4 covering a depth range of 262–209 cm, dating from approximately 480 BCE to 1050 CE. These findings correlate with existing records of *Cannabis*-type pollen. Thus, the method we propose is a helpful tool to track ancient hemp retting activities.

Keywords HPTLC · Cannabinol · Sediment · Biomarker · *Cannabis* · Hemp retting

Introduction

Cannabis has been used by humans for many centuries and is probably one of the oldest cultivated plants [1]. It is widely distributed around the world, and archaeological finds indicate its usage for more than 2500 years. For instance, almost complete ancient *Cannabis* plants as well as parts of it have been excavated from different tombs in the Jiayi and Yanghai cemetery located in Northwestern China dating back to the first millennium BCE [2, 3]. *Cannabis* is a versatile plant and has been used as medicine, food source (seeds and oil), fuel, and psychedelic drug and also as a construction material or for the production of textiles and paper. The production of hemp fibers, e.g., for the manufacturing of robes, requires the separation of the fibers from the stems through microbiological and physical processes occurring during retting. Traditionally, the extraction of the fibers from stems is performed in stagnant or slow-moving waters, thereby submerging the stems in water for several days. During this treatment plant material and among other substances, phytocannabinoids are released into the waters. Phytocannabinoids are unique to the *Cannabis* species. The predominant phytocannabinoids in drug- and fiber-type *Cannabis* are (-)-Δ^9-*trans*-tetrahydrocannabinolic acid (THCA) and cannabidiolic acid (CBDA) that are

Electronic supplementary material The online version of this article (https://doi.org/10.1007/s00216-020-02492-0) contains supplementary material, which is available to authorized users.

✉ Annemarie Elisabeth Kramell
annemarie.kramell@chemie.uni-halle.de

[1] Department of Organic Chemistry, Martin-Luther-University Halle-Wittenberg, Kurt-Mothes-Str. 2, 06120 Halle, Germany

[2] Department of Inorganic Chemistry, Martin-Luther-University Halle-Wittenberg, Kurt-Mothes-Str. 2, 06120 Halle, Germany

[3] Section Paleontology, Institute of Geological Sciences, Freie Universität Berlin, Malteserstr. 74-100, 12249 Berlin, Germany

transformed by a non-enzymatically decarboxylation upon heating after harvesting and during storage into their corresponding neutral forms, namely (-)-Δ^9-*trans*-tetrahydrocannabinol (Δ^9-THC) and cannabidiol (CBD). Phytocannabinoids accumulate in female flowers and in most aerial parts of the plant. In contrast, *Cannabis* pollen, seeds, and roots contain only low concentrations of these compounds [4]. The concentration of cannabinoids and the ratio Δ^9-THC:CBD depend on different parameters such as growth conditions, variety, age, harvest time, and storage conditions [4, 5]. Especially during storage, Δ^9-THC is relatively unstable whenever *Cannabis* products such as flowering tops, oils, and resins are exposed to air, light, heat, or acidic conditions [6]. Eventually, cannabinol (CBN) is one of the most important products of degradation [7, 8]. CBD also undergoes changes during long-term storage, e.g., the transformation to Δ^9-THC by an acid-catalyzed cyclization, followed by the decay of Δ^9-THC to CBN (Fig. 1) [8, 9]. Therefore, it is not surprising that CBN has been detected as the major degradation product of cannabinoids in dried *Cannabis* flowers dating from around 1896–1905 [10]. Studies concerning the CBN content in sedimentary records, however, are rare. Thus, Lavrieux et al. reported about the detection of CBN, preserved in sediment samples from lake Aydat in the French Massif Central, covering the past 1800 years [11], thereby relating the presence of CBN to the retting of locally grown *Cannabis* plants for fiber production. This finding was supported by the analysis of pollen and historical data. Thus, determination of CBN contents in sedimentary cores seems to be an excellent possibility to trace ancient water retting activities.

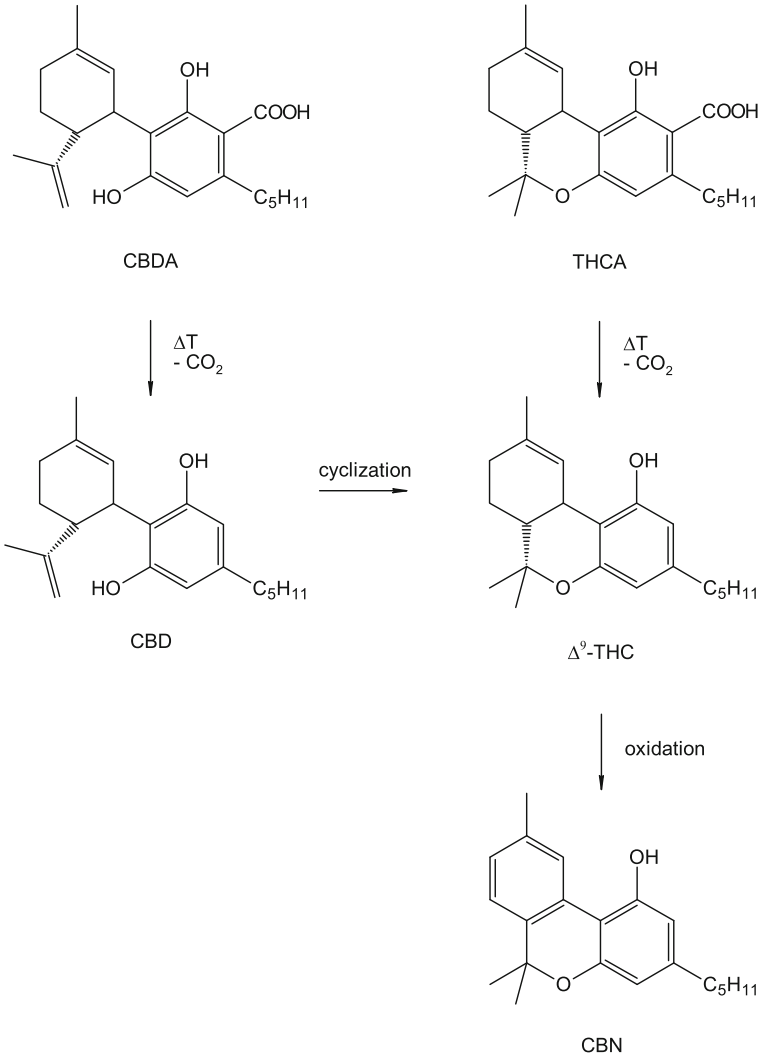

Fig. 1 Conversion of CBDA and THCA to CBD and THC as well as the formation of the main degradation product CBN

In a previous study, sediment samples from lake Aydat were investigated, and the detection of CBN was performed by gas chromatography mass spectrometry (GC-MS). However, this approach required a time-consuming derivatization with *N*,*O*-bis(trimethylsilyl)trifluoroacetamide (BSTFA). In general, different methods, e.g., GC-MS, liquid chromatography tandem mass spectrometry (LC-MS/MS), or (high-performance) thin-layer chromatography MS ((HP)TLC-MS) technique, are available for the quantification of cannabinoids in various matrices such as human blood, plasma, hair, urine, rodent tissues, or plant material [12–14]. Here, HPTLC combined with MS detection is a versatile and useful tool for the analysis of complex compounds in challenging matrices, thus enabling a relatively simple, rapid, and inexpensive qualitative and quantitative determination. However, the application of HPTLC-MS for the determination of CBN in sediment samples, a very complex matrix, has not yet been described so far.

In this study, we report on the development and validation of a HPTLC-electrospray ionization (ESI)-MS method for the identification and quantification of CBN as a molecular biomarker for ancient hemp retting in sedimentary records allowing a fast and accurate high-throughput screening of sediment samples. In this context, samples of a sediment core from a small lake in Northern India, covering a period from 2220 BCE to 1390 CE, were tested. Previous studies on these samples have already shown high percentages of *Cannabis*-type pollen, thus indicating an intense local retting of hemp [15].

Material and methods

Chemicals and materials

CBN (1 mg/mL in methanol, certified reference material), CBN-d_3 (100 μg/mL in methanol, certified reference material), CBD (1 mg/mL in methanol, certified reference material), and CBD-d_3 (100 μg/mL in methanol, certified reference material) were bought from Cerilliant; acetonitrile (HPLC gradient grade), methanol (HPLC gradient grade), *n*-hexane (HPLC grade), *n*-heptane (HPLC grade), and formic acid (98–100%) were obtained from VWR Chemicals; dichloromethane (HPLC grade) from Carl Roth, triethylamine from ACROS Organics, Fast Blue Salt B (FBS, dye content ~95%) from Sigma-Aldrich, Chromabond SiOH (1 ml/100 mg), Chromabond C_{18} ec (1 ml/ 100 mg) as well as TLC (thin-layer chromatography) plates (silica gel 60, ALUGRAM Xtra SIL G UV_{254} and octadecyl-modified silica, ALUGRAM RP-18 W/UV_{254}) from Macherey-Nagel, TLC plates (silica gel 60 without fluorescent indicator on aluminum sheets), and HPTLC (high-performance thin-layer chromatography) plates (silica gel 60 F_{254} MS-grade for matrix-assisted laser desorption/ionization (MALDI) and silica gel 60 F_{254} on glass plates) were purchased from Merck KGaA and analytical sea sand from Grüssig GmbH. Distilled diethyl ether and acetone were produced with a rotary evaporator from BÜCHI.

Preparation of standard solutions

A stock solution of CBN from Cerilliant (1 mg/mL in methanol) was diluted with methanol to obtain working solutions down to a concentration of 0.3 μg/mL. CBN-d_3 working solutions (2.5 μg/mL and 5.0 μg/mL) as internal standards were prepared in methanol. For the calibration, solutions holding different mixtures of CBN and CBN-d_3 were prepared (CBN, in the range of 1.0–6.2 μg/mL; CBN-d_3, 2.5 μg/mL), and for the validation of the HPTLC-ESI-MS method, different mixtures of CBN and CBN-d_3 were used (CBN, 1.4, 1.8, 2.2, 2.5, 3.4, 5.0, 5.4 μg/mL; CBN-d_3, 2.5 μg/mL).

Detection of CBN with FBS reagent (modified according to an application note from CAMAG [16])

The post-chromatographic detection reaction was performed with FBS reagent using CBN working solutions and sample extracts (25 μL aliquots) spotted onto TLC or HPTLC plates. For the preparation of the FBS reagent, FBS (250 mg) was completely dissolved in distilled water (10 mL) and was mixed with methanol (25 mL) and dichloromethane (15 mL). This reagent was always freshly prepared before use. (HP)TLC plates were developed in *n*-hexane/acetone/triethylamine (40:20:2 v/v/v; see Watanabe et al. [17]), sprayed with the reagent, and the presence of red spots indicated a positive response.

Detection of CBN with cerium-molybdenum reagent

In addition, post-chromatographic detection reactions were performed with cerium-molybdenum reagent using CBN working solutions and sample extracts (25 μL aliquots) spotted onto (HP)TLC plates. For the preparation of the cerium-molybdenum reagent, cerium(IV) sulfate (400 mg) and ammonium molybdate (20 g) were dissolved in 10% (v/v) sulfuric acid (400 mL). (HP)TLC plates were developed in *n*-heptane/diethyl ether/formic acid (75:25:0.3 v/v/v; according to an application note from CAMAG [16]), *n*-heptane/diethyl ether (90:10 v/v), or *n*-hexane/acetone/triethylamine (40:20:2 v/v/v), sprayed with the reagent, and blue spots became visible after exposure to heat.

Samples

Samples of a 3.55-m-long sediment core from Badanital (30° 29′ 50″ N, 78° 55′ 26 E, 2083 m a.s.l.), a small lake in the West Himalayan oak forest zone in Northern India, have been investigated. The core was retrieved using a piston corer in January 2008 (see Kotlia and Joshi [18]). Contiguous subsamples were taken in 1 cm slices and dried at 30 °C for storage and transportation to the pollen laboratory at the Institute of Geological Sciences, Freie Universität Berlin. Sediment samples, covering a period from 2220 BCE to 1390 CE, were examined concerning *Cannabis* pollen; they were categorized into real samples (positive samples), containing *Cannabis* pollen, and negative samples without *Cannabis* pollen. The procedure for pollen analyses is based on morphological characteristics as well as further results of the determination of palynomorphs; detailed results from accelerator mass spectrometry (AMS) radiocarbon dating using bulk sediment rich in organics were described by Demske et al. [15]. For the reconstruction of climatic changes based on geochemical parameters of sediment samples from Badanital lake, see Kotlia and Joshi [18].

HPTLC-ESI-MS analysis

Standard solutions and the extracts were spotted onto the TLC or HPTLC plates as 2 mm bands, in 25 μL aliquots, 20 mm from the bottom edge and 8 mm apart using a Linomat 5 (CAMAG, Switzerland). Plates were developed in a rectangular TLC developing chamber to a distance of 50 mm in 15 min using *n*-heptane/diethyl ether (90:10 v/v) as the developing solvent. For the optimization of the chromatographic separation, TLC and HPTLC plates as well as various developing solvents were tested, e.g., *n*-heptane/diethyl ether/formic acid (75:25:0.3 v/v/v) or *n*-hexane/acetone/triethylamine (40:20:2 v/v/v).

HPTLC plates were inspected both under white light and with under UV light at λ = 254 nm. Beside investigations by MS, different spray reagents were also used for the detection of CBN (see detection of CBN with FBS and cerium-molybdenum reagent).

A TLC-MS interface (Plate Express from Advion combined with an isocratic pump) was utilized for the elution of compounds from the HPTLC plates into an expression^{L} CMS (compact mass spectrometer from Advion, UK) system, equipped with an ESI ion source (negative mode, capillary temperature 250 °C, capillary voltage 180 V, source voltage offset 20, source voltage span 30, ESI source voltage 2500 V, source gas temperature 200 °C, MS scan range 200–400 *m/z*). Prior to the measurements, substance-specific parameters were determined by direct inlet of CBN working solutions. Methanol was used as eluent (flow rate 0.2 mL/min).

Offline HPTLC-ESI-HRMS analysis

Standard solutions were spotted onto HPTLC plates; HPTLC plates were developed in *n*-heptane/diethyl ether (90:10 v/v), and after 5 h, spots were marked; stationary phase was scraped from the plates and compounds were eluted with methanol (1 mL). This solution was filtered (0.2 μm PTFE) and utilized for HRMS experiments using a Q Exactive Plus mass spectrometer from Thermo Scientific equipped with an ESI ion source (negative mode, spray voltage 3287 V, spray current 1 μA, capillary temperature 320 °C, sheath gas flow rate 10 L/min, MS scan range 200–900 *m/z*).

Sample extraction and preparation

The remaining sediment samples analyzed for pollen were sent to the Department of Organic Chemistry, Martin-Luther-University Halle-Wittenberg (Halle), and used in the current study. An aliquot (1 g) of each sample was extracted with methanol/hexane (10 mL, 9:1 v/v) by the following procedure: 1 min on a vortex and 15 min ultrasonic bath at 30 °C including vortex again after 5 and 10 min. Subsequently, the suspension was centrifuged (10 min, 21 °C, 4200 rpm) in a centrifuge 5403 from Eppendorf. The extraction of the sample was repeated five times. The supernatants were combined, and the solution was evaporated to dryness on a rotary evaporator (temperature of the water bath, 30 °C). The residue was dissolved in *n*-heptane/diethyl ether (1 mL, 75:25 v/v) with the help of an ultrasonic bath at 30 °C for a few seconds. Afterwards, the sample extract was transferred to a Chromabond SiOH column conditioned with *n*-heptane/diethyl ether (75:25 v/v), the sample container was rinsed with *n*-heptane/diethyl ether (3 × 1 mL, 75:25 v/v), the rinse solution was also transferred onto the sorbent, and the analyte was eluted with *n*-heptane/diethyl ether (2 mL, 75:25 v/v). The eluate (fraction 1: combined solutions, approximately 6 mL) was evaporated to dryness on a rotary evaporator (temperature of the water bath, 30 °C), and the residue was dissolved in acetonitrile/water (500 μL, 70:30 v/v). The solution was transferred to a Chromabond C_{18} ec column conditioned with acetonitrile/water (70:30 v/v). The sample vessel was rinsed with acetonitrile/water (1 mL, 70:30 v/v), the rinse solution was also transferred onto the sorbent, and the analyte was eluted with acetonitrile/water (500 μL, 70:30 v/v, and 3 mL, 80:20 v/v). The eluate (fraction 2: combined solutions, approximately 5 mL) was evaporated to dryness on a rotary evaporator (temperature of the water bath, 50 °C). The residue was dissolved in methanol (1 mL) and transferred to a vial. The sample pot was rinsed with methanol (3 mL), and this solution was also transferred to this vial step-by-step. The sample solution in the vial was concentrated to dryness in a stream of argon with heat from a laboratory sand bath at 70 °C. The residue was solved in methanol (100 μL), and a defined

volume (25 μL) of the sample extract was spotted onto a HPTLC plate (Fig. 2).

For the optimization of the extraction procedure, various extraction times and further extracting agents were tested, e.g., dichloromethane/methanol (90:10 v/v and 1:1 v/v).

Determination of sediment pH

For the determination of the pH of a sample, a pH electrode from HANNA instruments was used. An aliquot (0.5 g) of the sediment sample was suspended in a solution of calcium chloride (0.01 M) at the ratio of 1:2.5. After the sedimentation, the pH was measured.

Determination of the loss on ignition (modified according to Heiri et al. [19])

The loss on ignition at 550 °C (LOI_{550}) was determined using a thermobalance STA 449C from Netzsch (reference: empty crucible of corundum). An aliquot of the sample (15–25 mg) was weighted in a crucible of corundum, and a stream of gas ($N_2/O_2 = 80/20$, 50 mL/min) was applied. Before each measurement, an equilibration of the thermobalance was performed for about 30 min at room temperature with current gas flow. Afterwards, the sample chamber was heated to 800 °C (heat rate 10 K/min). The weight loss is proportional to the amount of organic

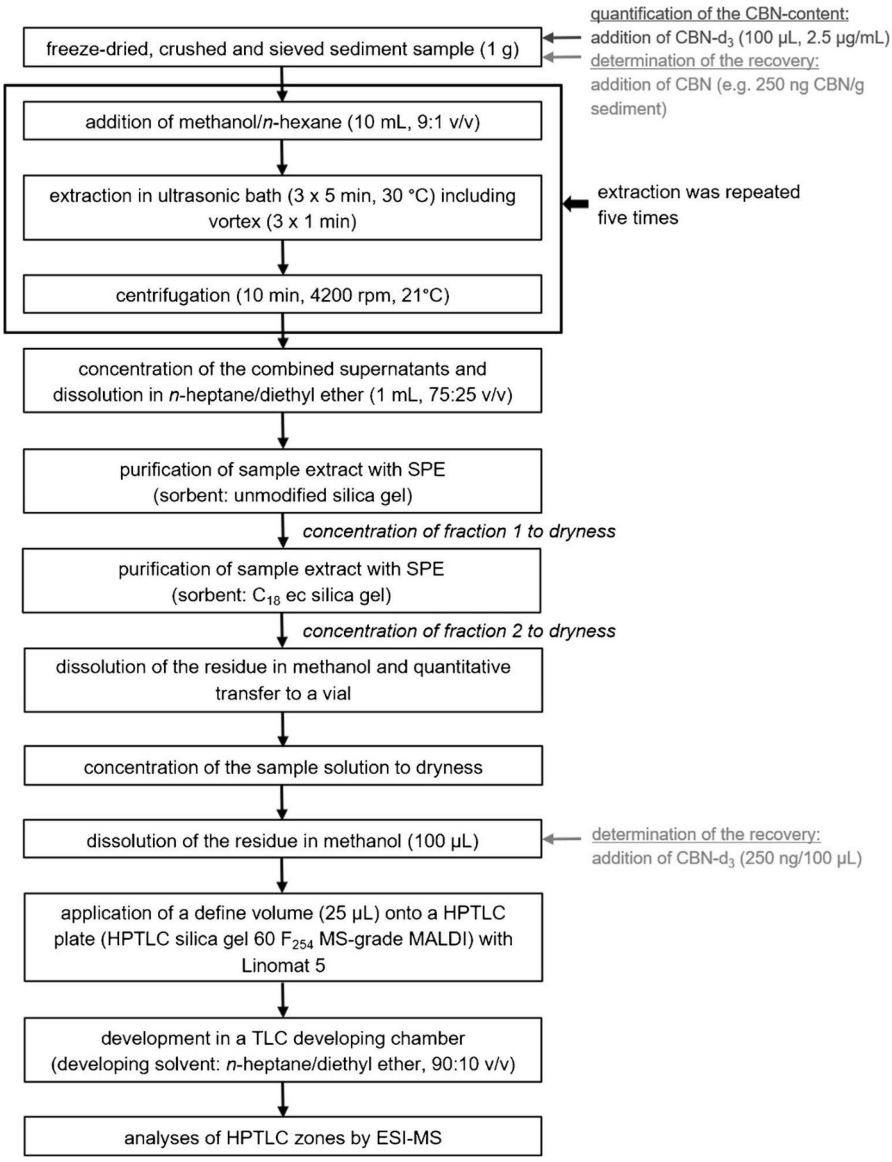

Fig. 2 Flow diagram for the extraction of the samples and cleanup protocol. For the quantification of the CBN content, internal standard CBN-d_3 was added after sample has been weighed. For the determination of the recovery, CBN-spiked sediment samples (approximately 140, 250, and 330 ng CBN/g sediment) were used, and the residue of the purification with reversed-phase sorbent was solved in a methanolic solution of CBN-d_3 (100 μL, 2.5 μg/mL) after having been transferred to a vial and before spotting the solution onto a HPTLC plate

carbon contained in samples. For the calculation, the following formula (1) was used:

$$LOI_{550} = ((DW_{105} - DW_{550})/DW_{105}) \times 100 \quad (1)$$

where LOI_{550} represents the LOI at 550 °C (as percentage), DW_{105} correspond to the dry weight of the sample before combustion, and DW_{550} to the dry weight of sample after heating to 550 °C (both in mg, see Heiri et al. [19]).

Determination of C/N content

The determination of the C and N content of the samples were performed with the analytical instrument "Vario EL" from the company Elementar.

Validation of the HPTLC-ESI-MS method

Specificity

The test for specificity was performed with a negative sample (without CBN) and a real sample (containing CBN) applying the post-chromatographic detection reaction with cerium-molybdenum reagent and HPTLC-ESI-MS using standard compounds. For HPTLC-ESI-MS experiments as well as for the detection of CBN with the cerium-molybdenum reagent, a sample extract was spotted onto a HPTLC plate; the HPTLC plate was developed in *n*-heptane/diethyl ether (90:10 v/v) and investigated by HPTLC-ESI-MS or sprayed with cerium-molybdenum reagent.

Linearity, limit of detection, and limit of quantification

The linearity of the calibration function was tested with the Mandel's test. Limit of detection (LOD) and limit of quantification (LOQ) were determined by means of a calibration curve method according to DIN 32645 [20], thereby spotting the calibration solutions (see preparation of standard solutions) onto HPTLC plates; the HPTLC plates were developed using *n*-heptane/diethyl ether (90:10 v/v) and investigated by HPTLC-ESI-MS. Each calibration solution was measured three times, and analyses were executed with average peak areas of the mass peaks of CBN (sum of *m/z* 309 and 354) and CBN-d_3 (sum of *m/z* 312 and 357). Average peak area ratios and CBN concentrations are depicted in Fig. S1 and Tab. S1 (see Electronic Supplementary Material, ESM).

Precision

For determining the repeatability, two to five replicate determinations on eight different days were carried out. For this purpose, a solution containing CBN and CBN-d_3 (CBN 3.4 μg/mL, CBN-d_3 2.5 μg/mL) was spotted onto HPTLC plates; HPTLC plates were developed using *n*-heptane/diethyl ether (90:10 v/v) and investigated by HPTLC-ESI-MS. For the interpretation of the repeatability, the relative standard deviation (RSD) of the CBN content was used. Furthermore, Dixon's Q test and Neumann trend test were applied for the identification of outliers or trends (see Table S2 of the ESM).

For determining the method precision, sediment sample BT-78 was utilized. Analyses were carried out with a number of six replicates and each aliquot of the sediment sample (approximately 1 g) was spiked with a defined concentration of CBN (100 μL; 3.4 μg/mL) and CBN-d_3 (100 μL; 2.5 μg/mL). Extractions and preparations of the different samples were performed independently of each other as described above. After SPE using a Chromabond C_{18} ec column, the residues were dissolved in methanol (100 μL) and defined volumes (25 μL) of the sample extracts were spotted onto HPTLC plates; HPTLC plates were developed in *n*-heptane/diethyl ether (90:10 v/v) and were investigated by HPTLC-ESI-MS. For the interpretation of the method precision, the relative standard deviation (RSD) of the CBN content was used. Furthermore, Dixon's Q test and Neumann trend test were applied for the identification of outliers or trends (see Table S2 of the ESM).

Trueness

The trueness was expressed in terms of recovery and bias. Bias calculation was performed for two concentration levels with a number of three replicates at each concentration (see Table S3 of the ESM). Sediment samples (approximately 1 g) were spiked with a defined concentration of CBN (100 μL; 5.4 μg/mL and 1.8 μg/mL) and CBN-d_3 (100 μL; 2.5 μg/mL). Extractions and preparations of the different samples as well as the planar chromatographic separations were performed independently of each other as described above. Real samples were used for bias calculation due to a limited sample amount. For the bias calculation, the following formula (2) was used:

$$\hat{\delta} = \bar{x} - T \quad (2)$$

where $\hat{\delta}$ represents the bias and T correspond to the "true" concentration and $\bar{x}$ to the mean value of the determined concentrations of the spiked sample materials.

Recovery

Three negative samples from different positions in the sedimentary core were used for the determination of the recovery. After the sediment samples have been weighed (approximately 1 g, see Fig. 2), defined concentrations of CBN (100 μL; 1.4, 2.5, and 3.4 μg/mL) were added and each concentration level was analyzed in duplicate (see Table S4 of

the ESM). Extractions and preparations of the different samples were performed independently of each other on different days as described above. After SPE using a Chromabond C_{18} ec column, the residues were dissolved in a methanolic solution of CBN-d_3 (100 μL; 2.5 μg/mL) and were spotted onto HPTLC plates; HPTLC plates were developed in *n*-heptane/diethyl ether (90:10 v/v) and were investigated by HPTLC-ESI-MS. The calculated CBN contents were compared with the target concentrations and the recovery rate was determined.

Stability of the standards

For testing the storage stability of standard solutions, solutions of CBN (50 and 100 μg/mL) were stored at − 12 °C in the dark, at room temperature (average temperature + 28 °C) in the dark and at room temperature exposed to sunlight. The different solutions were examined over a 4-week period. For analyses, solutions of CBN were diluted, CBN-d_3 was added, and the mixtures (CBN 2.2 and 5.0 μg/mL; CBN-d_3 2.5 μg/mL) were spotted onto HPTLC plates. Mass peak areas of CBN (sum of *m/z* 309 and 354) and CBN-d_3 (sum of *m/z* 312 and 357) were utilized for calculating the stability of CBN. For the identification of trends, a trend test by Neumann [20] was performed (see Table S5 of the ESM).

In addition, the stability of CBN and CBN-d_3 already having been spotted onto (HP)TLC plates was evaluated. For this purpose, a solution containing CBN and CBN-d_3 (CBN 5.0 μg/mL; CBN-d_3 5.0 μg/mL) was spotted in triplicate onto a TLC and a HPTLC plate. (HP)TLC plates were developed in *n*-heptane/diethyl ether (90:10 v/v) and were investigated by HPTLC-ESI-MS at a time interval of 3 h (measuring after 0.5, 1.5, and 3 h). Furthermore, investigations were performed on (HP)TLC plates spotted with CBN and CBN-d_3 without developing the chromatograms. For analyses, mass peak intensities of CBN (ratios of *m/z* 309 and 354) and CBN-d_3 (ratios of *m/z* 312 and 357) were utilized.

Results and discussion

Development of a HPTLC-ESI-MS method for the identification and quantification of CBN in sediment samples

Determination of CBN content in sediment samples was performed by HPTLC-ESI-MS. For this purpose, sediment samples were extracted followed by a subsequent elimination of disturbing matrix compounds using an orthogonal SPE sample preparation. Afterwards, purified extracts were spotted onto HPTLC plates, the HPTLC plates were developed and the HPTLC zones were analyzed by ESI-MS (MS scan range *m/z* 200–400). Mass spectra of standards eluted from HPTLC silica gel 60 plates show intense peaks at *m/z* 309 and 312, assigned to the quasi-molecular ions $[M\text{-}H]^-$ of CBN and CBN-d_3. In addition, extra mass peaks at *m/z* 354 (working solutions of CBN spotted onto HPTLC plates) and 357 (working solutions of CBN-d_3 spotted onto HPTLC plates) were observed (Fig. 3). These signals appear after the application of CBN and CBN-d_3 onto TLC or HPTLC silica gel 60 plates and were not found in fresh or aged (for 24 h) methanolic working solutions of CBN and CBN-d_3 or in the context of blanks (blanks for the whole method as well as investigations on TLC or HPTLC plates using different developing solvents without the addition of CBN or CBN-d_3). However, after development of the (HP)TLC plates, the proportion of these extra peaks increased compared with investigations without contact to a developing solvent. In this context, different developing solvents and stationary phases (octadecyl-modified TLC silica layers, unmodified (HP)TLC silica layers with and without fluorescent indicator on aluminum sheets and glass plates) were tested. Mass spectra of standards eluted from octadecyl-modified TLC silica layers show peaks at *m/z* 309 and 312. However, no signals at *m/z* 354 or 357 were observed. In contrast, in all experiments performed on unmodified silica layers, extra mass peaks at *m/z* 354 and 357 were detected. Furthermore, the proportion of these peaks increased in time. Immediately after application of the cannabinoids and the development of the HPTLC silica gel 60 plates, peak intensity ratios of *m/z* 309/354 and 312/357 were 10.1 (8.01E7/

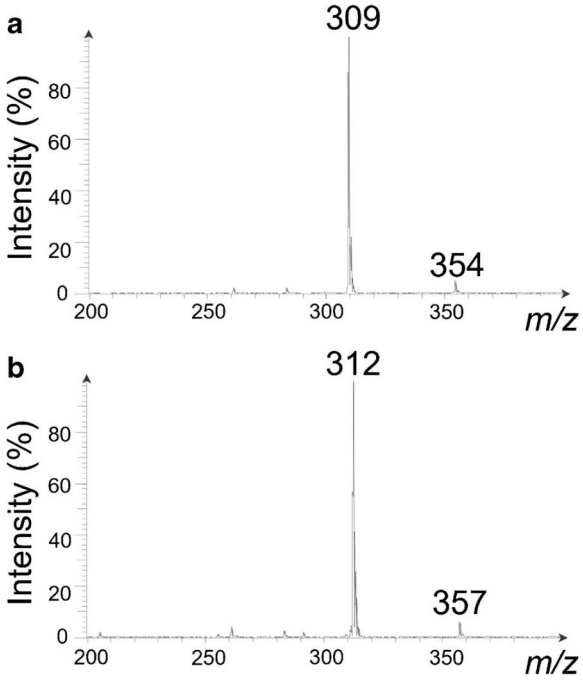

Fig. 3 MS spectrum of **a** CBN and **b** CBN-d_3 spotted onto a HPTLC silica gel 60 plate recorded immediately after chromatographic separation using *n*-heptane/diethyl ether (90:10 v/v) as developing solvent

7.91E6) and 8.3 (3.65E7/4.41E6, see Fig. S2a of the ESM). After 3 h, the ratios were in either case 0.3 (1.67E7/5.08E7 and 7.62E6/2.61E7, see Fig. S2b of the ESM). Thus, investigations were performed immediately after application and chromatographic separation and signals at *m/z* 354 and 357 were included in the quantitative determination of CBN.

Furthermore, methanolic working solutions of CBD and CBD-d_3 were spotted onto TLC or HPTLC silica gel 60 plates. After the development of the plates, besides intense peaks at *m/z* 313 and 316 (assigned to the quasi-molecular ions $[M\text{-}H]^-$), extra peaks with a mass shift of 45 were also detected at *m/z* 358 and 361 (see Fig. S3a and S3b of the ESM). As indicated by TLC and HRMS studies on CBN and CBN-d_3, the mass shift of 45 points to the presence of transient adducts with the silica gel from the plates. This will be subject to further studies.

In addition, different spray reagents were tested to find a pretest confirming the presence of CBN in sediment samples by a color reaction.

Optimization of mobile and stationary phase for planar chromatography

For the optimization of the planar chromatographic separation, different sorbents and solvents were tested. An acceptable separation of CBN and matrix compounds was found on TLC silica gel 60 sorbent using *n*-heptane/diethyl ether/formic acid (75:25:0.3 v/v/v) or *n*-hexane/acetone/triethylamine (40:20:2 v/v/v) as developing solvent (see Fig. S4 of the ESM). However, bands were rather diffused. Therefore, normal phase HPTLC on silica gel 60 was used to achieve sharper bands, thereby obtaining a satisfactory resolution of CBN and matrix compounds using *n*-heptane/diethyl ether (90:10 v/v) as the mobile phase.

Optimization of sample extraction and preparation

Different extracting agents and extraction times were tested using analytical sea sand spiked with CBN due to a limited sample amount (Table 1). An extraction in an ultrasonic bath with methanol/*n*-hexane (90:10 v/v) for 5 × 15 min provided satisfactory results concerning the recovery of CBN (recovery rate 97%). Sample handling was also optimized with CBN spiked sea sand samples.

Table 1 Optimization of sample extraction using different extracting agents and analytical sea sand spiked with CBN (extraction time 5 × 15 min)

Extracting agent	Recovery (%)
Methanol/*n*-hexane (90:10 v/v)	97
Dichloromethane/methanol (90:10 v/v)	90

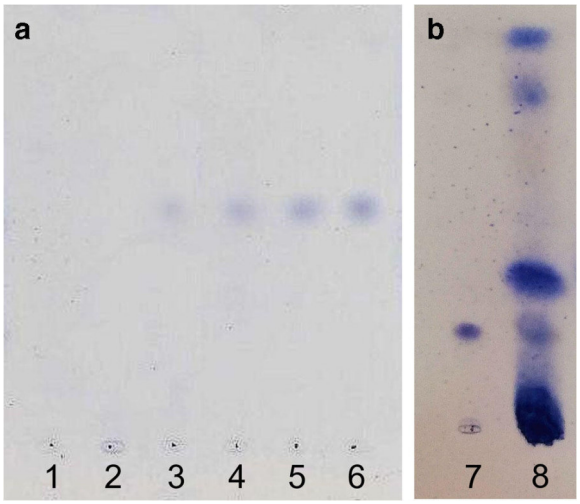

Fig. 4 HPTLC silica gel 60 plates developed using **a** *n*-heptane/diethyl ether/formic acid (75:25:0.3 v/v/v) or **b** *n*-heptane/diethyl ether (90:10 v/v) as developing solvent after derivatization with cerium-molybdenum reagent; observed under white light. Tracks 1–7 = CBN standard (from left to right increasing CBN concentration: 7.5, 15, 25, 55, 85, 125, 190 ng CBN/HPTLC zone); 8 = extract (extracting agent: methanol/hexane (10 mL, 9:1 v/v)) of real sample BT-96 spiked with CBN-d_3 (62.5 ng CBN-d_3/HPTLC zone)

For the determination of CBN in sediment matrices (extracts of real and spiked negative samples), two SPE columns were combined. Matrix simplification was carried out with a combination of normal phase and reversed phase sorbents. Some losses of CBN during this two-step purification procedure were eliminated through fine-tuning (recovery rate of

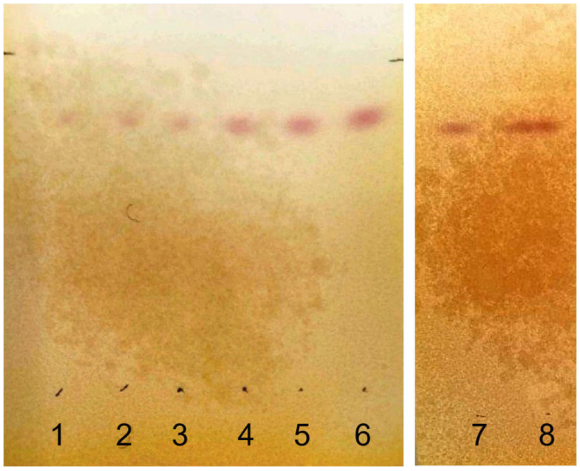

Fig. 5 HPTLC silica gel 60 plates developed using *n*-hexane/acetone/triethylamine (40:20:2 v/v/v) as developing solvent after derivatization with FBS reagent; observed under white light. Tracks 1–7 = CBN standard (from left to right increasing CBN concentration: 7.5, 15, 25, 55, 85, 125, 190 ng CBN/HPTLC zone); 8 = extract (extracting agent: methanol/hexane (10 mL, 9:1 v/v)) of real sample BT-96 spiked with CBN-d_3 (62.5 ng CBN-d_3/HPTLC zone)

Table 2 Chromatographic data for CBN and observed colors of the bands using different spray reagents

Developing solvent	R_F value		Band color	
	TLC plate	HPTLC plate	Cerium-molybdenum reagent	FBS reagent
n-Heptane/diethyl ether/formic acid (75:25:0.3 v/v/v)	0.4	0.5	Blue	None
n-Heptane/diethyl ether (90:10 v/v)	–	0.2		
n-Hexane/acetone/triethylamine (40:20:2 v/v/v)	0.6	0.8		Red

CBN for the whole procedure including extraction and purification: see validation results).

Detection of CBN by spray reagents

Different spray reagents were tested to confirm the presence of CBN in the sediment samples. The cerium-molybdenum reagent is suitable for the detection of low CBN concentrations up to 25.0 ng CBN/HPTLC zone using *n*-heptane/diethyl ether/formic acid (75:25:0.3 v/v/v, Fig. 4), *n*-heptane/diethyl ether (90:10 v/v), or *n*-hexane/acetone/triethylamine (40:20:2 v/v/v). CBN concentrations up to 7.5 ng CBN/HPTLC zone were detectable with the FBS reagent using *n*-hexane/acetone/triethylamine (40:20:2 v/v/v, Fig. 5). In the presence of the examined sediment matrices, exclusively CBN reacts under the described conditions with FBS resulting in red bands (FBS is known as a selective detection reagent for cannabinoids, see Fischedick et al. [21–23]). Thus, a post-chromatographic detection with FBS reagent was found to be appropriate as a pretest to confirm the presence of low CBN concentrations in sediment samples.

R_F values of CBN obtained by developing TLC or HPTLC plates in *n*-heptane/diethyl ether/formic acid (75:25:0.3 v/v/v), *n*-heptane/diethyl ether (90:10 v/v), and *n*-hexane/acetone/triethylamine (40:20:2 v/v/v) as well as observed colors of the bands are summarized in Table 2.

Validation results of HPTLC-ESI-MS method

Linearity, LOD, and LOQ were evaluated for CBN after chromatographic separation. The results from validation are summarized in Table 3 (further data see Table S1 and Fig. S1 of the ESM). LOD and LOQ were considered adequate for the purposes of the present study.

The developed HPTLC-ESI-MS method is specific for the determination of CBN in sediment samples. Post-chromatographic detection reaction with cerium-molybdenum reagent as well as the HPTLC-ESI-MS analyses on negative samples and real samples showed that CBN can be qualified and quantified even in the presence of interfering matrix components. Other related compounds being present in the complex sediment samples did not interfere with CBN during HPTLC-ESI-MS analyses. The method precision and the repeatability were determined with a RSD of 4.1% and 4.3% (see Table S2

Table 3 Linearity, LOD, and LOQ for CBN determination by HPTLC-ESI-MS (tv, test value; cv, characteristic value)

Key figures	Results
Range (ng CBN/HPTLC zone)	25–155
r^2 (coefficient of determination)	0.9979
Sy (residual standard deviation)	0.034
Sx (standard deviation for the method)	1.991
Residuals are normally distributed (R/s test, 99%)	Yes (tv = 3.32; cv = 2.86–4.34)
Residuals show a trend (Neumann trend test, 99%)	No (tv = 2.73; cv = 0.89)
Equation curve	y(x) = 0.0172x + 0.0245
	y: peak area ratio of CBN and CBN-d_3
	x: concentration of CBN (ng CBN/ HPTLC zone)
LOD (ng CBN/ HPTLC zone)	6.4
LOQ (ng CBN/ HPTLC zone)	20.7
Results of the Mandel's test according to DIN 32645	
Optimal regression model	Linear (tv = 0.02; cv = 9.64)
Linear regression acceptable	Yes

Table 4 CBN content of sediment samples and characteristics of these samples. Analyses of the CBN content including the described extraction and cleanup procedure were performed in duplicate

Estimated ages (ca cal years BP)	Sample ID	Depth in sedimentary core (cm)	pH$CaCl_2$	C content (%)	N content (%)	C/N (atomic)	LOI_{550} (%)	Average CBN content (ng CBN/HPTLC zone)	Average CBN content (ng CBN/g sediment)	PZ
Negative samples, without *Cannabis* pollen										
580	BT-270	86	4.7	4.4	0.3	17	*	< LOD	–	8
750	BT-192	164	5.1	3.9	0.6	8	7.1	< LOD	–	6
Real (positive samples), containing *Cannabis* pollen										
780	BT-174	182	4.9	4.5	0.1	53	8.0	25.9	99.2	5
880	BT-150	206	4.6	3.7	0.2	22	10.1	42.6	165.9	
950	BT-145	211	4.9	4.8	0.1	56	*	46.1	171.0	4
1000	BT-120	236	4.8	2.8	0.2	16	6.0	49.4	196.7	
1500	BT-102	254	4.8	3.9	0.4	11	7.6	88.8	348.5	
2200	BT-96	260	*	2.5	0.3	10	*	123.6	486.5	
2560	BT-91	265	5.0	2.3	0.2	13	5.8	70.1	271.7	3
2720	BT-85	271	*	1.3	0.2	8	*	37.0	145.5	
3020	BT-78	278	5.0	1.0	0.1	12	5.4	< LOQ	–	
Negative sample, without *Cannabis* pollen										
4200	BT-36	320	4.8	2.6	0.1	30	*	*	*	2

*Limited amount of sample

of the ESM), thereby classifying only one measured value as outliner by Dixon's test and was removed from the evaluation. The recovery rate of CBN after sample extraction and the described cleanup procedure (see sample extraction and preparation), determined with spiked negative samples from different positions in the sedimentary core, ranged from 63 to 82%, with an average recovery rate of 73% (see Table S4 of the ESM). Furthermore, no statistical difference has been observed between the mean and the "true" values (see bias calculation and Table S3 of the ESM). The storage stability of standard CBN solutions (2.2 and 5.0 μg/mL) was evaluated under different conditions (at − 12 °C in the dark, at room temperature in the dark, and exposed to sunlight). The tests showed that the concentration of CBN did not decrease more than 72% after 4 weeks (see Fig. S5 of the ESM). However, CBN underwent minor losses, maximal 84%, at a higher concentration of 5.0 μg/mL. Furthermore, no trend is discernible using a Neumann trend test.

In addition, it is conceivable to dissolve residues before the application onto HPTLC plates in a smaller volume of solvent (e.g., 30 μL instead of 100 μL) for increasing the concentration of the extract. This could enable a characterization of CBN in very low concentrations.

Thus, the method gives satisfactory results and allowed an appropriate examination of the CBN content in sediment samples.

Analysis of sediment samples

The quantitative determination of CBN in sediment samples was performed by HPTLC-ESI-MS. In this context, a series of twelve sediment samples of one core from a small lake in the Garhwal Himalaya, referred to as Badanital lake, was analyzed in duplicate. The results as well as the sample position in the sedimentary core and estimated ages (for age estimation based on radiocarbon dating, see Demske et al. [15]) of the investigated samples are summarized in Table 4. Prior to our investigations, palynological analyses were performed (for characteristics of the respective pollen zones (PZ), see Demske et al. [15]), and *Cannabis* pollen were proven in the sample material; these samples were categorized as real (positive) samples. In contrast, samples holding no *Cannabis* pollen were categorized as negative samples. For these negative samples, the absence of CBN was assumed. Post-chromatographic detection reactions with FBS as well as HPTLC-ESI-MS studies confirmed the absence of CBN or a CBN content lower than 6.4 ng CBN/HPTLC zone (LOD), i.e., 25.6 ng CBN/g sediment.

Furthermore, C and N contents were determined to estimate the content of organic matter of the sample material as well as the C/N ratios of organic matter. For investigated sediment samples, C contents correspond approximately to the total organic carbon (TOC) concentration due to pH values

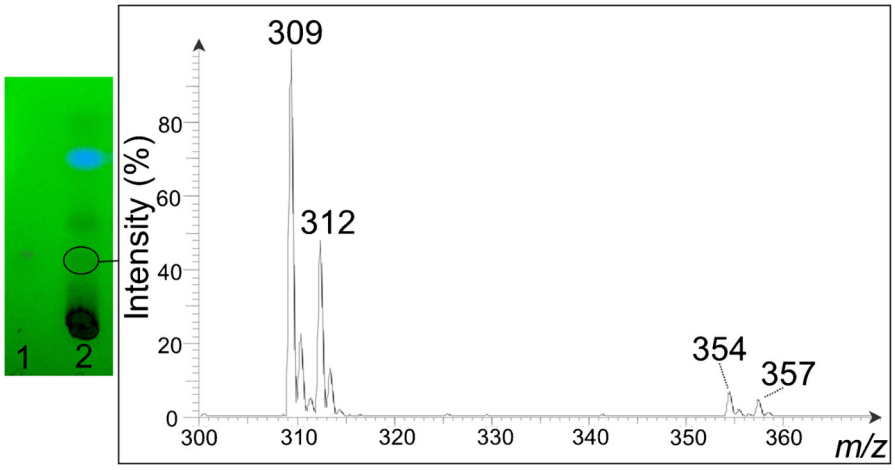

Fig. 6 HPTLC chromatogram of (1) CBN standard (190 ng CBN/HPTLC zone) and (2) an extract of real sample BT-102 spiked with CBN-d_3 (62.5 ng CBN-d_3/HPTLC zone) as well as a related MS spectrum (HPTLC silica gel 60 plate developed in *n*-heptane/diethyl ether (90:10 v/v); observed with an UV light source at 254 nm; extracting agent: methanol/hexane (10 mL, 9:1 v/v); after an orthogonal SPE sample preparation)

between 4.6 and 5.0 and the resulting absence of carbonate carbon. With C contents mostly between 3 and 4%, studied samples were rather rich in organic matter. Measured loss on ignition values at 550 °C (LOI_{550}), as a further parameter for estimating the organic content of the sediment samples (see Heiri et al. [19]), confirmed this finding. C/N ratios of 20 and greater indicating organic matter rather from vascular land plants than from phytoplankton (see Meyers and Teranes [24]) and match with findings of Demske et al. [15] (admixtures of plant fragments and woody material were described). C/N values of 8–13 point to organic matter from phytoplankton or a nearly equal mixture of algal and vascular plant contributions. For further geochemical parameters of sediment samples from Badanital lake or discussions concerning past vegetation or climatic changes, see Demske et al. and Kotlia and Joshi [15, 18].

The CBN content of the investigated real samples varied between 99.2 and 486.5 ng CBN/g sediment with a maximum content in PZ 4 at a depth of 260 cm. A characteristic HPTLC chromatogram of an extract and the corresponding MS spectrum is shown in Fig. 6. The data set indicates a correlation with the pollen records of Demske et al. [15]. A high pollen concentration of *Cannabis* type was also found in PZ 3 (293–262 cm; approximately 1620–480 BC) and 4 (262–209 cm; approximately 480 BC–1050 AD), followed by a decreasing contribution of *Cannabis* type in PZ 5 (209–173 cm; approximately 1050–1160 AD). The high percentages of *Cannabis* pollen were interpreted as an indicator of water retting of hemp and the confidential interval of intense retting at Badanital was dated from approximately 480 BC to 1050 AD. This hypothesis is largely corroborated by the record of sedimentary CBN. However, a systematic analysis of sediment core samples from Badanital lake is needed for a detailed discussion of the CBN content with regard to ancient retting activities. This remains the goal of additional investigations to be performed in the future.

Conclusion

In this paper, we report on the application of HPTLC-ESI-MS to identify and quantify the cannabinoid CBN, an unequivocal molecular biomarker for the *Cannabis* species and consequently a tracer for ancient water retting of *Cannabis* in sediment samples. In the course of method development, planar chromatographic separation, sample extraction, and the subsequent cleanup procedure, using an orthogonal SPE sample preparation, were optimized. To evaluate the potential of this method, parameter such as LOD, LOQ, linearity, recovery rate, method precision, and storage stability were determined. The validated method showed a satisfactory overall analytical performance and determined CBN contents of sediment samples from a small lake in Northern India match very well with pollen records reported in previous studies. In addition, different spray reagents for a post-chromatographic detection of CBN were tested. FBS reagent enables, under the selected conditions, a sensitive and specific detection of CBN in sediment samples.

In conclusion, HPTLC-ESI-MS is a relatively simple, rapid method enabling a high-throughput and low-cost screening of complex and challenging sediment samples as a natural archive for environmental changes and human activities. Considering the still fragmentary knowledge on ancient retting sites and fact that pollen records reflect the presence of *Cannabis*, however, not really the retting of *Cannabis*, this method is a promising approach to track more specifically the retting processes for reconstructing the *Cannabis* retting history.

Acknowledgments Open Access funding provided by Projekt DEAL. This work was supported by the German Research Foundation (DFG, project number 425225219). The authors are grateful to Maximilian Schneider and Senta Ludwig for the determination of the C and N contents and to Oliver Kraft for continuing support in the laboratory (Martin-Luther-Universität Halle-Wittenberg). Special thanks are due to Dr. Christian Ihling and Prof. Dr. Andrea Sinz for the HRMS measurements.

Compliance with ethical standards

Conflict of interest The authors declare that they have no conflict of interest.

References

1. Russo EB. History of cannabis and its preparations in Saga, science, and sobriquet. Chem Biodivers. 2007;4(8):1614–48. https://doi.org/10.1002/cbdv.200790144.
2. Jiang H, Wang L, Merlin MD, Clarke RC, Pan Y, Zhang Y, et al. *Ancient Cannabis burial shroud in a central Eurasian cemetery*. Econ Bot. 2016;70(3):213–21. https://doi.org/10.1007/s12231-016-9351-1.
3. Jiang H-E, Li X, Zhao Y-X, Ferguson DK, Hueber F, Bera S, et al. A new insight into *Cannabis sativa* (Cannabaceae) utilization from 2500-year-old Yanghai Tombs, Xinjiang, China. J Ethnopharmacol. 2006;108(3):414–22. https://doi.org/10.1016/j.jep.2006.05.034.
4. Andre CM, Hausman J-F, Guerriero G. *Cannabis sativa*: The Plant of the Thousand and One Molecules. Front Plant Sci. 2016;7:19. https://doi.org/10.3389/fpls.2016.00019.
5. Potter DJ. A review of the cultivation and processing of cannabis (Cannabis sativa L.) for production of prescription medicines in the UK. Drug Test Anal. 2014;6(1–2):31–8. https://doi.org/10.1002/dta.1531.
6. Pacifici R, Marchei E, Salvatore F, Guandalini L, Busardò Francesco P, Pichini S. Evaluation of cannabinoids concentration and stability in standardized preparations of cannabis tea and cannabis oil by ultra-high performance liquid chromatography tandem mass spectrometry. Clin Chem Lab Med. 2017;55(10):1555–63. https://doi.org/10.1515/cclm-2016-1060.
7. Trofin IG, Vlad C, Dabija G, Filipescu L. Influence of storage conditions on the chemical potency of herbal cannabis. Rev Chim. 2011;62(6):639–45.
8. Trofin IG, Dabija G, Vaireanu D-I, Filipescu L. Long - term storage and cannabis oil stability. Rev Chim. 2012;63(3):293–7.
9. Trofin IG, Dabija G, Vaireanu D-I, Filipescu L. The influence of long-term storage conditions on the stability of cannabinoids derived from cannabis resin. Rev Chim. 2012;63(4):422–7.
10. Harvey DJ. Stability of cannabinoids in dried samples of cannabis dating from around 1896–1905. J Ethnopharmacol. 1990;28(1):117–28. https://doi.org/10.1016/0378-8741(90)90068-5.
11. Lavrieux M, Jacob J, Disnar J-R, Bréheret J-G, Le Milbeau C, Miras Y, et al. Sedimentary cannabinol tracks the history of hemp retting. Geology. 2013;41(7):751–4. https://doi.org/10.1130/g34073.1.
12. Citti C, Braghiroli D, Vandelli MA, Cannazza G. Pharmaceutical and biomedical analysis of cannabinoids: a critical review. J Pharm Biomed Anal. 2018;147:565–79. https://doi.org/10.1016/j.jpba.2017.06.003.
13. Leghissa A, Hildenbrand ZL, Schug KA. A review of methods for the chemical characterization of cannabis natural products. J Sep Sci. 2018;41(1):398–415. https://doi.org/10.1002/jssc.201701003.
14. Vozella V, Zibardi C, Ahmed F, Piomelli D. Fast and sensitive quantification of Δ(9)-tetrahydrocannabinol and its main oxidative metabolites by liquid chromatography/tandem mass spectrometry. Cannabis Cannabinoid Res. 2019;4(2):110–23. https://doi.org/10.1089/can.2018.0075.
15. Demske D, Tarasov PE, Leipe C, Kotlia BS, Joshi LM, Long T. Record of vegetation, climate change, human impact and retting of hemp in Garhwal Himalaya (India) during the past 4600 years. Holocene. 2016;26(10):1661–75.
16. Camag. Identification and quantification of different cannabinoids in *Cannabis sativa*. https://www.camag.com/en/tlc_hptlc/camag_laboratory/methods.cfm?ao=-1. 2017. Accessed 3rd April 2019.
17. Watanabe K, Yamaori S, Funahashi T, Kimura T, Yamamoto I. 8-Hydroxycannabinol: a new metabolite of cannabinol formed by human hepatic microsomes. Forensic Toxicol. 2006;24(2):80–2. https://doi.org/10.1007/s11419-006-0016-0.
18. Kotlia BS, Joshi LM. Late Holocene climatic changes in Garhwal Himalaya. Curr Sci. 2013;104(7):911–9.
19. Heiri O, Lotter AF, Lemcke G. Loss on ignition as a method for estimating organic and carbonate content in sediments: reproducibility and comparability of results. J Paleolimnol. 2001;25(1):101–10. https://doi.org/10.1023/a:1008119611481.
20. Kromidas S. Handbuch Validierung in der Analytik. Weinheim: Wiley-VCH; 2011.
21. Fischedick JT, Glas R, Hazekamp A, Verpoorte R. A qualitative and quantitative HPTLC densitometry method for the analysis of cannabinoids in Cannabis sativa L. Phytochem Anal. 2009;20(5):421–6. https://doi.org/10.1002/pca.1143.
22. Hazekamp A, Peltenburg A, Verpoorte R, Giroud C. Chromatographic and spectroscopic data of cannabinoids from Cannabis sativa L. J Liq Chromatogr Relat Technol. 2005;28(15):2361–82. https://doi.org/10.1080/10826070500187558.
23. Corrigan D, Lynch JJ. An investigation of potential staining reagents for the Glandular Trichomes of *Cannabis sativa*. Planta Med. 1980;40(S 1):163–9. https://doi.org/10.1055/s-2008-1075020.
24. Meyers PA, Teranes JL. Sediment organic matter. In: Last WM, Smol JP, editors. Tracking environmental change using lake sediments: physical and geochemical methods. Dordrecht: Springer Netherlands; 2001. p. 239–69.

Analytical and Bioanalytical Chemistry

Electronic Supplementary Material

Identification and quantification of cannabinol as a biomarker for local hemp retting in an ancient sedimentary record by HPTLC-ESI-MS

Theresa Schmidt, Annemarie Elisabeth Kramell, Florian Oehler, Ralph Kluge,
Dieter Demske, Pavel E Tarasov, René Csuk

Table of content

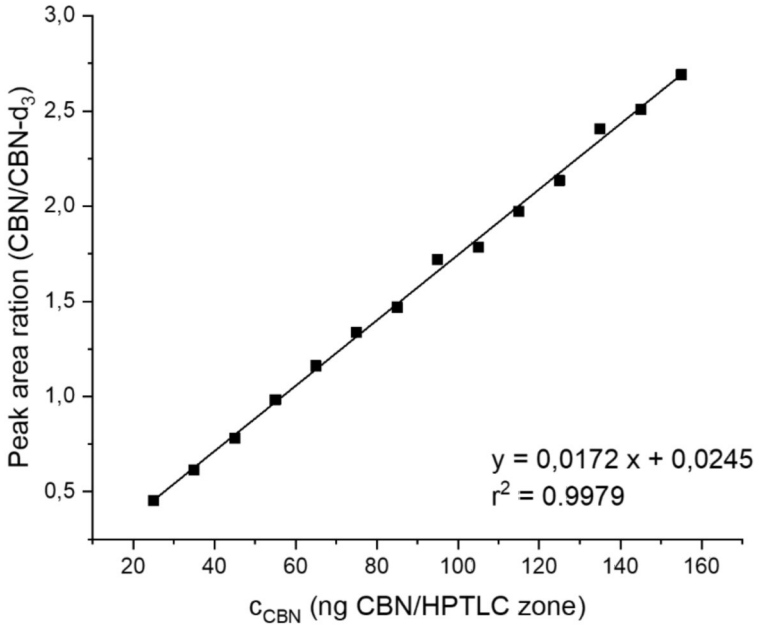

Fig. S1 Calibration curve obtained from CBN in the range 25 – 155 ng CBN/HPTLC zone with 62,5 ng CBN-d_3/HPTLC zone after chromatographic separation

Tab. S1 CBN concentration of calibration solutions and related average peak area ratios of CBN (sum of mass peaks at *m/z* 309 and 354) and CBN-d_3 (sum of mass peaks at *m/z* 312 and 357) received from analyses on calibration solutions in triplicate (25 - 155 ng CBN/HPTLC zone; 62,5 ng CBN-d_3/HPTLC zone) after chromatographic separation

c_{CBN} (ng CBN/HPTLC zone)	**Average peak area ratio (∑ *m/z* 309+354)/(∑ *m/z* 312+357)**
25	0.4534
35	0.6139
45	0.7816
55	0.9831
65	1.1609
75	1.3379
85	1.4685
95	1.7203
105	1.7835
115	1.9735
125	2.1344
135	2.4072
145	2.5084
155	2.6911

Tab. S2 Data set for experiments concerning the precision

Repeatability (n = 24; measured value classified as outliner by Dixon's test was rejected)	
Key figure	**Result**
Mean (ng CBN/HPTLC zone)	88.76
SD (standard deviation in ng CBN/HPTLC zone)	3.82
RSD (relative standard deviation in %)	4.30
Results of Neumann trend test	
Test value	30.80
Characteristic value (99 %)	1.11
No trend was observed with a statistical safety of 99 %	
Method precision using sediment sample BT-78 (n = 6; no measured value was classified as outliner by Dixon's test)	
Key figure	**Result**
Mean (ng CBN/HPTLC zone)	131.90
SD (standard deviation in ng CBN/HPTLC zone)	5.36
RSD (relative standard deviation in %)	4.06
Results of Neumann trend test	
Test value	2.69
Characteristic value (99 %)	0.58
No trend was observed with a statistical safety of 99 %	

Tab. S3 Data set for experiments concerning the trueness

Bias calculation with sediment sample BT-102 (spiked with CBN 100 µL, 5.4 µg/ml, i.e. 135 ng CBN/HPTLC zone; average CBN content of the untreated sediment sample: 88.8 ng CBN/HPTLC zone)	
Key figure	**Result**
Mean (ng CBN/HPTLC zone)	237.89
True concentration (ng CBN/HPTLC zone)	223.8
Bias (ng CBN/HPTLC zone)	14.09
Results of Student's t-test	
SD (standard deviation in ng CBN/HPTLC zone)	15.85
Test value	1.54
Critical value [t(2;0.99)]	9.93
no statistical difference between the mean and the "true" values	
Bias calculation with sediment sample BT-145 (spiked with CBN 100 µL, 1.8 µg/ml, i.e. 45 ng CBN/HPTLC zone; average CBN content of the untreated sediment sample: 46.1 ng CBN/HPTLC zone)	
Key figure	**Result**
Mean (ng CBN/HPTLC zone)	104.83
True concentration (ng CBN/HPTLC zone)	91.1
Bias (ng CBN/HPTLC zone)	13.73
Results of Student's t-test	
SD (standard deviation in ng CBN/HPTLC zone)	2.90
Test value	8.20
Critical value [t(2;0.99)]	9.93
no statistical difference between the mean and the "true" values	

Tab. S4 Recovery of the method determined using negative samples spiked with CBN and characteristics of these samples (62,5 ng CBN-d_3/HPTLC zone). Two aliquotes of each sediment sample were used for calculation

Estimated ages (ca cal yrs BP)	Sample ID	Depth in sedimentary core (cm)	Calculated CBN content (ng CBN/HPTLC zone	Calculated CBN content (ng CBN/g sediment)	Target content of CBN (ng CBN/g sediment)	Recovery (%)
380	BT-270.1	86	64.6	249.3	328.2	76
	BT-270.2		66.1	256.4	329.8	78
730	BT-192.1	164	42.8	170.1	248.8	68
	BT-192.2		44.8	174.6	239.9	72
4250	BT-36.1	320	22.1*	87.9	139.2	63
	BT-36.2		28.6	113.7	139.0	82

* below lowest concentration used for calibration; however above LOQ

Tab. S5 Data set for experiments concerning the storage stability of CBN standard solutions (n = 11)

Key figure	Result
2.2 µg/mL, RT, light	
Mean (% initial CBN concentration)	98.26
SD (standard deviation in % initial CBN concentration)	8.31
Results of Neumann trend test	
Test value	1.97
Characteristic value (99 %)	0.7915
No trend was observed with a statistical safety of 99 %	
2.2 µg/mL, RT, dark	
Mean (% initial CBN concentration)	85.97
SD (standard deviation in % initial CBN concentration)	8.68
Results of Neumann trend test	
Test value	1.84
Characteristic value (99 %)	0.7915
No trend was observed with a statistical safety of 99 %	
2.2 µg/mL, -12 °C, dark	
Mean (% initial CBN concentration)	91.04
SD (standard deviation in % initial CBN concentration)	7.94
Results of Neumann trend test	
Test value	1.45
Characteristic value (99 %)	0.7915
No trend was observed with a statistical safety of 99 %	
5.0 µg/mL, RT, light	
Mean (% initial CBN concentration)	103.48
SD (standard deviation in % initial CBN concentration)	6.17
Results of Neumann trend test	
Test value	1.62
Characteristic value (99 %)	0.7915
No trend was observed with a statistical safety of 99 %	
5.0 µg/mL, RT, dark	
Mean (% initial CBN concentration)	104.39
SD (standard deviation in % initial CBN concentration)	9.12
Results of Neumann trend test	
Test value	1.73
Characteristic value (99 %)	0.7915
No trend was observed with a statistical safety of 99 %	
5.0 µg/mL, -12 °C, dark	
Mean (% initial CBN concentration)	97.76
SD (standard deviation in % initial CBN concentration)	9.14
Results of Neumann trend test	
Test value	2.07
Characteristic value (99 %)	0.7915
No trend was observed with a statistical safety of 99 %	

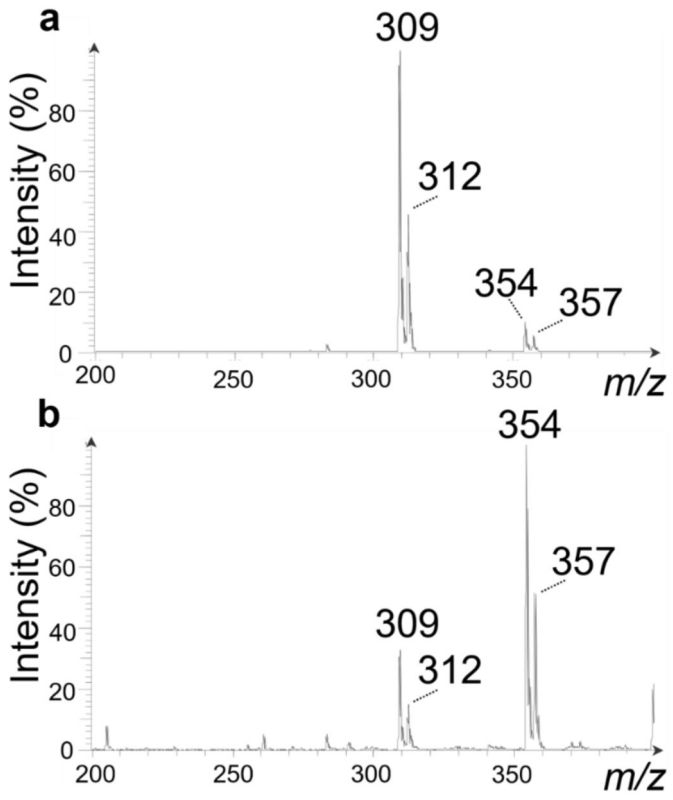

Fig. S2 MS spectrum of a mixture of CBN and CBN-d_3 spotted onto a HPTLC silica gel 60 plate recorded (a) immediately after chromatographic separation and (b) after 3 h [developing solvent: *n*-heptane/diethyl ether (90:10 v/v)]

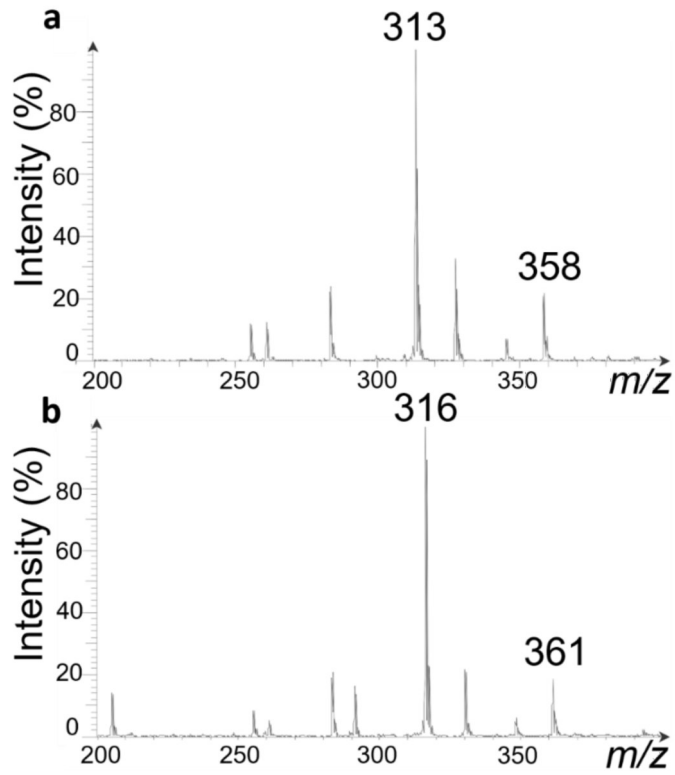

Fig. S3 MS spectrum of (a) CBD and (b) CBD-d_3 spotted onto a HPTLC silica gel 60 plate using *n*-heptane/diethyl ether (90:10 v/v)] as developing solvent

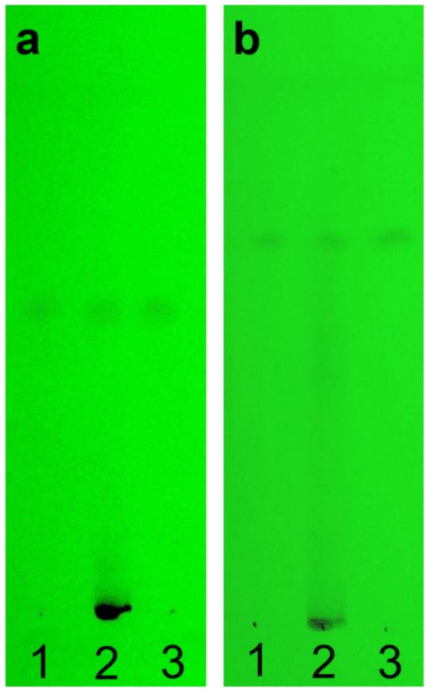

Fig. S4 TLC silica gel 60 plates developed using (a) *n*-heptane/diethyl ether/formic acid (75:25:0.3 v/v/v) and (b) *n*-hexane/acetone/triethylamine (40:20:2 v/v/v) as developing solvent; observed with an UV light source at 254 nm. Tracks: 1 = CBN standard (62,5ng CBN/TLC zone; 125 ng CBN-d_3/TLC zone); 2 = diluted extract [extracting agent: dichloromethane/methanol (1:1 v/v); without a SPE sample preparation] of negative sample BT-270 spiked with CBN (62.5 ng CBN/TLC zone; 125 ng CBN-d_3/HPTLC zone); 3 = CBN standard (125 ng CBN/TLC zone; 125 ng CBN-d_3/TLC zone)

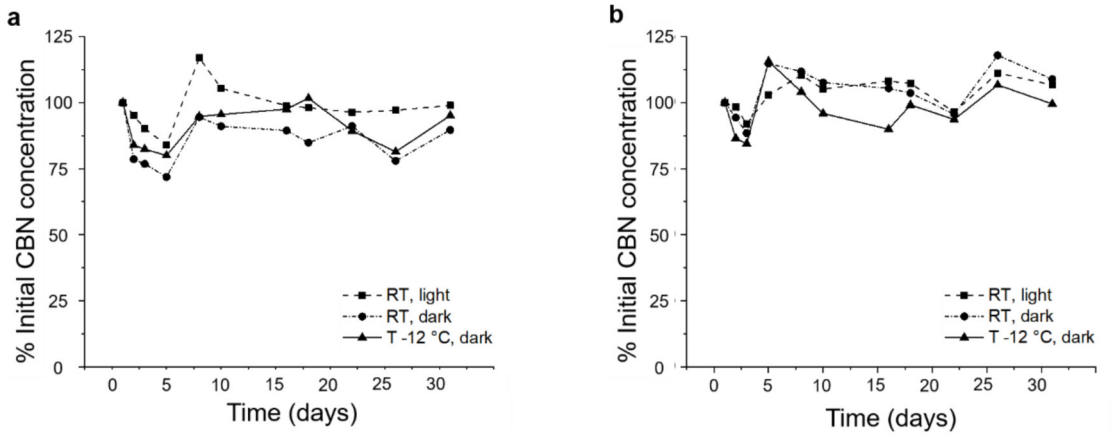

Fig. S5 Variation of CBN concentration in working solutions of CBN stored at -12 °C in the dark, at room temperature in the dark and at room temperature exposed to sunlight, over a period of 31 days. Initial concentration of CBN (a) 2.2 µg/mL; (b) 5.0 µg/mL

P2

Results in Chemistry 3 (2021) 100234

Contents lists available at ScienceDirect

Results in Chemistry

journal homepage: www.sciencedirect.com/journal/results-in-chemistry

Separating the true from the false: A rapid HPTLC-ESI-MS method for the determination of cannabinoids in different oils☆

Theresa Schmidt, Jacqueline Stommel, Tim Kohlmann, Annemarie E. Kramell, René Csuk *

Martin-Luther University Halle-Wittenberg, Organic Chemistry, Kurt-Mothes, Str. 2, D-06120 Halle (Saale), Germany

ARTICLE INFO

Keywords:
CBD oils
Cannabidiol
Tetrahydrocannabinol
Cannabinoids
Cannabis
HPTLC

ABSTRACT

Cannabis is one of the oldest cultivated plant, which has been used by humankind for thousands of years due to its biological properties and a wide range of applications. In total, hemp plants contain over 500 different substances while the characteristic components are the cannabinoids. The most important cannabinoids are (-)-Δ^9-*trans*-tetrahydrocannabinol (Δ^9-THC), cannabidiol (CBD), and cannabinol (CBN – the latter being an oxidation product resulting from Δ^9-THC). In the course of recent years, a paradigm shift has taken place with regard to the use of products and ingredients derived from hemp, especially CBD. Thus, an ever-increasing number of products containing CBD are on the market; this ranges from classic CBD oil to CBD chewing gum and even CBD shampoo. Despite an increasing presence of these products in the market, the regulation of cannabinoids in these products is very inconsistent in different countries, except for Δ^9-THC whose limit is 0.2% for many products and many countries. The enormous abundance of CBD-containing products calls for the development of new analytical techniques that allow a reliable and quick determination of the main cannabinoids usually found in hemp. This seems all the more necessary since previous examinations of CBD oils often revealed a difference between the declared amount and the actual content of the ingredients. Many methods usually applied to determine cannabinoids are rather time-consuming and associated with high costs. In this study, we developed and validated a sensitive, simple, reliable as well as fast method for the determination of CBN, CBD and Δ^9-THC in commercially available CBD oils using high-performance thin-layer chromatography (HPTLC) combined with electrospray ionization mass spectrometry (ESI-MS). Thus, for this method, a recovery rate of $\geq$ 90% was determined. This procedure enables both qualitative and quantitative analyses of CBN, CBD and Δ^9-THC in CBD oils of different matrices such as hempseed oil, olive oil or sunflower oil. Thus, this method is a helpful and fast tool to investigate a broad variety of commercially available CBD oils.

1. Introduction

Several CBD (cannabidiol)-based products obtained from flowers and leaves of hemp varieties are distributed in the different retail sectors, such as shops selling items of daily use, “hemp” shops and in internet shops. The products are marketed in a variety of forms, such as oils, balms, capsules, sprays and even as foodstuffs like gummy bears or chewing gums. CBD oils are prepared from the concentrated solvent extracts made from cannabis flowers or leaves, that have been diluted with edible oils such as olive, sunflower or hemp seed oil. For extraction, organic solvents (e.g. ethanol and isopropyl alcohol) or supercritical fluids (CO_2) are exploited [1]. Besides CBD, phyto-cannabinoids such as Δ^9-THC [(-)-Δ^9-*trans*-tetrahydrocannabinol] and other plant components are co-extracted. As a consequence, varying amounts of these compounds are found in CBD oils; their amount depends on the used hemp variety, the cultivation conditions of the hemp plants, the extraction procedure and the subsequent treatment of the extracts [1-3]. Previous studies reported on an inaccurate labeling of some CBD-based products sold online regarding their CBD and Δ^9-THC content because of a lack of specific regulations for the manufacturing process or due to missing quality standards [4,5]. For instance, a study from the USA revealed – with respect to CBD – approximately 25% of the examined

☆ Professor René Csuk, the corresponding author on this paper is a member of the advisory board but this author had no involvement in the peer review process used to assess this work submitted to Results in Chemistry. This paper was assessed and the corresponding peer review managed by Professor Yilun Ying, an editor working on Results in Chemistry.

* Corresponding author.
E-mail address: rene.csuk@chemie.uni-halle.de (R. Csuk).

https://doi.org/10.1016/j.rechem.2021.100234
Received 30 July 2021; Accepted 1 November 2021
Available online 6 November 2021

oils were under-labeled, 30% were over-labeled and only 45% were accurately labeled [5]. Furthermore, Δ^9-THC was detected up to a concentration of 6.43 mg/mL for approximately 21% of the tested CBD products (oils, tinctures and vaporization liquids). These findings agree with studies of the US Food and Drug Administration and have triggered warning letters to several businesses [4]. Inaccurate labeling of some CBD or cannabis oils concerning the CBD and Δ^9-THC content was also proven for products from the European market [1,6]. Relatively high Δ^9-THC contents of some products, however, are of concern because of the psychotropic properties of Δ^9-THC and several adverse effects of orally administered Δ^9-THC such as nausea, vomiting, panic, paranoid reactions and probably tachycardia as well as hypotension [7]. Some case reports of consumers described Δ^9-THC-like side effects after the consumption of CBD products [6,8]. Studies of Lachenmeier et al. revealed that some CBD oils and CBD oil supplements exceed the Δ^9-THC LOAEL (lowest observed adverse effect level) of 2.5 mg Δ^9-THC per day and were assessed as harmful to health [6]. In contrast to Δ^9-THC, CBD is not a controlled substance in the European Union since this compound is not psychoactive. It is an anticonvulsant, neuroprotective antioxidant, analgesic and anti-nausea active molecule [9] and may be a useful treatment for a number of medical conditions [10]. However, there is only a pre-clinical evidence for most indications, with the exception of the treatment of two rare, severe forms of childhood-onset epilepsy. Since 2019, the CBD-based medicinal product Epidyolex is approved in the European Union for the treatment of these forms of childhood-onset epilepsy [11].

CDB oils are available in internet shops, drug stores or organic shops; they are marketed as sleeping aids, for pain relief or for stress reduction. However, dubious advertising texts representing CBD based products as some kind of “miracle cures” can also be found on some websites, e.g. for self-medicating of cancer [4,6].

Usually, chromatographic methods such as (U)HPLC [(ultra) high performance liquid chromatography] or gas chromatography (GC) are used for the detection and determination of cannabinoids in oil samples [5,6,12-15]. Furthermore, high-performance thin-layer chromatography (HPTLC) analysis of commercially available cannabis oils applying RP-18 HPTLC plates and 100% acetonitrile as developing solvent, were described by Yotoriyama et al. [15]. Here cannabinoids such as CBD and Δ^9-THC were detected by a post-chromatographic detection reaction with FBS (Fast Blue Salt B) reagent. However, due to the low detection sensitivity, no cannabinoid was detected in extracts from examined oils.

In this study, we report on the development and validation of a HPTLC-ESI-MS (electrospray ionization mass spectrometry) method for the identification and quantification of CBD, Δ^9-THC and CBN (cannabinol) in CBD oils purchased from different internet shops, enabling a fast and accurate high-throughput screening of CBD oils based on olive, sunflower or hemp seed oil matrices. CBN is one of the most important degradation products of CBD and Δ^9-THC found in Cannabis oils exposed to air, and light during storage [16].

2. Results and discussion

2.1. Development of a fast HPTLC-ESI-MS method for the identification and quantification of the three main cannabinoids (CBN, CBD, Δ⁹-THC) in commercially available CBD oils

The content of CBN, CBD and Δ^9-THC of commercially available CBD oils, purchased from internet shops, was determined by a combination of planar chromatography via HPTLC and ESI-MS. The examined CBD oils are mixtures of hemp seed extracts and a carrier oil, for exmple hemp seed oil, sunflower oil or olive oil; as a consequence, the matrix of the oils differs depending on the individual carrier oil. In addition to the three main cannabinoids, other ingredients were also detected in the oils, such as cannabidiolic acid (CBDA, *m/z* 357) or Δ^9-tetrahydrocannabinolic acid (Δ^9-THCA, *m/z* 357), which can also have an impact on the subsequent analysis. For full MS spectra of some CBD oil samples see Supplementary Material Fig. 1. Besides the peak of CBD and Δ^9-THC, which can not be distinguished by direct infusion (because they have the same molecular weight) there are only a few more signals – depending on the carrier oil. During the first extraction tests it could estrablished that for the given concentration of CBD in the oils, a higher dilution is required to allow a simple and rapid detection of CBN, CBD and Δ^9-THC using HPTLC-ESI-MS. If the concentration of CBD on the HPTLC plate is too high, other spots will overlap, making it thus impossible to determine a specific analyte with HPTLC-ESI-MS. For analyses, CBD oils were diluted with *n*-hexane. The dilution factor of CBD oil/*n*-hexane (0.1:100, w/v) enables a satisfactory resolution as well as a separation of the cannabinoids using HPTLC plates and due to the high dilution – no interfering matrix components were detected (see Fig. 1).

Thus, an elimination of matrix compounds, e.g. by a SPE (solid-phase extraction) sample preparation, is not necessary. CBD oil/*n*-hexane mixtures were spotted onto HPTLC plates, these plates were developed using *n*–hexane/diethyl ether (80:20 v/v) [17] and the HPTLC zones were analyzed by ESI-MS (MS scan range *m/z* 200–400). For optimization of the chromatographic separation, different solvents were tested. The cannabinoids were nicely separated, for example with *n*-hexane/acetone/triethylamine (40:20:2 v/v/v) [18], *n*-heptane/diethyl ether/formic acid (40:20:0.3 v/v/v) [19] or cyclohexane/isopropyl ether/triethyl amine (52:40:8 v/v/v) [20]. Many elution systems gave no clean separation of the cannabinoids or even, no separation at all. An excellent separation, however, showing the largest distance between the bands of CBN, CBD and Δ^9-THC gave a mixture of *n*–hexane/diethyl ether (80:20 v/v) (see Fig. 2). For an unambiguous determination of CBD and Δ^9-THC by HPTLC-ESI-MS, an adequate separation of these isomers – with respect to the size and dimensions of the elution head – is mandatory.

Also, different ratios of *n*–hexane/diethyl ether were tested (60:40 v/v; 75:25 v/v; 85:15 v/v; 90:10 v/v). However, an appropriate resolution between the analyte bands enabling the determination of CBD and Δ^9-THC contents in oils by HPTLC-MS was only achieved using *n*–hexane/diethyl ether with a ratio of 80:20 v/v as developing solvent (Table 1). Thus, an influence of the individual spots among each other and their

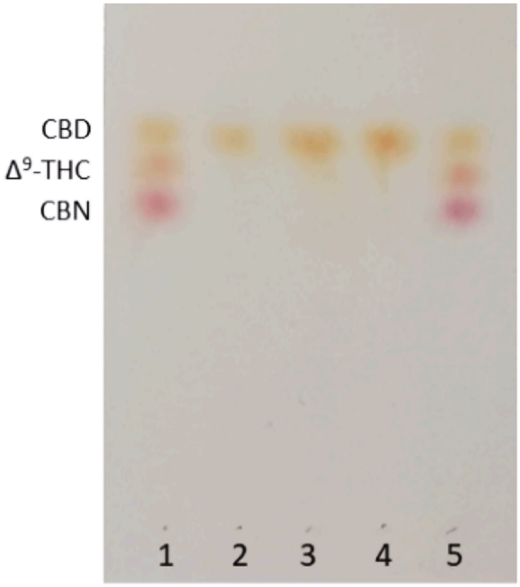

Fig. 1. Chromatographic separation of CBD oil/*n*-hexane (0.1:100 w/v) with *n*-hexane/diethyl ether (80:20 v/v) [spot 1 and 5: 250 ng cannabinoid standard (CBN, CBD, Δ^9-THC)/HPTLC zone; spot 2: CBD-Oil-1; spot 3: CBD-Oil-5; spot 4: CBD-Oil-7]; detection of the analyte bands with FBS reagent.

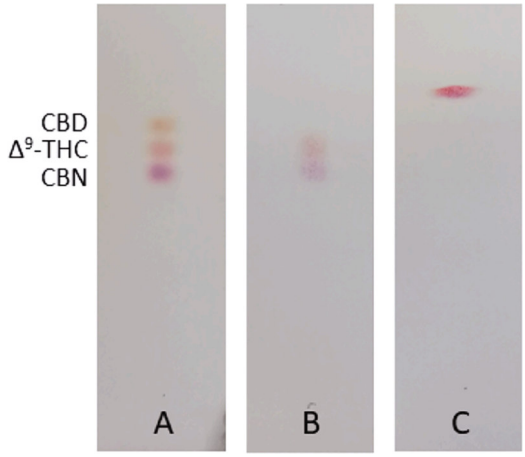

Fig. 2. Optimization of the chromatographic separation of a cannabinoid standard solution (CBN, CBD, Δ^9-THC) employing different elution solvents; A: *n*–hexane/diethylether (80:20 v/v); B: *n*-hexane/acetone/triethylamine (40:20:2 v/v/v); C: *n*-heptane/diethylether/formic acid (40:20:0.3 v/v/v); detection of the analyte bands with FBS reagent.

Table 1
Retention factors (rf) of CBN, CBD and Δ^9-THC after separation with different ratios of *n*-hexane/diethyl ether as developing solvent and color of the cannabinoid bands after detection with FBS spray reagent.

Ratio of *n*-hexane/diethyl ether	rf_{CBN}	rf_{CBD}	$rf_{\Delta 9\text{-THC}}$
60:40 v/v	0.73	0.81	0.77
75: 25 v/v	0.77	0.86	0.84
80:20 v/v	0.53	0.71	0.63
85:15 v/v	0.68	0.81	0.74
90:10 v/v	0.88	0.93	0.98
Color of cannabinoid band	Magenta	Orange	Red

content determination can be excluded.

Deuterated cannabinoids were used for quantification of the analyzed cannabinoid content evaluating peak area ratios (peak area of non-deuterated cannabinoid to peak area of deuterated cannabinoid). Mass spectra of standards eluted from HPTLC silica gel 60 plates show for each analyzed cannabinoid intense peaks which can assigned to the quasi-molecular ions $[M-H]^-$ of the non-deuterated and deuterated cannabinoids (CBN/CBN-d_3: *m/z* 309 and 312; CBD/CBD-d_3: *m/z* 313 and 316; Δ^9-THC/Δ^9-THC-d_3: *m/z* 313 and 316). Furthermore, extra mass peaks were observed for working solutions of CBN, CBD and Δ^9-THC spotted onto HPTLC plates (CBN/CBN-d_3: *m/z* 354 and 356; CBD/CBD-d_3: *m/z* 327, 358 and 330, 361; Δ^9-THC/Δ^9-THC-d_3: *m/z* 345, 358 and 348, 361; see Fig. 3. This observation is also known from previous investigations [21]. The signals appear after the application of the cannabinoid standards onto the HPTLC plate, but they are not detectable in fresh or aged methanolic working solutions or by measurements of the silica gel of the HPTLC plate. It was also observed that the more time elapsed between development of the chromatogram and the measurement by HPTLC-ESI-MS, the higher the proportion of the extra mass peaks. For this reason, it was possible to exclude the possibility that these signals were impurities from the solvents or from the HPTLC plates. Also, comprehensive TLC and HRMS studies on CBN and CBN-d_3 indicated that theses peaks point to the presence of transient adducts with silica gel from the HPTLC plates. Experiments with CBD and CBD-d_3 also indicate a formation of adduct ions. Thus, additional peaks (see above) were included in the quantitative determination of CBN, CBD and Δ^9-THC. Furthermore, investigations were performed immediately after chromatographic separation because of the increasing peak intensities in the ESI-MS of the additional peaks with advancing time.

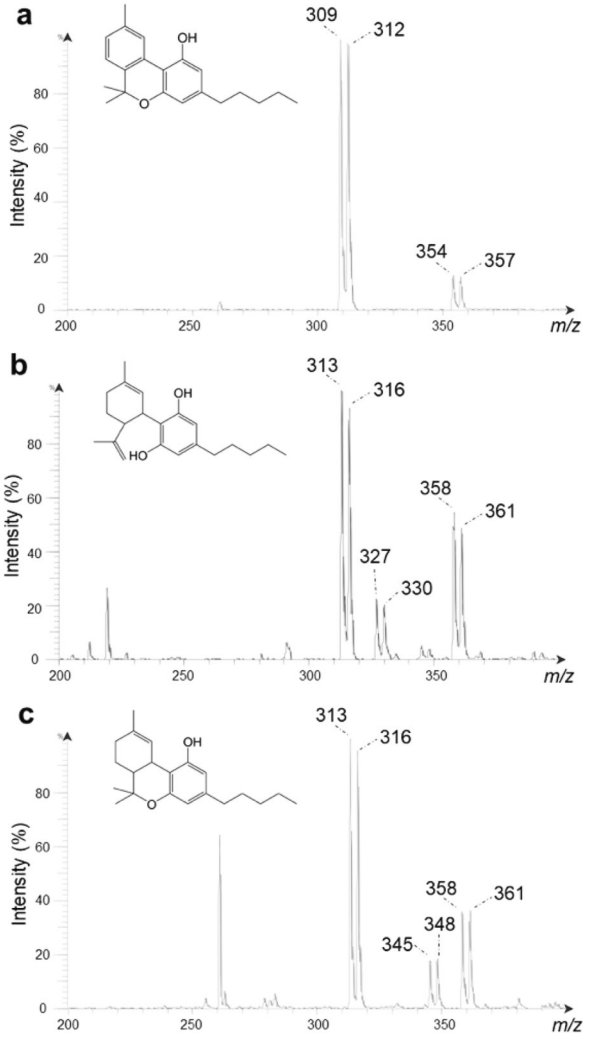

Fig. 3. MS spectrum of (a) CBN, (b) CBD and (c) Δ^9-THC spotted onto a HPTLC silica gel 60 plate recorded immediately after chromatographic separation using *n*-hexane/diethyl ether (80:20 v/v) as developing solvent and the structure of each analyzed cannabinoid.

2.2. Detection for HPTLC spots of CBN, CBD and Δ^9-THC

The detection of the cannabinoid spots with the light of an UV lamp ($\lambda = 254$ nm) is of limited value since only the CBN spot can be detected. Other wavelengths could not be observed due to the incorporated fluorescence indicator ($\lambda_{max} = 254$ nm) on the HPTLC plates. For CBD and Δ^9-THC, other detection methods have to be used in order to determine the spot area for the HPTLC-ESI-MS measurements. Thereby, an unambiguous detection of the individual spots is necessary since the spots must be marked. Subsequent, only the marked spots were extracted with methanol (by the elution head of the *plate express* unit), and the analytes were guided to the ESI-MS source. To establish the different UV absorption of the cannabinoids, their respective UV spectra were determined.

The cannabinoids showed two main absorption bands in methanol in the UV range from 200 to 350 nm (Fig. 4). At the natural neutral pH value being present in the methanolic solutions, it can be assumed that only the completely protonated compounds are present. The pK_a of Δ^9-THC is 10.6 [22], therefore two pH units below this ensures that only the

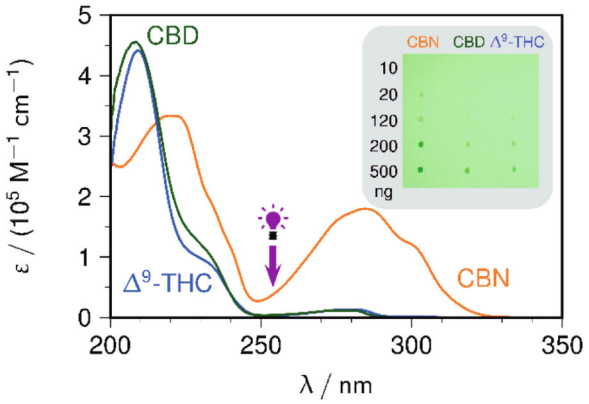

Fig. 4. Absorption spectra of CBN (orange), CBD (green) and Δ^9-THC (blue) in methanol (10 µg / ml), the wavelength of the UV lamp at 254 nm used for the HPTLC spot detection is indicated by a violet arrow; Inset: HPTLC plate with F_{254} fluorescence indicator with spots of CBN, CBD and THC (diameter 1.5 mm, dissolved in methanol and air-dried) with amounts of 10, 20, 120, 200 and 500 ng cannabinoid per spot under 245 nm light, darkened points indicate a sufficient amount of cannabinoid for visual detection. (For interpretation of the references to color in this figure legend, the reader is referred to the web version of this article.)

neutral form exists. In the case of CBN and CBD, no experimental pK_a values are available in the literature, but they should still be >9, based on a comparison with the core structure resorcinol (pK_a = 9.32 [23]). This is also supported by computational pK_a calculations for the two compounds [24]. Additionally, the presence of CBD in a single protonation state, is underlined by the fact that the absorption spectra between Δ^9-THC and CBD are remarkably similar both in the location of the absorption bands and in the extinction coefficient. The cyclization obviously has no influence on the absorption of the cannabinoids. The absorption band at 280 nm is characteristic of the phenolic core structure and shows the HOMO-LUMO $\pi \rightarrow \pi^*$ transition [24,25]. Δ^9-THC has two poorly separated maxima at 276 and 283 nm and CBD some at 274 and 281 nm. In addition, a clearly more intense band with maxima at 209 nm for Δ^9-THC and CBD exists. However, the absorption spectrum of CBN differs significantly from the other two. CBN shows a pronounced band with a maximum at 285 nm and a shoulder at 298 nm and an extinction coefficient at 280 nm that is about 15 times higher than that of the other two derivatives. The reason for this is the additional conjugation via the second aromatic ring in CBN. The second major absorption band has a maximum at 221 nm. The high extinction coefficient of the CBN at 254 nm ($\varepsilon_{254} = 3800\ M^{-1}\ cm^{-1}$) enables easy visual detection of the CBN spots on the HPTLC plate using a standard 254 nm UV lamp. This is particularly important because, in contrast to spray reagents, non-destructive direct detection is possible here. The inset in Fig. 4 shows an HPTLC plate with F_{254} fluorescence indicator and spots of CBN, CBD and Δ^9-THC (diameter 1.5 mm, dissolved in methanol and air-dried) with amounts of 10, 20, 120, 200 and 500 ng cannabinoid per spot under 245 nm light. Even 20 ng of CBN can be clearly recognized as darkened spots. In the case of Δ^9-THC and CBD, this visual detection is only possible with significantly larger quantities above 120 ng due to the small extinction coefficients with $\varepsilon_{254} < 360\ M^{-1}\ cm^{-1}$.

After the elution of the analyte bands with *n*–hexane/diethyl ether (80:20 v/v), the visual detection limit of CBD and Δ^9-THC was significantly decreased thus not allowing a visual inspection of the individual spots (see Fig. 5).

Based on these results, a spray reagent was needed to optimally mark the analyte zones for the elution head so that the analytes could be measured with as little loss as possible.

For the detection of cannabinoids, different spray reagents were tested, and the FBS reagent showed the best results. From literature, the

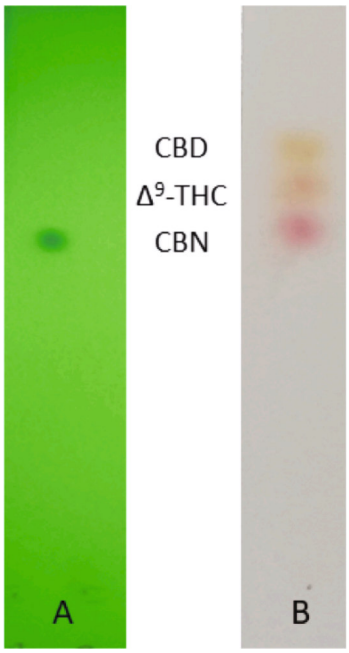

Fig. 5. Cannabinoid standard solution (CBN, CBD, Δ^9-THC) after chromatographic separation with *n*–hexane/diethyl ether (80:20 v/v); A: detection of the analyte bands with UV light by 254 nm; B: detection of the analyte bands with FBS reagent.

FBS reagent is known as a selective and sensitive detection reagent for the post-chromatographic detection of cannabinoids such as CBN, CBD and Δ^9-THC [21,26-28]. After staining with FBS reagent, differently colored cannabinoid bands were observed (see Table 1). As described in a previous study of Hazekamp et al. [27], FBS reagent is more sensitive for the detection of cannabinoid bands than UV-detection at λ = 254 nm. This is particularly relevant for CBD and Δ^9-THC, because low concentrations of these compounds, spotted onto HPTLC plates, are not detectable under UV light at λ = 254 nm (see above). Thus, FBS reagent is a suitable complement for the detection of cannabinoids by ESI-MS.

2.3. *Validation results of HPTLC-ESI-MS method*

Linearity, LOD and LOQ of the HPTLC-ESI-MS method were evaluated after chromatographic separation. Furthermore, these parameters were assessed after direct infusion ESI-MS. The results from the validation are summarized in Table 2 (further data see Supplementary Material, Tables 1–7 and Figs. 2–7). LOD and LOQ were considered adequate for the purposes of the present study.

Examined CBD oils were diluted with olive, sunflower and hemp seed oils during the manufacturing process. Thus, these edible oils were used for the determination of validation parameters such recovery rates, bias and method precision.

The developed HPTLC-ESI-MS method is specific for the determination of CBN, CBD and Δ^9-THC in examined CBD oils. The post-chromatographic detection with FBS reagent and the HPTLC-ESI-MS analyses of olive oil, sunflower oil, hemp seed oil and CBD oil samples showed that the analyzed cannabinoids (CBN, CBD, Δ^9-THC) can be qualified and quantified in the presence of matrix components. Other related compounds being present in examined CBD oils did not interfere with CBN CBD and Δ^9-THC during HPTLC-ESI-MS analyses. Also, the system precision and the method precision were determined with a RSD of 4.8% and 6.8% for CBN, 4.0% and 4.3% for CBD as well as 9.6% and 7.0% for Δ^9-THC (see Supplementary Material, Tables 8–12). For

Table 2
Linearity, LOD, and LOQ for CBN, CBD and Δ^9-THC determination by HPTLC-ESI-MS (tv…test value; cv…characteristic value).

Key figures	Results		
	CBN	CBD	Δ^9-THC
Range (ng/HPTLC zone)	25–160	50–500	35–160
r^2 (coefficient of determination)	0.9982	0.9962	0.9931
Sy (residual standard deviation)	0.105	0.038	0.039
Sx (standard deviation for the method)	7.790	9.960	3.809
Residuals are normally distributed (R/s test, 99%)	Yes (tv = 3.58; cv = 2.51–3.87)	Yes (tv = 3.49; cv = 2.51–3.87)	Yes (tv = 3.22; cv = 2.51 – 3.87)
Residuals show a trend (Neumann trend test, 99%)	No (tv = 1.79; cv = 0.75)	No (tv = 1.93; cv = 0.75)	No (cv = 3.06; cv = 0.75)
Equation curve	y(x) = 0.0127x − 0.0086y: peak area ratio of CBN and CBN-d_3x: concentration of CBN (ng CBN/ HPTLC zone)	y(x) = 0.0038x + 0.0295y: peak area ratio of CBD and CBD-d_3x: concentration of CBD (ng CBD/ HPTLC zone)	y(x) = 0.0103x − 0.0278y: peak area ratio of Δ^9-THC and Δ^9-THC-d_3x: concentration of Δ^9-THC (ng Δ^9-THC/HPTLC zone)
LOD (ng/ HPTLC zone)	3.6	16.6	7.0
LOQ (ng/ HPTLC zone)	16.6	38.9	29.3
Results of the Mandel's test according to DIN 32,645			
Optimal regression model	Linear (tv = 1.79; cv = 0.75)	Linear (tv = 0.61; cv = 12.24)	Linear (tv = 0.12; cv = 12.24)
Linear regression acceptable	Yes	Yes	Yes

measured values of precision, no trend was observed and the two measured values, which were classified as outliner by Dixon's test, were removed from the evaluation. Recovery rates of the cannabinoids after sample preparation were determined with samples of olive oil, sunflower oil and hemp seed oil in triplicate at two different concentration levels. The recovery rate of CBN range from 77.6% to 98.4% (average recovery rate of 89.5%), CBD from 81.4% to 99.7% (average recovery rate of 89.4%) and Δ^9-THC from 79.5% to 101.3% (average recovery rate of 92.8%). The recovery rates of CBN, CBD and Δ^9-THC for oil samples spiked with analytes before picking an aliquot for subsequently dilution with *n*-hexane are 96.2% for CBN, 87.0% for CBD and 98.1% for Δ^9-THC. No statistical difference has been observed between the mean and the "true" values (see Supplementary Material, Tables 16–18). Furthermore, the recovery rates of CBD, Δ^9-THC and CBN for the above-described spiking experiments (see recovery) were very similar (see Supplementary Material, Tables 13–15). The storage stability of cannabinoid standard solutions was evaluated under different conditions (at –12 °C in the dark, at room temperature in the dark and exposed to sunlight). In a previous work the stability of CBN standard solution over a period of four weeks was evaluated and no trend was observed [21]. For this work, the stability of CBN, CBD and Δ^9-THC were observed over a period of six months. The tests showed that the deviation for the concentration of CBN is not higher than 81%, for CBD the measured concentration does not exceed 65% of the initial concentration, and for Δ^9-THC the concentration did not decrease more than 76% (for diagrams see Supplementary Material Figs. 8–10). By using a Neumann trend test, no trend was observed and no measured value was identified as outlier by Dixion's test. Furthermore, it was evident that over a period of six months the measured concentration of all analyzed cannabinoids decreased more when the standard solutions were stored at room temperature exposed to sunlight, as compared to their storage at room temperature in the dark or at −12 °C in the dark. Based on these results and the maximum average change of the concentration related to the initial concentration for CBN (3% for 2 μg/mL and 4 μg/mL), CBD (4% for 2 μg/mL; 1% for 4 μg/mL) and Δ^9-THC (2% for 2 μg/mL; 3% for 4 μg/mL), it can be concluded that the standard solutions are stable over a long period when they were stored at −12 °C in the dark.

In summary, the method gives satisfactory results and enables a sensitive as well as selective, fast and simple determination of CBN, CBD and Δ^9-THC contents in commercially available CBD oils.

2.4. Analysis of CBD oils

The quantitative determination of the main cannabinoids CBN, CBD and Δ^9-THC in commercially available CBD oils was performed by HPTLC-ESI-MS. Therefore, fifteen commercially available CBD oils were analyzed each in triplicate. The results of the determination of CBN, CBD and Δ^9-THC of these samples were summarized as average amount in Table 3. Commercially available and for household use declared olive oil, sunflower oil and hempseed oil were used as negative samples. Post-chromatographic detection reactions with FBS as well as HPTLC-ESI-MS studies confirmed the absence of CBN, CBD and Δ^9-THC content in these negative oil samples.

CBN is a degradation product from the oxidation process from Δ^9-THC, and the detection of CBN is a good evidence for oxidation during the extraction or inadequate storage condition, so the quality of the CBD oil can be evaluated. In all analyzed oil samples, the content of CBN was determined under LOD (3.6 ng CBN/HPTLC zone) or was not measurable. Just in case of CBD-Oil-14 the CBN content was over limit of detection but far below under limit of quantification, which also does not allow to make a conclusion about the CBN content in the analyzed CBD oil. For this reason, the CBN content is not listed in the subsequent table.

The triplicate test results of the CBD and Δ^9-THC content were averaged and are reported by weight percentage. The variation of CBD in the analyzed CBD oil samples is between 1.2 and 11.3%. The declared CBD content of each CBD oil is summarized in Table 3, which varied between 1.8 and 33.0%. The analyzed CBD content from CBD-Oil-1 to CBD-Oil-4 is – except to a difference of maximal 0.4% – similar to the declared CBD content. For CBD-Oil-9 there is a difference of 0.6% between the determined and advertised CBD content, but for the CBD oils 7, 8, 10, 14 and 15 there was just an insignificant difference of 0.1% between the measured and declared CBD content. The CBD amount of CBD-Oil-5 was determined with 11.3%, but the declared CBD content was only 10% and was the highest determined deviation with 1.3%. Most of the determined CBD amounts were over the declared CBD content, with some exceptions. For example, CBD-Oil-6 showed a difference of 1.1% and in CBD-Oil-11 to 13 there was no CBD measurable or detectable at all.

The obtained results from Δ^9-THC content show that 12 out of 15 CBD oils contain Δ^9-THC; this finding is important to note due to its potential of intoxicating activity [13]. The Δ^9-THC content was mainly

Table 3
Declared CBD contents in weight percent (% w/w), oil matrices (O…olive oil; S…sunflower oil; H…hempseed oil), average CBD and Δ^9-THC content in the analyzed CBD oil samples in ng/HPTLC zone and in weight percent (% w/w) as well as in µg/g and countries of product origin of the examined CBD oils. Analyses of the CBD and Δ^9-THC content including the described preparation and separation procedure were performed in triplicate (LOD…limit of detection; LOQ…limit of quantification).

		Declared CBD content (% w/w)	Average CBD content (ng CBD/HPTLC zone)	Average CBD content (µg/g)	Determined CBD content (% w/w)	Average Δ^9-THC content (ng Δ^9-THC /HPTLC zone)	Determined THC content (% w/w)	Product origin
CBD-Oil-1	O	5	204.7	52721.2	5.3	<LOQ	–	Switzerland
CBD-Oil-2	O	2.5	95.3	26697.3	2.7	<LOQ	–	Switzerland
CBD-Oil-3	O	5	190.7	53891.1	5.4	<LOQ	–	Germany
CBD-Oil-4	S	5	171.9	51057.7	5.1	<LOQ	–	Switzerland
CBD-Oil-5	S	10	385.4	113414.3	11.3	45.2	1.3	Switzerland
CBD-Oil-6	H	5	146.4	39436.1	3.9	<LOQ	–	Germany
CBD-Oil-7	H	10	374.5	100635.6	10.1	30.4	0.8	Austria
CBD-Oil-8	H	5	170.7	49189.3	4.9	<LOQ	–	Austria
CBD-Oil-9	H	1.8	40.0	11786.2	1.2	<LOQ	–	USA
CBD-Oil-10	H	5	161.6	50105.7	5.0	<LOQ	–	Germany
CBD-Oil-11	H	3.6	<LOD	–	–	<LOD	–	China
CBD-Oil-12	H	16	<LOD	–	–	<LOD	–	New Zealand
CBD-Oil-13	H	33	<LOD	–	–	<LOD	–	United Kingdom (UK)
CBD-Oil-14	H	5	181.5	49173.2	4.9	<LOQ	–	Netherlands
CBD-Oil-15	H	5	188.5	49000.7	4.9	<LOQ	–	Germany

under LOD and LOQ, thus a detailed determination of the amount was not possible. For better categorization of the Δ^9-THC content in relation to the European limit value of 0.2% [29] the Δ^9-THC content should be determined by other methods again (for example see Pavlovic et al. [13]). Two of all Δ^9-THC positive oil samples (CBD-Oil-5 and CBD-Oil-7) contain an increased content (1.3 and 0.8%). This is much higher than admitted in the EU and contradicts the declaration of the manufacturer declaring this CBD oil as Δ^9-THC-free. Both CBD oils with a Δ^9-THC content over 0.2% have a CBD content nearly 10%, so it can be assumed that the higher the CBD content of the oil was determined, the higher was also their the Δ^9-THC content. An interference between CBD and Δ^9-THC during the HPTLC-ESI-MS method was not observed and can be excluded (see Development of HPTLC-ESI-MS method) but it can be supposed that this correlation is due to the extraction process, which is, however, not described in the package insert. The variation in the results show the importance of the regulations regarding the amount of Δ^9-THC in commercially available CBD oil that should specify the latter.

Most of the analyzed CBD oils had an accurate labeling of their CBD content. The three wrong labeled CBD oils, where no CBD was determined, have some flavor added (e.g. peppermint) which might influence the results. As a conclusion, our HPTLC-ESI-MS method is a suitable and fast method to measure the CBD content in commercially available CBD oils.

3. Conclusions

In this publication, we report the application of a sensitive and selective HPTLC-ESI-MS for identification and quantification of CBN, CBD and Δ^9-THC content in CBD oils. During method development, the chromatographic separation between the analyzed cannabinoids was optimized. For the evaluation of the potential of the method validation parameter such as LOD, LOQ, linearity, recovery rate, precision, trueness and storage stability were determined. The validated method showed satisfactory results, and most of the tested CBD oil samples had correct labeling with respect to their advertised cannabinoid content.

In conclusion, this HPTLC-ESI-MS method is a simple, fast and low-cost method for the qualification and quantification of the three main cannabinoids CBN, CBD and Δ^9-THC in commercially available CBD oils. Only about 30 min are needed to completely characterize an oil and determine its cannabinoid content, whereby up to five CBD oils can be applied and measured per HPTLC plate. The regulations and analytical methods for cannabinoid analysis and use are still very unregulated in Germany and usually very labor-intensive and time-consuming, e.g. using HPLC following previous extraction procedures. For the developed HPTLC-ESI-MS method, no clean-up procedure nor an extraction of the target analytes is necessary. The oil sample can be used without any preparation; due to the high dilution the matrix does not interfere with the target analytes. Furthermore, no time-consuming derivatization of the analytes are required such as its often the case by GC or HPLC methods. Our method can be used for a rapid verification of specified cannabinoid contents in CBD oils providing also a high sample throughput. By determining the cannabinoid content, the classification in existing regulations and comparison with the existing limits is possible but also incorrectly declared products can be detected.

4. Experimental

4.1. Chemicals and materials

Analytical cannabinoid standards CBN, CBD, Δ^9-THC (1 mg/mL in methanol, certified reference material) and CBN-d_3, CBD-d_3, Δ^9-THC-d_3 (100 μg/mL in methanol, certified reference material) were bought from Cerilliant and Supelco; acetonitrile (HPLC super gradient grade) was obtained from Honeywell Riedel-de Haën; methanol (HPLC gradient grade) from VWR Chemicals; *n*-hexane (HPLC grade) from VWR Chemicals and Fisher scientific; dichloromethane (HPLC grade) from Carl Roth; triethylamine from ARCOS Organics; Fast Blue Salt B (FBS, dye content ~ 95%) from Sigma-Aldrich and HPTLC plates [silica gel 60 F_{254} MS-grade for matrix-assisted laser desorption/ionization (MALDI)] were purchased from Merck KGaA. Distilled diethyl ether and acetone were produced with a rotary evaporator from BÜCHI.

4.2. Preparation of standard solutions

Stock solutions of CBN, CBD and Δ^9-THC from Cerilliant and Supelco (1 mg/mL in methanol) were diluted with methanol to obtain working solutions down to a concentration of 1 μg/mL. CBN–d_3, Δ^9-THC-d_3 (3.6 μg/mL) as well as CBD-d_3 (3.6 and 11.0 μg/mL) working solutions as internal standards were prepared in methanol. For calibration, different mixtures of CBN/CBN-d_3, CBD/CBD-d_3 and Δ^9-THC/Δ^9-THC-d_3 were prepared (CBN and Δ^9-THC: in the range of 1.0–6.4 μg/mL, CBN- d_3 and Δ^9-THC-d_3: 3.6 μg/mL; CBD: in the range of 1.0–6.4 μg/mL and 2.0–20.0 μg/mL, CBD- d_3: 3.6 and 11.0 μg/mL). For the validation of the HPTLC-ESI-MS method, different mixtures of CBN/CBN-d_3, CBD/CBD-d_3 and Δ^9-THC/Δ^9-THC-d_3 were utilized (CBN and Δ^9-THC: 2.4, 3.4, 4.8 μg/mL; CBN- d_3 and Δ^9-THC-d_3: 3.6 μg/mL; CBD: 3.4, 6.0, 16.0 μg/mL; CBD-d_3: 3.6 and 11.0 μg/mL).

4.3. Detection for HPTLC spots of CBN, CBD and Δ^9-THC

For investigations concerning the UV–vis activity of cannabinoids, working solutions of CBN, CBD and Δ^9-THC (10 μg/mL) were prepared. Spectra of absorption were recorded in the range of $\lambda = 200$–350 nm. For measurements, a Shimadzu UV-1800 spectrophotometer was used. Furthermore, working solutions of CBN, CBD and Δ^9-THC were spotted onto HPTLC plates, HPTLC plates were developed in *n*-hexane/diethyl ether (80:20 v/v) and investigated under UV light at $\lambda = 254$ nm.

The detection of the cannabinoid spots occurred with the FBS spray reagent (modified according to an application note from CAMAG [19]). FBS reagent was used for a post-chromatographic detection of cannabinoid working solutions (25 μL aliquots) spotted onto HPTLC plates. For the preparation of the FBS reagent, FBS (10 mg) was completely dissolved in distilled water (2 mL) and was mixed with methanol (10 mL) and dichloromethane (6 mL). FBS reagent was freshly prepared before use and was applied to the HPTLC plates with a 10 mL nebulizer. HPTLC plates were developed in *n*-hexane/diethyl ether (80:20 v/v; see Pacifici et al. [30]) and sprayed with a mixture of methanol/triethylamine (80:20 v/v). After drying, HPTLC plates were sprayed with the FBS reagent. Reddish colored spots (CBN: magenta;CBD: orange; Δ^9-THC: red) indicated a positive response.

4.4. Oil samples

Fifteen CBD oils with different CBD concentrations, primary commercially available in Germany and surrounding countries, were purchased from different internet shops between August 2019 and February 2021 (for main characteristics of the oils see Table 3, not for all used CBD oils details regarding the addition of purified/synthetic CBD or the extraction procedure of cannabis flowers or leaves were available but if there was an information the oil was extracted with the CO_2 extraction procedure). The names of the vendors and manufacturers were withheld due to a lack of consent for disclosure. Oils were stored as recommended by the manufacturer between 2 and 8 °C (CBD-Oil-4 to 15) or at room temperature (CBD-Oil-1 to 3). Commercially available olive and sunflower oils were categorized as negative samples, assuming the absence of cannabinoids. Furthermore, hemp seed oil was used as reference material, which could be contaminated with cannabinoid containing resins from the flowers and leaves of hemp plants during hemp seed processing but for the developed method this CBD concentration is under the limit of detection why it did not affect the determination of the CBD content in CBD oils.

4.5. Preparation of oil samples

An aliquot (100 mg) of each oil sample (CBD oils, olive oil, sunflower oil, hempseed oil) was filled with *n*-hexane to a volume of 100 mL. After thorough mixing, an aliquot (10 μL) of this solution was transferred to a vial and was concentrated to dryness in an argon stream with heat from a laboratory sand bath at 50 °C. The residue was dissolved in methanol (100 μL), and a defined volume (25 μL) of the solution was spotted onto a HPTLC plate. For quantification of the cannabinoid content, deuterated internal standards of CBN, CBD and Δ^9-THC were added after the transfer of a 10 μL aliquot into a vial.

4.6. HPTLC-ESI-MS analysis (modified according to Schmidt et al. [21])

Standard solutions of CBN, CBD as well as Δ^9-THC and prepared oil samples were spotted onto HPTLC plates as 2 mm bands, in 25 μL aliquots, 15 mm from the bottom edge and 7 mm apart using a Linomat 5 (CAMAG, Switzerland). Plates were developed in a TLC developing chamber with a flat bottom to a distance of 50 mm in 12 min using *n*-hexane/diethyl ether (80:20 v/v) as developing solvent. For the optimization of the chromatographic separation of the cannabinoids various developing solvents were tested, e.g. *n*-hexane/acetone/triethylamine (40:20:2 v/v/v) or cyclohexane/diisopropylether/triethylamine (52:40:8 v/v/v).

Beside the investigation by ESI-MS, FBS spray reagent was used for the detection of CBN, CBD and Δ^9-THC (see detection of cannabinoids with FBS reagent). For the detection of CBN, HPTLC plates were also inspected with an UV light source at $\lambda = 254$ nm.

For the elution of the analyte, compounds from the HPTLC plates into an expression^L CMS (compact mass spectrometer from Advion, United Kingdom) system, equipped with an ESI ion source, a TLC-MS interface (Plate Express from Advion combined with an isocratic pump, dimensions of the elution head: 2x4 mm) was utilized (for instrument parameter see Schmidt et al. [21]). Substance-specific parameters were determined by direct infusion ESI-MS of CBN, CBD and Δ^9-THC working solutions (2.0, 5.0, 8.0 μg/mL).

4.7. Validation of the HPTLC-ESI-MS method

4.7.1. Specificity

A test for specificity was conducted with olive oil, sunflower oil and hemp seed oil by a post-chromatographic detection reaction with FBS reagent and HPTLC-ESI-MS using working solutions of cannabinoid standards (5.0 μg/mL). For the detection of CBN, CBD and Δ^9-THC with FBS reagent as well as for HPTLC-ESI-MS experiments, prepared oil samples (see preparation of oil samples) and working solutions of cannabinoids were spotted onto HPTLC plates, HPTLC plates were developed in *n*–hexane/diethyl ether (80:20 v/v) and investigated by HPTLC-ESI-MS or sprayed with FBS for staining cannabinoid bands.

4.7.2. Linearity, limit of detection (LOD) and limit of quantitation (LOQ)

The linearity of the calibration curves was tested with the Mandel's test. The determination of LOD and LOQ was performed using the calibration curve method according to DIN 32,645 [31]. Therefore, calibration solutions of CBN, CBD and Δ^9-THC (see preparation of standard

solutions) were measured via direct infusion by ESI-MS or were spotted onto HPLTC plates, HPTLC plates were developed using *n*–hexane/diethyl ether (80:20 v/v) and investigated by HPTLC-ESI-MS. Analyses were performed in triplicate and executed with average peak areas of the mass peaks of the respective analytes (ESI-MS: CBN: *m/z* 309; CBD: *m/z* 313; Δ^9-THC: *m/z* 313; HPTLC-ESI-MS: CBN: *m/z* 309, 354; CBD: *m/z* 313, 327, 358; Δ^9-THC: *m/z* 313, 345, 358) and the internal standards (ESI-MS: CBN-d_3: *m/z* 312; CBD-d_3: *m/z* 316; Δ^9-THC-d_3: *m/z* 316; HPTLC-ESI-MS: CBN-d_3: *m/z* 312, 357; CBD-d_3: *m/z* 316, 330, 361; Δ^9-THC-d_3: *m/z* 316, 348, 361). Average peak area ratios and cannabinoid concentrations were presented in Tables 1–3 (see Supplementary Material).

4.7.3. Precision

For determining the system precision, methanolic solutions containing mixtures of CBN/CBN-d_3, CBD/CBD-d_3 and Δ^9-THC/Δ^9-THC-d_3 (CBN, CBD, Δ^9-THC: 3.4 μg/mL; deuterated cannabinoids: 3.6 μg/mL) were used. Each solution was measured six times on three different days by direct infusion ESI-MS and HPTLC-ESI-MS. For HPTLC-ESI-MS experiments, solutions were spotted onto HPTLC plates, HPTLC plates were developed using *n*–hexane/diethyl ether (80:20 v/v) and investigated by HPTLC-ESI-MS. For the interpretation of the system precision, relative standard deviations (RSD) of the cannabinoid contents were used. In addition, Dixon's Q test and Neumann trend test were applied for the identification of outliners or trends (see Supplementary Material, Tables 8 and 9).

For determining the method precision, an aliquot of each oil (olive oil, sunflower oil and hemp seed oil; 100 mg of each oil) was filled with *n*-hexane to a volume of 100 mL. After thorough mixing, aliquots (10 μL) of these *n*-hexane/oil mixtures were transferred to vials, spiked with a defined concentration of each analyzed cannabinoid (CBN, Δ^9-THC: 40 μL, 10 μg/mL, CBD: 120 μL, 10 μg/mL) and the internal standards (CBN-d_3, Δ^9-THC-d_3: 100 μL, 3.6 μg/mL; CBD-d_3: 11 μL, 100 μg/mL) and concentrated to dryness in an argon stream. Before measurement, the residues were dissolved in methanol (100 μL) and defined volumes (25 μL) were spotted onto HPTLC plates. The HPTLC plates were developed in *n*–hexane/diethyl ether (80:20 v/v) and were investigated by HPTLC-ESI-MS. Analyses were carried out with a number of six replicates for each oil. Preparations of the oil samples were executed independently of each other. The interpretation of the method precision based on the relative standard deviations (RSD) of the cannabinoid contents. Additionally, Dixon's Q test and Neumann trend test were implemented for the identification of outliners or trends (see Supplementary Material, Tables 10–12).

For the analysis of the system and method precision the average peak areas of the mass peaks of the analytes (ESI-MS: CBN: *m/z* 309; CBD: *m/z* 313; Δ^9-THC: *m/z* 313; HPTLC-ESI-MS: CBN: *m/z* 309, 354; CBD: *m/z* 313, 327, 358; Δ^9-THC: *m/z* 313, 345, 358) and the internal standards (ESI-MS: CBN-d_3: *m/z* 312; CBD-d_3: *m/z* 316; Δ^9-THC-d_3: *m/z* 316; HPTLC-ESI-MS: CBN-d_3: *m/z* 312, 357; CBD-d_3: *m/z* 316, 330, 361; Δ^9-THC-d_3: *m/z* 316, 348, 361) were used.

4.7.4. Trueness

For interpretation of trueness, terms of recovery and bias were considered. The described studies were performed using olive, sunflower and hemp seed oils.

4.7.5. Recovery

For the determination of recovery of the developed procedure, an aliquot (100 mg) of each oil was filled with *n*-hexane to a volume of 100 mL. After thorough mixing, an aliquot (10 μL) of this *n*-hexane/oil mixture was transferred to a vial, spiked with a defined concentration of each cannabinoid (CBN, CBD, Δ^9-THC: 24 μL and 48 μL; 10 μg/mL) and concentrated to dryness in an argon stream. The residue was solved in a methanolic solution of internal standards (CBN-d_3, Δ^9-THC- d_3: 100 μL, 3.6 μg/mL; CBD-d_3: 100 μL, 11.0 μg/mL) and a defined volume (25 μL) of the solution was spotted onto a HPTLC plate. The HPTLC-plate was developed in *n*–hexane/diethyl ether (80:20 v/v) and investigated by HPTLC-ESI-MS. Each concentration level was analyzed in triplicate (see Supplementary Material, Tables 13–15). For interpretation of the recovery the average peak areas of the mass peaks of the analytes (CBN: *m/z* 309, 354; CBD: *m/z* 313, 327, 358; Δ^9-THC: *m/z* 313, 345, 358) and the internal standards (CBN-d_3: *m/z* 312, 357; CBD-d_3: *m/z* 316, 330, 361; Δ^9-THC-d_3: *m/z* 316, 348, 361) were used. To confirm the results, three olive oil samples (100 mg) were spiked with a defined concentration of CBN, CBD and Δ^9-THC (CBN: 400 μg/mL; CBD: 1 mg/mL; Δ^9-THC: 400 μg/mL) before filling with *n*-hexane and picking aliquots (10 μL) of the with cannabinoids spiked *n*-hexane/oil mixtures. The preparation of the oil samples was performed independent of each other on different days as described above.

The calculated cannabinoid contents were compared with the average target concentrations and then the recovery rate was determined.

4.7.6. Bias calculation

Bias calculation was performed for two concentration levels of each cannabinoid with a number of three replicates at each concentration. Each aliquot (10 μL) of the *n*-hexane/oil mixtures (see above) was spiked with a defined concentration of CBN (24 μL and 48 μL; 10 μg/mL), CBD (60 μL and 160 μL; 10 μg/mL) and Δ^9-THC (24 μL and 48 μL; 10 μg/mL) as well as the appropriate internal standard (CBN-d_3, Δ^9-THC-d_3: 100 μL, 3.6 μg/mL; CBD-d_3: 11 μL, 100 μg/mL). Preparations of the oils and chromatographic separation by HPTLC (see preparation of oil samples) were performed independently of each other. For the bias calculation, the

$$\widehat{\delta} = \bar{x} - T \tag{1}$$

following formula (1) was used:where $\widehat{\delta}$ represents the bias and T correspond to the "true" concentration and $\bar{x}$ to the mean value of the determined cannabinoid concentration of the spiked oil samples.

4.8. Stability of the standards

The stability of the standard solutions of CBN, CBD and Δ^9-THC were tested through storage these solutions at different conditions (oriented by the procedure of Schmidt et al. [21]). Standard solutions were stored at −12 °C in the dark, at room temperature (average temperature 27 °C) in the dark and at room temperature exposed to sunlight. The different cannabinoid solutions (50 and 100 μg/mL) were investigated over a ten-week period. Furthermore, some irregular measurements over a period of six months were performed. For the analyses, the stored solutions of CBN, CBD and Δ^9-THC were diluted (2.0 and 4.0 μg/mL) and the internal standards (CBN-d_3, CBD-d_3, Δ^9-THC-d_3; 3.6 μg/mL) were added. Subsequently, these solutions were measured using direct infusion ESI-MS. Each solution was analyzed three times and for the interpretation of the stability, the average mass peak area of the non-deuterated and deuterated cannabinoids (CBN: *m/z* 309; CBD: *m/z* 313, Δ^9-THC: *m/z* 313, CBN-d_3: *m/z* 312; CBD-d_3: *m/z* 316, Δ^9-THC-d_3: *m/z* 316) were utilized. For identification of trend or outliners, a trend test by Neumann [31] and a Dixon's Q test were performed (see Supplementary Material, Table 19).

CRediT authorship contribution statement

Theresa Schmidt: Validation, Investigation, Writing – original draft, Writing – review & editing. **Jacqueline Stommel:** Investigation. **Tim Kohlmann:** Investigation, Writing – review & editing. **Annemarie E. Kramell:** Conceptualization, Validation, Writing – original draft, Writing – review & editing. **René Csuk:** Conceptualization, Validation, Writing – review & editing.

Declaration of Competing Interest

The authors declare that they have no known competing financial interests or personal relationships that could have appeared to influence the work reported in this paper.

Acknowledgement

We like to thank M. Schneider for his help in the lab.

Appendix A. Supplementary data

Supplementary data to this article can be found online at https://doi.org/10.1016/j.rechem.2021.100234.

References

[1] A. Hazekamp, The trouble with CBD oil, Med. Cannabis Cannabinoids 1 (1) (2018) 65–72.
[2] G. Magagnini, G. Grassi, S. Kotiranta, The effect of light spectrum on the morphology and cannabinoid content of Cannabis sativa L. Med. Cannabis Cannabinoids 1 (1) (2018) 19–27.
[3] T. Glivar, J. Eržen, S. Kreft, M. Zagožen, A. Čerenak, B. Čeh, E. Tavčar Benković, Cannabinoid content in industrial hemp (Cannabis sativa L.) varieties grown in Slovenia, Ind. Crops Prod. 145 (2020) 112082, https://doi.org/10.1016/j.indcrop.2019.112082.
[4] Administration, FDA, Warning Letters and Test Results for Cannabidiol-Related Products. https://www.fda.gov/news-events/public-health-focus/warning-letters-and-test-results-cannabidiol-related-products (23.02.2021).
[5] M.O. Bonn-Miller, M.J.E. Loflin, B.F. Thomas, J.P. Marcu, T. Hyke, R. Vandrey, Labeling accuracy of cannabidiol extracts sold online, JAMA 318 (17) (2017) 1708–1709.
[6] D. Lachenmeier, S. Habel, B. Fischer, F. Herbi, Y. Zerbe, V. Bock, T. Rajcic de Rezende, S. Walch, C. Sproll, Are side effects of cannabidiol (CBD) products caused by tetrahydrocannabinol (THC) contamination? [version 3; peer review: 2 approved, 1 approved with reservations], F1000Res. 8 (1394) (2020).
[7] European Commission, Scientific Opinion on the risks for human health related to the presence of tetrahydrocannabinol (THC) in milk and other food of animal origin. EFSA J. 13 (6) (2015) 4141.
[8] M. Wheeler, J.W. Merten, B.T. Gordon, H. Hamadi, CBD (Cannabidiol) product attitudes, knowledge, and use among young adults, Subst. Use Misuse 55 (7) (2020) 1138–1145.
[9] S. Pisanti, A.M. Malfitano, E. Ciaglia, A. Lamberti, R. Ranieri, G. Cuomo, M. Abate, G. Faggiana, M.C. Proto, D. Fiore, C. Laezza, M. Bifulco, Cannabidiol: state of the art and new challenges for therapeutic applications, Pharmacol. Therapeut. 175 (2017) 133–150.
[10] WHO, Cannabidiol (CBD) – critical review report, in: Expert Committee on Drug Dependence, Geneva, Switzerland, 2018.
[11] C.M. Williams, G.J. Stephens, Development of cannabidiol as a treatment for severe childhood epilepsies, Br. J. Pharmacol. 177 (24) (2020) 5509–5517.
[12] M. Kitamura, Y. Kiba, R. Suzuki, N. Tomida, A. Uwaya, F. Isami, S. Deng, Cannabidiol content and in vitro biological activities of commercial cannabidiol oils and hemp seed oils. Medicines (Basel, Switzerland) 7 (9) (2020).
[13] R. Pavlovic, G. Nenna, L. Calvi, S. Panseri, G. Borgonovo, L. Giupponi, G. Cannazza, A. Giorgi, Quality traits of "cannabidiol oils": cannabinoids content, terpene fingerprint and oxidation stability of European commercially available preparations, Molecules 23 (5) (2018) 1230, https://doi.org/10.3390/molecules23051230.
[14] Y. Urasaki, C. Beaumont, M. Workman, J.N. Talbot, D.K. Hill, T.T. Le, Potency assessment of CBD oils by their effects on cell signaling pathways, Nutrients 12 (2) (2020) 357, https://doi.org/10.3390/nu12020357.
[15] M. Yotoriyama, E. Ishiharajima, Y. Kato, A. Nagato, S. Sekita, K. Watanabe, I. Yamamoto, Identification and determination of cannabinoids in both commercially available and cannabis oils stored long term, J. Health Sci. 51 (4) (2005) 483–487.
[16] I.G. Trofin, G. Dabija, D.-I. Vaireanu, L. Filipescu, Long – term storage and cannabis oil stability, Rev. Chim. 63 (3) (2012) 293–297.
[17] N. Galand, D. Ernouf, F. Montigny, J. Dollet, J. Pothier, Separation and identification of cannabis components by different planar chromatography techniques (TLC, AMD, OPLC), J. Chromatogr. Sci. 42 (3) (2004) 130–134.
[18] K. Watanabe, S. Yamaori, T. Funahashi, T. Kimura, I. Yamamoto, 8-Hydroxycannabinol: a new metabolite of cannabinol formed by human hepatic microsomes, Forensic Toxicol. 24 (2) (2006) 80–82.
[19] Identification and quantification of different cannabinoids in *Cannabis sativa*. https://www.camag.com/en/tlc_hptlc/camag_laboratory/methods.cfm?ao=-1. Last accessed 03.04.2019, 14:24.
[20] P. Sharma, M.M. Bharath, P. Murthy, Qualitative high performance thin layer chromatography (HPTLC) analysis of cannabinoids in urine samples of Cannabis abusers, Indian J. Med. Res. 132 (2010) 201–208.
[21] T. Schmidt, A.E. Kramell, F. Oehler, R. Kluge, D. Demske, P.E. Tarasov, R. Csuk, Identification and quantification of cannabinol as a biomarker for local hemp retting in an ancient sedimentary record by HPTLC-ESI-MS, Anal. BioanalChem. 412 (11) (2020) 2633–2644.
[22] E.R. Garrett, C.A. Hunt, Physicochemical properties, solubility, and protein binding of Δ9 -tetrahydrocannabinol, J. Pharm. Sci. 63 (7) (1974) 1056–1064.
[23] R.C. Wheast, Handbook of Chemistry and Physics, CRC Press, Boca Raton, 1983.
[24] J. Vacek, J. Vostalova, B. Papouskova, D. Skarupova, M. Kos, M. Kabelac, J. Storch, Antioxidant function of phytocannabinoids: molecular basis of their stability and cytoprotective properties under UV-irradiation, Free Radical Biol. Med. 164 (2021) 258–270.
[25] N.D. Coggeshall, E.M. Lang, Influence of solvent, hydrogen bonding, temperature and conjugation on the ultraviolet spectra of phenols and aromatic hydrocarbons1, J. Am. Chem. Soc. 70 (10) (1948) 3283–3292.
[26] J.T. Fischedick, R. Glas, A. Hazekamp, R. Verpoorte, A qualitative and quantitative HPTLC densitometry method for the analysis of cannabinoids in Cannabis sativa L, Phytochem. Anal. 20 (5) (2009) 421–426.
[27] A. Hazekamp, A. Peltenburg, R. Verpoorte, C. Giroud, Chromatographic and spectroscopic data of cannabinoids from Cannabis sativa L. J. Liq. Chromatogr. Rel. Techol. 28 (15) (2005) 2361–2382.
[28] D. Corrigan, J. Lynch, An investigation of potential staining reagents for the glandular trichomes of Cannabis sativa, Planta Med. 40 (S 1) (1980) 163–169.
[29] Regulation (EU) No 1307/2013 of the European Parliament and of the Council of 17 December 2013 establishing rules for direct payments to farmers under support schemes within the framework of the common agricultural policy and repealing Council Regulation (EC) No 637/2008 and Council Regulation (EC) No 73/2009, 2013.
[30] R. Pacifici, E. Marchei, F. Salvatore, L. Guandalini, F.P. Busardò, S. Pichini, Evaluation of cannabinoids concentration and stability in standardized preparations of cannabis tea and cannabis oil by ultra-high performance liquid chromatography tandem mass spectrometry, Clin. Chem. Lab. Med. 55 (10) (2017) 1555–1563.
[31] S. Kromidas, Handbuch Validierung in der Analytik, vol. 2, Wiley-VCH Verlag & Co. KGaA, Weinheim, 2011.

Separating the true from the false: A rapid HPTLC-ESI-MS method for the determination of cannabinoids in different oils

Theresa Schmidt [1], Jacqueline Stommel [1], Tim Kohlmann [1], Annemarie E. Kramell [1], René Csuk [1,*]

[1] Martin-Luther University Halle-Wittenberg, Organic Chemistry, Kurt-Mothes, Str. 2, D-06120 Halle (Saale), Germany; theresa.schmidt@chemie.uni-halle.de (T.S.); jac.stommel@googlemailcom (J.S.); tim.kohlmann@chemie.uni-halle.de (T.K.); annemarie.kramell@chemie.uni-halle.de (A.K); rene.csuk@chemie.uni-halle.de (R.C.)

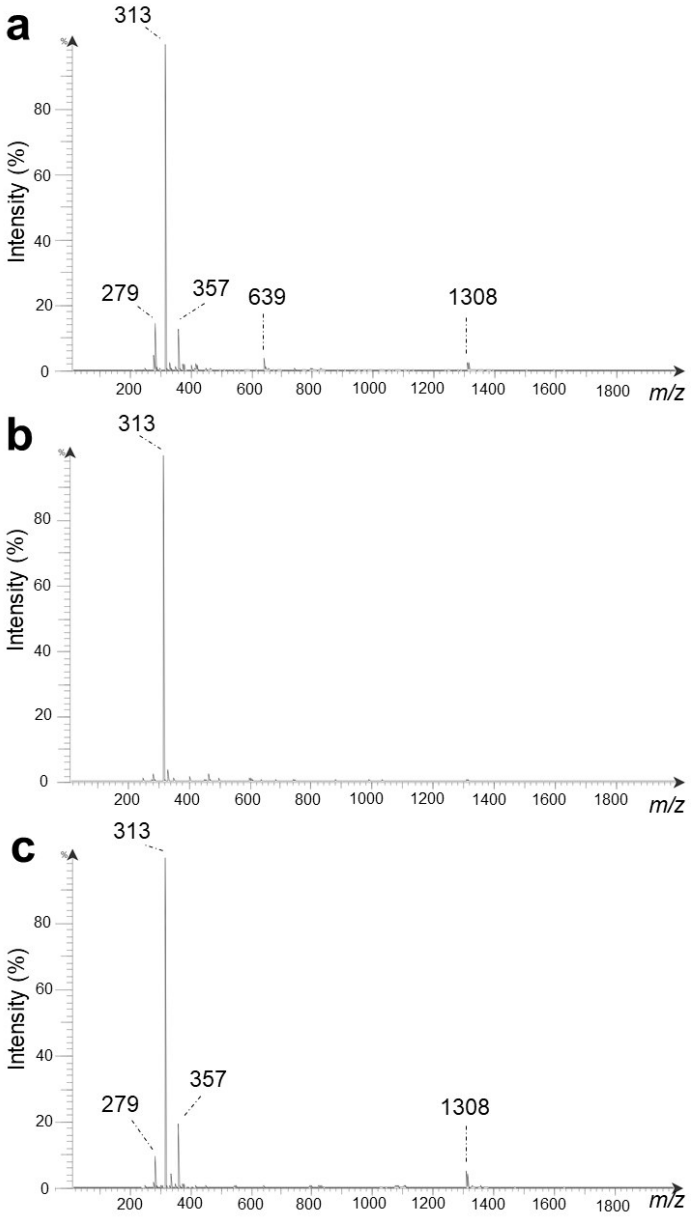

Figure 1. Full scan MS-Spektrum of a methanolic extract of 100 mg of (a) CBD-Oil-7 [with hemp seed oil as carrier oil], (b) CBD-Oil-1 [with olive oil as carrier oil] and (c) CBD-Oil-1 [with sunflower oil as carrier oil] measured via direct infusion with ESI-MS.

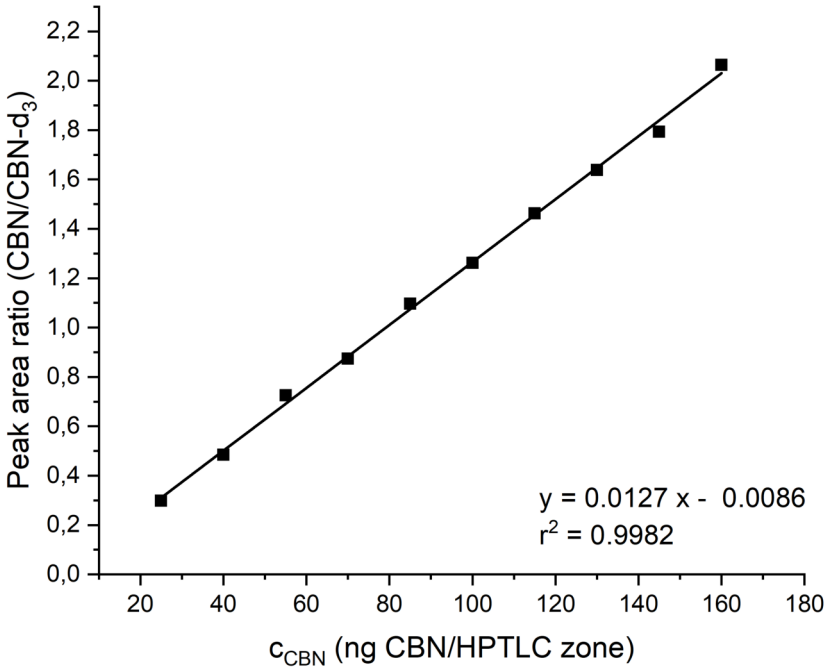

Figure 2. Calibration curve obtained from CBN in the range 25 – 160 ng CBN/HPTLC zone with 90 ng CBN-d_3/HPTLC zone after chromatographic separation.

Table 1. CBN concentration of calibration solutions and related average peak area ratios of CBN (sum of mass peaks at *m/z* 309 and 354) and CBN-d_3 (sum of mass peaks at *m/z* 312 and 357) received from analyses on calibration solutions in triplicate (25 - 160 ng CBN/HPTLC zone; 90 ng CBN-d_3/HPTLC zone) after chromatographic separation.

c_{CBN} (ng CBN/HPTLC zone)	**Average peak area ratio (∑ *m/z* 309+354)/(∑ *m/z* 312+357)**
25	0.2985
40	0.4845
55	0.7260
70	0.8743
85	1.0966
100	1.2622
115	1.4627
130	1.6378
145	1.7929
160	2.0634

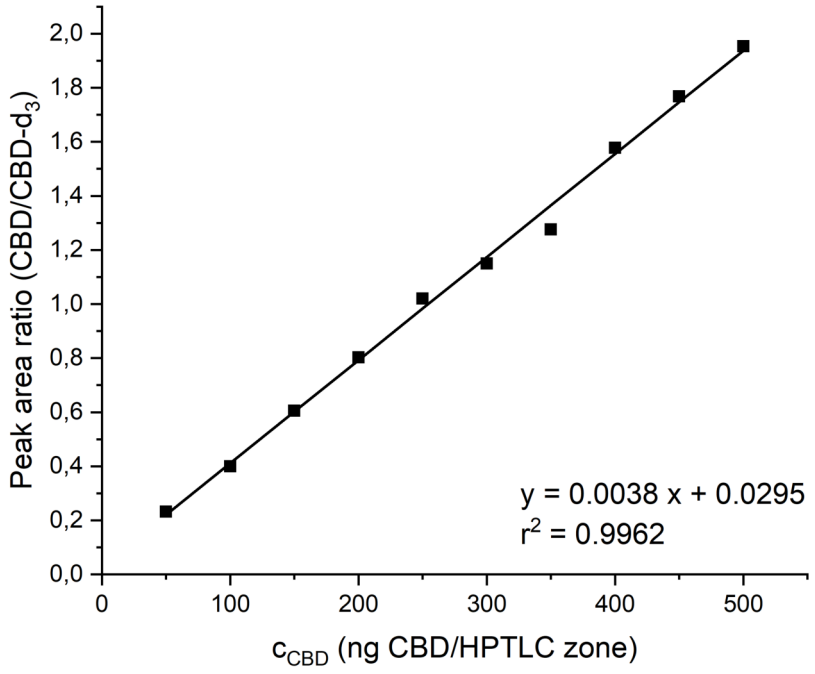

Figure 3. Calibration curve obtained from CBD in the range 50 – 500 ng CBD/HPTLC zone with 275 ng CBD-d_3/HPTLC zone after chromatographic separation.

Table 2 CBD concentration of calibration solutions and related average peak area ratios of CBD (sum of mass peaks at *m/z* 313, 327 and 358) and CBD-d_3 (sum of mass peaks at *m/z* 316, 330 and 361) received from analyses on calibration solutions in triplicate (50 - 500 ng CBD/HPTLC zone; 275 ng CBD-d_3/HPTLC zone) after chromatographic separation.

c_{CBD} (ng CBD/HPTLC zone)	Average peak area ratio (∑ *m/z* 313+327+358)/(∑ *m/z* 316+330+361)
50	0.2327
100	0.4002
150	0.6051
200	0.8033
250	1.0205
300	1.1499
350	1.2758
400	1.5781
450	1.7686
500	1.9532

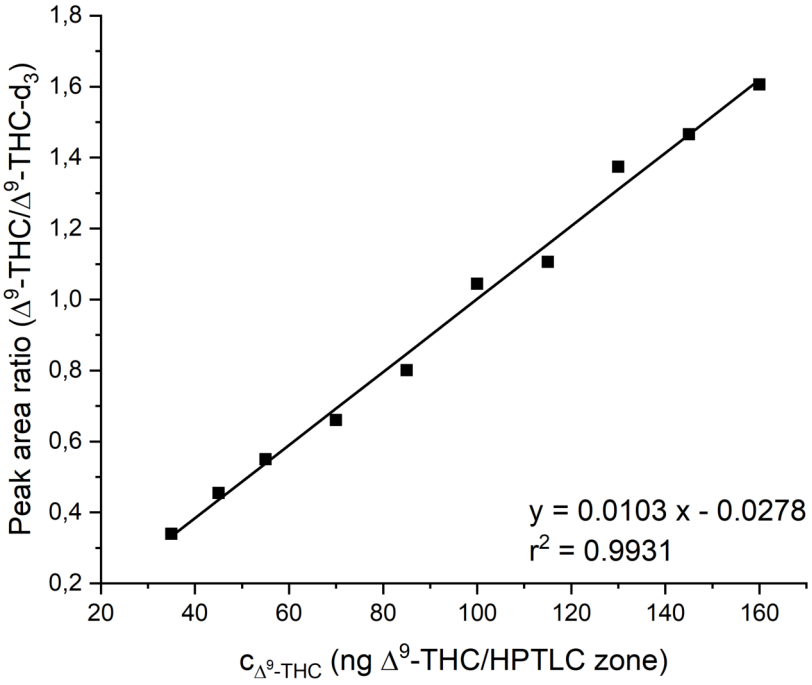

Figure 4. Calibration curve obtained from Δ9-THC in the range 35 – 160 ng Δ^9-THC/HPTLC zone with 90 ng Δ^9-THC-d_3/HPTLC zone after chromatographic separation.

Table 3. Δ^9-THC concentration of calibration solutions and related average peak area ratios of Δ^9-THC (sum of mass peaks at *m/z* 313, 345 and 358) and Δ^9-THC-d_3/(sum of mass peaks at *m/z* 316, 348 and 361) received from analyses on calibration solutions in triplicate (35 - 160 ng Δ^9-THC/HPTLC zone; 90 ng Δ9-THC-d_3/HPTLC zone) after chromatographic separation.

$c_{\Delta 9\text{-THC}}$(ng Δ^9-THC/HPTLC zone)	**Average peak area ratio (∑ *m/z* 313+327+358)/(∑ *m/z* 316+330+361)**
35	0.3393
45	0.4546
55	0.5498
70	0.6604
85	0.8010
100	1.0441
115	1.1056
130	1.3740
145	1.4654
160	1.6055

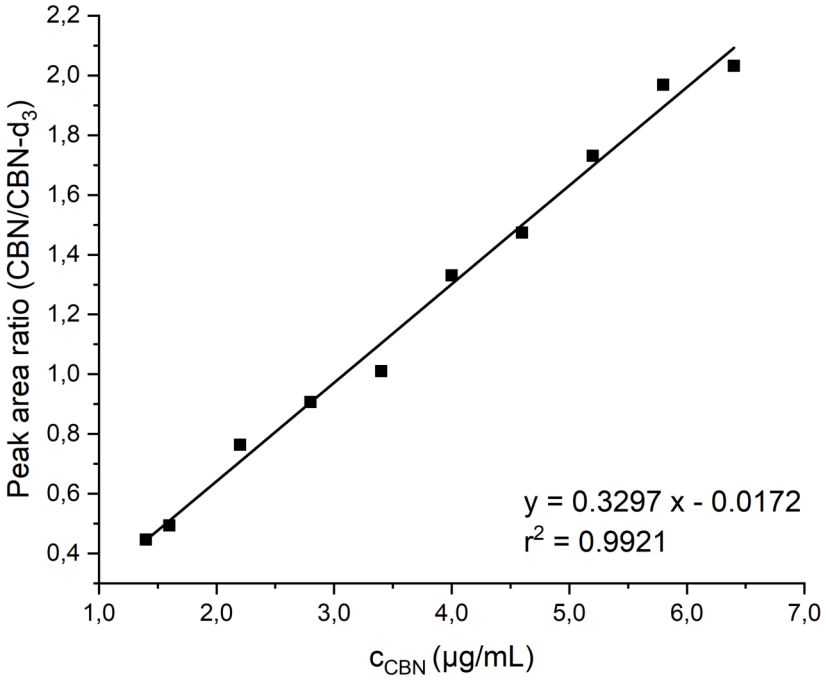

Figure 5. Calibration curve obtained from CBN in the range 1.4 – 6.4 µg CBN/mL with 3.6 µg CBN-d_3/mL by direct infusion.

Table 4. CBN concentration of calibration solutions and related average peak area ratios of CBN (*m*/*z* 309) and CBN-d_3 (*m*/*z* 312) received from analyses on calibration solutions in triplicate (1.4 – 6.4 µg CBN/mL with 3.6 µg CBN-d_3/mL) by direct infusion.

c_{CBN} (µg/mL)	Average peak area ratio (*m*/*z* 309)/(*m*/*z* 312)
1.4	0.4463
1.6	0.4942
2.2	0.7640
2.8	0.9067
3.4	1.0098
4.0	1.3309
4.6	1.4735
5.2	1.7306
5.8	1.9689
6.4	2.0318

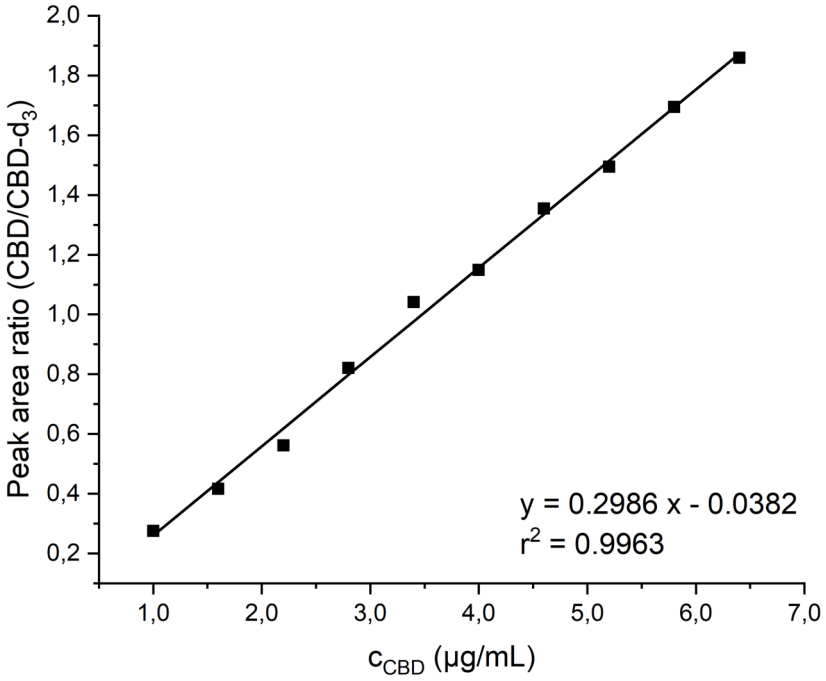

Figure 6. Calibration curve obtained from CBD in the range 1.0 – 6.4 µg CBD/mL with 3.6 µg CBN-d_3/mL by direct infusion.

Table 5. CBD concentration of calibration solutions and related average peak area ratios of CBD (*m*/*z* 313) and CBD-d_3 (*m*/*z* 316) received from analyses on calibration solutions in triplicate (1.0 – 6.4 µg CBD/mL with 3.6 µg CBN-d_3/mL) by direct infusion.

c_{CBD} (µg/mL)	Average peak area ratio (*m*/*z* 313)/(*m*/*z* 316)
1.0	0.2755
1.6	0.4165
2.2	0.5613
2.8	0.8213
3.4	1.0411
4.0	1.1490
4.6	1.3548
5.2	1.4937
5.8	1.6940
6.4	1.8585

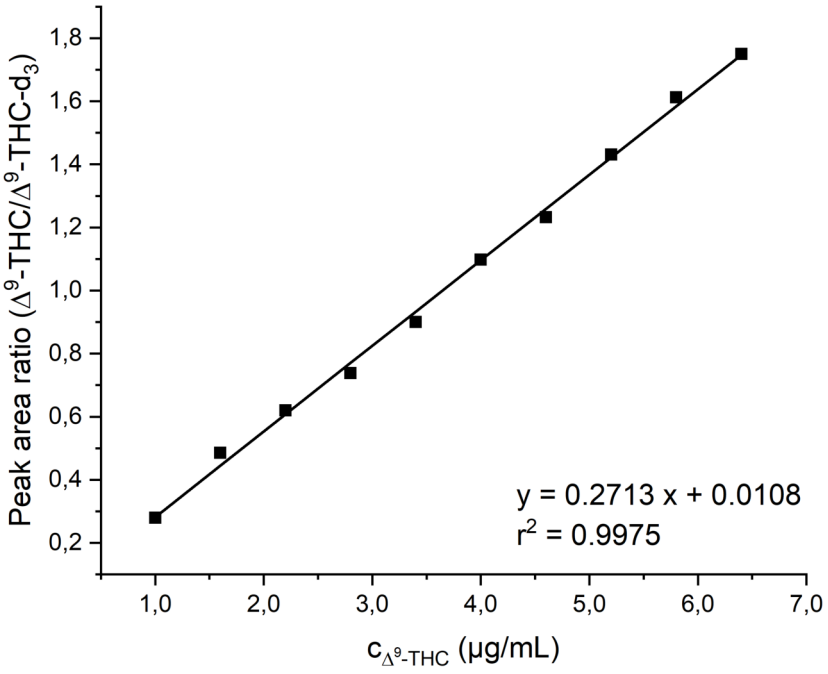

Figure 7. Calibration curve obtained from Δ^9-THC in the range 1.0 – 6.4 µg Δ^9-THC/mL with 3.6 µg Δ^9-THC-d_3/mL by direct infusion.

Table 6. Δ^9-THCconcentration of calibration solutions and related average peak area ratios of Δ^9-THC (*m*/*z* 313) and Δ^9-THC-d_3 (*m*/*z* 316) received from analyses on calibration solutions in triplicate (1.0 – 6.4 µg Δ^9-THC/mL with 3.6 µg Δ^9-THC-d_3/mL) by direct infusion.

$c_{\Delta^9\text{-THC}}$ (µg/mL)	Average peak area ratio (*m*/*z* 313)/(*m*/*z* 316)
1.0	0.2796
1.6	0.4850
2.2	0.6196
2.8	0.7379
3.4	0.9006
4.0	1.0978
4.6	1.2321
5.2	1.4308
5.8	1.6120
6.4	1.7497

Table 7. Linearity, LOD, and LOQ for CBN, CBD and Δ^9-THC determination by direct infusion via ESI-MS (tv…test value; cv…characteristic value).

Key figures	**Results**		
	CBN	**CBD**	**Δ^9-THC**
Range (µg/mL)	1.4 - 6.4	1.0 - 6.4	1.0 - 6.4
r^2 (coefficient of determination)	0.9921	0.9963	0.9975
Sy (residual standard deviation)	0.055	0.035	0.026
Sx (standard deviation for the method)	0.166	0.117	0.096
Residuals are normally distributed (R/s test, 99 %)	Yes (tv = 3.32; cv = 2.51 – 3.87)	Yes (tv =3.78; cv = 2.51 - 3.87)	Yes (tv = 3.2; cv = 2.51 – 3.87)
Residuals show a trend (Neumann trend test, 99 %)	No (tv = 2.34; cv = 0.75)	No (tv = 1.76; cv = 0.75)	No (tv = 1.53; cv = 0.75)
Equation curve	y(x) = 0.3297x - 0.0172 y: peak area ratio of CBN and CBN-d_3 x: concentration of CBN (µg/mL)	y(x) = 0.2986x - 0.0382 peak area ratio of CBD and CBD-d_3 x: concentration of CBD (µg/mL)	y(x) = 0.2713x + 0.0108 y: peak area ratio of Δ^9-THC and Δ^9-THC-d_3 x: concentration of Δ^9-THC (µg/mL) 0.2
LOD (µg/mL)	0.3	0.2	0.8
LOQ (µg/mL)	1.3	1.0	
Results of the Mandel's test according to DIN 32645			
Optimal regression model	Linear (tv = 0; cv = 0.75)	Linear (tv = 0.59; cv = 12.24)	Linear (tv = 2.21;cv = 12.24)
Linear regression acceptable	Yes	Yes	Yes

Table 8. Data set for experiments concerning the system precision for CBN, CBD and Δ^9-THC by HPTLC-ESI-MS.

Repeatability (n = 18; no measured value was classified as outliner by Dixon's test)			
Key figure	**CBN**	**CBD**	**Δ^9-THC**
Mean (ng/HPTLC zone)	82.69	261.21	93.26
SD (standard deviation in ng/HPTLC zone)	3.99	10.36	8.91
RSD (relative standard deviation in %)	4.83	3.97	9.56
Results of Neumann trend test			
Test value	1.32	1.34	1.53
Characteristic value (99 %)	0.99	0.99	0.99
No trend was observed with a statistical safety of 99 %			

Table 9. Data set for experiments concerning the system precision for CBN, CBD and Δ⁹-THC by direct infusion via ESI-MS.

Repeatability (n = 18; no measured value was classified as outliner by Dixon's test)			
Key figure	**CBN**	**CBD**	**Δ⁹-THC**
Mean (µg/mL)	3.23	3.13	3.71
SD (standard deviation in µg/mL)	0.13	0.09	0.39
RSD (relative standard deviation in %)	4.07	2.89	10.45
Results of Neumann trend test			
Test value	1.32	1.84	1.37
Characteristic value (99 %)	0.99	0.99	0.99
No trend was observed with a statistical safety of 99 %			

Table 10. Data set for experiments concerning the method precision (matrix: olive oil) for CBN, CBD and Δ⁹-THC by HPTLC-ESI-MS.

Method precision using olive oil as matrix ($n_{CBN,CBD}$ = 6; $n_{\Delta 9\text{-}THC}$ = 5; measured value classified as outliner by Dixon's test was rejected)			
Key figure	**CBN**	**CBD**	**Δ⁹-THC**
Mean (ng/HPTLC zone)	91.68	271.80	93.57
SD (standard deviation in ng/HPTLC zone)	9.83	8.04	3.04
RSD (relative standard deviation in %)	10.72	2.96	3.25
Results of Neumann trend test			
Test value	1.90	1.94	0.78
Characteristic value (99 %)	0.58	0.58	0.54
No trend was observed with a statistical safety of 99 %			

Table 11. Data set for experiments concerning the method precision (matrix: sunflower oil) for CBN, CBD and Δ⁹-THC by HPTLC-ESI-MS.

Method precision using sunflower oil as matrix ($n_{CBD,\Delta 9\text{-}THC}$ = 6; n_{CBN} = 5; measured value classified as outliner by Dixon's test was rejected)			
Key figure	**CBN**	**CBD**	**Δ⁹-THC**
Mean (ng/HPTLC zone)	89.67	276.93	105.49
SD (standard deviation in ng/HPTLC zone)	2.91	11.23	8.95
RSD (relative standard deviation in %)	3.24	4.06	8.48
Results of Neumann trend test			
Test value	1.01	2.09	2.76
Characteristic value (99 %)	0.54	0.58	0.58
No trend was observed with a statistical safety of 99 %			

Table 12. Data set for experiments concerning the method precision (matrix: hempseed oil) for CBN, CBD and Δ⁹-THC by HPTLC-ESI-MS.

Method precision using hempseed oil as matrix (n = 6; no measured value was classified as outliner by Dixon's test)			
Key figure	**CBN**	**CBD**	**Δ⁹-THC**
Mean (ng/HPTLC zone)	95.09	287.58	105.90
SD (standard deviation in ng/HPTLC zone)	6.20	16.48	10.00
RSD (relative standard deviation in %)	6.52	5.73	9.44
Results of Neumann trend test			
Test value	1.24	1.00	2.48
Characteristic value (99 %)	0.58	0.58	0.58
No trend was observed with a statistical safety of 99 %			

Table 13. Recovery of the method determined using olive oil, sunflower oil and hempseed oil spiked with CBN and characteristics of these samples (90 ng CBN-d_3/HPTLC zone).

Sample ID	Matrix	Calculated CBN content (ng CBN/HPTLC zone	Calculated CBN content (ng CBN/100 mg oil)	Target content of CBN (ng CBN/100 mg oil)	Recovery (%)
CBN-1	olive oil	56.8	227.4	240	94.73
CBN-2		46.6	186.2	240	77.59
CBN-3		51.6	206.6	240	86.08
CBN-4		108.9	435.5	480	90.73
CBN-5		110.2	440.7	480	91.80
CBN-6		111.9	447.8	480	93.28
CBN-7	sunflower oil	51.0	204.0	240	85.00
CBN-8		51.6	206.4	240	86.01
CBN-9		53.9	215.8	240	89.91
CBN-10		114.5	458.0	480	95.42
CBN-11		106.4	425.5	480	88.65
CBN-12		107.6	430.5	480	89.68
CBN-13	hempseed oil	48.0	192.0	240	79.98
CBN-14		52.9	211.6	240	88.16
CBN-15		51.3	205,2	240	85.52
CBN-16		118.1	472,6	480	98.45
CBN-17		117.4	469,5	480	97.82
CBN-18		110.2	440,8	480	91.82
samples spiked before filling with n-hexane and picking aliquots					
CBN-19	olive oil	93.6	374,4	400	93.59
CBN-20		95.6	382,6	400	95.64
CBN-21		99.3	397,0	400	99.26

Table 14. Recovery of the method determined using negative samples spiked with CBD and characteristics of these samples (275 ng CBD-d_3/HPTLC zone).

Sample ID	Matrix	Calculated CBD content (ng CBD/HPTLC zone	Calculated CBD content (ng CBD/100 mg oil)	Target content of CBD (ng CBD/100 mg oil)	Recovery (%)
CBD-1	olive oil	149.5	597.9	600	99.65
CBD-2		141.4	565.7	600	94.29
CBD-3		134.0	536.0	600	89.33
CBD-4		354.7	1418.7	1600	88.67
CBD-5		325.7	1302.7	1600	81.42
CBD-6		328.8	1315.3	1600	82.21
CBD-7	sunflower oil	133.4	533.8	600	88.96
CBD-8		128.5	513.9	600	85.66
CBD-9		136.7	546.8	600	91.14
CBD-10		390.1	1560.3	1600	97.52
CBD-11		379.7	1519.0	1600	94.93
CBD-12		350.0	1399.8	1600	87.49
CBD-13	hempseed oil	136.3	545.4	600	90.89
CBD-14		133.8	535.1	600	89.18
CBD-15		136.2	544.9	600	90.81
CBD-16		372.2	1488.7	1600	93.04
CBD-17		323.3	1293.1	1600	80.82
CBD-18		335.0	1340.2	1600	83.76
samples spiked before filling with n-hexane and picking aliquots					
CBD-19	olive oil	221.8	887.1	1200	88.71
CBD-20		222.8	891.4	1200	89.12
CBD-21		215.3	861.3	1200	86.13

Table 15. Recovery of the method determined using negative samples spiked with Δ^9-THC and characteristics of these samples (90 ng Δ^9-THC-d_3/HPTLC zone).

Sample ID	Matrix	Calculated Δ^9-THC content (ng Δ^9-THC/HPTLC zone	Calculated Δ^9-THC content (ng Δ^9-THC/100 mg oil)	Target content of Δ^9-THC (ng Δ^9-THC/100 mg oil)	Recovery (%)
THC-1	olive oil	59.1	236.6	240	98.58
THC-2		56.9	227.7	240	94.87
THC-3		58.5	234.1	240	97.53
THC-4		108.0	432.1	480	90.03
THC-5		98.4	393.5	480	81.99
THC-6		121.6	486.4	480	101.34
THC-7	sunflower oil	56.5	226.1	240	94.20
THC-8		58.4	233.8	240	97.40
THC-9		58.1	232.3	240	96.77
THC-10		117.4	469.7	480	97.86
THC-11		119.2	477.0	480	99.38
THC-12		102.1	408.5	480	85.10
THC-13	hempseed oil	47.7	190.9	240	79.54
THC-14		57.8	231.1	240	96.31
THC-15		56.9	227.7	240	94.87
THC-16		100.3	401.3	480	83.61
THC-17		97.5	390.1	480	81.26
THC-18		119.2	476.7	480	99.32
samples spiked before filling with n-hexane and picking aliquots					
THC-19	olive oil	99.1	396.4	400	99.10
THC-20		95.1	380.4	400	95.10
THC-21		100.1	400.5	400	100.12

Table 16 Data set for experiments concerning the bias calculation (matrix: olive oil) for CBN, CBD and Δ⁹-THC by HPTLC-ESI-MS.

Bias calculation with olive oil as matrix (spiked with CBN (24 µL; 10 µg/mL), CBD (60 µL; 10 µg/mL) and Δ⁹-THC (24 µL; 10 µg/mL), i.e. 60 ng CBN/HPTLC zone)			
Key figure	**CBN**	**CBD**	**Δ⁹-THC**
Mean (ng CBN/HPTLC zone)	59.02	146.21	52.52
True concentration (ng CBN/HPTLC zone)	60	150	60
Bias (ng CBN/HPTLC zone)	-0.98	-3.79	-7.47
Results of Student's t-test			
SD (standard deviation in ng CBN/HPTLC zone)	4.36	1.44	4.95
Test value	-0.39	-4.56	-2.62
Critical value [t(2;0.95)]	4.303	4.303	4.303
no statistical difference between the mean and the "true" values			
Bias calculation with olive oil as matrix (spiked with CBN (48 µL; 10 µg/mL), CBD (160 µL; 10 µg/mL) and Δ⁹-THC (48 µL; 10 µg/mL), i.e. 120 ng CBN/HPTLC zone)			
Key figure	**CBN**	**CBD**	**Δ⁹-THC**
Mean (ng CBN/HPTLC zone)	115.10	397.10	104.50
True concentration (ng CBN/HPTLC zone)	120	400	120
Bias (ng CBN/HPTLC zone)	-4.89	-2.90	-15.49
Results of Student's t-test			
SD (standard deviation in ng CBN/HPTLC zone)	5.86	20.04	10.77
Test value	-1.45	-0.25	-2.49
Critical value [t(2;0.95)]	4.303	4.303	4.303
no statistical difference between the mean and the "true" values			

Table 17. Data set for experiments concerning the bias calculation (matrix: sunflower oil) for CBN, CBD and Δ⁹-THC by HPTLC-ESI-MS.

Bias calculation with sunflower oil as matrix (spiked with CBN (24 µL; 10 µg/mL), CBD (60 µL; 10 µg/mL) and Δ⁹-THC (24 µL; 10 µg/mL), i.e. 60 ng CBN/HPTLC zone)			
Key figure	**CBN**	**CBD**	**Δ⁹-THC**
Mean (ng CBN/HPTLC zone)	59.61	139.48	55.02
True concentration (ng CBN/HPTLC zone)	60	150	60
Bias (ng CBN/HPTLC zone)	-0.38	-10.52	-4.98
Results of Student's t-test			
SD (standard deviation in ng CBN/HPTLC zone)	5.63	10.18	9.60
Test value	-0.12	-1.79	-0,90
Critical value [t(2;0.95)]	4.303	4.303	4.303
no statistical difference between the mean and the "true" values			
Bias calculation with sunflower oil as matrix (spiked with CBN (48 µL; 10 µg/mL), CBD (160 µL; 10 µg/mL) and Δ⁹-THC (48 µL; 10 µg/mL), i.e. 120 ng CBN/HPTLC zone)			
Key figure	**CBN**	**CBD**	**Δ⁹-THC**
Mean (ng CBN/HPTLC zone)	109.07	413.18	108.94
True concentration (ng CBN/HPTLC zone)	120	400	120
Bias (ng CBN/HPTLC zone)	-10.93	13.18	-11.06
Results of Student's t-test			
SD (standard deviation in ng CBN/HPTLC zone)	5.06	9.77	11.66
Test value	-3,74	2.34	-1.64
Critical value [t(2;0.95)]	4.303	4.303	4.303
no statistical difference between the mean and the "true" values			

Table 18. Data set for experiments concerning the bias calculation (matrix: hempseed oil) for CBN, CBD and Δ^9-THC by HPTLC-ESI-MS.

Bias calculation with hempseed oil as matrix (spiked with CBN (24 µL; 10 µg/mL), CBD (60 µL; 10 µg/mL) and Δ^9-THC (24 µL; 10 µg/mL), i.e. 60 ng CBN/HPTLC zone)			
Key figure	**CBN**	**CBD**	**Δ^9-THC**
Mean (ng CBN/HPTLC zone)	62.81	146.26	63.26
True concentration (ng CBN/HPTLC zone)	60	150	60
Bias (ng CBN/HPTLC zone)	2.81	-3.73	3.26
Results of Student's t-test			
SD (standard deviation in ng CBN/HPTLC zone)	1.80	0.96	5.61
Test value	2.71	-6.71	1.01
Critical value [t(2;0.95)]	4.303	4.303	4.303
no statistical difference between the mean and the "true" values			
Bias calculation with hempseed oil as matrix (spiked with CBN (48 µL; 10 µg/mL), CBD (160 µL; 10 µg/mL) and Δ^9-THC (48 µL; 10 µg/mL), i.e. 120 ng CBN/HPTLC zone)			
Key figure	**CBN**	**CBD**	**Δ^9-THC**
Mean (ng CBN/HPTLC zone)	110,892343	415,2336873	106,5878162
True concentration (ng CBN/HPTLC zone)	120	400	120
Bias (ng CBN/HPTLC zone)	-9,1077	15,2337	-13,4122
Results of Student's t-test			
SD (standard deviation in ng CBN/HPTLC zone)	1.35	7.73	10.02
Test value	-11.72	3.41	-2.32
Critical value [t(2;0.95)]	4.303	4.303	4.303
no statistical difference between the mean and the "true" values			

Table 19. Data set for experiments concerning the storage stability of CBN, CBD and Δ^9-HC by direct infusion via ESI-MS (n=14; $n_{CBD\ (2\ \mu g/mL\ RT,\ dark)}$ =13 ; $n_{THC\ (2\ \mu g/mL\ RT,\ dark)}$ =13; $n_{THC\ (4\ \mu g/mL\ RT,\ dark)}$ =13; $n_{THC\ (4\ \mu g/mL\ RT,\ light)}$ =13; measured value classified as outliner by Dixon's test was rejected).

Key figure	**CBN**	**CBD**	**Δ^9-THC**
2 µg/mL, RT, light			
Mean (% initial concentration)	95.10	92.17	98.41
SD (standard deviation in % initial concentration)	5.00	8.77	8.79
Results of Neumann trend test			
Test value	29.87	1.68	2.17
Characteristic value (99 %)	0.89	0.89	0.89
No trend was observed with a statistical safety of 99 %			
2 µg/mL, RT, dark			
Mean (% initial concentration)	104.15	101.20	98.24
SD (standard deviation in % initial concentration)	7.06	4.50	5.30
Results of Neumann trend test			
Test value	1.15	1.40	2.38
Characteristic value (99 %)	0.89	0.86	0.8618
No trend was observed with a statistical safety of 99 %			
2 µg/mL, -12 °C, dark			
Mean (% initial concentration)	102.98	103.68	102.23
SD (standard deviation in % initial concentration)	6.50	12.33	8.74
Results of Neumann trend test			
Test value	0.93	1.05	2.25
Characteristic value (99 %)	0.89	0.89	0.89
No trend was observed with a statistical safety of 99 %			
4.0 µg/mL, RT, light			
Mean (% initial concentration)	111.66	96.05	94.64
SD (standard deviation in % initial concentration)	7.63	4.88	11.14
Results of Neumann trend test			
Test value	15.96	1.88	0.86
Characteristic value (99 %)	0.89	0.89	2.18
No trend was observed with a statistical safety of 99 %			
4.0 µg/mL, RT, dark			
Mean (% initial concentration)	104.75	97.96	99.60
SD (standard deviation in % initial concentration)	6.51	3.20	7.87
Results of Neumann trend test			
Test value	1,70	1.94	1.85
Characteristic value (99 %)	0.89	0.89	0.86
No trend was observed with a statistical safety of 99 %			
4.0 µg/mL, -12 °C, dark			
Mean (% initial concentration)	103.04	100.96	96,71
SD (standard deviation in % initial concentration)	9.63	4.14	8.44
Results of Neumann trend test			
Test value	1.71	1.81	1.06
Characteristic value (99 %)	0.89	0.89	0.89
No trend was observed with a statistical safety of 99 %			

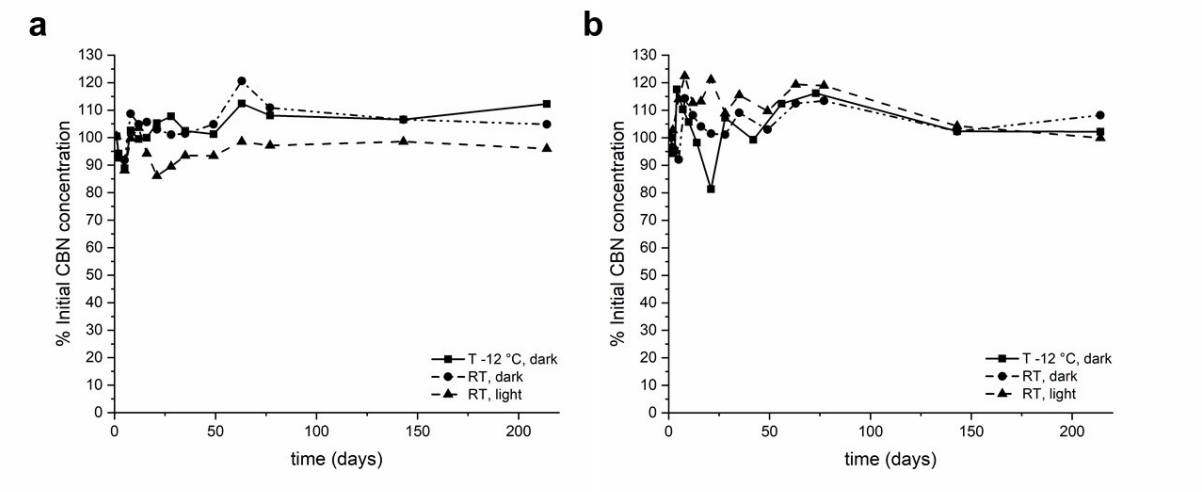

Figure 8. Variation of CBN concentration in working solutions of CBN stored at -12 °C in the dark, at room temperature in the dark and at room temperature exposed to sunlight, over a period of 214 days. Initial concentration of CBN (a) 2.0 μg/mL; (b) 4.0 μg/mL.

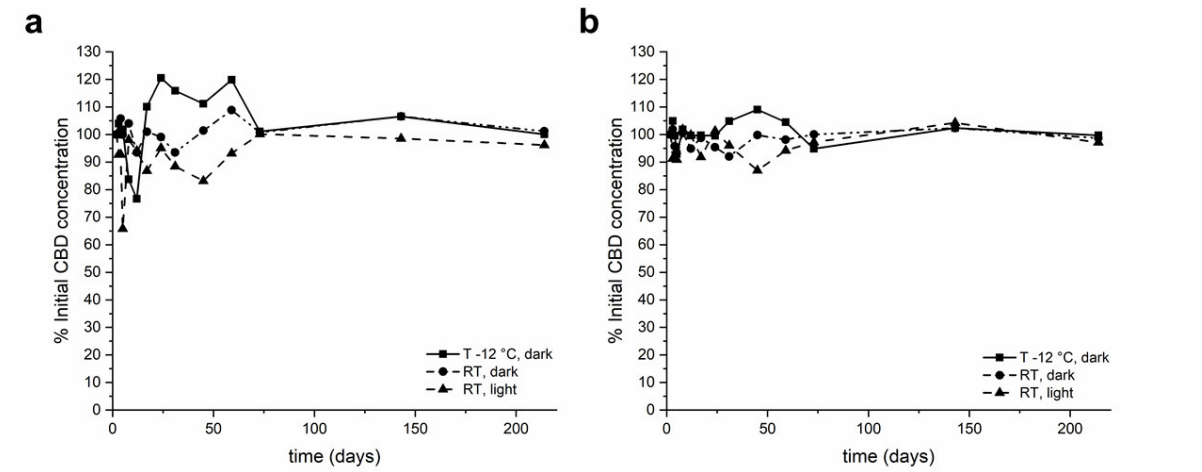

Figure 9. Variation of CBD concentration in working solutions of CBD stored at -12 °C in the dark, at room temperature in the dark and at room temperature exposed to sunlight, over a period of 214 days. Initial concentration of CBD (a) 2.0 μg/mL; (b) 4.0 μg/mL.

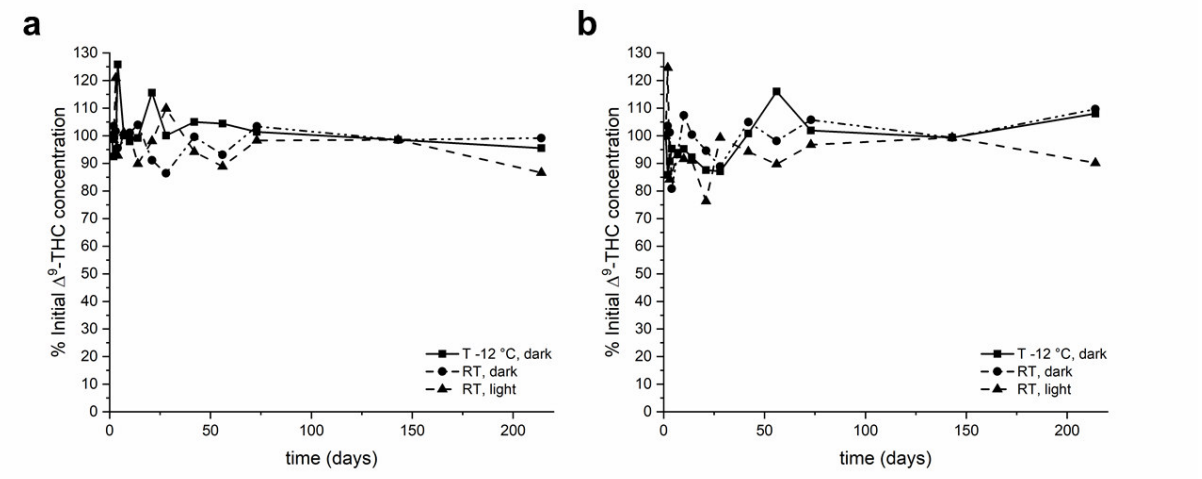

Figure 10. Variation of Δ^9-THC concentration in working solutions of Δ^9-THC stored at -12 °C in the dark, at room temperature in the dark and at room temperature exposed to sunlight, over a period of 214 days. Initial concentration of Δ^9-THC (a) 2.0 μg/mL; (b) 4.0 μg/mL.

P3

Received: 5 April 2023 | Revised: 19 July 2023 | Accepted: 21 July 2023

DOI: 10.1002/pca.3273

RESEARCH ARTICLE

Phytochemical Analysis WILEY

TLC and HPTLC-APCI-MS for the rapid discrimination of plant resins frequently used for lacquers and varnishes by artists and conservators

Marcel Schendzielorz | Theresa Schmidt | Nils Puchalla | René Csuk | Annemarie E. Kramell

Department of Organic Chemistry, Martin-Luther-University Halle-Wittenberg, Halle, Germany

Correspondence
Annemarie Elisabeth Kramell, Department of Organic Chemistry, Institute of Chemistry, Martin-Luther-University Halle-Wittenberg, Kurt-Mothes-Straße 2, 06120 Halle, Germany.
Email: annemarie.kramell@chemie.uni-halle.de

Funding information
ALAGO ART & STRINGS GmbH

Abstract

Introduction: Depending on their terpenoid and phenolic constituents plant resins can be classified as diterpenoid, triterpenoid or phenolic resins; thereby the profile of diterpenes and triterpenes is considered as genus- or even species-specific.

Objectives: We aimed to develop a simple, rapid, inexpensive, sensitive and specific method for the identification of resin-specific triterpenoid and phenolic compounds in plant resins using (HP)TLC [(high-performance) thin-layer chromatography] combined with APCI-MS (atmospheric pressure chemical ionisation mass spectrometry) and post-chromatographic detection reactions.

Methods: Twenty resin samples from different plant species were analysed. Different extraction procedures, post-chromatographic detection reagents as well as various sorbents and solvents for planar chromatography were tested. To evaluate the potential of the optimised (HP)TLC-APCI-MS methods, parameter such as limit of detection (LOD) was determined for selected marker compounds.

Results: Our protocol enabled qualitative analyses of chemotaxonomic molecular markers in natural resins such as dammar, mastic, olibanum and benzoin. For the first time, the application of thionyl chloride-stannic chloride reagent for a specific post-chromatographic detection of triterpenes is reported, sometimes even allowing discrimination between isomers based on their characteristic colour sequences. For triterpene acids, triterpene alcohols and phenolic compounds, detection limits of 2–20 ng/TLC zone and a system precision with a relative standard deviation (RSD) in the range of 3.9%–7.0% were achieved by (HP)TLC-APCI-MS. The applicability of the method for the analysis of resin-based varnishes was successfully tested on a mastic-based varnish. Thus, the method we propose is a helpful tool for the discrimination of resins and resin-based varnishes with respect to their botanical origin.

Marcel Schendzielorz and Theresa Schmidt contributed equally to this work.

KEYWORDS
benzoin balsam, HPTLC-MS, plant resin, triterpene, varnish

1 | INTRODUCTION

Plant resins are metabolic by-products of plant tissues that have been used for thousands of years for various applications, for example, as adhesives, hydro-repellents, coating and sealing agents or in the formulation of fragrances, flavours and pharmaceuticals.[1] They are very complex mixtures of different volatile as well as non-volatile compounds and can be classified as terpenoid or phenolic resins based on their constituents. Terpenoid resins make up the majority of these resins; they contain various monoterpenes, sesquiterpenes, diterpenes and triterpenes. Thereby, monoterpenes and sesquiterpenes are present in the volatile fraction of most resins, while diterpenes and triterpenes are non-volatile or very low volatile resin components. Since diterpenes and triterpenes are rarely found together in the same resin, a further subdivision into diterpene and triterpene resins is possible.[2,3]

Diterpenoid resins are produced by trees of the subfamily *Caesalpinioideae* or conifers such as pines of the genus *Pinus* (*Pinaceae* family). Sandarac, *Juniperus* and cypress resins, which are extracted from plants of the *Cupressaceae* family, also belong to the conifer resins and thus to the class of diterpenoid resins. These resins contain mainly bicyclic and tricyclic diterpenoids holding a labdane- or pimarane-type structure.[4,5] Resins of the *Pinaceae* family, such as pine resins, differ markedly in chemical composition from those of the *Cupressaceae* family. Pine resins, for instance, contain predominantly tricyclic diterpenoid acids with either abietane or pimarane skeletons.[5,6]

Triterpenoid resins are produced by various broad-leaved trees, for example, of the *Burseraceae*, *Dipterocarpaceae* or *Anacardiaceae* family. Resins from the *Burseraceae* family include olibanum or frankincense, obtained from several *Boswellia* species. *Boswellia* resins were already used by ancient cultures either in the preparation of perfumes, cosmetics and medicines or in fumigation during embalming ceremonies. In a few cases, the use of *Boswellia* resins as tempera paint binding media is also reported.[7] In the last decades, anti-inflammatory and antidepressant properties of triterpenoid boswellic acids and diterpenoid incensole derivates in *Boswellia* resins received large interest in the scientific world.[8] White dammar, however, is derived from various plants of the genera *Hopea* and *Shorea* (*Dipterocarpaceae* family) and mastic from trees of the genus *Pistacia* (*Anacardiaceae* family). Both, white dammar and mastic, are frequently used in the formulation of varnishes for easel paintings. In addition to their protective function, varnishes saturate the colours and give the painting a glossy appearance. Painting conservators in particular apply dammar and mastic on a large scale. Furthermore, mastic is utilised as incense or as an adhesive. Mastic holds many components in common with white dammar, but differs significantly in composition from *Boswellia* resins. In general, triterpenoid resins consist of pentacyclic and tetracyclic triterpenes belonging, for example, to oleanane, ursane, lupane, dammarane or euphane type molecules (Supporting Information Figure S1). Tetracyclic triterpenes based on the dammarane or euphane skeleton are characterised by the presence of a hydroxy or a keto group at position C-3. Furthermore, the lateral chain of tetracyclic triterpenic components often bears functional groups. A hydroxy or keto group at C-3 is also common for pentacyclic triterpenes based on oleanane, ursane or lupane type molecules. In addition, pentacyclic triterpenes are often oxidised at C-28 to alcohols, aldehydes or carboxylic acids.[5,6]

In addition to the terpenoid resins, there is a much smaller but also important group of phenolic resins. These resins contain no or hardly any terpenes, but esters of benzoic acid (**9**) and cinnamic acid (**10**) with benzenoid alcohols.[5,6] Benzoin as well as storax are well-known phenolic resins. The later results from *Liquidambar* spp. and *Altingia* spp. (*Altingiaceae* family).[6] Benzoin exudes from *Styrax* trees and shrubs (*Styracaceae* family). According to their origin, a distinction is made between Sumatra and Siam benzoin balsams. Siam benzoin balsam is mainly tapped in Laos and Thailand from *Styrax tonkinensis* (Pierre) Craib ex Hartwich. Sumatra benzoin balsam is produced by *Styrax benzoin* Dryand and *Styrax paralleloneurum* Perk, both native to tropical forests of North Sumatra. Analysis showed that Siam benzoin balsam is composed of **9** and esters of **9** and **10**. In contrast, Sumatra benzoin balsam contain **10** and its esters as well as a low content of **9** and respective esters.[9,10] Besides aromatic compounds, triterpenoid acids such as siaresinolic and sumaresinolic acid have also been identified in benzoin. A comparison of benzoin balsams shows that siaresinolic acid was found only in Siam benzoin balsam, while sumaresinolic acid was detected in both, Siam and Sumatra benzoin balsams.[10] Similar to benzoin balsams, storax resins obtained from *Liquidambar* species are also characterised by the presence of triterpenoid acids. For example, oleanonic acid and 3-epi-oleanolic acid have been identified in the resin of *Liquidambar orientalis* Mill.[11,12] Benzoin and storax are known for their pharmacological and odoriferous properties and used as incense in religious ceremonies, often in combination with *Boswellia* resins.[5,10] In addition, benzoin was used for the production of red lacquers. For instance, the red-coloured resin dragon's blood was often mixed with other red resins such as benzoin or shellac to intensify or modify the colour.[13]

The metabolic characterisation of plant resins has been the subject of several studies, and in particular the profile of diterpenes and triterpenes can be considered as genus-specific or sometimes even species-specific and allows distinction between different resin types.[5,6,14–16] Diterpenes and triterpenes as well as phenolic compounds in plant resins or varnishes can be analysed by numerous analytical methods. HPLC (high-performance liquid chromatography) in combination with MS (mass spectrometry) or UV (ultraviolet) detection as well as GC–MS (gas chromatography–mass spectrometry or THM-GC–MS (GC–MS with thermally-assisted hydrolysis and

methylation) are the most common techniques for the determination and quantification of diterpenoids/triterpenoids and phenolic compounds in various resins, with derivatisation of target structures required for GC applications.[4,10,12,17–23] The composition of varnishes on artworks as well as ageing products of plant resins has been studied, for instance, by MALDI-TOF-MS (matrix-assisted laser desorption/ionisation time-of-flight-mass spectrometry), GALDI-TOF-MS (graphite-assisted laser desorption/ionisation time-of-flight-mass spectrometry) or TOF-SIMS (time-of-flight secondary ion mass spectrometry).[24–28] These techniques allow the analysis of resins without any time-consuming sample preparation or derivatisation. However, the distinction between isomers is only possible to a limited extent, for example, by principal component analysis, which reveals the differences in the fragmentation pattern of the isomers.[28] Furthermore, planar chromatography is a powerful tool, especially for the screening of diterpenoids and triterpenoids in extracts of plant resins, thus enabling relatively simple, inexpensive and fast analyses without a time-consuming sample pretreatment.[29–31] However, diterpenoids and triterpenoids lack chromophores, so the sensitivity of UV detection is rather low. In addition, the characterisation of diterpenoid/triterpenoid compounds with similar structures and polarities remains a challenging task.

In this work, we report on the development of simple, rapid, sensitive and specific TLC (thin-layer chromatography) and (HP)TLC-APCI-MS [(high-performance) thin-layer chromatography-atmospheric pressure chemical ionisation-mass spectrometry) methods for the identification of triterpenoid and phenolic compounds in various plant resins to allow a discrimination of these resins with respect to their botanical origin. In this context, natural resins such as dammar, mastic, olibanum and benzoin, produced by different plant species, were analysed for resin-specific triterpenes and phenolic compounds. Furthermore, the potential of preliminary investigations using APCI-MS and specific post-chromatographic detection reactions was evaluated to provide first indications of resin composition. The applicability of the methods for the analysis of resin-based varnishes on wooden objects was tested on a wooden sample with a thin varnish film of mastic.

2 | MATERIAL AND METHODS

2.1 | Chemicals and materials

Acetone (HPLC grade), chloroform (HPLC grade), *n*-heptane (HPLC grade), *n*-hexane (HPLC grade), methanol (HPLC grade) and sulphuric acid (> 95%) were purchased from Fisher Scientific; acetonitrile (HPLC gradient grade) and formic acid (98%) were obtained from Riedel-de Haën; dichloromethane, ethanol and ethyl acetate from Carl Roth; acetic acid from J. T. Baker (99%); thionyl chloride (99.7%) from Acros Organics; **10** (97%), **9** (> 99.5%) and stannic chloride (99%) from Sigma-Aldrich; **1** from abcr GmbH; **2** (98.9%) from ChromaDex; **3** (99%) from PhytoLab GmbH & Co. KG Germany; **4** (≥ 97%) from Enzo Life Sciences Germany; **5** (98%) from Betulines Czech; **6** (> 96%) Tokyo Chemical Industry Co. Ltd; **7** (98.6%) from Carbone Scientific UK; **8** from ubichem UK; sumaresinolic acid (> 95%) from Biosynth Carbosynth Group; syringe filters [0.2 μm polytetrafluoroethylene (PTFE)], Normal-phase (NP)-TLC plates (silica gel 60, ALUGRAM Xtra SIL G/UV_{254}) as well as reversed-phase (RP)-HPTLC/TLC plates (partial octadecyl-modified silica, ALUGRAM RP-18 W/UV_{254}) from Macherey-Nagel; cerium(IV) sulphate (98%) was bought from Merck KGaA. Details of the resins used can be found in Supporting Information Table S1. Wooden panels (1 cm × 3.5 cm × 0.14 cm) with and without a mastic resin layer (see Figure S2) were prepared by Leonhard Rank (conservator, Cologne, Germany).

For natural ageing, dammar samples were kept in the dark in a closed box. Artificial ageing of resins was carried out under UV lamps (254 nm) for 163 h or in an oven for 21 h at 100°C. For ageing studies, powdered resins were stored on a glass surface.

2.2 | Preparation of stock solutions

Solutions (1 mg/mL) of triterpenic and phenolic standard compounds **1**–**10** were individually prepared in methanol, stored at −20°C and diluted with methanol to obtain working solutions down to a concentration of 1 μg/mL.

2.3 | Chromatography

Working solutions and extracts were applied on the (HP)TLC plates as 1 mm bands, in 2 aliquots using a Linomat 5 (CAMAG, Muttenz, Switzerland, track distance: 10 mm, distance from the lower edge: 15 mm, distance from left edge: 10 mm). Thereafter, each plate was developed in a pre-saturated ADC2 development chamber (CAMAG, Muttenz, Switzerland, migration distance: 85 mm) or a conventional TLC developing chamber using acetonitrile/water (95:5 v/v), acetonitrile/water (7:1 v/v) or 2% acetic acid in *n*-hexane/ethyl acetate (5:1 v/v) as developing solvent (see Section 3.2.3). For the optimisation of the chromatographic separation, different (HP)TLC plates as well as various developing solvents were tested, for example, various ratios of *n*-hexane/ethyl acetate, acetonitrile/water or methanol/water (with and without acetic acid addition).

(HP)TLC plates were inspected both under white light and with UV light at $\lambda = 254$ nm. Beside investigations by MS, different post-chromatographic detection reagents were also used for the identification of target structures (see Sections 2.4 and 2.5).

2.4 | Detection of triterpenes with thionyl chloride and stannic chloride (reagent A, modified according to Noller et al.[32])

The post-chromatographic detection reaction was performed with thionyl chloride and stannic chloride using working solutions of triterpenes and sample extracts applied on (HP)TLC plates. For the preparation of reagent A, anhydrous stannic chloride (0.2 mL) was dissolved

in thionyl chloride (20 mL). The reagent was prepared fresh daily. After development and drying, the (HP)TLC plates were immersed in the reagent for about 1 s and coloured bands became visible after some seconds or several minutes. For the optimisation of the detection reaction, pure thionyl chloride as well as various ratios of thionyl chloride and stannic chloride were tested (e.g., thionyl chloride/stannic chloride 1000:1, 100:1, 10:1 v/v).

2.5 | Detection of triterpenes with cerium-molybdenum reagent

Furthermore, post-chromatographic detection reactions were performed with cerium-molybdenum reagent (for the preparation of the cerium-molybdenum reagent see Schmidt et al.[33]). The reagent was stored in the fridge. After development and drying, the TLC plates were immersed in the reagent for about 1 s and blue bands became visible after exposure to heat.

2.6 | (HP)TLC-MS coupling

A TLC-MS interface (Plate Express from Advion combined with an isocratic pump) was utilised for the elution of compounds from the (HP)TLC plates into an expression^{L} CMS (compact mass spectrometer from Advion, Ithaca, NY, USA) system, equipped with an electrospray ionisation (ESI) ion source (negative and positive mode) or a APCI ion source (negative and positive mode, capillary temperature: 200/250°C, source voltage offset: 15/20 V, source voltage dynamic: 10/20 V, source gas temperature: 200/350°C, MS scan range *m/z* 100–600). Data acquisition and processing were performed with Mass Express and Data Express software (Advion). Prior to the measurements, substance-specific parameters were determined by direct inlet of respective working solutions. Methanol was used as eluent (flow rate 0.2 mL/min).

2.7 | Sample extraction and preparation (modified according to Mathe et al.[21] as well as Ganzera and Khan[18])

Resins (1 g) were powdered and an aliquot (250 mg) of each resin was extracted with methanol (3 mL) by sonicating the homogenised material for 10 min. After centrifugation (5 min, 22°C, 3000 rpm), the supernatant was filtered (0.2 µm, PTFE). This procedure was repeated three times. The supernatants were combined, and a defined volume (2 µL) of the sample extract was spotted onto a (HP)TLC plate. For the optimisation of the extraction procedure, further extracting agents were tested, for example, chloroform and *n*-hexane. For the calculation of extraction efficiency, the supernatant was concentrated to dryness and the residue was weighed (see Table S4). Furthermore, the insoluble residue was dried and weighed (see Table S5).

Thin wooden panels with and without a mastic-based varnish were also extracted three times with methanol (3 × 3 mL) by sonicating the homogenised material for 10 min. The supernatants were combined, and a defined volume (2 µL) of the sample extracts was spotted onto a (HP)TLC plate.

2.8 | Limit of detection

Limit of detection (LOD) was determined using the signal-to-noise ratio ($S/N \geq 3$). For calibration, stock solutions were diluted with methanol down to a concentration of 1 µg/mL. Calibration solutions were measured via direct injection (5 µL aliquots) by APCI-MS or applied on the (HP)TLC plates [NP- and RP-(HP)TLC plates; 2 µL aliquots]. (HP)TLC plates were developed using acetonitrile/water (95:5 v/v), acetonitrile/water (7:1 v/v) or 2% acetic acid in *n*-hexane/ethyl acetate (5:1 v/v) and investigated by (HP)TLC-APCI-MS. Experiments with NP-TLC plates were performed before and after development. Each calibration solution was measured three times, and analyses were executed with peak areas of characteristic mass peaks of the respective standard compound.

2.9 | System precision

For determining the system precision, methanolic solutions of **3**, **5**, **6**, **9** and **10** were used (1, 0.1 or 0.01 mg/mL). Each solution was measured six times by APCI-MS (direct injection) and (HP)TLC-APCI-MS. For (HP)TLC-APCI-MS experiments, solutions were spotted onto RP- or NP-(HP)TLC plates, (HP)TLC plates were developed using acetonitrile/water (95:5 v/v), acetonitrile/water (7:1 v/v) or 2% acetic acid in *n*-hexane/ethyl acetate (5:1 v/v) and investigated by (HP)TLC-APCI-MS. For the interpretation of the system precision, relative standard deviations (RSDs) of peak areas of characteristic mass peaks of **3**, **5**, **6**, **9** and **10** were used (positive mode; **3**: *m/z* 409, 453, 513; **5**: *m/z* 409, 423; **6**: *m/z* 409, 437, 455; negative mode; **9**: *m/z* 121; **10**: *m/z* 147). In addition, Dixon's Q test and Neumann trend test were applied for the identification of outliers or trends.

3 | RESULTS AND DISCUSSION

3.1 | Resin-specific triterpenoid and phenolic compounds

Discrimination between plant resins such as dammar, mastic, olibanum and benzoin is based on the selection of chemotaxonomic molecular markers, detectable in fresh/unaged and aged resins. The plant resins studied are commonly used triterpenoid or phenolic resins, whose molecular composition has already been investigated by several research groups. The photochemical and thermal ageing of triterpenoid resins have also been extensively studied. GALDI-MS studies by Dietemann et al. have shown, for example, that plant resins such as

dammar and mastic are oxidised quite quickly even when kept in darkness.[25] The commercially available resins are therefore usually in an advanced stage of oxidation and degradation.[26] Ageing of triterpenes results in a wide variety of products, formed by autoxidative chain reactions. Groups of signals spaced by 14 and 16 Da indicate the incorporation of different numbers of oxygen atoms as well as the simultaneous loss of hydrogen, for example, by allylic oxidation or oxidation from alcohols to acids.[25,26]

A selection of triterpenoid and phenolic compounds (for structural formula see Figure S3) that can be used as markers to distinguish plant resins is listed in Table 1.

3.2 | Development of a (HP)TLC-APCI-MS method for the identification of triterpenoid and phenolic marker compounds in plant resins

Identification of triterpenoid and phenolic marker compounds was performed by (HP)TLC-APCI-MS. For this purpose, plant resins were extracted; filtered extracts were applied on (HP)TLC plates, the plates were developed using a suitable developing solvent (see Section 3.2.3) and TLC zones were analysed by APCI-MS. In the course of method development, several parameters were optimised to allow detection of marker compounds in the presence of complex resin samples.

3.2.1 | Characterisation of triterpenoid and phenolic marker compounds by APCI-MS

Initially, the ability to ionise triterpenoid and phenolic marker compounds using ESI and APCI conditions [direct injection and ESI/APCI-(HP)TLC-MS experiments] was tested. Best results were obtained for the triterpenes by APCI in positive ionisation mode with a set of characteristic ions that provide information about the presence of functional groups ($[M + H]^+$, $[M + H - H_2O]^+$ and $[M + H - HCOOH]^+$; Table S2). In accordance with literature, dehydration of protonated triterpene alcohols as a dominating process in the APCI source resulting in $[M + H - H_2O]^+$ ions was observed.[35,38] Furthermore, fragment ions corresponding to $[M + H - HCOOH]^+$ are characteristic of triterpene acids with a carboxylic acid group in position 17 or 4 such as **2**, **6**, **7**, and **8**.[37–40] However, the carboxylic acid substituent present on **4** was not split off under APCI conditions. Instead, a fragment ion peak at *m/z* 441 was found for **4** in positive ionisation mode due to the presence of a hydroxy substituent and the resulting elimination of water ($[M + H - H_2O]^+$). In negative ionisation mode, triterpene acids were detected with acceptable peak intensities by APCI as deprotonated ions $[M - H]^-$. For the detection of the triterpene alcohols **1** and **5**, however, the negative ionisation mode is inappropriate. Phenolic compounds **9** and **10** were detected with satisfactory peak intensities by ESI and APCI as deprotonated ions $[M - H]^-$ in negative ionisation mode.

As a consequence, subsequent experiments were performed by [(HP)TLC]-APCI-MS in positive and negative ionisation mode.

3.2.2 | Characterisation of target structures by post-chromatographic detection reagents

Most triterpenoid marker substances cannot be detected by an inspection under UV light at $\lambda = 254$ nm or 366 nm. Therefore, different reagents were tested to confirm the presence of triterpenoid and phenolic marker compounds in extracts of plant resins. In addition to well-known reagents for the detection of terpenoids (e.g., anisaldehyde reagent[41,42] and vanillin–sulphuric acid reagent[43]), cerium-molybdenum reagent as well as the application of thionyl chloride and stannic chloride (reagent A) were tested. The cerium-molybdenum reagent is suitable for the detection of various oxidisable substances found in extracts of natural resins – this also includes triterpenoid and phenolic marker compounds. However, all stainable compounds showed a blue coloration. A more specific post-chromatographic detection reaction, suitable for the detection of triterpenes, can be performed with thionyl chloride and stannic chloride.

TABLE 1 Triterpenoid and phenolic marker compounds used to identify the plant resins studied.

Label	Name	Structure type	Biomarker for	Reference
1	α-Amyrin	Ursane	Various triterpenoid resins, e.g. elemi, white dammar, *Boswellia* resin, myrrh (unaged and aged)	6,15,24,34
2	β-Boswellic acid	Ursane	*Boswellia* resin (unaged and aged)	6,21
3	Acetyl-11-keto-β-boswellic acid	Ursane	*Boswellia* resin (unaged)	22
4	Dammarenolic acid	Dammarane	Dammar (white) (unaged and aged)	15,24,27,35
5	Lupeol	Lupane	Various triterpenoid resins, e.g. mastic, *Boswellia* resin (unaged and aged)	6,19,25,36
6	Moronic acid	Oleanane	Mastic (unaged and aged)	6,15,16,27,35
7	Oleanolic acid	Oleanane	Various triterpenoid resins, e.g. dammar, mastic (unaged)	25,28,37
8	Ursolic acid	Ursane	Dammar (unaged)	25,28,37
9	Benzoic acid	Phenolic compound	Benzoin (unaged)	6,10
10	Cinnamic acid	Phenolic compound	Benzoin (unaged)	6,10

Highly coloured solutions of triterpenes as well as characteristic sequences of colours, sometimes even allowing a distinction between isomeric compounds such as **1** and β-amyrin, using the thionyl chloride and stannic chloride reagent were first described by Noller et al.[32]

In this work, thionyl chloride and stannic chloride were used for the first time for post-chromatographic detection reactions of triterpenes. Initially, tests with different ratios of thionyl chloride and stannic chloride (1000:1, 100:1, 10:1 v/v) and thionyl chloride without addition of stannic chloride were carried out. A ratio of thionyl chloride/stannic chloride 100:1 v/v has proven to be suitable for the detection of triterpenoid marker compounds. Characteristic colour changes of seven triterpenes are listed in Table S3. As already described by Noller et al., the use of thionyl chloride in combination with stannic chloride allows a distinction between structural isomers.[32] For example, **2** and **8**, both triterpenes with the same molecular formula differing only in the positions of a methyl and a carboxylic acid group, show markedly different colour changes. Thus, for the characterisation of triterpenes, characteristic sequences of colours can be used in addition to retardation factor (R_F) values (see Table 2). However, phenolic marker compounds such as **9** and **10** as well as the triterpenoid compound **3** with an acetylated hydroxy group in position 3 cannot be stained with reagent A. A strong decrease in colour intensity was also found by Noller et al. for triterpenes holding esterified hydroxyl groups.[32] Studies on the stainability of acetylated triterpenes are the subject of additional investigations to be performed in future.

3.2.3 | Optimisation of mobile and stationary phase for planar chromatography

For the determination of triterpenoid and phenolic marker compounds in methanolic resin extracts, a variety of sorbents and solvents was tested. For this purpose, working solutions of standard compounds, resin extracts and extracts mixed with defined concentrations of standard compounds were applied on different (HP)TLC sorbents. After development and inspection under white light and with UV light at λ = 254 nm, (HP)TLC plates were investigated by (HP)TLC-APCI-MS or immersed in post-chromatographic detection reagents (see Section 3.2.2). (HP)TLC-APCI-MS studies showed that the use of RP-18 HPTLC plates results in a low background signal and an increase of peak areas for many triterpene acids – partly by a factor of 10–100 – as compared to TLC silica gel sorbent. Thus, octadecyl-modified silica HPTLC sorbent was preferred for HPTLC-APCI-MS experiments of triterpenoid resins.

For extracts of dammar and mastic, a satisfactory separation of triterpenoid marker and matrix compounds was found on partial octadecyl-modified silica HPTLC sorbent using acetonitrile/water (95:5 v/v) as developing solvent. Optimised TLC conditions for the analysis of **2** and **3** in the examined *Boswellia* resin extracts included the use of partial octadecyl-modified silica HPTLC plates and as a developing solvent methanol/water (7:1 v/v). For methanolic extracts of benzoin, no optimal separation of phenolic marker and matrix compounds was achieved with RP-18 (HP)TLC plates. Consequently, tests were performed with TLC silica gel sorbent. Here a satisfactory separation of marker and matrix compounds as well as suitable detection limits (see Section 3.2.5) for phenolic marker compounds **9** and **10** were observed with 2% acetic acid in *n*-hexane/ethyl acetate (5:1 v/v) as developing solvent. However, the R_F values for **9** (R_F = 0.32) and **10** (R_F = 0.30) are quite similar under these conditions. Thus, TLC-APCI-MS analysis is of great importance to distinguish between UV-active substances **9** and **10**, both of which cannot be stained with reagent A. The latter chromatographic system [TLC silica gel sorbent, 2% acetic acid in *n*-hexane/ethyl acetate (5:1 v/v)] also leads to an acceptable separation of extractable dammar, mastic and *Boswellia* resin components and can be used for preliminary investigations with regard to the composition of plant resins by a post-chromatographic

TABLE 2 Chromatographic data and retardation factor (R_F) values for triterpenoid and phenolic marker compounds. After dipping in cerium-molybdenum reagent all marker compounds show a blue coloration. For characteristic sequences of colours produced by dipping in reagent A see Supporting Information Table S3.

	Developing solvent and (high-performance) thin-layer chromatography [(HP)TLC] sorbent		
	Acetonitrile/water (95:5 v/v) RP-18 W	Methanol/water (7:1 v/v) RP-18 W	2% Acetic acid in *n*-hexane/ethyl acetate (5:1 v/v) Silica gel 60
Compound	R_F values		
1	0.31	–	0.38
2	0.55	0.41	0.28
3	0.67	0.60	0.25
4	0.67	–	0.22
5	0.37	–	0.37
6	0.66	–	0.20
7	0.57	–	0.28
8	0.54	–	0.27
9	–	–	0.32
10	–	–	0.30

detection reaction with reagent A. For the earlier reasons, RP-18 HPTLC plates were preferred for HPTLC-APCI-MS studies on dammar, mastic and *Boswellia* resins containing triterpene acids as marker compounds, whereas TLC silica gel plates were used for TLC-APCI-MS studies on benzoin balsam as well as for the preliminary study of the resin extracts.

The R_F values and coloration of marker compounds after derivatisation with reagent A or cerium-molybdenum reagent are presented in Tables 2 and S3.

3.2.4 | Optimisation of the extraction procedure

Extraction solvents of varying polarity were compared with respect to extraction efficiency, extract composition and the removal of polymeric fractions present in various resins such as dammar or mastic resins. For this purpose, powdered and homogenised plant resins (250 mg) were extracted three times by sonicating using, for instance, methanol, *n*-hexane or chloroform as extraction solvent. Afterwards, filtered supernatants were applied on the (HP)TLC plates; the (HP)TLC plates were developed and investigated by (HP)TLC-APCI-MS. For comparison, average peak areas of characteristic mass peaks of triterpenoid and phenolic marker compounds were determined. Furthermore, the extraction efficiency in terms of weight (Tables S4 and S5) as well as the chromatographic separation of marker and matrix compounds were considered. In accordance with the literature, methanol has proven to be a suitable solvent for the extraction of triterpenoid and phenolic marker compounds from the examined resins.[17,18,21,29,37] In addition, experiments were carried out with significantly lower sample amounts (8–9 mg resin). For this purpose, powdered resins were extracted with methanol. After centrifugation and filtration, the supernatants were concentrated to dryness. Subsequently, the residues were dissolved in methanol (300–500 µL) and used for analyses. Detection of marker compounds was possible even when using the lower sample amounts.

3.2.5 | Evaluation of the limit of detection and the system precision

LOD and system precisions were evaluated for selected triterpenoid and phenolic marker compounds by APCI-MS (direct injection) and (HP)TLC-APCI-MS (see Table 3). In this context, the influence of the chromatographic system on detection limits was investigated. For **3**, **5** and **6**, detection limits of 5–50 ng/injection and 2–20 ng/TLC zone were determined by APCI-MS (direct injection) and RP-HPTLC-APCI-MS using acetonitrile/water (95:5 v/v) or methanol/water (7:1 v/v) as developing solvent. For **5**, a detection limit of 20 ng **5**/TLC zone could also be determined with NP (in this case it means silica gel sorbent) plates. The use of NP-TLC plates, however, increases the detection limits for triterpene acids such as **3** and **6** to 2000 ng **3**/TLC zone [developing solvent: 2% acetic acid in *n*-hexane/ethyl acetate (5:1 v/v)], 200 ng **3**/TLC zone (without development of the TLC plates) and 200 ng **6**/TLC zone (with and without development of the TLC plates). As mentioned earlier, octadecyl-modified silica HPTLC sorbent was preferred for HPTLC-APCI-MS experiments on triterpenoid compounds (see Section 3.2.3). For phenolic compounds **9** and **10**, satisfactory detection limits of 5 ng/injection and 2 ng/TLC zone were determined by APCI-MS (direct injection) and NP-TLC-APCI-MS using 2% acetic acid in *n*-hexane/ethyl acetate (5:1 v/v) as developing solvent. System precisions were determined for **3**, **5**, **6**, **9** and **10** with an RSD in the range of 0.8%–10.4%. Thus, the data were considered adequate for the purposes of the present study.

3.3 | Preliminary investigations by APCI-MS (direct injection)

For preliminary investigations with regard to the composition of plant resins by APCI-MS, an aliquot of the respective methanolic resin extract was directly injected into the mass spectrometer and analysed without prior chromatographic separation. Obtained mass spectra

TABLE 3 Limit of detection (LOD) for selected marker compounds and relative standard deviations (RSDs) of peak areas of characteristic mass peaks of **3**, **5**, **6**, **9** and **10,** determined by atmospheric pressure chemical ionisation mass spectrometry (APCI-MS) (direct injection), normal-phase thin-layer chromatography (NP-TLC)-APCI-MS and reversed-phase high-performance thin-layer chromatography (RP-HPTLC)-APCI-MS.

	LOD (ng/injection or ng/TLC zone)				RSD (%)	
Compound	APCI-MS (direct injection)	NP-TLC-APCI-MS	NP-TLC-APCI-MS (without development of the TLC plates)	RP-HPTLC-APCI-MS	APCI-MS (direct injection)	(HP)TLC-APCI-MS
3	5	2000	200	2	10.4	3.9 (RP-HPTLC)
5	5	20	20	20	7.6	12.3
6	50	200	200	20	4.7	5.5 (RP-HPTLC)
9	5	2	–	–	4.3	6.0 (NP-TLC)
10	5	2	–	–	0.8	7.0 (NP-TLC)

were analysed with respect to the presence (or absence) of characteristic peaks for triterpenoid and phenolic marker compounds. Further information on the resins studied is given in Table S1.

In APCI mass spectra of dammar samples **D1–D4** (plant family *Dipterocarpaceae*), recorded in positive and negative ionisation mode, characteristic peaks of the triterpenoid marker compound **4** at *m/z* 441 ($[M + H - H_2O]^+$) and 457 ($[M\text{-}H]^-$) can be seen as base peaks or intense signals (Figure 1). Furthermore, intense signals at *m/z* 425 and 409 indicate the presence of white dammar ingredients such as dammaradienone (*m/z* 425 $[M + H]^+$), dammaradienol (*m/z* 409 $[M + H - H_2O]^+$), **1** (*m/z* 409 $[M + H - H_2O]^+$) or hydroxydammarenone (*m/z* 425, $[M + H - H_2O]^+$).[25,35,37,44] The latter is a major component of both, dammar and mastic. Signals with mass differences of 16 Da indicate the presence of corresponding oxidation products (see Section 3.1). A similar oxidation pattern resulting from autoxidation of hydroxydammarenone during storage was observed, for example, by Dietemann et al.[25] However, in naturally and thermally aged as well as photoaged dammar samples, the relative intensity of the signals, for example, at *m/z* 425, 441, 457 and 473, does not increase significantly (positive mode, Figure S4). In addition, signals at *m/z* 457 and 473 can also be detected in the extracts of other resin samples and are consequently not characteristic for aged dammer or mastic samples. Further investigation on oxidation products should be the subject of future studies. Mass spectra of sample **D5** differ significantly from spectra of **D1–D4**. Characteristic signals of **4** are absent or show a much lower intensity in mass spectra of **D5** (Figure 1). However, an intensive signal at *m/z* 409 can also be observed for **D5** in positive ionisation mode (Figure 1). **D5** is traded under the name "dammar dark" and probably originates from a *Canarium* species (plant family *Burseraceae*). Several resins of the genus *Canarium* have been marketed under the name elemi, with Manila elemi from *Canarium luzonicum* (Blume) A. Gray or *Canarium commune* L. in particular being used in Fine Arts.[34] Furthermore, a brownish-black resin with the commercial name black dammar can be obtained from trees of the species *Canarium strictum* Roxb.[37,45] Both resins, Manila elemi and black dammar, contain various triterpenes such as **1** or β-amyrin, to which an intensive signal at *m/z* 409 as well as less intense signals at *m/z* 425 and 423 can be attributed (see Table S2).[5,34,46] Moreover, **4** does not represent a triterpenoid marker compound for these *Canarium* resins. Thus, **D5** is correctly identified as no (white) dammar resin sample in the preliminary investigations by APCI-MS.

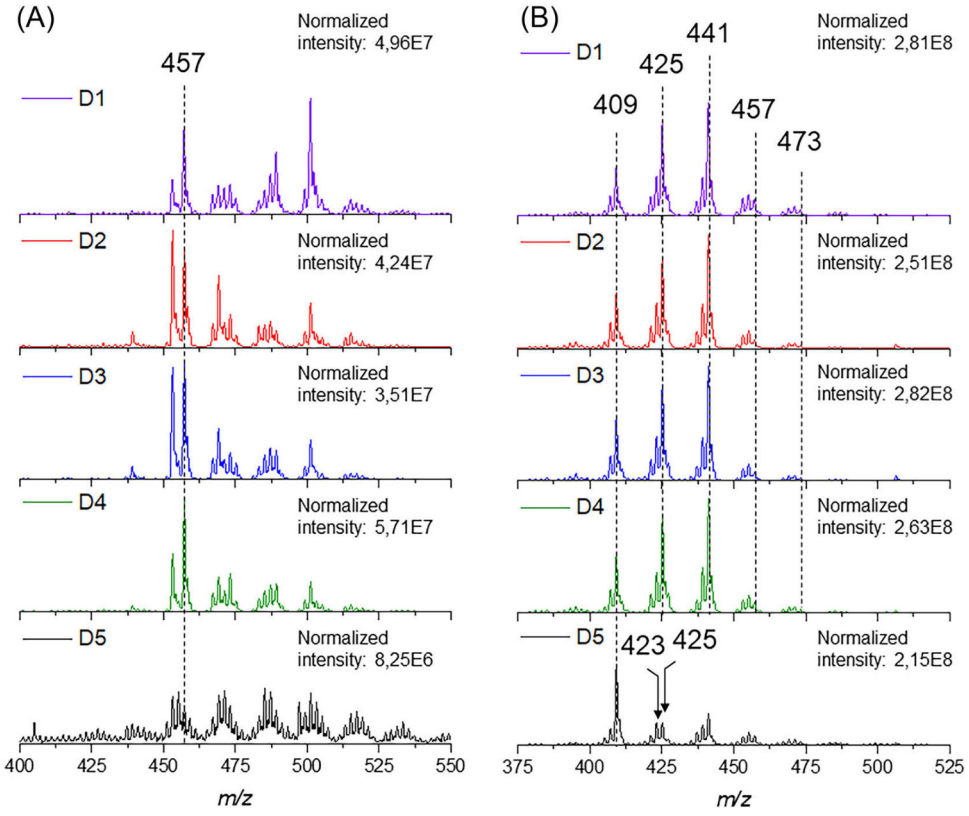

FIGURE 1 APCI mass spectra (direct injection) of methanolic extracts of dammar samples **D1–D5**. MS detection was performed in (A) negative mode (molecular ion of **4**: *m/z* 457) and (B) positive mode (fragment ions of **4**: *m/z* 441; **1** and β-amyrin: *m/z* 425, 423, 409; triterpenes contained in dammar with a dammarane skeleton such as hydroxydammarenone or dammaradienol: *m/z* 425, 409; putative products of autoxidative chain reactions: *m/z* 457, 473).

Intense signals at *m/z* 425 and 409 can also be detected in positive ionisation mode under APCI conditions in extracts of mastic samples **M1–M4** (Figure 2). As mentioned earlier, components such as hydroxydammarenone occur both in dammar and mastic. However, these signals can also be assigned to other triterpenoid components of mastic such as **5** (fragment ions of **5**: *m/z* 425, 409) or β-amyrin (expected fragment ions of β-amyrin: *m/z* 425, 423, 409[42,47]).[25] Furthermore, characteristic signals of the protonated and deprotonated marker compound **6** at *m/z* 455 ($[M + H]^+$) and 453 ($[M - H]^-$) are found as intense peaks in APCI mass spectra of **M1–M4** (Figure 2). For isomeric triterpene acids contained as minor components in mastic, for example, masticadienonic acid, isomasticadienonic acid or oleanonic acid, however, signals at *m/z* 455 (positive mode) or 453 (negative mode) would also be expected.[37]

Mass spectra of *Boswellia* resin extracts are more heterogeneous. However, in APCI mass spectra of samples *Boswellia* **1–5** characteristic peaks at *m/z* 513 ($[M + H]^+$) and 511 ($[M - H]^-$) assigned to protonated and deprotonated **3** are found as base or intense peaks (Figures S5A–D, S5A and S6A). In addition, signals at *m/z* 455 ($[M - H]^-$) and 497 ($[M - H]^-$) corresponding, for instance, to deprotonated boswellic acid (α-BA and **2**) or acetylated boswellic acid (α-ABA and β-ABA), are detected.[14,21] A characteristic signal of deprotonated boswellic acid at *m/z* 455 ($[M - H]^-$) is also prominent in mass spectra of sample *Boswellia* **6**, which is traded as "Weihrauch Borena (*Boswellia neglecta*)" (Figure S5E). As expected for a *Boswellia neglecta* resin, characteristic signals of **3** (negative and positive mode, Figures S6B and S7B) as well as the signal at *m/z* 497 (negative mode) were missing in mass spectra of this sample. Resins of *Boswellia neglecta* are characterised by very low concentrations of **3** and ABA and a medium concentration of boswellic acid compared to other *Boswellia* species.[22,48] Thus, first indications of the presence or absence of boswellic acids can be obtained by APCI-MS. Furthermore, characteristic signals at *m/z* 425, 423 and 409 of triterpenes such as **1** and **5**, also contained in *Boswellia* resins (see Table 1), were detected by APCI-MS in positive mode (Figure S7).

Characteristic peaks at *m/z* 121 ($[M - H]^-$) and 147 ($[M - H]^-$), indicating the presence of **9** and **10**, are found in APCI mass spectra of the benzoin extracts of **B1–B3** (**B1**: designated as Gummi Benzoe, without further details; **B2** and **B3**: traded as a Sumatra benzoin balsam, Figure S8). As expected, a characteristic peak of **9** at *m/z* 121 and no evidence for the presence of free **10** was found in sample **B4**, traded as a Siam benzoin balsam (Figure S8). Previous studies have shown that **9** was detected in both, Sumatra and Siam benzoin balsam, while quite important proportions of **10** were detected rather

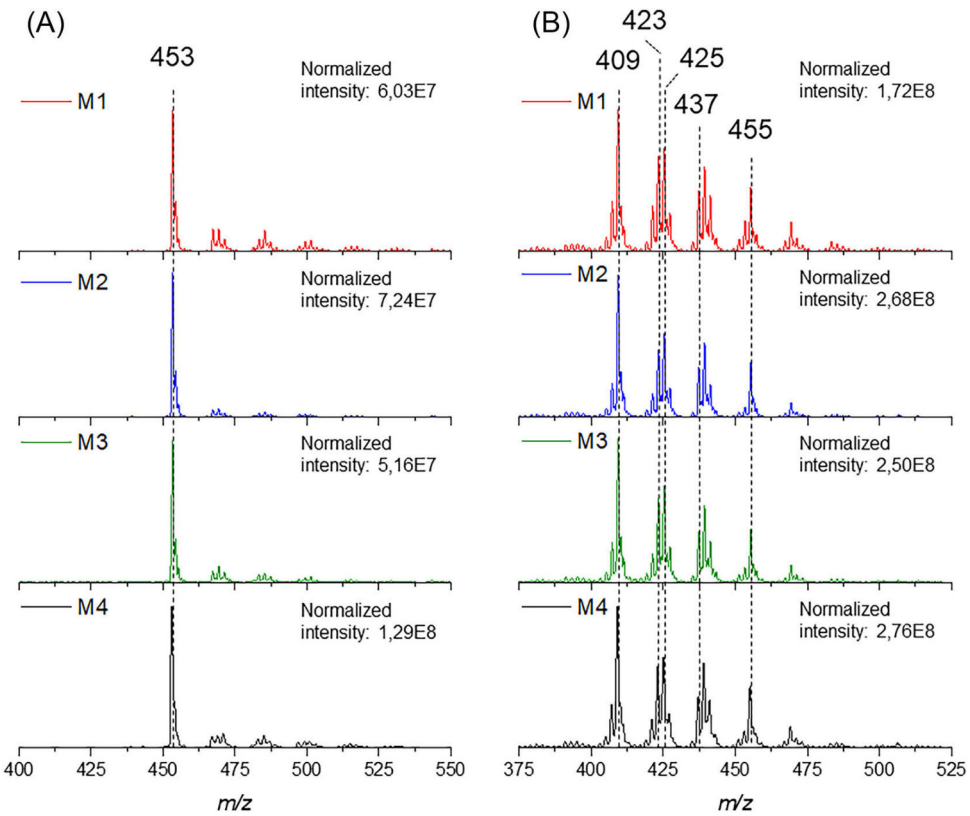

FIGURE 2 APCI mass spectra (direct injection) of methanolic extracts of mastic samples **M1–M4**. MS detection was performed in (A) negative mode (molecular ion of **6**: *m/z* 453) and (B) positive mode [(fragment) ions of **6**: *m/z* 455, 437, 409; **5**: *m/z* 425, 409; β-amyrin: *m/z* 425, 423, 409; hydroxydammarenone as a major component of mastic: *m/z* 425].

in Sumatra benzoin balsams.[10] However, in addition to a signal for **9** at *m/z* 121, an intensive characteristic signal of **10** at *m/z* 147 was also observed for sample **B5**, designated as Siam benzoin balsam. This finding is surprising, as the intensive characteristic signal of **10** is atypical for a Siam benzoin balsam and suggest a Sumatra benzoin balsam or an adulterated Siam benzoin balsam. However, further investigations, for example, by GC–MS or HPLC-ELDS (evaporative light scattering detector; see Burger et al.[10]), are required to verify the results. These investigations will be the subject of future studies.

Furthermore, APCI mass spectra of **B1–B5**, recorded in negative ionisation mode, show intense signals at *m/z* 469 and 471. These signals can probably be assigned to deprotonated siaresinolic or sumaresinolic acids (isomeric structures, both 472 Da) and deprotonated oxidised derivatives with a carbonyl group instead of a hydroxy group (470 Da). Sumaresinolic acid is well-known as a minor component in Sumatra and Siam benzoin balsams. Siaresinolic acid, however, is found only in Siam benzoin.[10,49] For a more detailed characterisation of **B1–B5**, further investigations by APCI-TLC-MS are required. It should be noted that **9**, **10** and respective ester derivatives are not reliable markers for a discrimination between ancient phenolic resins due to their high volatility and water solubility as well as cross-reactions (transesterification) with other constituents of the sample during ageing processes. Furthermore, the double bond of cinnamates might be cleaved by oxidative processes.[12] In contrast to **9** and **10** as well as respective ester derivatives, triterpenes such as sumaresinolic and siaresinolic acid are promising marker compounds for strongly aged phenolic resins, for example, from archaeological sites (see Section 1 and Courel et al.[12]).

For all extracts studied, characteristic signals of triterpenoid and phenolic marker compounds can be detected by APCI-MS. However, the distinction between isomeric structures in these complex multi-component mixtures is possible only to a limited extent without a chromatographic separation of these components. Consequently, (HP) TLC-APCI-MS studies are indispensable for further characterisation of natural resins (see Section 3.5).

3.4 | Preliminary investigations by planar chromatography and post-chromatographic detection reactions

For preliminary investigations with regard to the composition of the plant resins by TLC and post-chromatographic detection reactions, methanolic resin extracts were applied on TLC silica gel 60 sorbent and TLC plates were developed using 2% acetic acid in *n*-hexane/ethyl acetate (5:1 v/v). After an inspection under white light and with UV light at $\lambda = 254$ nm, TLC plates were immersed in reagent A.

Samples **B1–B5** and *Boswellia* **1–6** show characteristic bands and colour changes allowing a distinction between these resins. The obtained chromatograms of **B1–B3** (**B1**: designated as Gummi Benzoe, without further details; **B2** and **B3**: Sumatra benzoin balsams) show a uniform spot pattern with characteristic UV-active bands for **9** and/or **10**, however, with similar R_F values as already noted earlier (see Section 3.2.3, Figure S9). A characteristic UV-active band for **9** is also present in track 6 of sample **B4** (Siam benzoin balsam). Furthermore, a band stainable with reagent A (sequence of colours: red-brown → purple → purple-grey → grey → grey-green) and a R_F value of 0.15 indicates the presence of sumaresinolic acid in **B1–B4** (Figure S10). As already mentioned, sumaresinolic acid is contained in benzoin balsam from Sumatra and Siam. It should be noted that sample **B5** (designated as Siam benzoin balsam) shows a similar pattern to samples **B1–B3**, which is distinctly different from sample **B4** (Figures S9 and S10). This finding supports the assumption that sample **B5** is a Sumatra benzoin balsam or an adulterated Siam benzoin balsam (see Section 3.3).

Characteristic bands at R_F 0.28 with colour changes typical for **2** can be observed for *Boswellia* resins *Boswellia* **1–5** (Figure S11). In addition, the chromatograms of *Boswellia* **1–5** show at a R_F value of 0.25 a characteristic UV-active band for **3** that is not stainable with reagent A (Figure S12). An exception are extracts of the resin sample *Boswellia* **6**. These sample extracts show a spot pattern different from other *Boswellia* resins; for example, no indication of the presence of **3** and only a small amount of **2** was found (Figures S13 and S14). As mentioned earlier, *Boswellia* species such as *Boswellia neglecta* are characterised by a rather low concentration of boswellic acids (see Section 3.3).

Chromatograms of mastic samples **M1–M4** and dammar samples **D1–D4** are very similar (Figures 3 and S15–S17). However, different colour sequences can be observed for some stainable bands. Furthermore, marker compound **6** is not sufficiently separated from matrix components of samples **M1–M4** under these conditions (Figure S15), whereas marker compound **4** is clearly detectable in extracts of **D1–D4** (Figure 3). Artificially and naturally aged dammar samples also show characteristic bands with colour changes typical for **4** (see Section 2.1). Compared to **D1–D4**, the chromatogram of sample **D5** (*Canarium* resin) shows only one intense stainable band with a R_F value of 0.44 (sequence of colours: orange → red-brown → brown → grey-brown → grey-purple, Figure 3) and, as expected, differs significantly from chromatograms of **D1–D4** (white dammar).

Thus, characteristic spot patterns obtained after a planar chromatographic separation of extract ingredients, in combination with the sequence of colours observable after derivatisation with reagent A, are helpful to obtain the first hints about the resin composition.

3.5 | Characterisation of triterpenoid and phenolic resins by (HP)TLC-APCI-MS and post-chromatographic detection reactions

The characterisation of plant resins was performed by (HP)TLC-APCI-MS. Results of preliminary investigations using APCI-MS (direct injection) and post-chromatographic detection reactions provide initial information on the composition of the resins studied and help to choose suitable chromatographic conditions enabling a separation of

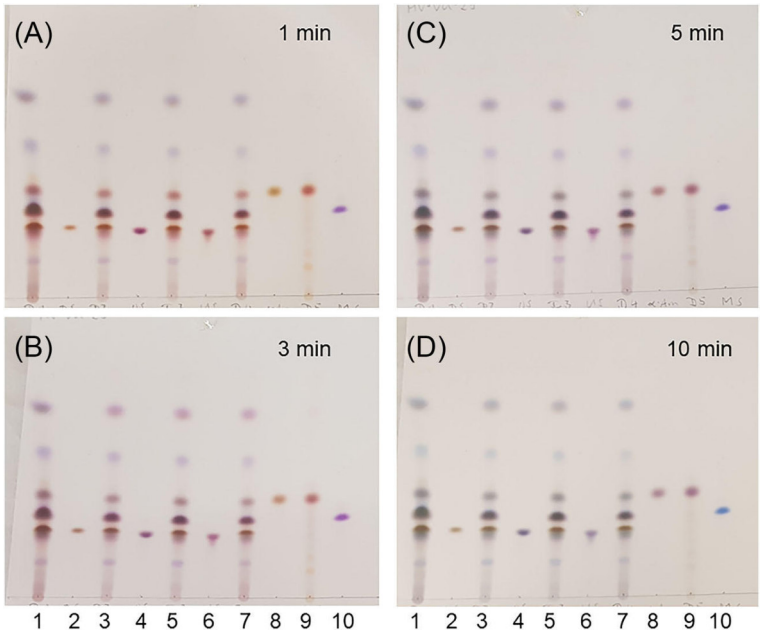

FIGURE 3 TLC chromatogram of methanolic dammar extracts and respected marker compounds developed on silica gel plates using 2% acetic acid in *n*-hexane/ethyl acetate (5:1 v/v) as mobile phase. TLC plates were viewed under white light (A) 1 min, (B) 3 min, (C) 5 min and (D) 10 min after derivatisation with reagent A. Tracks 1, 3, 5, 7, 9 = methanolic resin extracts (1: **D1**; 3: **D2**; 5: **D3**; 7: **D4**; 9: **D5**). Tracks 2, 4, 6, 8, 10 = methanolic solutions of marker compounds [2: **4** (dammarenolic acid); 4: **7** (oleanolic acid); 6: **8** (ursolic acid); 8: **1** (α-amyrin), 10: **6** (moronic acid); 2 µg/TLC zone each].

resin components. Identification of selected triterpenoid and phenolic compounds was achieved by APCI-MS spectra, R_F values and the presence or absence of characteristic colour changes after derivatisation with reagent A.

For dammar samples **D1–D4**, APCI mass spectra of the stainable band (typical colour sequence for **4**, see Table S3) at R_F 0.67 show intense peaks at *m/z* 441 (positive mode) and 457 (negative mode) correspond to the triterpenoid marker compound **4**. In contrast, **4** cannot be detected in the extract of sample **D5**. As already discussed, the composition and thus MS spectra and (HP)TLC chromatograms of white dammar (**D1–D4**) and the *Canarium* resin **D5** differ significantly (see Sections 3.3 and 3.4).

Compound **6** with a R_F value of 0.66 (colour sequence see Table S3) and characteristic signals at *m/z* 455, 437, 409 (positive mode) and 453 (negative mode) was identified in mastic samples **M1–M4**.

Characteristic signals of the triterpenoid marker compound **3** at *m/z* 513 (positive mode) and 511 (negative mode) are found at R_F 0.60 (non-stainable with reagent A) as intense peaks in APCI mass spectra of *Boswellia* **1–5**. The simultaneous presence of smaller peaks at *m/z* 453 and 409 in positive mode corresponding to fragment ions of **3** confirms the detection of **3** (see Table S2). Furthermore, bands with R_F values of 0.41 (typical colour sequence for **2**, see Table S3) and a characteristic signal of **2** at *m/z* 455 (negative mode) are found for *Boswellia* **1–5**. In contrast, no evidence of the presence of **3** was found in extracts of *Boswellia* **6**. Thus, **2** and **3** are suitable marker compounds for *Boswellia* resins, with the exception of sample *Boswellia* **6**. *Boswellia* **6** is traded as a *Boswellia neglecta* resin, which has a very low concentration of **3** compared to other *Boswellia* species (see Section 3.3). However, the composition of *Boswellia* **6** extracts should be verified by another method, for example, GC–MS, in future studies.

Phenolic marker compounds **9** and/or **10** with characteristic peaks at *m/z* 121 and 147 (negative mode) were detected in benzoin extracts **B1–B5** at R_F values of 0.32 and 0.30, respectively (NP-TLC-MS experiments). As noted earlier, bands of **9** and **10** can be detected under UV light at 254 nm, however, cannot be stained with reagent A (see Section 3.2.2 and Figures S9 and S10). The presence of sumaresinolic acid in benzoin extracts **B1–B5** can be confirmed by RP-HPTLC-APCI-MS. A characteristic signal of sumaresinolic acid at *m/z* 471 is found at R_F 0.70 as an intense peak in APCI mass spectra of **B1–B5** (Figure S18). As expected, the use of silica gel plates is unsuitable for the detection of the triterpene acid sumaresinolic acid by TLC-MS and results in a low intensity signal at *m/z* 471. Unfortunately, no optimal separation of **9**, **10** and matrix compounds was achieved with octadecyl-modified silica HPTLC sorbent. Therefore, two independent experiments using NP- and RP-(HP)TLC plates are required for the detection of **9**, **10** and sumaresinolic acid in benzoin extracts by TLC-MS.

Thus, the identification of triterpenoid and phenolic marker compounds, which allow discrimination of plant resins, by (HP)TLC-APCI-MS and specific detection reactions with reagent A was successful for all natural resins tested. In summary, (HP)TLC-APCI-MS in combination with specific post-chromatographic detection reactions is a simple, fast, inexpensive, sensitive and specific method for screening resins and resin-based varnishes for botanical origin that can analyse a large number of samples simultaneously (for a comparison with other techniques see Table S6).

3.6 | Case study: Analysis on a mastic varnish

Extracts of a 1-year-old mastic varnish – naturally aged as a thin film on a wooden panel – and an unvarnished wooden panel were

analysed by HPTLC-APCI-MS. Initially, the preliminary investigations described earlier were carried out. APCI mass spectra and (HP)TLC chromatograms of the mastic-based varnish look very similar to the studied mastic samples **M1–M4** (Figures S15 and S16). Thus, for the subsequent studies by HPTLC-APCI-MS, RP-18 HPTLC plates and acetonitrile/water (95:5 v/v) as developing solvent were used for the chromatographic separation of the resin components. Corresponding analyses confirm the presence of the triterpenoid marker compound **6** for the varnished sample and thus the presence of mastic, a natural triterpenoid resin often used by conservators. In comparison, no marker compound was detected in the extract of the unvarnished wooden panel.

ACKNOWLEDGEMENTS

This work was supported by ALAGO ART & STRINGS GmbH. The authors would like to thank Leonhard Rank (Cologne, Germany) for providing natural resins and for preparing a varnished wooden sample. Open Access funding enabled and organized by Projekt DEAL.

DATA AVAILABILITY STATEMENT

All data are included in the Supporting Information section.

ORCID

Annemarie E. Kramell https://orcid.org/0000-0002-2417-6372

REFERENCES

1. Moyler DA, Clery RA. The Aromatic Resins: Their Chemistry and Uses. In: Swift KAD, ed. *Flavours and fragrances*. Woodhead Publishing; 2005:96-115. doi:10.1533/9781845698249.2.96
2. Dilworth LL, Riley CK, Stennett DK. Chapter 5—plant constituents: carbohydrates, oils, resins, balsams, and plant hormones. In: Badal S, Delgoda R, eds. *Pharmacognosy*. Academic Press; 2017:61-80. doi:10.1016/B978-0-12-802104-0.00005-6
3. Mills JS, White R. *The organic chemistry of museum objects*. Butterworth & Co; 1987. doi:10.1016/B978-0-408-11810-1.50006-4
4. Kononenko I, de Viguerie L, Rochut S, Walter P. Qualitative and quantitative studies of chemical composition of sandarac resin by GC-MS. *Environ Sci Pollut Res*. 2017;24(3):2160-2165. doi:10.1007/s11356-016-7261-5
5. Mills JS, White R. Natural resins of art and archaeology their sources, chemistry, and identification. *Stud Conserv*. 1977;22(1):12-31. doi:10.1179/sic.1977.003
6. Colombini MP, Modugno F. Organic materials in art and archaeology. In: Colombini MP, Modugno F, eds. *Organic mass spectrometry in art and archaeology*. John Wiley & Sons; 2009:3-36. doi:10.1002/9780470741917.ch1
7. Dietemann P, Neugebauer W, Baumer U, et al. Analysis of complex tempera binding media combining chromatographic techniques, fluorescent staining for proteins and FTIR-FPA imaging. In: Beltinger K, Nadolny J, eds. *Painting in tempera, c 1900*. SIK-ISEA/Archetype Publications; 2016:183-203.
8. Al-Harrasi A, Csuk R, Khan A, Hussain J. Distribution of the anti-inflammatory and anti-depressant compounds: incensole and incensole acetate in genus *Boswellia*. *Phytochemistry*. 2019;161:28-40. doi:10.1016/j.phytochem.2019.01.007
9. Pastorova I, de Koster CG, Boon JJ. Analytical study of free and ester bound benzoic and cinnamic acids of gum benzoin resins by GC–MS and HPLC–frit FAB–MS. *Phytochem Anal*. 1997;8(2):63-73. doi:10.1002/(SICI)1099-1565(199703)8:2%3C63::AID-PCA337%3E3.0.CO;2-Y
10. Burger P, Casale A, Kerdudo A, et al. New insights in the chemical composition of benzoin balsams. *Food Chem*. 2016;210:613-622. doi:10.1016/j.foodchem.2016.05.015
11. Pastorova I, Weeding T, Boon JJ. 3-Phenylpropanylcinnamate, a copolymer unit in Siegburgite fossil resin: a proposed marker for the Hammamelidaceae. *Org Geochem*. 1998;29(5):1381-1393. doi:10.1016/S0146-6380(98)00068-0
12. Courel B, Adam P, Schaeffer P. The potential of triterpenoids as chemotaxonomic tools to identify and differentiate genuine, adulterated and archaeological balsams. *Microchem J*. 2019;147:411-421. doi:10.1016/j.microc.2019.03.035
13. Baumer U, Dietemann P. Identification and differentiation of dragon's blood in works of art using gas chromatography/mass spectrometry. *Anal Bioanal Chem*. 2010;397(3):1363-1376. doi:10.1007/s00216-010-3620-0
14. Paul M. Chemotaxonomic investigations on resins of the frankincense species *Boswellia papyrifera*, *Boswellia serrata* and *Boswellia sacra*, respectively, *Boswellia carterii*: a qualitative and quantitative approach by chromatographic and spectroscopic methodology [PhD thesis]. Saarland Universität; 2012.
15. Cartoni G, Russo MV, Spinelli F, Talarico F. GC-MS characterisation and identification of natural terpenic resins employed in works of art. *Ann Chim*. 2004;94(11):767-782. doi:10.1002/adic.200490098
16. Steigenberger G, Herm C. Natural resins and balsams from an eighteenth-century pharmaceutical collection analysed by gas chromatography/mass spectrometry. *Anal Bioanal Chem*. 2011;401(6):1771-1784. doi:10.1007/s00216-011-5169-y
17. Büchele B, Zugmaier W, Simmet T. Analysis of pentacyclic triterpenic acids from frankincense gum resins and related phytopharmaceuticals by high-performance liquid chromatography. Identification of lupeolic acid, a novel pentacyclic triterpene. *J Chromatogr B*. 2003;791(1):21-30. doi:10.1016/S1570-0232(03)00160-0
18. Ganzera M, Khan IA. A reversed phase high performance liquid chromatography method for the analysis of boswellic acids in *Boswellia serrata*. *Planta Med*. 2001;67(08):778-780. doi:10.1055/s-2001-18346
19. Marner F-J, Freyer A, Lex J. Triterpenoids from gum mastic, the resin of *Pistacia lentiscus*. *Phytochemistry*. 1991;30(11):3709-3712. doi:10.1016/0031-9422(91)80095-I
20. Papageorgiou VP, Bakola-Christianopoulou MN, Apazidou KK, Psarros EE. Gas chromatographic–mass spectroscopic analysis of the acidic triterpenic fraction of mastic gum. *J Chromatogr A*. 1997;769(2):263-273. doi:10.1016/S0021-9673(96)01032-1
21. Mathe C, Culioli G, Archier P, Vieillescazes C. High-performance liquid chromatographic analysis of triterpenoids in commercial frankincense. *Chromatographia*. 2004;60(9):493-499. doi:10.1365/s10337-004-0417-3
22. Schmiech M, Lang SJ, Werner K, Rashan LJ, Syrovets T, Simmet T. Comparative analysis of pentacyclic triterpenic acid compositions in oleogum resins of different *Boswellia* species and their in vitro cytotoxicity against treatment-resistant human breast cancer cells. *Molecules*. 2019;24(11):2153-2172. doi:10.3390/molecules24112153
23. Decq L, Stoffelen P, Cattersel V, et al. Quality control of natural resins used in historical European lacquer reconstructions with some reflections on the composition of sandarac resin (*Tetraclinis articulata* [Vahl] mast.). *J Anal Appl Pyrolysis*. 2021;158:105159. doi:10.1016/j.jaap.2021.105159
24. Dietemann P, Higgitt C, Kälin M, Edelmann MJ, Knochenmuss R, Zenobi R. Aging and yellowing of triterpenoid resin varnishes—influence of aging conditions and resin composition. *J Cult Herit*. 2009;10(1):30-40. doi:10.1016/j.culher.2008.04.007
25. Dietemann P, Kälin M, Zumbühl S, Knochenmuss R, Wülfert S, Zenobi R. A mass spectrometry and electron paramagnetic resonance study of photochemical and thermal aging of triterpenoid varnishes. *Anal Chem*. 2001;73(9):2087-2096. doi:10.1021/ac000754w

26. Dietemann P. Towards more stable natural resin varnishes for paintings—the aging of triterpenoid resins and varnishes [PhD thesis]; 2003.
27. Scalarone D, Duursma MC, Boon JJ, Chiantore O. MALDI-TOF mass spectrometry on cellulosic surfaces of fresh and photo-aged di- and triterpenoid varnish resins. *J Mass Spectrom*. 2005;40(12):1527-1535. doi:10.1002/jms.893
28. Tortora L, Biocca P, Sotgiu G, de Notaristefani F, Urbini M, Ioele M. Oleanolic and ursolic acid in dammar and mastic resin: isomer discrimination by using ToF-SIMS and multivariate statistics. *Surf Interface Anal*. 2016;48(7):398-403. doi:10.1002/sia.5991
29. Krohn K, Rao MS, Raman NV, Khalilullah M. High-performance thin layer chromatographic analysis of anti-inflammatory triterpenoids from *Boswellia serrata* Roxb. *Phytochem Anal*. 2001;12(6):374-376. doi:10.1002/pca.606
30. Pozharitskaya ON, Ivanova SA, Shikov AN, Makarov VG. Separation and quantification of terpenoids of *Boswellia serrata* Roxb. Extract by planar chromatography techniques (TLC and AMD). *J Sep Sci*. 2006; 29(14):2245-2250. doi:10.1002/jssc.200600078
31. Salomé-Abarca LF, van der Pas J, Kim HK, van Uffelen GA, Klinkhamer PGL, Choi YH. Metabolic discrimination of pine resins using multiple analytical platforms. *Phytochemistry*. 2018;155:37-44. doi:10.1016/j.phytochem.2018.07.011
32. Noller CR, Smith RA, Harris GH, Walker JW. Saponins and sapogenins. XX. Some color reactions of triterpenoid sapogenins. *J Am Chem Soc*. 1942;64(12):3047-3049. doi:10.1021/ja01264a511
33. Schmidt T, Kramell AE, Oehler F, et al. Identification and quantification of cannabinol as a biomarker for local hemp retting in an ancient sedimentary record by HPTLC-ESI-MS. *Anal Bioanal Chem*. 2020; 412(11):2633-2644. doi:10.1007/s00216-020-02492-0
34. De la Cruz-Cañizares J, Doménech-Carbó M-T, Gimeno-Adelantado J-V, Mateo-Castro R, Bosch-Reig F. Study of Burseraceae resins used in binding media and varnishes from artworks by gas chromatography–mass spectrometry and pyrolysis-gas chromatography–mass spectrometry. *J Chromatogr A*. 2005; 1093(1-2):177-194. doi:10.1016/j.chroma.2005.07.058
35. van der Doelen GA, van den Berg KJ, Boon JJ, Shibayama N, René de la Rie E, Genuit WJL. Analysis of fresh triterpenoid resins and aged triterpenoid varnishes by high-performance liquid chromatography–atmospheric pressure chemical ionisation (tandem) mass spectrometry. *J Chromatogr A*. 1998;809(1-2):21-37. doi:10.1016/S0021-9673(98)00186-1
36. Badria FA, Mikhaeil BR, Maatooq GT, Amer MMA. Immunomodulatory triterpenoids from the oleogum resin of *Boswellia carterii* Birdwood. *Z Naturforsch*. 2003;58(7-8):505-516. doi:10.1515/znc-2003-7-811
37. van Doelen GA. Molecular studies of fresh and aged triterpenoid varnishes [PhD thesis]. University of Amsterdam; 1999.
38. Kosyakov DS, Ul'yanovskii NV, Falev DI. Determination of triterpenoids from birch bark by liquid chromatography-tandem mass spectrometry. *J Anal Chem*. 2014;69(13):1264-1269. doi:10.1134/S1061934814130061
39. Novotny L, Abdel-Hamid ME, Hamza H, Masterova I, Grancai D. Development of LC–MS method for determination of ursolic acid: application to the analysis of ursolic acid in *Staphylea holocarpa* Hemsl. *J Pharm Biomed Anal*. 2003;31(5):961-968. doi:10.1016/S0731-7085(02)00706-9
40. Tarvainen M, Suomela J-P, Kallio H, Yang B. Triterpene acids in *Plantago major*: identification, quantification and comparison of different extraction methods. *Chromatographia*. 2010;71(3):279-284. doi:10.1365/s10337-009-1439-7
41. Paul M, Brüning G, Bergmann J, Jauch J. A thin-layer chromatography method for the identification of three different olibanum resins (*Boswellia serrata*, *Boswellia papyrifera* and *Boswellia carterii*, respectively, *Boswellia sacra*). *Phytochem Anal*. 2012;23(2):184-189. doi:10.1002/pca.1341
42. Martelanc M, Vovk I, Simonovska B. Separation and identification of some common isomeric plant triterpenoids by thin-layer chromatography and high-performance liquid chromatography. *J Chromatogr A*. 2009;1216(38):6662-6670. doi:10.1016/j.chroma.2009.07.038
43. Shai LJ, McGaw LJ, Aderogba MA, Mdee LK, Eloff JN. Four pentacyclic triterpenoids with antifungal and antibacterial activity from *Curtisia dentata* (Burm.f) C.A. Sm. leaves. *J Ethnopharmacol*. 2008;119(2):238-244. doi:10.1016/j.jep.2008.06.036
44. Vahur S, Teearu A, Haljasorg T, Burk P, Leito I, Kaljurand I. Analysis of dammar resin with MALDI-FT-ICR-MS and APCI-FT-ICR-MS. *J Mass Spectrom*. 2012;47(3):392-409. doi:10.1002/jms.2971
45. Varghese A, Ticktin T. Regional variation in non-timber forest product harvest strategies, trade, and ecological impacts: the case of black dammar (*Canarium strictum* Roxb.) use and conservation in the Nilgiri Biosphere Reserve, India. *Ecol Soc*. 2008;13(2):art11. doi:10.5751/ES-02555-130211
46. Hinge VK, Wagh AD, Paknikar SK, Bhattacharyya SC. Terpenoids—LXXI: constituents of Indian black dammar resin. *Tetrahedron*. 1965; 21(11):3197-3203. doi:10.1016/S0040-4020(01)96937-6
47. Liu R, Carballo-Arce A-F, Singh R, et al. A selective ion HPLC-APCI-MS method for the quantification of pentacyclic triterpenes in an anxiolytic botanical dietary supplement for the animal health market. *Nat Prod Commun*. 2019;14(1):11-14. doi:10.1177/1934578X1901400104
48. Schmiech M, Ulrich J, Lang SJ, et al. 11-keto-α-Boswellic acid, a novel triterpenoid from *Boswellia* spp. with chemotaxonomic potential and antitumor activity against triple-negative breast cancer cells. *Molecules*. 2021;26(2):366-391. doi:10.3390/molecules26020366
49. Hovaneissian M, Archier P, Mathe C, Culioli G, Vieillescazes C. Analytical investigation of styrax and benzoin balsams by HPLC- PAD-fluorimetry and GC-MS. *Phytochem Anal*. 2008;19(4):301-310. doi:10.1002/pca.1048

SUPPORTING INFORMATION

Additional supporting information can be found online in the Supporting Information section at the end of this article.

How to cite this article: Schendzielorz M, Schmidt T, Puchalla N, Csuk R, Kramell AE. TLC and HPTLC-APCI-MS for the rapid discrimination of plant resins frequently used for lacquers and varnishes by artists and conservators. *Phytochemical Analysis*. 2024;35(1):64-76. doi:10.1002/pca.3273

Supporting Information

TLC and HPTLC-APCI-MS for the rapid discrimination of plant resins frequently used for lacquers and varnishes by artists and conservators

Marcel Schendzielorz [1,#], Theresa Schmidt [1,#], Nils Puchalla [1], René Csuk [1], Annemarie E. Kramell [1]

[1] Department of Organic Chemistry, Martin-Luther-University Halle-Wittenberg, Kurt-Mothes-Straße 2, 06120 Halle, Germany

[#] Marcel Schendzielorz and Theresa Schmidt contributed equally to this work

Correspondence

Annemarie Elisabeth Kramell, Department of Organic Chemistry, Institute of Chemistry, Martin-Luther-University Halle-Wittenberg, Kurt-Mothes-Straße 2, 06120 Halle, Germany.

Email: annemarie.kramell@chemie.uni-halle.de

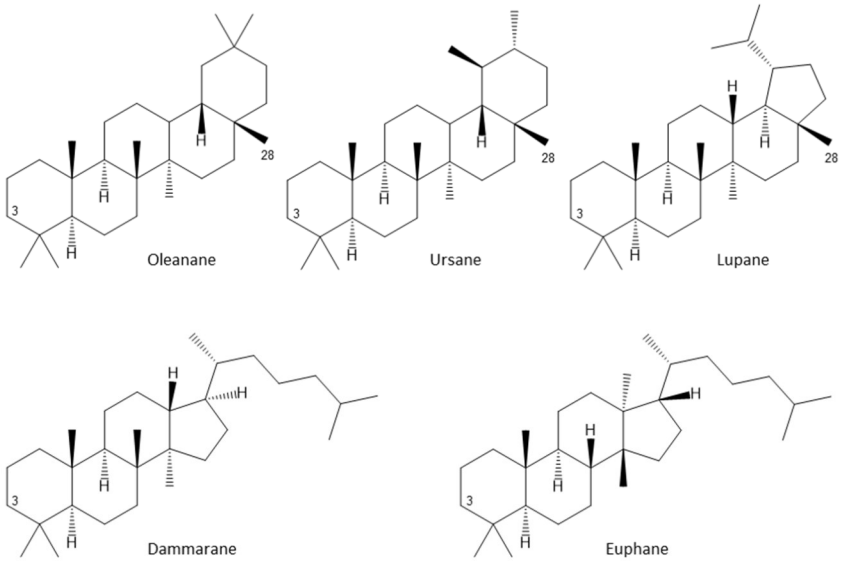

Figure S1 Pentacyclic and tetracyclic triterpenes - oleanane, ursane, lupane, dammarane and euphane skeleton.

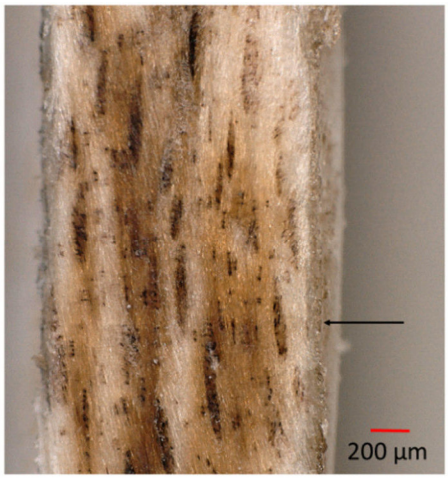

Figure S2 Cross section of a wooden panel with a mastic-based varnish. The arrow marks the varnished side.

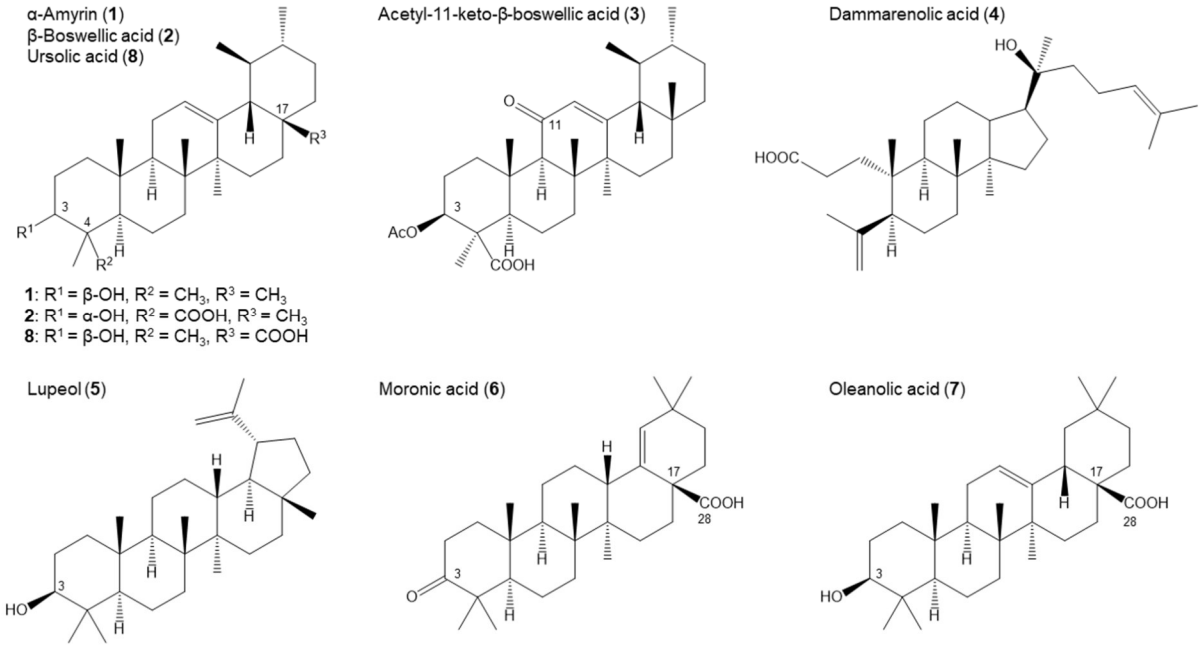

Figure S3 Triterpenes used as biomarkers for triterpenoid resins such as dammar, mastic or olibanum.

Table S1 Plant resin samples used for studies.

Plant resin	Sample ID	Plant family	Plant species	Supplier	Specification
Benzoin	B 1	*Styracaceae*	not specified	Kremer Pigmente, Aichstetten	Gummi Benzoe
	B 2		*Styrax benzoin* Dryand	Rauchtum, Brunnthal	Benzoe Sumatra
	B 3		*Styrax benzoin* Dryand	Seelenrauch, Weyhe	Benzoe Sumatra
	B 4		*Styrax tonkinensis* (Pierre) Craib ex Hartwich	Seelenrauch, Weyhe	Benzoe Siam
	B 5		*Styrax tonkinensis* (Pierre) Craib ex Hartwich	Rauchtum, Brunnthal	Benzoe Siam, Thailand
Dammar	D 1	*Dipterocarpaceae*	not specified	Kremer Pigmente, Aichstetten	Dammar resin
	D 2		not specified	Fine Art Encaustic, Weilheim/Teck	White dammar – dammar resin
	D 3		not specified	Justingredients, Chepstow, UK	Dammar gum
	D 4		*Shorea wiesneri*	Rauchtum, Brunnthal	Dammar white, India
	D 5	*Burseraceae*	*Canarium* species	Rauchtum, Brunnthal	Dammar dark, India
Mastic	M 1	*Anacardiaceae*	not specified	Kremer Pigmente, Aichstetten	Gummi mastic, Chios, Greek
	M 2		not specified	Chios Gum Mastic Growers Association	Gum mastic, Chios
	M 3		*Pistacia lentiscus* L.	Rauchtum, Brunnthal	Mastic – Mastiha, Chios, Greek
	M 4		*Pistacia lentiscus* L.	Seelenrauch, Weyhe	Mastic
Olibanum/ frankincense (*Boswellia* resin)	*Boswellia* 1	*Burseraceae*	not specified	Kremer Pigmente, Aichstetten	Gummi Olibanum
	Boswellia 2		*Boswellia carteri* Birdw.	Rauchtum, Brunnthal	Weihrauch Bejo, Somalia
	Boswellia 3		*Boswellia serrata* Roxb.	Rauchtum, Brunnthal	Weihrauch Salai-Guggal, India
	Boswellia 4		*Boswellia sacra* Flueck.		Royal Al-Hojari, Grade 1, Oman
	Boswellia 5		*Boswellia papyrifera* (Del.) Hochst.	AMAHOFF, Roßtal	Eritrea-Olibanum, Ethiopia
	Boswellia 6		*Boswellia neglecta* S. Moore	Rauchtum, Brunnthal	Weihrauch Borena, Ethiopia

Table S2 Characteristic (fragment) ions of triterpenoid and phenolic marker compounds under APCI (direct injection) conditions in positive and negative ionization mode.

Label	Compound	APCI-MS positive mode *m/z* (rel. Int.; %)	APCI-MS negative mode *m/z* (rel. Int.; %)	Comment
Triterpenes				
1	α-Amyrin	409 (100) 423 (22) 425 (20)	-	$[M+H-H_2O]^+$ $[M+H-2H_2]^+$ $[M+H-H_2]^+$
2	β-Boswellic acid	409 (57) 411 (37) 439 (100) 453 (81) 457 (10)	455 (100)	$[M+H-HCOOH-H_2]^+$ $[M+H-HCOOH]^+$ $[M+H-H_2O]^+$ $[M+H-2H_2]^+$ $[M+H]^+$ $[M-H]^-$
3	Acetyl-11-keto-β-boswellic acid	409 (60) 453 (17) 513 (100)	511 (100)	$[M+H-AcOH-CO_2]^+$ $[M+H-AcOH]^+$ $[M+H]^+$ $[M-H]^-$
4	Dammarenolic acid	441 (100)	457 (100)	$[M+H-H_2O]^+$ $[M-H]^-$
5	Lupeol	409 (100) 425 (18)	-	$[M+H-H_2O]^+$ $[M+H-H_2]^+$
6	Moronic acid	409 (100) 437 (20) 455 (45)	453 (100)	$[M+H-HCOOH]^+$ $[M+H-H_2O]^+$ $[M+H]^+$ $[M-H]^-$
7	Oleanolic acid	411 (25) 439 (100)	455 (100)	$[M+H-HCOOH]^+$ $[M+H-H_2O]^+$ $[M-H]^-$
8	Ursolic acid	411 (50) 439 (100)	455 (100)	$[M+H-HCOOH]^+$ $[M+H-H_2O]^+$ $[M-H]^-$
Phenolic compounds				
9	Benzoic acid	-	121 (100)	$[M-H]^-$
10	Cinnamic acid	-	147 (100)	$[M-H]^-$

Table S3 Post-chromatographic detection reactions of triterpenes with thionyl chloride-stannic chloride reagent (reagent A). Characteristic sequence of colors produced on TLC silica gel sorbent (observation period: one hour; developing solvent: 2 % acetic acid in n-hexane/ethyl acetate (5:1 v/v); concentration: 2 µg triterpene/TLC zone). Comparable color changes can be observed with RP-C18 (HP)TLC-plates.

Triterpenes	**thionyl chloride without addition of stannic chloride ***	**thionyl chloride/stannic chloride**		
		1000:1 v/v	**100:1 v/v**	**10:1 v/v**
1	Yellow → orange → brown → purple → gray	Brown → orange → red-purple → pale pink	Brown → orange → brown → purple → gray	Yellow → brown → gray-brown→ gray
2	Gray → gray-purple → gray	Gray → pale brown → light blue → colorless	Yellow-brown → brown → red-brown → purple → blue-purple → blue-gray	Yellow → red-brown → red → purple
4	Pale gray → pale brown → pale green → pale gray	Yellow-brown → orange → ochre → brown-green	Pale yellow → orange → orange-brown → light brown → pale yellow	Orange → red → red-brown → purple → gay-purple
5	Yellow → orange → brown-gray → gray	Yellow-brown → red-brown → brown-gray	Yellow-brown → orange → red-brown → brown-gray → gray	Yellow → brown → red-brown → brown-gray → purple → gray- brown
6	Pale purple → pale blue-gray → light gray → colorless	Purple → blue-purple → blue-gray → pale gray	Purple → blue-purple → blue-gryay → pale gray	Yellow-brown → purple → blue-purple → dark blue → blue-gray
7	Pink → purple → blue-gray → blue-green	Pink → purple → light blue → blue-green	Pink → purple → blue → blue-green	Orange → red → red-brown → purple → blue → gray-green
8	Pale pink → purple → blue-gray → gray	Ligth pink → blue-purple → blue-gray → gray-green	Ligth pink → pink → purple → blue-gray → gray-green	Yellow-orange → red-purple → purple → blue-green → gray

* clearly paler color reactions

Table S4 Extraction efficiency in terms of weight (x_e). Extraction solvent: methanol. Calculation: $x_e = m_r/m_0$ with m_r … mass of the extractable fraction and m_0 … mass of the resin before extraction.

Plant resin	**Sample ID**	**Extraction efficiency in terms of weight (%)**
Benzoin	**B 1**	99
	B 2	98
	B 3	97
	B 4	97
	B 5	99
Dammar	**D 1**	74
	D 2	73
	D 3	76
	D 4	74
	D 5	18
Mastic	**M 1**	84
	M 2	87
	M 3	90
	M 4	86
Olibanum/frankincense (*Boswellia* resin)	***Boswellia* 1**	75
	***Boswellia* 2**	70
	***Boswellia* 3**	62
	***Boswellia* 4**	67
	***Boswellia* 5**	75
	***Boswellia* 6**	64

Table S5 Comparison of extraction solvents with regard to extraction efficiency in terms of weight (x_e).
Calculation: $x_e = 1 - (m_r/m_0)$ with m_r … mass of the insoluble residue and m_0 … mass of the resin before extraction.

Extraction solvent	**Extraction efficiency in terms of weight (%)**			
	Benzoin **B 1**	Dammar **D 1**	Mastic **M 1**	*Boswellia* resin ***Boswellia* 1**
n-Hexane	0	32	23	43
Chloroform	64	70	100	37
Methanol	99	74	81	74

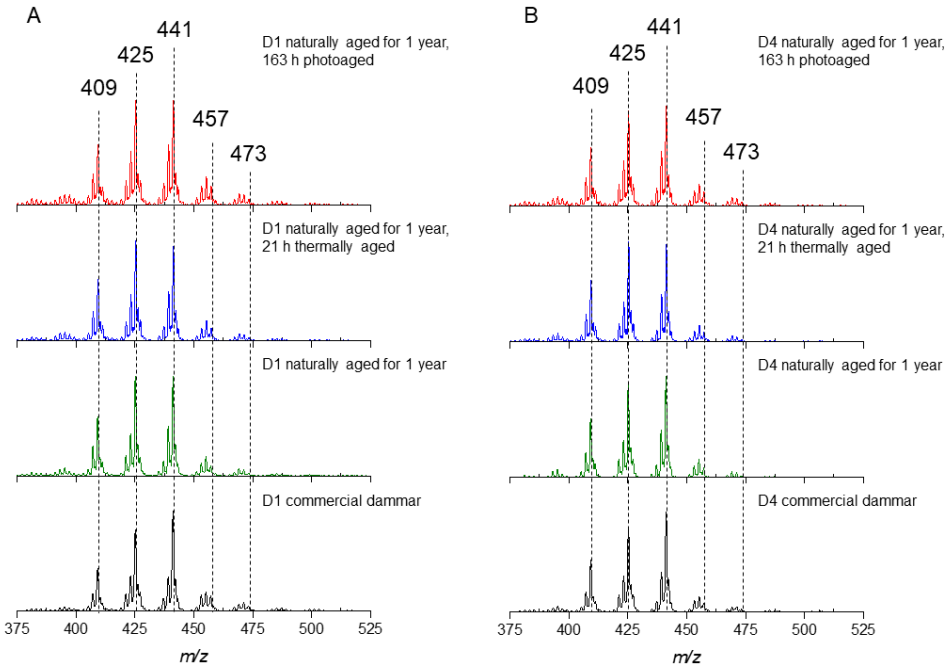

Figure S4 APCI mass spectra (direct injection) of methanolic extracts of commercial (unaged), naturally (aged for 1 year in darkness) and artificially (21 h, 100 °C or 163 h, 254 nm) aged dammar samples; a) **D 1** and b) **D 4** samples. MS detection was performed in positive mode [fragment ions of **4**: *m/z* 441; **1** and β-amyrin: *m/z* 425, 423, 409; triterpenes contained in dammar with a dammarane skeleton such as hydroxydammarenone or dammaradienol: *m/z* 425, 409; putative products of autoxidative chain reactions: *m/z* 457, 473]

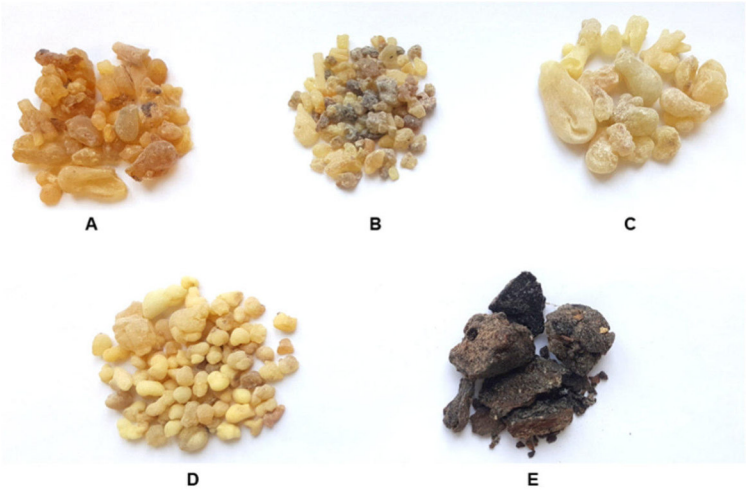

Figure S5 *Boswellia* resin samples ***Boswellia* 2-6** used for studies. a) *B. carteri* Birdw., b) *B. serrata* Roxb., c) *B. sacra* Flueck., d) *B. papyrifera* (Del.) Hochst., e) *B. neglecta* S. Moore.

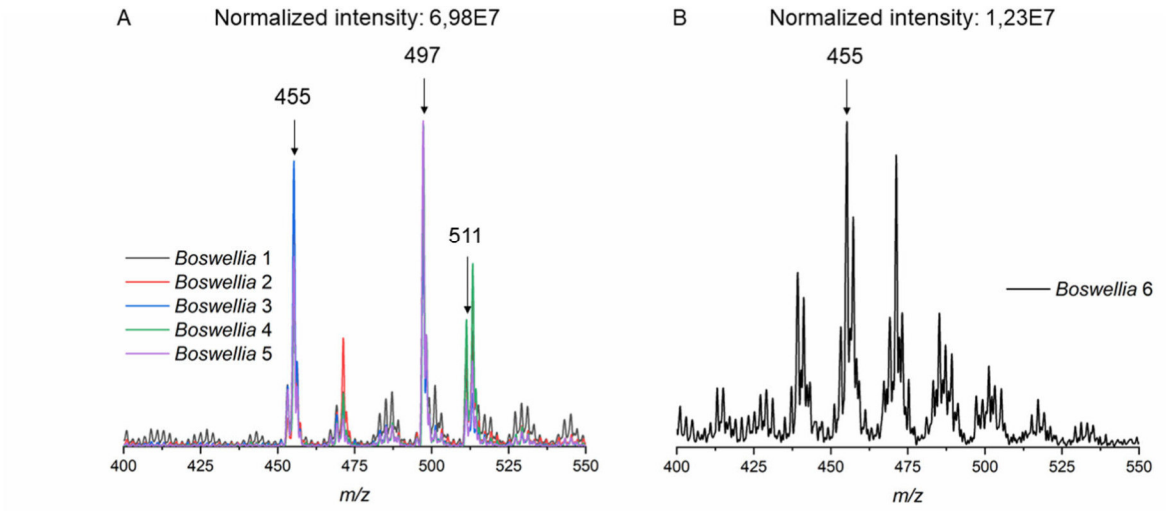

Figure S6 APCI mass spectra (direct injection) of methanolic extracts of *Boswellia* resin samples a) ***Boswellia* 1-5** and b) ***Boswellia* 6**. MS detection was performed in negative mode [molecular ion of **3**: *m/z* 511; boswellic acid (α-BA and **2**): *m/z* 455; acetylated boswellic acid (α-ABA and β-ABA): *m/z* 497].

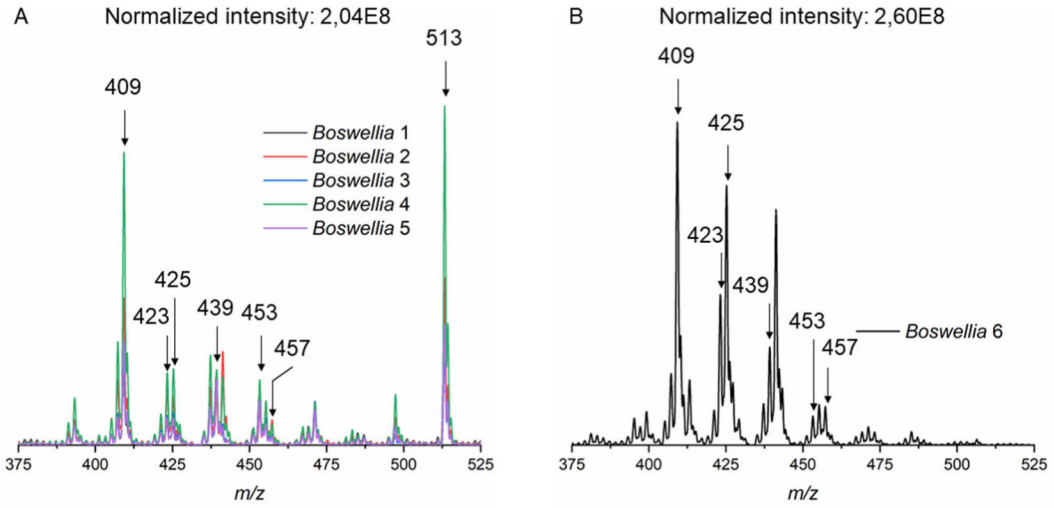

Figure S7 APCI mass spectra (direct injection) of methanolic extracts of *Boswellia* resin samples a) ***Boswellia* 1-5** and b) ***Boswellia* 6**. MS detection was performed in positive mode [(fragment) ions of **3**: *m/z* 513, 453, 409; boswellic acid (α-BA and **2**): *m/z* 457, 453, 439, 409; **5**: *m/z* 425, 409; **1**: *m/z* 425, 423, 409].

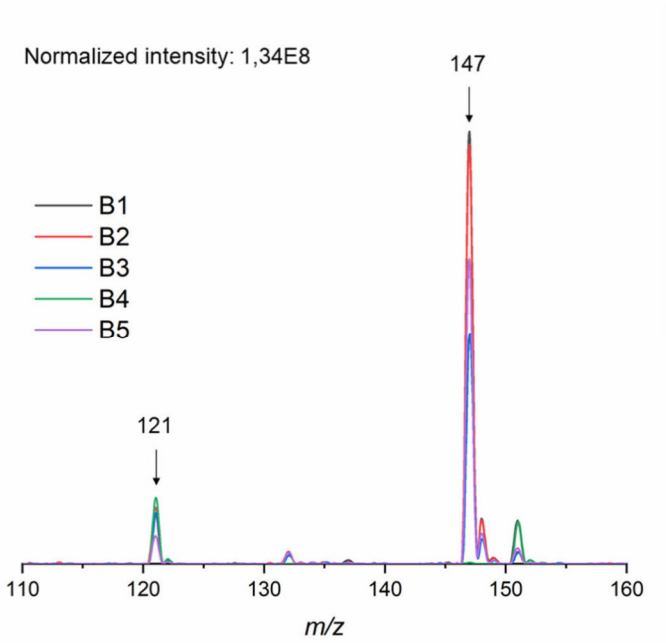

Figure S8 APCI mass spectra (direct injection) of methanolic extracts of benzoin samples **B 1-5**. MS detection was performed in negative mode [deprotonated ions $[M-H]^-$ of **9**: *m/z* 121; **10**: *m/z* 147].

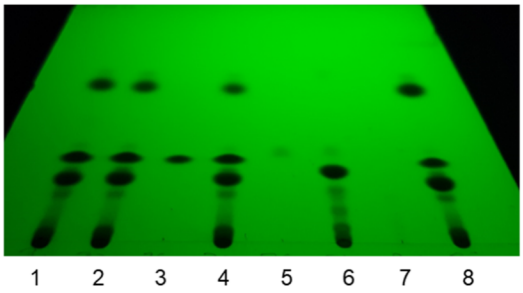

Figure S9 TLC chromatogram of methanolic extracts of benzoin samples and respected marker compounds developed on silica gel plates using 2 % acetic acid in *n*-hexane/ethyl acetate (5:1 v/v) as mobile phase. TLC plates were viewed with an UV light source at 254 nm. Tracks 1, 3, 4, 7, 8 = methanolic resin extracts (1: **B 1**; 2: **B 2**; 4: **B 3**; 6: **B 4**; 8: **B 5**). Tracks 3, 5, 7 = methanolic solutions of marker compounds [3: **10** (cinnamic acid); 5: **9** (benzoic acid); 7: sumaresinolic acid (not detectable under these conditions); 2 µg/TLC zone each].

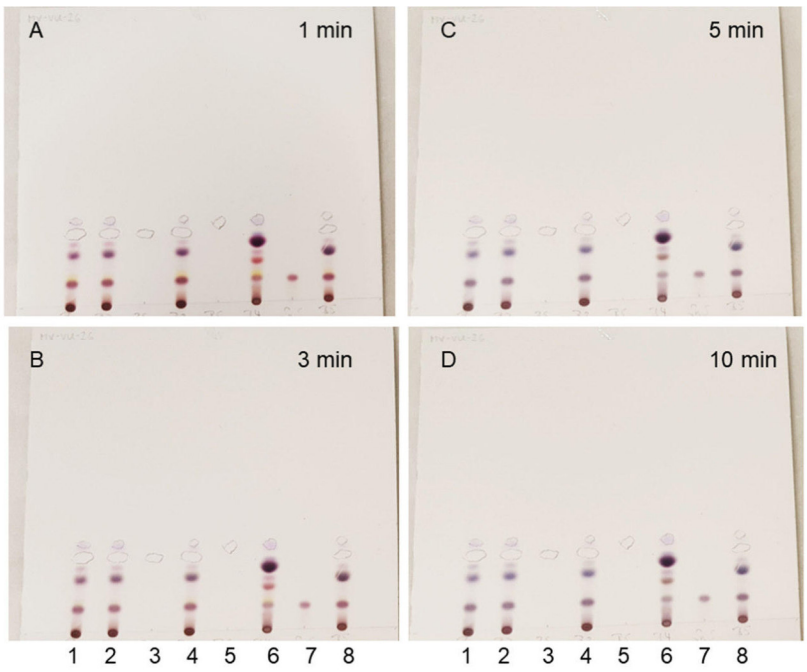

Figure S10 TLC chromatogram of methanolic extracts of benzoin samples and respected marker compounds developed on silica gel plates using 2 % acetic acid in *n*-hexane/ethyl acetate (5:1 v/v) as mobile phase. TLC plates were viewed under white light a) 1 min, b) 3 min, c) 5 min and d) 10 min after derivatization with reagent A. Tracks 1, 3, 4, 7, 8 = methanolic resin extracts (1: **B 1**; 2: **B 2**; 4: **B 3**; 6: **B 4**; 8: **B 5**). Tracks 3, 5, 7 = methanolic solutions of marker compounds [3: **10** (cinnamic acid, not stainable with reagent A); 5: **9** (benzoic acid, not stainable with reagent A); 7: sumaresinolic acid; 2 µg/TLC zone each (R_F: 0.15)].

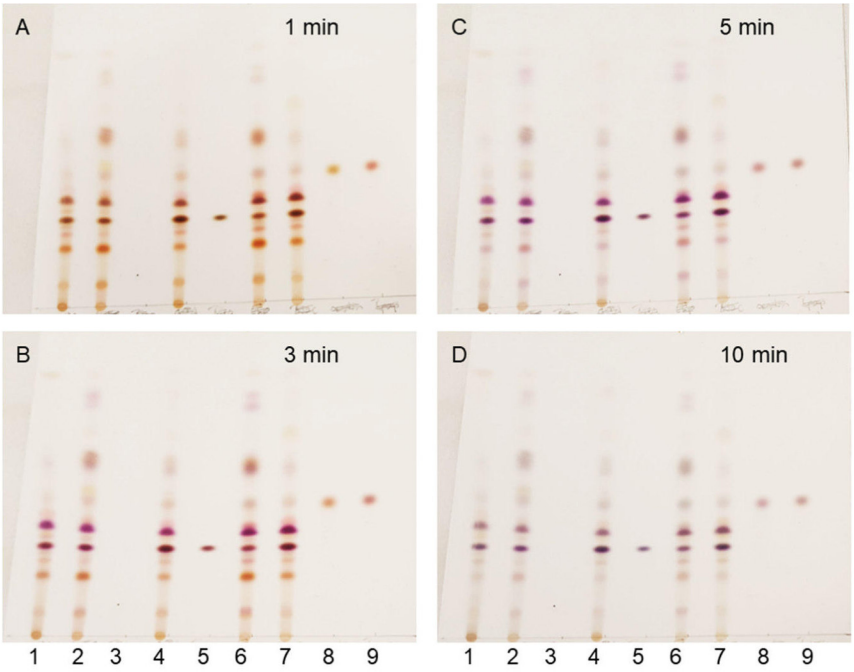

Figure S11 TLC chromatogram of methanolic *Boswellia* resin extracts and respected marker compounds developed on silica gel plates using 2 % acetic acid in *n*-hexane/ethyl acetate (5:1 v/v) as mobile phase. TLC plates were viewed under white light a) 1 min, b) 3 min, c) 5 min and d) 10 min after derivatization with reagent A. Tracks 1, 2, 4, 6, 7 = methanolic resin extracts (1: ***Boswellia* 1**; 2: ***Boswellia* 2**; 4: ***Boswellia* 3**; 6: ***Boswellia* 4**; 7: ***Boswellia* 5**). Tracks 3, 5, 8, 9 = methanolic solutions of marker compounds [3: **3** (acetyl-11-keto-β-boswellic acid, not stainable with reagent A); 5: **2** (β-boswellic acid); 8: **1** (α-amyrin); 9: **5** (lupeol); 2 µg/TLC zone each].

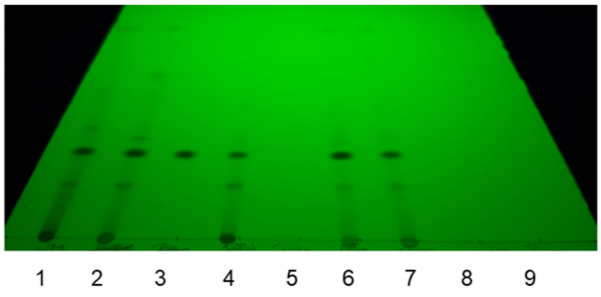

Figure S12 TLC chromatogram of methanolic *Boswellia* resin extracts and respected marker compounds developed on silica gel plates using 2 % acetic acid in *n*-hexane/ethyl acetate (5:1 v/v) as mobile phase. TLC plates were viewed with an UV light source at 254 nm. Tracks 1, 2, 4, 6, 7 = methanolic resin extracts (1: ***Boswellia* 1**; 2: ***Boswellia* 2**; 4: ***Boswellia* 3**; 6: ***Boswellia* 4**; 7: ***Boswellia* 5**). Tracks 3, 5, 8, 9 = methanolic solutions of marker compounds [3: **3** (acetyl-11-keto-β-boswellic acid); 5: **2** (β-boswellic acid, not detectable under these conditions); 8: **1** (α-amyrin, not detectable under these conditions); 9: **5** (lupeol, not detectable under these conditions); 2 µg/TLC zone each].

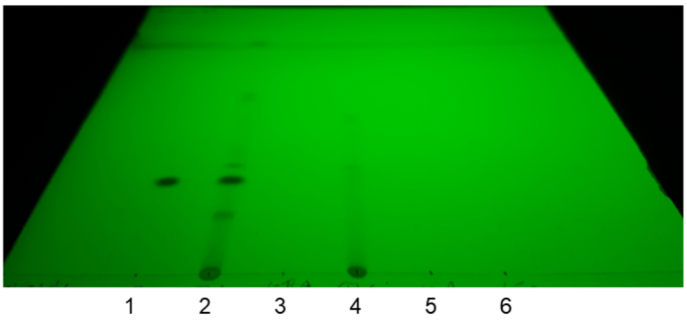

Figure S13 TLC chromatogram of methanolic *Boswellia* resin extracts and respected marker compounds developed on silica gel plates using 2 % acetic acid in *n*-hexane/ethyl acetate (5:1 v/v) as mobile phase. TLC plates were viewed with an UV light source at 254 nm. Tracks 2, 4 = methanolic resin extracts (2: ***Boswellia* 1**; 4: ***Boswellia* 6**). Tracks 1, 3, 5, 6 = methanolic solutions of marker compounds [1: **3** (acetyl-11-keto-β-boswellic acid); 3: **2** (β-boswellic acid, not detectable under these conditions); 5: **1** (α-amyrin, not detectable under these conditions); 6: **5** (lupeol, not detectable under these conditions); 2 µg/TLC zone each].

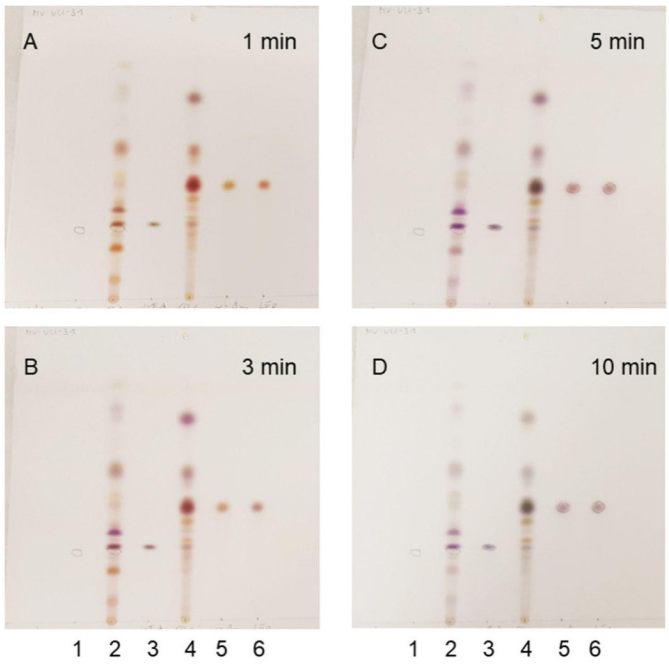

Figure S14 TLC chromatogram of methanolic *Boswellia* resin extracts and respected marker compounds developed on silica gel plates using 2 % acetic acid in *n*-hexane/ethyl acetate (5:1 v/v) as mobile phase. TLC plates were viewed under white light a) 1 min, b) 3 min, c) 5 min and d) 10 min after derivatization with reagent A. Tracks 2, 4 = methanolic resin extracts (2: ***Boswellia* 1**; 4: ***Boswellia* 6**). Tracks 1, 3, 5, 6 = methanolic solutions of marker compounds [1: **3** (acetyl-11-keto-β-boswellic acid, not stainable with reagent A); 3: **2** (β-boswellic acid); 5: **1** (α-amyrin); 6: **5** (lupeol); 2 µg/TLC zone each].

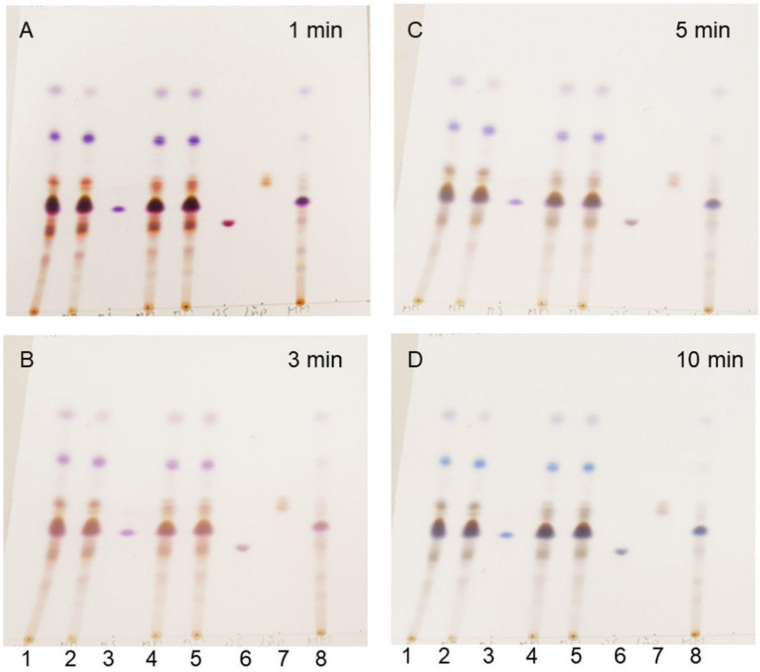

Figure S15 TLC chromatogram of methanolic mastic extracts and respected marker compounds developed on silica gel plates using 2 % acetic acid in *n*-hexane/ethyl acetate (5:1 v/v) as mobile phase. TLC plates were viewed under white light a) 1 min, b) 3 min, c) 5 min and d) 10 min after derivatization with reagent A. Tracks 1, 2, 4, 5 = methanolic resin extracts (1: **M 1**; 2: **M 2**; 4: **M 3**; 5: **M4**). Tracks 3, 6, 7 = methanolic solutions of marker compounds [3: **6** (moronic acid); 6: **7** (oleanolic acid); 7: **5** (lupeol); 2 µg/TLC zone each]. Track 8 = methanolic extract of a mastic-based varnish from a wooden panel (see 3.6).

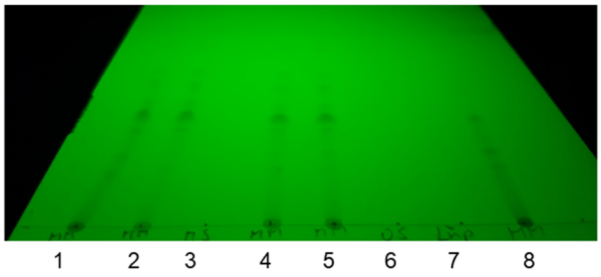

Figure S16 TLC chromatogram of methanolic mastic extracts and respected marker compounds developed on silica gel plates using 2 % acetic acid in *n*-hexane/ethyl acetate (5:1 v/v) as mobile phase. TLC plates were viewed with an UV light source at 254 nm. Tracks 1, 2, 4, 5 = methanolic resin extracts (1: **M 1**; 2: **M 2**; 4: **M 3**; 5: **M4**). Tracks 3, 6, 7 = methanolic solutions of marker compounds, not detectable under these conditions [3: **6** (moronic acid); 6: **7** (oleanolic acid); 7: **5** (lupeol); 2 µg/TLC zone each]. Track 8 = methanolic extract of a mastic-based varnish from a wooden panel (see 3.6).

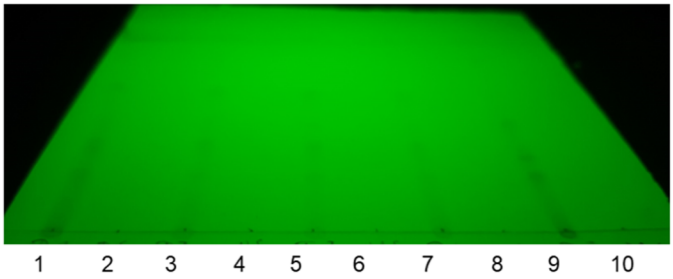

Figure S17 TLC chromatogram of methanolic dammar extracts and respected marker compounds developed on silica gel plates using 2 % acetic acid in *n*-hexane/ethyl acetate (5:1 v/v) as mobile phase. TLC plates were viewed with an UV light source at 254 nm. Tracks 1, 3, 5, 7, 9 = methanolic resin extracts (1: **D 1**; 3: **D 2**; 5: **D 3**; 7: **D 4**; 9: **D 5**). Tracks 2, 4, 6, 8, 10 = methanolic solutions of marker compounds, not detectable under these conditions [2: **4** (dammarenolic acid); 4: **7** (oleanolic acid); 6: **8** (ursolic acid); 8: **1** (α-amyrin), 10: **6** (moronic acid); 2 µg/TLC zone each].

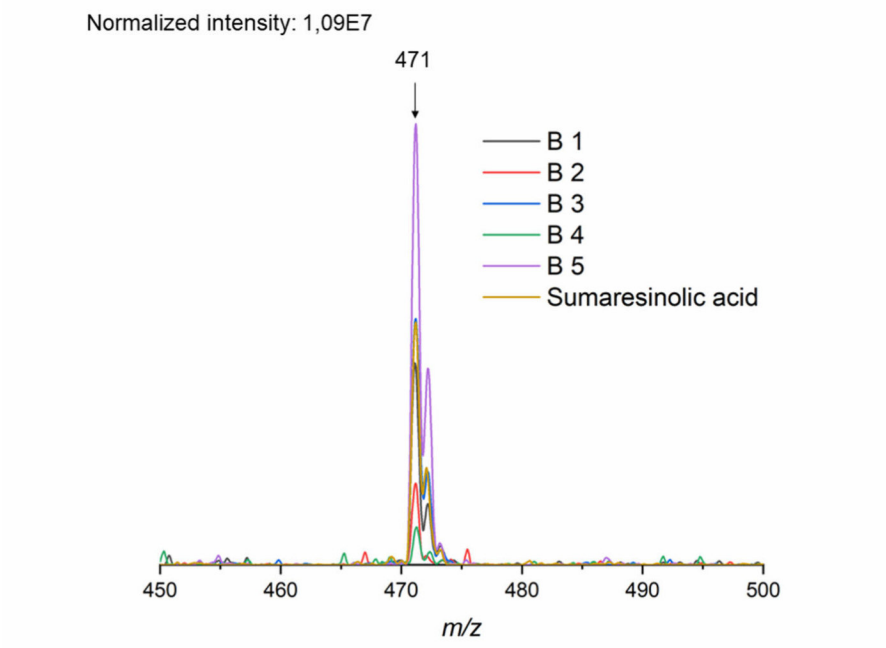

Figure S18 APCI mass spectra at R_F 0.70 of methanolic extracts of benzoin samples **B 1-5** and a methanolic solution of sumaresinolic acid (2 µg/HPTLC zone) spotted onto octadecyl-modified silica HPTLC plates. RP-HPTLC plates were developed using acetonitrile/water (95:5 v/v) and investigated by HPTLC-APCI-MS. MS detection was performed in negative mode [deprotonated ion $[M-H]^-$ of sumaresinolic acid: *m/z* 471].

Table S6 Comparison of the TLC and (HP)TLC-APCI-MS methods described in this study with other methods for the determination of triterpenes and phenolic compounds in various resins.

Ref.	Technique	Sample preparation	Analysis time	Identification of the compounds was based on…	LOD	Repeatability	Investigated material	Description
This study	TLC, HPTLC-APCI-MS	Extraction with MeOH by sonicating (RT, 3 x 10 min), centrifugation/filtration	TLC/HPTLC: 28.5 min for developing/drying, 1-10 min for post-chromatographic detection reactions (10 x 20 cm plates: up to 17 samples simultaneously) few seconds per (HP)TLC-APCI-MS analysis	R_F values, mass spectra, characteristic color sequences	2-20 ng/TLC zone [selected marker compounds, (HP)TLC-APCI-MS]	Coefficient of variation ±3.9 – 7.0 % (n=6) [selected marker compounds, (HP)TLC-APCI-MS]	Dammar, mastic, *Boswellia* and benzoin samples	Separation and identification of triterpenoid and phenolic compounds
(1)	HPLC-DAD	Soxhlet extraction with MeOH (RT, 3 h)	50/66 min per HPLC run	Retention times, UV-spectra	0.9-84 ng/injection	Coefficient of variation ±2% (n=6)	Frankincense resins, phytopharmaceuticals	Separation and quantification of 12 pentacyclic triterpenic acids
(2)	HPLC-DAD-ELDS, HPTLC (non-volatile compounds) GC-MS, GC-FID (volatile compounds)	Solubilized in ethanol, filtration	HPTLC: 5 min for developing/drying, < 10 min for post-chromatographic detection reactions with sulfuric anisaldehyde reagent; 40 min per HPLC run; 75 min per GC run	Retention times, R_F values, mass spectra, UV spectra	-	-	Benzoin samples	Separation and quantification of volatile compounds (vanillin, benzoic acid, cinnamic acid, benzyl benzoate) and non-volatile compounds (coniferyl benzoate, *p*-coumaryl cinnamate, cinnamyl cinnamate)
(3)	THM-GC/MS	Thermochemolysis in presence of tetramethylammonium hydroxid (0.2 min)	39 min per GC run	Retention times, mass spectra	-	Standard deviation (n=3) of selected markers for different temperature programs are given	Resins, gums and oils – e.g. of the genera *Tetraclinis*, *Callitris, Juniperus, Agathis*	Separation and identification of marker compounds (e.g. monoterpenes such as linalool, diterpenes, triterpenes, cinnamic and benzoic acids)
(4-6)	GALDI-TOF-MS	A suspension of graphite particles and a solution of the sample were pipetted sequentially onto a sample tip	Few minutes	Mass spectra	-	-	Dammar and mastic varnishes/resins (freshly harvested, commercially available, naturally and artificially aged samples)	Identification of triterpenes and related oxidation products without prior chromatographic separation
(7)	TOF-SIMS	Deposited of diluted samples on silicon wafer by spin coating technique	120 s per analysis (area: 500 × 500 µm^2)	High-resolution mass spectra, PCA (principal component analysis) using a selection of 61 peaks	-	-	Dammar and mastic resins	Identification of oleanolic and ursolic acids without prior chromatographic separation

References

1. Büchele B, Zugmaier W, Simmet T. Analysis of pentacyclic triterpenic acids from frankincense gum resins and related phytopharmaceuticals by high-performance liquid chromatography. Identification of lupeolic acid, a novel pentacyclic triterpene. *J Chromatogr B* 2003;791(1):21-30. https://doi.org/10.1016/S1570-0232(03)00160-0.
2. Burger P, Casale A, Kerdudo A, Michel T, Laville R, Chagnaud F, et al. New insights in the chemical composition of benzoin balsams. *Food Chem* 2016;210:613-22. https://doi.org/10.1016/j.foodchem.2016.05.015.
3. Decq L, Stoffelen P, Cattersel V, Mazurek J, Fremout W, Veenhoven J, et al. Quality control of natural resins used in historical European lacquer reconstructions with some reflections on the composition of sandarac resin (Tetraclinis articulata (Vahl) Mast.). *J Anal Appl Pyrolysis* 2021;158:105159. https://doi.org/10.1016/j.jaap.2021.105159.
4. Dietemann P, Kälin M, Zumbühl S, Knochenmuss R, Wülfert S, Zenobi R. A Mass Spectrometry and Electron Paramagnetic Resonance Study of Photochemical and Thermal Aging of Triterpenoid Varnishes. *Anal Chem* 2001;73(9):2087-96. 10.1021/ac000754w.
5. Dietemann P, Higgitt C, Kälin M, Edelmann MJ, Knochenmuss R, Zenobi R. Aging and yellowing of triterpenoid resin varnishes – Influence of aging conditions and resin composition. *J Cult Herit* 2009;10(1):30-40. https://doi.org/10.1016/j.culher.2008.04.007.
6. Dietemann P. Towards More Stable Natural Resin Varnishes for Paintings -The Aging of Triterpenoid Resins and Varnishes [PhD thesis]. Zurich: ETH; 2003.
7. Tortora L, Biocca P, Sotgiu G, de Notaristefani F, Urbini M, Ioele M. Oleanolic and ursolic acid in dammar and mastic resin: isomer discrimination by using ToF-SIMS and multivariate statistics. *Surf Interface Anal* 2016;48(7):398-403. https://doi.org/10.1002/sia.5991.

P4

scientific reports

Check for updates

OPEN

Degumming and characterization of *Bombyx mori* and non-mulberry silks from Saturniidae silkworms

Theresa Schmidt, Nils Puchalla, Marcel Schendzielorz & Annemarie E. Kramell✉

In this study, cocoons and degummed silk samples of *Bombyx mori* and twenty Saturniidae species of the genera *Actias*, *Attacus*, *Argema*, *Antheraea*, *Caligula*, *Callosamia*, *Cricula*, *Epiphora*, *Hyalophora*, *Loepa*, *Samia* and *Saturnia* are studied to gain an insight into their morphology, chemical composition and physical structure. For this purpose, silk samples are characterized by optical microscopy and FTIR spectroscopy in attenuated total reflection mode (ATR-FTIR spectroscopy). Furthermore, degummed silk samples are analyzed for their amino acid (AA) composition by GC-FID. In the course of method development, various degumming methods are tested using alkalis, citric acid, enzymes and detergents. A mixture of 0.1% sodium carbonate and 2.5% ethylenediamine proves to be an effective agent for degumming Saturniidae and *B. mori* cocoons. After hydrolysis of the fibroin filaments with 6 N hydrochloric acid and derivatization with propyl chloroformate, fifteen AAs are identified and qualified. This method shows a satisfactory overall analytical performance with an average recovery rate of 95% at the medium concentration level. The chemical composition of the different silks was considered comparatively. Within a genus, the analyses usually show a high degree of similarity in AA composition and the resulting structural indices, whereas differences are found between genera.

Silk is one of the most exclusive fibers in the world and has been used for textile production for several thousand years. The earliest direct biomolecular evidence for the existence of silk is from tombs dated 9000–8500 BP in Jiahu, China[1]. For centuries, the domesticated silkworm [*Bombyx mori* L. (BM), family Bombycidae], also known as mulberry silk moth, has been the most important producer of silk. These mulberry feeding silkworms originated from the Chinese wild silkworm *Bombyx mandarina* Moore that occurs throughout Asia, where modern sericulture and silkworm domestication were initiated[2,3]. Beside BM and *B. mandarina*, several wild or semi-domesticated moth larvaes produce silks with remarkable mechanical properties that have attracted large interest in the scientific world[4–7]. These non-mulberry feeding silkworm species are diverse and have a wide distribution throughout the world. Among non-mulberry silk moth the most well-known species, belonging to the family Saturniidae, are *Antheraea pernyi* Guérin-Méneville [APe, Chinese temperate (oak) tasar/tussah], *A. proylei* Jolly (Indian oak tasar, hybrid of *A. roylei* Moore and APe[8]), *A. mylitta* Drury (AM, Indian tropical tasar), *A. assamensis* Helfer (Indian muga), *Samia cynthia* Drury (SCy, Indian eri), and *A. yamamai* Guérin-Méneville (Japanese oak silk). Some species have great economic importance and are cultivated not only for textile production. For instance, APe, which uses oaks (various *Quercus* species) as host plants, is also used in traditional medicine, cosmetic products as animal feed, farm fertilizer and a food source for human consumption[9–11]. To meet this demand, thousands of hectares of oak are under cultivation today in China, India and Korea for silk, egg, larva and pupae production[10]. In contrast, silks from wild silk moth such as *Pachypasa otus* Drury (Lasiocampidae family), the source of Coan silk, have only historical significance[12].

A cocoon, whose primary function is to protect the developing moth against its natural enemies and climate conditions, is a multilayer composite material composed of two proteins, namely fibroin and sericin. Sericin, also known as gum, is a glue-like protein, which coats and binds together filaments of the protein fibroin into an intact cocoon. The structure and composition of the water-soluble sericin coating of BM has been the subject of several studies[13–15]. The sericin coating composed of two or more layers that cover the outside of the fibroin filaments. These layers of sericin consists mainly of AAs with a polar side chain such as Ser, Asp and Thr, with the amount of polar AAs in the sericin layers gradually decreasing from the outer to the inner layer. In production of silk threads and fabrics, sericin must be removed to obtain glossy, soft, smooth and dyeable materials. Conventional degumming processes, during which sericin is fully/partially hydrolyzed or solubilized, are based on the use of soap, alkalis, organic acids, enzymes or detergents[16,17]. In addition, various extraction processes, such as using

Department of Organic Chemistry, Martin-Luther-University Halle-Wittenberg, Kurt-Mothes-Straße 2, 06120 Halle, Germany. ✉email: annemarie.kramell@chemie.uni-halle.de

water at high temperature and pressure can be used for the removal of sericin[18]. In contrast to sericin, fibroin is insoluble in water, has a fibrous nature and contains a high proportion of amino acids (AAs) with non-polar side chains[19]. Silk fibroin from BM is composed of three proteins, heavy chain fibroin (FibH, 350 kDa), light chain fibroin (FibL 26 kDa) and P25 (also known as fibrohexamerin, 30 kDa), and consists mainly of Ala- (alanine) and Gly- (glycine) rich repetitive motifs[19]. The BM fibroin elementary unit consists of six disulfide-linked FibH and FibL dimers and one P25 glycoprotein molecule[20]. However, the AA sequence and composition of silk fibroin from non-mulberry silkworms differs from BM[21,22]. In this context, the chemical composition of various *Antheraea* species was studied in particular[23]. For instance, fibroin of commercial *Antheraea* species such as APe, AM and *A. assamensis* is characterized by a significantly higher content of Ala as well as a higher ratio of basic to acidic and hydrophilic to hydrophobic AAs compared to BM fibroin[7,24,25]. In addition, significant differences in mechanical properties and structural morphologies were found between silks of BM and other species[5,21]. Silk filaments of BM, for example, have a triangular cross-sectional shape, while wild silk is mostly elongated rectangular or a wedge-shaped[5,24]. In order to better understand the structural and chemical composition of non-mulberry silks, different techniques are used, e.g. (Wide-angle) X-ray diffraction, IR and Raman spectroscopy[21,23,24,26–28]. In addition, AA analyses using an Amino Acid Analyzer (AAA) as well as MS analyses of trypsinized cocoons or silks are used to characterize and identify silk proteins[13,22,23,28].

In this study, we report on the development and validation of a GC-FID method for the identification and quantification of fifteen AAs in silk fibroin of twenty-one silkworm species. Cocoons of BM and non-mulberry silkworms in the tribes *Saturniini* and *Attacini* (family Saturniidae) were degummed and the obtained fibroin filaments were analyzed for their AA composition. In this context, different degumming methods were tested, using optical microscopy and FTIR spectroscopy in attenuated total reflection mode (ATR-FTIR spectroscopy) as well as degumming ratio to monitor the degumming process and characterize the degummed silks. AA compositions, morphologies and ATR-FTIR spectra of the silk samples were compared and differences between silks produced by Saturniidae or Bombycidae moths were discussed. The aim of this study is to contribute basic knowledge on degumming of BM and Saturniidae cocoons, the chemical composition and the physical structure of the degummed silk filaments. Furthermore, the potential of AA analyses, microscopic and ATR-FTIR spectroscopic studies to distinguish between Saturniidae silks was investigated.

Experimental section

Chemicals and material

L-Alanine (Ala; 99%), L-isoleucine (Ile; 99%), L-proline (Pro; 99%), L-cysteine (Cys; > 98%), L-lysine (Lys; 98%), L-norleucine (Nle; 99%) and 3-picoline (99%) were obtained from Alfa Aesar. Glycine (Gly; ≥ 99%) were purchased from Tokyo Chemical Industry (TCI); L-leucin (Leu; ≥ 99%), L-valine (Val; ≥ 99%), L-glutamic acid (Glu; ≥ 99%), L-aspartic acid (Asp; ≥ 99%), L-threonine (Thr; ≥ 99%), L-phenylalanine (Phe; ≥ 99%) and L-methionine (Met; ≥ 99%) from CARL ROTH GmbH + Co. KG; L-serine (Ser; > 99%), L-histidine (His; ≥ 99%) sodium carbonate (Na_2CO_3; anhydrous), sodium hydrogen carbonate ($NaHCO_3$), citric acid (99%), ethylene diamine (≥ 99%), phenol (≥ 99%), 3,3′-dithiodipropionic acid (DTDPA, 99%) and sericin BM (silkworm) from Sigma-Aldrich; tryptophane (Trp; 99%), propyl chloroformate (98%) and *n*-Propanol (> 99%, extra pure) from Acros Organics; isooctane (ACS, Reag. Ph. Eur) from VWR Chemicals; chloroform (≥ 99.8%), concentrated hydrochloric acid (HCl; 37%) and sulphuric acid (≥ 95%) from Fisher Scientific and papain from carica papaya (3.0 U mg^{-1}) was bought from Fluka Chemicals. Handcrafted Savon de Marseille soap was obtained from the Savonnerie Fer à Cheval; Marseille, France. The industrial degumming detergent Perlavin LMO in combination with the sequestering solution Periquest APG (alkyl polyglycoside) was bought from Dr. Petry—Textile Auxiliaries, Reutlingen, Germany. The pineapples were purchased from a local market.

Cocoons and silk samples

BM cocoons were obtained from World of Butterflies & Moths (Lincolnshire, England), a Chinese web store and from the Francke Foundations in Halle/Saale (silk worms were cultivated within the framework of a pedagogical project). Degummed BM silk and cocoons of AM (Indian tasar silkmoth) were purchased from Seidentraum (organic peace silk, Sternenfels, Germany). Cocoons of *Attacus atlas* L. (AtA) were obtained from the butterfly house of Jonsdorf (Germany); other non-mulberry silkworm cocoons from World of Butterflies & Moths (Lincolnshire, England) or from Worldwide Butterflies (England).

Optical microscopy (OM) and ATR-FTIR spectroscopy

The surface morphology of the cocoons (outside and inside) and degummed silken filaments was characterized using a VHX-6000 digital microscope from KEYENCE. For ATR-FTIR analysis, a Perkin Elmer UATR two spectrometer was used. ATR-FTIR spectra were acquired with 64 or 256 scans over the range of 4000 to 400 cm^{-1} at a spectral resolution of 4 cm^{-1}. All samples were scanned on 2 to 5 different positions. Background was collected each time before all ATR-FTIR spectra of silk samples were collected. Spectral data analysis, including baseline correction, smoothing and deconvolution of amide I bands (1600–1700 cm^{-1}) were performed using Spectrum 10 software (Perkin Elmer) and PeakFit 4.12 (Systat Software Inc.) according to the literature[29–31]. The numbers and positions of peaks were defined from the results of second derivatives spectra and fixed during the deconvolution process. The data (e.g. β-sheet content) obtained from the spectra were the mean and standard deviations taken from separate deconvolutions from at least three separate samples. Assignment of adsorption peaks in the amide I band: the peak from 1619 to 1624 cm^{-1} is assigned to β-sheet conformation; the small peak from 1687 to 1692 cm^{-1} to β-turn conformation of the hairpin-folded antiparallel β-sheet structure; and the peak centered at 1653–1662 cm^{-1} to random coil, helical conformation, or both.

Degumming

Sericin removal was performed by different methods: alkaline or acidic methods with Na_2CO_3, $NaHCO_3$, ethylenediamine or citric acid, enzymatic processes with papain or pineapple juice and methods with detergents such as Marseille soap or industrially used Perlavin LMO (modified according to[16,17,28,32,33]. After degumming, the fibers were immediately rinsed thoroughly with distilled water until a neutral pH value was achieved and dried at 100 °C until constant weight was reached. The degumming ratio D_r (%), which correspond to the amount of sericin and non-sericin components (including wax, pigments, sugars and other impurities) removed by different degumming treatment, was expressed in terms of percentage weight loss using the weights of the dried silk samples before (W_0) and after (W_1) degumming (see Feng et al.[34]). For the D_r calculation, the following Eq. (1) was used:

$$D_r(\%) = \frac{W_0 - W_1}{W_0} * 100 \quad (1)$$

In addition, microscopic and ATR-FTIR spectroscopic examinations were carried out to assess the efficiency of the degumming process. Degumming methods were first applied to cocoons of BM, and subsequently the studies were extended to non-mulberry silkworm cocoons, e.g. of AtA and AM. Pupae, plant parts and coarse impurities were removed with tweezers before degumming. All experiments were repeated three times.

In alkaline method, cocoons were treated with an aqueous solution of Na_2CO_3 (1 g L^{-1}) at 95 °C for 30–90 min. To optimize the degumming process, the reaction time (30, 60, 90, 120 min), concentration of the Na_2CO_3 solution (between 0.1 and 5 g L^{-1}) and the temperature of the water bath (80 °C, 90 °C and 95 °C) were varied.

Furthermore, cocoons were degummed at 95 °C for 30–120 min using different concentrations of ethylenediamine (2.5 and 10% v/v) or $NaHCO_3$ (0.5 and 1% w/v). As alternative method, cocoons were boiled at 95 °C in an aqueous solution containing Na_2CO_3 (1 g L^{-1}) and ethylenediamine (2.5% w/w). This study was conducted for 30, 60, 90 and 120 min. The recommended reaction time for BM cocoons is 30–60 min. However, reaction times of up to 300 min are required for decoating of non-mulberry cocoons.

In addition to alkaline degumming described above, an acidic approach using citric acid (1 and 2 g L^{-1-}; reaction time: 120, 240 min; temperature of the degumming bath: 95 °C), an enzyme-based method with papain (1 g L^{-1}; reaction time: 120, 240 min; temperature of the degumming bath: 90 °C; pH value of the degumming bath: 6) and the use of an industrial detergent (1 g L^{-1} Periquest APG as a nonionic surfactant and 5 g L^{-1} Perlavin LMO as a detergent based on natural soaps with additional fiber-protective components—specifically designed for degumming silk; reaction time: 60, 90 and 120 min; temperature of the degumming bath: 95 °C) were evaluated. Prior to silk degumming with Periquest APG and Perlavin LMO, the degumming bath was adjusted to pH 10 with a NaOH solution.

Conventional degumming methods using Marseille soap (1 and 2 g L^{-1}; pH value of the degumming bath: 8–10) or fresh pineapple juice, which is known to be a reservoir of proteolytic enzymes, were also tested. For the conventional soap process, the degumming bath was heated to 95 °C and process was continued for 120 min at this temperature. The degumming using the juice of a pineapple was carried out at 90 °C for 120 and 240 min, respectively. For this purpose, pineapples were peeled, cut and blended using a mixer. The filtrate was used to remove the sericin coating.

AA analysis by GC-FID

Preparation of standard solutions

Stock solutions (50 mM) of (L-)AAs were individually prepared in aqueous hydrochloric acid (0.1 M) and diluted with aqueous hydrochloric acid (0.1 M) to obtain working solutions down to a concentration of 1 mM. Nle (50 mM) was used as an internal standard.

Hydrolysis of Silk Fibroin (modified according to Vilaplana et al.[35])

Hydrolysis of the degummed silk samples (1–10 mg) was performed with hydrochloric acid (1000 µL, 6 N) at 110 °C for 24 h. As stabilization reagents, phenol in water (50 µL, 1%) and 3,3′-dithiodipropionic acid (50 µL, 1%) in an aqueous solution of NaOH (0.2 M) were added to all samples. The hydrolysate was concentrated to dryness at 90 °C using a nitrogen stream and the residue was dissolved in hydrochloric acid (200 µL, 0.1 M). Aliquotes (25–200 µL) were used for AA derivatization.

AA derivatization with propyl chloroformate (modified according to the EZ:faast kit derivatization protocol from Phenomenex)

Aliquotes of AA working solutions or hydrolysates (25–200 µL) were diluted up to a volume of 225 µL with distilled water. Subsequently, derivatization reagent 1 (100 µL, 77% *n*-propanol and 23% 3-picoline)[36] was added and the solution was thorough vortexed for 20 s. In the next step, derivatization reagent 2 (70 µL, 17.4% propyl chloroformate, 11% isooctane and 71.6% chloroform)[36] was added, the solution was mixed again for 20 s and remained at room temperature for 1 min. Then the solution was heated to 40 °C for 3 min and vortexed rigorous for 20 s. Finally, isooctane (250 µL) was added and it was mixed again. An aliquote of the organic phase (2.5 µL) was injected into the gas chromatograph.

GC-FID analysis

Samples were analyzed with a Shimadzu gas chromatograph GC-2025, equipped with an AOC-20i injector (injection volume: 2.5 µL, split mode, split ratio 15:1), an AOC-20 s autosampler and a flame ionization detector (FID; hydrogen and air flows were set at 40 and 400 mL min^{-1}). Chromatographic separation was performed on

a Zebron ZB-50 column (15 m × 0.25 mm × 0.15 µm, Phenomenex). The injection port was held at 320 °C and the detector operated at 310 °C. The column oven temperature was initially set to 100 °C, held for 30 s and then ramped with 20 °C min^{-1} to 300 °C, held for 6 min; the carrier gas was nitrogen at a constant column flow of 1.10 mL min^{-1} (linear velocity: 35.7 cm s^{-1}). All analyses were performed in triplicate.

Principal component analysis (PCA)
PCA of AA composition was performed with Gly and Ala content as well as the amount of polar and non-polar AA residues as independent variables, using Origin 2019 (OriginLab Corporation, US). The first two components account for 98% of the variance of the data.

Validation experiments

Specificity
To determine the specificity of the method, a mixture of all AAs studied was measured by GC-FID after derivatization with PCF [for retention times see Table S1, Supplementary Information (SI)]. Furthermore, hydrolysates of degummed BM and non-mulberry silkworm silk as well as blank samples (without AA or protein addition) were analyzed by GC-FID.

Linearity, limit of detection (LOD) and limit of quantification (LOQ)
For the calibration, solutions were prepared with different mixtures of proteinogenic AAs and Nle [AAs: in the range of min 0.6 to max 20.4 mM with Nle as internal standard (50 µL, 50 mM); additionally extended concentration range for Ala and Gly: 6.6–24.8 mM with Nle as internal standard (110 µL, 50 mM)]. Each calibration solution was measured three times and analyses were executed with average peak area ratios of the respective AA and Nle. The linearity of each calibration function was tested with the Mandel's test. Limit of detection (LOD) and limit of quantification (LOQ) were determined by means of a calibration curve method according to DIN 32645[37]. These validation data are shown in Table S1, SI.

Precision
For determining the repeatability, six replicate measurements were carried out for two different concentrations (Table S1, SI). For this purpose, solutions containing respective AAs and Nle as internal standard were prepared, derivatized and analyzed with GC-FID. Ala and Gly were analyzed separately from the other AAs due to the high concentration differences. For the interpretation of the repeatability, the relative standard deviation (RSD) of the respective AA concentration was used. For determining the method precision, six BM silk samples (10 mg), degummed with method 4–2 (see Table 1), were hydrolyzed and independently derivatized in the presence of the internal standard Nle. Aliquots (2.5 µL) of the organic phases were analyzed by GC-FID. For the interpretation of the method precision, the RSD of the AA concentrations was used (Table S1, SI). Furthermore, Dixon's Q test and Neumann trend test were applied for the identification of outliers or trends.

Recovery
The calculation of the recovery rate for each AA was performed for three concentration levels with a number of three replicates (Table S1, SI). For this purpose, degummed silken filaments of BM (10 mg, degumming method 4–2, see Table 1) were spiked with a defined AA concentration, hydrolyzed with hydrochloric acid at 110 °C for 24 h and derivatized with PCF/*n*-propanol as described above. Hydrolysis, derivatization and GC-FID analysis of the spiked silk samples were performed independently of each other on different days. The calculated AA concentrations were compared with the target concentrations and the recovery rate was determined. The average AA concentrations of degummed silken filaments of BM, determined in the course of the method precision, were used for the calculation of the target concentrations.

Stability of the standards
An aliquote of a working solution containing Nle as internal standard and AAs studied (equimolar mixture) was derivatized with PCF and stored at room temperature in the autosampler of the gas chromatograph. The solution was examined over a 24 h period and analyses were repeated three times with eight independently prepared solutions. Dixon's Q test and Neumann trend test were applied for the identification of outliers or trends. The investigation of the long-term stability of AA mixtures in 0.1 M hydrochloric acid, stored at 4 °C in the dark and examined over a 7-week period, was carried out during parallel ongoing studies (see Puchalla[38]).

Results and discussion

The subjects of the studies were, in addition to BM silks (family Bombycidae), cocoons and degummed fibers from twenty non-mulberry feeding silkworms species of the genera *Actias*, *Attacus*, *Argema*, *Antheraea*, *Caligula*, *Callosamia*, *Cricula*, *Epiphora*, *Hyalophora*, *Loepa*, *Samia* and *Saturnia* which belong to the family Saturniidae. In some cases, several silk samples of the same species, but from different regions were examined.

Degumming of mulberry and non-mulberry silkworm cocoons

Degumming of BM cocoons
Different approaches were compared to remove the globular glue protein sericin from silk filaments of BM (Table 1), using microscopic and ATR-FTIR spectroscopic studies as well as the average degumming ratio D_r to evaluate the degumming efficiency. As shown in Table 1, the degumming ratio of BM cocoons using 0.5–1% $NaHCO_3$, 0.1% Na_2CO_3 and/or 2.5% ethylenediamine as degumming agent for 30–90 min at 95 °C is about

Degumming method	Method ID	D_r [%]		
		BM	AM	AtA
Alkaline				
Na_2CO_3 (1 g L^{-1}), 30 min, 95 °C	1–1	34	–	
Na_2CO_3 (1 g L^{-1}), 60 min, 95 °C	1–2	31	–	
Na_2CO_3 (1 g L^{-1}), 90 min, 95 °C	1–3	28	–	–
$NaHCO_3$ (0.5%), 120 min, 95 °C	2–1	28	–	
$NaHCO_3$ (1%), 120 min, 95 °C	2–2	29	–	
Ethylenediamine (2.5%), 30 min, 95 °C	3–1	36	–	
Ethylenediamine (2.5%), 60 min, 95 °C	3–2	29	23	19
Ethylenediamine (2.5%), 90 min, 95 °C	3–3	30	23	19
Ethylenediamine (2.5%), 120 min, 95 °C	3–4	34	–	–
Ethylenediamine (10%), 120 min, 95 °C	3–5	38	–	–
Na_2CO_3 (1 g L^{-1}) and ethylenediamine (2.5%), 30 min, 95 °C	4–1	32	28	–
Na_2CO_3 (1 g L^{-1}) and ethylenediamine (2.5%), 60 min, 95 °C	4–2	31	24	16
Na_2CO_3 (1 g L^{-1}) and ethylenediamine (2.5%), 90 min, 95 °C	4–3	31	24	17
Na_2CO_3 (1 g L^{-1}) and ethylenediamine (2.5%), 120 min, 95 °C	4–4	–	–	22
Acidic				
Citric acid (1 g L^{-1}), 120 min, 95 °C	5–1	9	–	–
Citric acid (1 g L^{-1}), 240 min, 95 °C	5–2	11	–	–
Citric acid (2 g L^{-1}), 120 min, 95 °C	5–3	11	–	–
Detergent-based				
Marseille soap (1 g L^{-1}), 120 min, 95 °C	6–1	23	–	–
Marseille soap (2 g L^{-1}), 120 min, 95 °C	6–2	28	–	–
Periquest APG (1 g L^{-1}) and Perlavin LMO (5 g L^{-1}), 60 min, 95 °C	7–1	34	11	16
Periquest APG (1 g L^{-1}) and Perlavin LMO (5 g L^{-1}), 90 min, 95 °C	7–2	34	10	18
Periquest APG (1 g L^{-1}) and Perlavin LMO (5 g L^{-1}), 120 min, 95 °C	7–3	32	–	–
Enzyme-based				
Papain (1 g L^{-1}), 120 min, 90 °C	8–1	23	–	–
Papain (1 g L^{-1}), 240 min, 90 °C	8–2	25	–	–
Pineapple juice, 120 min, 90 °C	9–1	9	–	–
Pineapple juice, 240 min, 90 °C	9–2	18	–	–

Table 1. Degumming ratio of different degumming methods using mulberry and non-mulberry silkworm cocoons.

30–35%. A degumming ratio of approximately 30–35% can also be achieved with Marseille soap (2 g L^{-1}) or the nonionic surfactant Periquest APG in combination with Perlavin LMO, with degumming in both cases taking place under alkaline conditions (pH 8–10). In contrast, a degumming ratio of 9–18% is observed for the acidic and enzyme-based methods using 0.1–0.2% citric acid or pineapple juice as degumming agent. Since the sericin content on the cocoon shell of commercially available BM varieties is usually about 20–30%[14,39], a degumming ratio < 20% indicates incomplete degumming. Microscopic examination showing residual sericin on the silken filaments degummed with 0.1–0.2% citric acid (D_r 9–11%) or pineapple juice (D_r 9–18%) confirms incomplete sericin removal (Figure S1A, SI). A degumming rate of 25% is obtained when using papain for 240 min at 90 °C. However, traces of sericin can be observed on some filaments. To increase the degumming efficiency, for example, the use of papain in the presence of urea or treatment with 15–30% citric acid would be conceivable (see Biswal et al.[16]).

In agreement with previous experiments[39], the determined degumming ratio of the alkaline and detergent-based methods of about 30–35% indicates complete removal of the sericin gum from the silk filaments. Microscopic observations show that silken filaments degummed with 0.1% Na_2CO_3 and/or 2.5% ethylenediamine for 30–90 min at 95 °C or using Periquest APG/ Perlavin LMO for 60–120 min at 95 °C are smooth and without residual sericin (Figure S1B, SI). And also during the treatment with Marseille soap (2 g L^{-1}) or 0.5–1% $NaHCO_3$ for 120 min at 95 °C, twin silk filaments were transformed into monofilament structure. ATR-FTIR spectra of silken filaments treated with these degumming agents show prominent bands at 975, 998 and 1695 cm^{-1} assigned to a – Gly – Ala – peptide backbone and β-sheets indicating a high level of protein crystallinity (Figure S2, SI). Since fibroin has a higher degree of crystallinity than sericin due to stacked β-sheets, the relative intensity of β-sheet peaks serve as indicators of degumming efficiency (see Refs.[16,26]). Studies on untreated BM cocoons show that these bands are masked by the presence of a sericin coating. Furthermore, the intensity of the signature peaks for sericin at around 1400 cm^{-1} and 1070 cm^{-1} is significantly reduced for all degummed samples compared to the untreated cocoons[40].

In addition, investigations on the AA composition of degummed silk samples were carried out (see AA analysis by GC-FID). For silken filaments degummed with alkaline and detergent-based methods, with the exception of samples treated with Marseille soap, a Ser content of 3.1 to 6.1 mol% was determined (for AA composition see Table S2, SI). The Ser content of silk samples treated with Marseille soap (2 g L^{-1}) or papain (240 min) is 7.7 and 6.0 mol%, respectively. In contrast, samples degummed with 0.1–0.2% citric acid or pineapple juice have a Ser content of 9.6–11.1 mol%. A similar trend can be observed for Thr. For instance, alkaline and Periquest APG/Perlavin LMO-based treatments result in Thr contents of 0.7–1.1 mol%, while Thr contents of 1.5–2.5 mol% were determined for silk samples treated with citric acid or pineapple juice. Also, commercially degummed silk filaments used for textile production have Ser and Thr contents of 5.5 and 0.8 mol%, respectively. Thus, the content of Ser and Thr, both AAs with a polar side chain, is also an excellent indicator of degumming efficiency of BM cocoons. However, it should be noted that treatment of silk samples under extremely acidic and alkaline pH conditions also leads to hydrolysis of peptide bonds in silk fibroin. This hydrolysis occurs mainly in the amorphous spacers within the fibroin chains, which are more sensitive to degradative effects than the crystalline regions. A significant reduction in the AAs Asp, Thr, Ser (polar side chains) Ile and Leu (hydrophobic side chains), which are found mainly in the amorphous regions, is well known for such samples[35]. However, no meaningful decrease in Asx (Asp + Asn, see validation experiments) and Ile content was observed for silk samples degummed by the alkaline and detergent-based methods discussed above (pH value of the degumming baths was in the range of 8 to 10).

Studies by, for example, Dou and Zuo[41] or Zhao et al. show a correlation between degumming agent concentration, temperature, treatment time and various properties of silk fibers such as mechanical strength, wettability and morphology[39]. Harsh conditions, i.e. long treatment time and/or high concentration of the degumming agent, lead to partial degradation of fibroin fibers and a degumming ratio > 35%, which indicates loss of fibroin protein. For instance, brittle fibers reduced in diameter and a degumming ratio of 38% were observed when BM cocoons were treated with 10% ethylenediamine for 120 min at 95 °C (method 3–5, pH value of the degumming bath: 12, see Table 1).

Degumming of non-mulberry silkworm cocoons

In a next step, selected alkaline and Periquest APG/Perlavin LMO-based methods were tested for degumming AM and AtA cocoons (Table 1, Figures S3 and S4, SI), cocoons spun by commercial used silk moth species in the tribes *Saturniini* and *Attacini* (family Saturniidae). AM cocoons have a very hard and compact shell, while AtA cocoons are soft in nature and have an intermediate sericin content compared to BM and AM cocoons[26]. The degumming ratio of AM samples ranged from 28% for filaments degummed with a mixture of Na_2CO_3 and ethylenediamine to 10% for cocoons treated with Periquest APG and Perlavin LMO. Degumming ratios of 16–22% were determined for AtA cocoons using ethylenediamine or ethylenediamine in combination with Na_2CO_3 for 60–120 min at 95 °C, while values of 16–18% were obtained with Periquest APG/Perlavin LMO-based methods. For AM and AtA samples treated with a mixture of Na_2CO_3 and ethylenediamine (AM: 30–90 min, D_r 24–28%; AtA: 120 min, D_r 22%), the separation of two brins of fibroin is clearly seen under microscope (Figures S3B and S4B, SI). Furthermore, these degummed silk filaments are smooth and not degraded, indicating high degumming efficiency without destruction of the filaments at the macroscopic level. In contrast, detergent-based methods tested result in unseparated brins of fibroin and thus incomplete degumming (AM: D_r 10–11%, Figure S3A; AtA: D_r 16–18%, Figure S4A, SI). AA analysis shows that Ser content (Ser + Pro, see validation experiments) of AM fibroin ranges from 5.4 to 6.4 mol% and the Thr content ranges from 0.6 to 1.2 mol% for all degumming methods (see Table S3 for AA composition, SI). And also in samples of AtA, Ser (Ser + Pro) and Thr content is not a suitable indicator of degumming efficiency (see Table S4 for AA composition, SI). However, ATR-FTIR spectra of silken filaments of AtA and AM, degummed with ethylenediamine or ethylenediamine/Na_2CO_3, show that the intensity of the band at around 1052 cm^{-1} assigned to sericin C–O stretching[26] is significantly reduced compared to the untreated cocoons and the incompletely degummed samples (Figures S5 and S6, SI).

A mixture of 0.1% Na_2CO_3 and 2.5% ethylenediamine was used to degum cocoons of several other non-mulberry feeding silkworm species (tribes *Saturniini* and *Attacini*) that exhibited a wide variety of morphologies and architectures, with porosity ranging from loose meshes to full shells (see Cocoon and fiber morphologies). The progress of the degumming process was monitored by microscopic examinations of the filaments, adjusting the treatment time if necessary. Average degumming ratios, indicative of the removal of adhering constituents (sericin, calcium oxalate, wax, pigemts etc.), and the corresponding treatment times are summarized in Table S5, SI. After degumming, smooth silk filaments were obtained, and twin silk filaments were transformed into monofilament structure. For a comparison between the species, degummed silk samples were characterized by ATR-FTIR spectroscopy and analyzed with respect to their AA composition (see Between-species comparison).

Differences between BM and non-mulberry silkworm cocoons in terms of sericin content, sericin structure and the content of non-protein components such as calcium oxalate crystals are well known and can be attributed to different habitats and host plants[26,42]. In general, harsher conditions are often required for the removal of sericin from silk filaments of non-mulberry silkworms[43]. Thus, ethylenediamine is often used as an effective agent for degumming of non-mulberry silk[25,44]. And also in our studies, ethylenediamine in combination with Na_2CO_3 shows a great result as degumming agent for non-mulberry silkworm cocoons.

Between-species comparison

Cocoon and fiber morphologies

As already mentioned, the appearance and dimensions of the examined cocoons are partly very different, whereby also within a genus sometimes substantial differences can be determined. For instance, cocoons spun by different *Antheraea*, *Actias* and *Hyalophora* silk moth species vary significantly in architectural features (Figure S7, SI).

In addition, some species such as *Hyalophora cecropia* (HC) are known to produce discrete dimorphic cocoons that are either large and fluffy (baggy) or significantly smaller and tightly woven (compact)[45]. In our study, only baggy HC cocoons were analyzed. Moreover, cocoons of the wild eri silkworm *Samia canningii* (SCa) differ significantly from the cocoons of domestic *Samia* species used commercially for silk production (Figure S7R-T, SI). Non-mulberry silk cocoons mostly have microscale crystals on the outer surface, and some crystals are also seen on the inner surface. The examined Saturniidae silkworm cocoon fibers have a flat and ribbon-like structure with an oval to rectangular cross-section, while the cross section of BM filaments has a triangular shape (Figures S1, S3, S4 and S8, SI).

ATR-FTIR analysis

For further characterization, cocoons and degummed silk samples were analyzed by ATR-FTIR spectroscopy (Figures S9-S11, SI). As outlined in previous studies, this approach enables the identification and quantification of, for example, calcium oxalate, serine, polyalanine $(A)_n$ β-sheets, polyalanineglycine $(AG)_n$ β-sheets, tannins and phenolic compounds present in native silk feedstock and cocoons[26].

In agreement with the studies of Boulet-Audet et al.[26], an intense band at about 1315 cm^{-1} was observed in the spectra of the untreated *Antheraea* cocoons, especially on the outside of the cocoons, which is assigned to the calcium oxalate vibrational modes and thus indicates a high calcium oxalate content. In contrast, a weak or no characteristic band for calcium oxalate was found on the inner and outer surfaces of the untreated cocoons of *Argema mimosae* (ArM), *Caligula cachara* (CC), *Loepa katinka* (LK) and BM (Figures S2 and S9, SI). Moreover, all degummed non-mulberry silk samples show a characteristic peak at 963 cm^{-1}, corresponding to the β-sheet conformation of polyalanine $(A)_n$. This peak is specific to wild silk spun, e.g., by Saturniidae silk moths and cannot be observed in spectra of BM silk (see Figure S2)[26,46]. Our results suggest that degummed silk of *Actias selene* (AcS) has the lowest amount of $(A)_n$, followed by ArM silk, while a much higher $(A)_n$ amount was determined for *Epiphora bauhiniae* (EB), *Callosamia promethea* (CaP), HC and *Samia* silk (Fig. 1). Main characteristic features of degummed BM silk, whose β-sheets consist of polyalanineglycine $(AG)_n$ segments, are the peaks at 975 and 998 cm^{-1}. As described above (see Degumming of BM cocoons), these bands are clearly visible in the ATR-FTIR spectra of degummed BM silk. Furthermore, it is known from previous studies that the silk of *B. mandarina* has a high amount of $(AG)_n$ β-sheets[26]. In contrast, most Saturniidae silks are poor in $(AG)_n$ β-sheets. Thus, these characteristic peaks are not observed in the IR spectra of degummed and untreated non-mulberry silk samples. To obtain a further quantitative understanding of the composition of different secondary structures, including β-sheet, β-turn, α-helix and random coil, peak deconvolution analyses were carried out on the amide I bands (1600–1700 cm^{-1}, see Refs.[29–31,47]). The deconvolution results revealing the quantitative content of the secondary structure of the degummed silk samples are summarized in Table S6 and Figure S12, SI. The β-sheet content in *Actias*, ArM, AM, CC, LK and *Hyalophora gloveri* (HG) silk is slightly lower compared with APe, AtA, CaP, EB, *Samia* and BM silk. These results show that silk from (semi-)domesticated silkworms such as APe, SCy ricini and BM, in particular, has a higher β-sheet content, which is in good agreement with previous studies[29]. However, an increased β-sheet content can also be found in some wild silks such as EB or CaP. In summary, the analysis of ATR-FTIR spectra enables to discriminate easily between silk of the *Bombyx* genus and Saturniidae silks. Furthermore, some general tendencies can be observed for Saturniidae cocoons and silk, such as a relatively high calcium oxalate content in *Antheraea* cocoons.

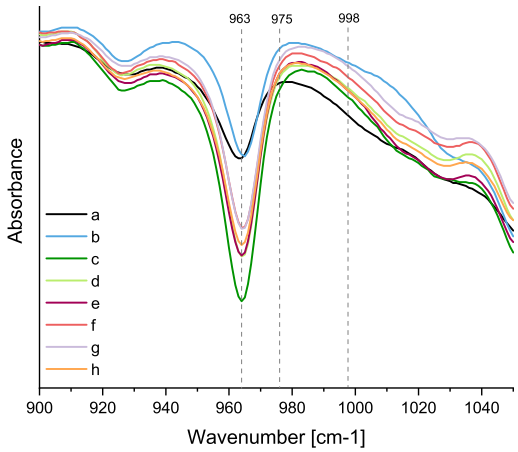

Figure 1. ATR-FTIR spectra of silk degummed with a mixture of 0.1% Na_2CO_3 and 2.5% ethylenediamine at 95 °C: (**a**) AcS, (**b**) ArM, (**c**) EB, (**d**) CaP, (**e**) HC, (f) SCy ricini, (**g**) SCa (**h**) Eri silk moth.

AA composition of degummed filaments

AA analyses were performed on degummed silks that showed no sericin residues on the filament surface. For this purpose, the silk samples were hydrolyzed with 6 N hydrochloric acid and after derivatization with propyl chloroformate, the AAs were analyzed by GC-FID (see AA analysis by GC-FID and AA analysis by GC-FID—validation experiments). Fifteen AAs were identified and quantified in hydrolysates of degummed silks, namely Ala, Gly, Val, Leu, Ser (Ser + Pro, see validation experiments), Asx (Asp + Asn), Glx (Gln + Glu), Phe, Cys, Lys, His, Tyr, Ile, Met and Thr. It should be noted that the amount of Arg and Trp was not determined and therefore these AAs are not part of the further considerations.

Tables 2 and S4-S5 (SI) and Figs. 2, 3 summarize the AA composition of the studied BM (family Bombycidae) and non-mulberry silks (family Saturniidae), degummed with a mixture of 0.1% Na_2CO_3 and 2.5%

Tribe	Genus	Species	Description (Supplier)	Sample ID	Comparative AA composition							
					Ala + Gly [mol%]	Gly/Ala	100LC/SC[a]	P [mol%][b]	NP [mol%][c]	P/N[d]	Ser + Pro + Thr + Tyr [mol%][e]	B/A[f]
Saturniini	*Actias*	*Actias luna*	America	AcL	64.8	0.8	36	16	84	0.2	15.0	1.1
		Actias selene	Thailand	AcS	62.9	0.9	27	23	77	0.3	23.9	1.1
	Argema	*Argema mimosae*	Kenya	ArM	58.7	0.9	53	18	82	0.2	15.1	1.9
	Antheraea	*Antheraea pernyi*	China	APe-1	75.7	0.7	27	12	88	0.1	9.4	0.8
			North Korea	APe-2	79.6	0.7	22	11	89	0.1	7.2	0.7
		Antheraea polyphemus	North USA	APo-1	74.6	0.7	27	14	86	0.2	11.2	0.8
			North America	APo-2	75.7	0.8	26	13	88	0.1	10.8	1.0
		Antheraea mylitta	–	AM-1	77.4	0.8	19	14.1	85.9	0.2	12.6	0.9
			–	AM-2	77.6	0.7	23	12.4	87.6	0.1	9.2	0.8
			Tussar silk moth	AM-3	78.0	0.7	24	11.3	88.7	0.1	9.6	1.0
	Caligula	*Caligula cachara*	India	CC	66.7	0.7	34	17	83	0.2	12.6	1.7
	Cricula	*Cricula trifenestrata*	India	CrT	68.3	0.9	33	16	84	0.2	14.9	2.1
	Loepa	*Loepa katinka*	India	LK	70.0	0.7	37	13	87	0.1	13.3	1.8
	Saturnia	*Saturnia pavonia*	Europe	SaPa-1	68.1	0.9	34	16	84	0.2	11.6	1.6
			England	SaPa-2	63.7	1.0	41	20	80	0.2	13.5	0.9
		Saturnia pyri	France	SaPy-1	63.4	0.8	40	20	80	0.3	14.0	0.8
			Europe	SaPy-2	62.7	0.8	38	22	78	0.3	14.4	0.7
Attacini	*Attacus*	*Attacus atlas*	Jonsdorf (butterfly house)	AtA	83.6	0.7	14	9.9	90.2	0.1	8.2	0.9
	Callosamia	*Callosamia promethea*	North America	CaP	76.7	0.8	27	11	89	0.1	9.6	1.4
	Epiphora	*Epiphora bauhiniae*	Kenya	EB	78.5	0.8	23	11	89	0.1	8.4	1.1
	Hyalophora	*Hyalophora gloveri*	America	HG	77.0	0.7	25	12	89	0.1	8.8	0.8
		Hyalophora cecropia	America	HC	75.2	0.7	29	13	87	0.1	10.3	0.7
	Samia	*Samia canningii* (wild eri silk moth)	India	SCa	77.0	0.7	26	11	89	0.1	10.7	1.4
		Samia cynthia ricini	Thailand	SCy ricini	78.0	0.8	25	10	90	0.1	8.5	1.5
		Eri silk moth	–	S-1	78.1	0.9	25	10	90	0.1	7.3	1.1
			India	S-2	79.3	0.8	24	10	90	0.1	8.1	1.3
	Bombyx	*Bombyx mori*	Chinese web store	BM-1	80.2	1.7	17	12.2	87.9	0.1	9.1	0.4
			Halle (Saale)	BM-2	77.9	1.6	22	11.6	88.4	0.1	8.7	0.9
			China	BM-3	76.5	1.6	26	13.9	86.1	0.2	7.3	1.1

Table 2. AA composition of non-mulberry (Saturniini and Attacini) as well as BM silks degummed with Na_2CO_3 (1 g L^{-1}) and ethylenediamine (2.5%) at 95 °C. [a]Ratio between long chain (LC: other AAs) and short chain (SC: Ala, Gly, Ser, Thr) AAs; [b]Polar AAs: acidic, basic and hydroxyl AAs; [c]Non-polar AAs: other AAs; [d]Ratio between polar and non-polar AA residues; [e]AAs with hydroxyl groups: Ser, Thr, Tyr; [f]Ratio between basic (Lys, His) and acidic (Asx, Glx) AAs.

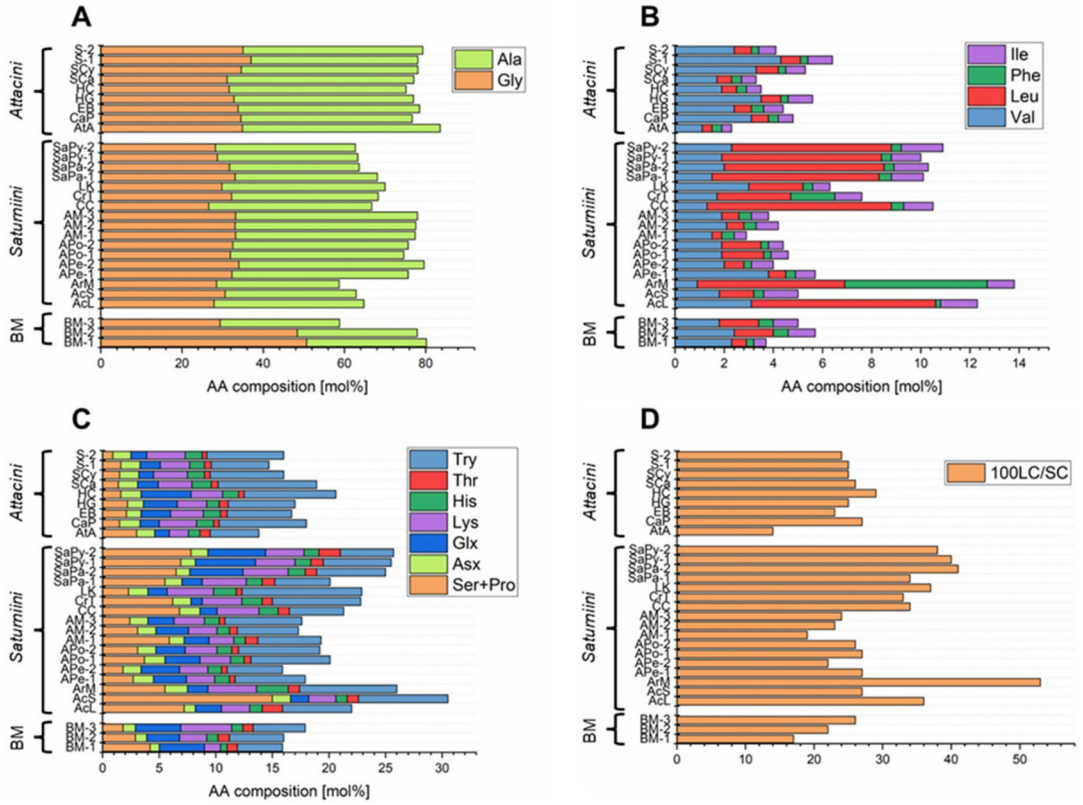

Figure 2. (**A**–**C**) AA composition and the (**D**) 100LC/SC ratio of BM and non-mulberry silks (family Saturniidae), degummed with a mixture of 0.1% Na_2CO_3 and 2.5% ethylenediamine at 95 °C (for sample ID assignment see Table 2).

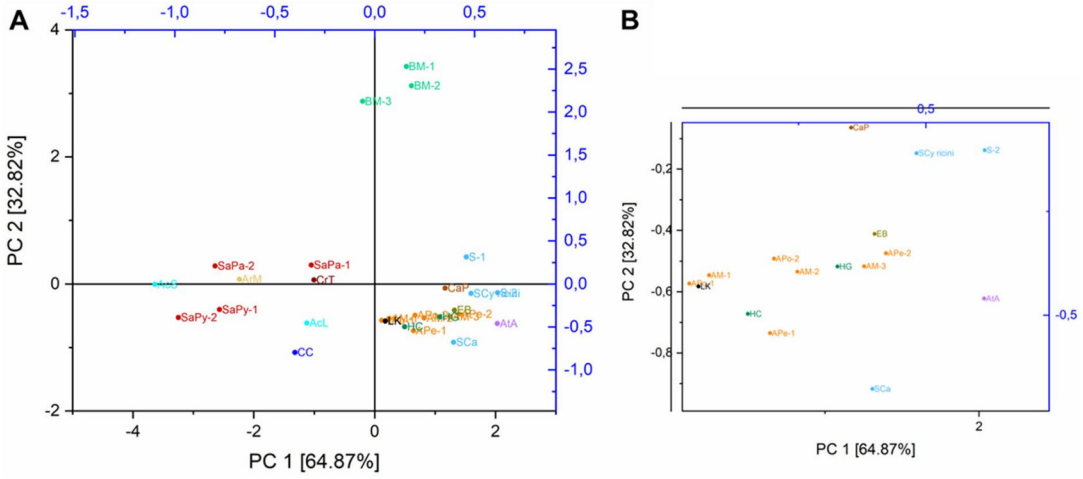

Figure 3. (**A**) PCA score plot of BM and non-mulberry silks (family Saturniidae), degummed with a mixture of 0.1% Na_2CO_3 and 2.5% ethylenediamine at 95 °C, (**B**) zoom of the right area (for sample ID assignment see Table 2).

ethylenediamine. Ala and Gly are predominant in BM and non-mulberry fibroin and account for approximately between 60 and 85 mol% of the total AA content, with Ala content (between 35 and 49 mol%) being higher than Gly content (between 27 and 37 mol%) in non-mulberry silks. Exceptions to this are silk samples of AcS, ArM, *Cricula trifenestrata* (CrT) and *Saturnia pavonia* (SaPa). In these samples, the Ala and Gly content is about 30–35 mol% and the Gly/Ala ratio is thus around 1. In contrast, the Ala content of BM silk is about 30 mol%, while the Gly content is approximately 50 mol% (Table S5, SI). Consequently, the ratio of Gly/Ala for fibroin of non-mulberry species belonging to the family Saturniidae is lower than that for BM, suggesting a difference in the primary structure and/or organization of residues in the fibroin (non-mulberry silk: Gly/Ala ≤ 1; BM: Gly/Ala ≈ 1.6–1.7; Gly/Ala of BM silk in other studies: 1.45[24]). In addition, bulky and/or polar AAs such as Tyr or Leu are more abundant in many of the non-mulberry silks examined than in BM fibroin. For instance, the content of bulky AAs is significantly increased in *Actias luna* (AcL, Tyr: 6.1 mol%, Leu: 7.5 mol%, Phe: < LOQ), ArM (Tyr: 8.6 mol%, Leu: 6.0 mol%, Phe: 5.8 mol%) or *Saturnia pyri* (SaPy, Tyr: 4.7–6.0 mol%, Leu: 6.5 mol%, Phe: < LOQ) fibroin compared to BM fibroin (Tyr: 4.0–4.8 mol%, Leu: 0.6–1.6 mol%, Phe: mostly < LOQ). As reported by various authors these compositional differences have implications for structure that can be described by the long chain/short chain (100LC/SC) ratio[23,27]. Since a high proportion of bulky side groups is found in the amorphous region of silk, this structural index is often used in providing insight on the relative degree of crystallinity in fibroin. The 100LC/SC ratio of BM fibroin is 17–26 which is lower than that of non-mulberry silks such as AcL (100LC/SC: 36), SaPy (100LC/SC: 38–40) or ArM (100LC/SC: 53). A Gly/Ala ratio < 1 and a 100LC/SC ratio higher than for BM silk fibroin has already been described in several studies for wild silks such as silk of *Gonometa* species (Lasiocampidae), suggesting a lower structural regularity and thus a lower rigidity and a higher extensibility compared to BM silk[27]. However, we have found that the 100LC/SC ratio is also in the range 20–25 for some of the non-mulberry silks studied, e.g., EB (100LC/SC: 23) or *Antheraea* species (100LC/SC: 19–27).

The AA composition of AcL (Ser + Pro: 7.2 mol%, Thr: 1.8 mol%), ArM (Ser + Pro: 5.5 mol%, Thr: 1.0 mol%) and SaPy (Ser + Pro: 6.9–7.8 mol%, Thr: 1.1–1.9 mol%) silk is also characterized by a high Ser + Pro and Thr content, with the total amount of Ser + Pro, Thr and Tyr (AAs with hydroxyl groups: Ser, Thr, Tyr) ranging from 14 to 15 mol%. Furthermore, a relatively high content of the basic AAs Lys (4.3 mol%) and His (2.8 mol%) was found in the silk samples of ArM. In comparison, the total amount of Lys and His (2.0–5.5 mol%, method 4–2, see Table 1) and AAs with hydroxyl groups (7.3–9.1 mol%, method 4–2, see Table 1) in BM silk is low. The ratio of polar:non-polar (P:NP) AAs in AcL, ArM and SaPy silk samples is approximately 20:80. In contrast, a P:NP ratio of about 10:90 was determined for BM silk as well as for other non-mulberry silks (e.g. silk of *Samia* species). The higher ratio of basic to acidic (B/A) AAs for wild silks compared to BM silk, mentioned at the beginning (see Refs.[23,24]), cannot be confirmed for all silks examined. However, a comparison with the literature values is difficult here, since many wild silks have a high Arg content, which cannot be determined with the chosen method (see Hušek[48]).

In agreement with Lucas et al., it can be stated that there are no precise relationships between the AA compositions of the different fibroins and their biological classifications. However, some generally valid conclusions can be drawn[49]. Within a genus, for example, there is usually a close similarity between the structural indices, which can be useful parameters for inferring physical structure and chemical reactivity of silks. However, several studies have reported comparable structural indices in silk fibroin from different strains. For instance, Lucas et al. describes a high similarity between the AA composition of BM and *Bena prasinana* fibroin, the latter being a small British moth, which belongs to the Cymbidae family[49]. Consequently, for characterization of silks, it is recommended to combine the results of AA analyses with e.g. microscopic and spectroscopic data.

Principal component analysis (PCA)

The use of PCA of AA composition contribute to distinguishing between BM and non-mulberry silks. As shown in Fig. 3, *Antheraea* (sample ID: APe-1, APe-2, APo-1, APo-2, AM-1, AM-2, AM-3; marked orange) and *Hyalophora* (sample ID: HG, HC; marked dark green) silks were positioned close to each other, showing that the silks of these species have greater similarity to each other, in relation to silk from the genus *Saturnia* (sample ID: SaPa-1, SaPa-2, SaPy-1, SaPy-2; marked red), *Actias* (sample ID: AcL, AcS; marked light blue) or *Bombyx* (sample ID: BM-1, BM-2, BM-3; marked green). However, with the data set available, it is not possible to distinguish between the tribes *Saturniini* and *Attacini*. Increasing the size of the data set is the subject of future studies.

AA analysis by GC-FID—validation experiments

The results of the validation study for AA analyses using GC-FID are summarized in Table S1, SI. Retention times of derivatized AAs were determined using AA standard solutions. Chromatograms of hydrolyzed silk samples of non-mulberry and mulberry silkworms as well as blank samples were free from interference. However, coelution is observed for Pro and Ser derivatives. Since the Ser content in BM silk is known to be significantly higher than the Pro content (0.6%[50]), only the Ser content is given for hydrolysates of BM silk. Many non-mulberry silks also contain significantly less Pro than Ser[24,25]. However, for non-mulberry silk, it is reported as Ser + Pro content. Calibration plots (concentration of AA versus peak area ratio of AA and internal standards) are linear in the respective selected range (min 0.6 mM, max 24.8 mM). For all AAs considered, an R^2 value > 0,973 was obtained, and both LODs and LOQs were considered adequate for the purposes of the present study. The repeatability, expressed by relative standard deviations (RSD), ranged from 0.03% for Phe to 2.5% for His. To determine the method precision, hydrolysis of 10 mg BM silk, degummed by method 4–2 (see Table 1), was processed six times and RSDs of AA concentrations were calculated. The RSD values for the AAs Ala and Gly, which are predominant in fibroin, are satisfactory at 2.2 and 2.1%, respectively. RSD values of low abundant AAs, meaning AAs present in fibroin at < 5 mol%, range from 3.9% for Asx (Asp + Asn) to 9.9% for Val. The Cys and Met concentrations of the hydrolysates are below the LOQ and LOD, respectively. Thus, no values for method precision are given for

these AAs. Trp, a low abundant AA of BM silk[50], is decomposed during treatment with hydrochloric acid (see Rutherfurd and Gilani[51]) and cannot be determined using this method. In addition, it should be noted that Asn and Gln are deaminated during acid hydrolysis to Asp and Glu[51]. Thus, after hydrolysis with 6 N hydrochloric acid, values for Asp and Glu are reported as the sum of the acid and amide derivatives (Asx or Glx). Recovery tests were made by spiking degummed BM silk with defined concentrations of AAs. The recovery rate of the different AAs after hydrolysis and derivatization ranged from 69% for Asx to 120% for Gly with an average recovery rate of 89% at the low, 95% at the medium and 87% at the high concentration level. The stability of a solution with derivatized AAs was evaluated at room temperature over a 24 h period. The tests show that the deviation for the AA concentrations is not higher than 10% after 10 h; within 24 h a maximum deviation of 25% is observed (Figure S13, SI). Consequently, samples were measured within 10 h after derivatization (for storage stability of not derivatized AAs in 0.1 M hydrochloric acid, see Ref[38,51]).

Conclusion

Degummed silk samples of twenty silkworm species of the family Saturniidae were analyzed for their AA composition. For comparison, cocoons of BM, the most important silk producer for centuries, were degummed and analyzed. In this context, alkaline, acidic, enzymatic and detergent-based degumming methods were tested and degumming ratios determined. A mixture of 0.1% Na_2CO_3 and 2.5% ethylenediamine was found to be an effective agent for degumming Saturniidae and BM cocoons. Degummed silks were hydrolyzed with 6 N hydrochloric acid, and after derivatization with propyl chloroformate, AAs were identified and quantified by GC-FID. To evaluate the potential of this method, parameter such as LOD, LOQ, linearity, recovery rate, method precision, and stability of derivatized AAs were determined. The validated method showed a satisfactory overall analytical performance. As expected, the AA composition and resulting structural indices of Saturniidae fibroin filaments differ significantly from those of BM silk. Moreover, major differences were found between some Saturniidae species. Within a genus, however, a high degree of similarity can usually be observed between the structural indices. In addition, the structural indices, such as the long chain/short chain ratio (100LC/SC), which provide information about the relative degree of crystallinity of fibroin, allow conclusions to be drawn about physical and chemical properties of silks. A PCA of AA composition, conducted on this rather small data panel, reveals, for instance, significant differences between *Antheraea*, *Saturnia* and *Bombyx* silk. Chemometric analyses on a larger data set are the subject of future studies. The silk samples were also characterized by optical microscopy and ATR-FTIR spectroscopy. As already outlined in previous studies, both techniques enable to discriminate between BM and Saturniidae silks. In addition, these methods have been successfully used to monitor the degumming process. ATR-FTIR spectroscopic studies also reveal general tendencies for Saturniidae cocoons and silk, such as a low proportion of polyalanine $(A)_n$ β-sheets in degummed AcS silk or a relatively high calcium oxalate content in *Antheraea* cocoons.

Data availability

The datasets generated and analyzed during the current study are available from the corresponding author upon request.

Received: 21 April 2023; Accepted: 1 November 2023
Published online: 09 November 2023

References

1. Gong, Y., Li, L., Gong, D., Yin, H. & Zhang, J. Biomolecular evidence of silk from 8,500 years ago. *PLoS ONE* **11**, 0168042. https://doi.org/10.1371/journal.pone.0168042 (2016).
2. Arunkumar, K. P., Metta, M. & Nagaraju, J. Molecular phylogeny of silkmoths reveals the origin of domesticated silkmoth, *Bombyx mori* from Chinese *Bombyx mandarina* and paternal inheritance of *Antheraea proylei* mitochondrial DNA. *Mol. Phylogenet. Evol.* **40**, 419–427. https://doi.org/10.1016/j.ympev.2006.02.023 (2006).
3. Xia, Q. *et al.* Complete resequencing of 40 genomes reveals domestication events and genes in silkworm (*Bombyx*). *Science* **326**, 433–436. https://doi.org/10.1126/science.1176620 (2009).
4. Nakazawa, Y. & Asakura, T. High-resolution ^{13}C CP/MAS NMR study on structure and structural transition of *Antheraea pernyi* silk fibroin containing poly(L-alanine) and Gly-rich regions. *Macromolecules* **35**, 2393–2400. https://doi.org/10.1021/ma011999t (2002).
5. Zhang, J. *et al.* Mechanical properties and structure of silkworm cocoons: A comparative study of *Bombyx mori*, *Antheraea assamensis*, *Antheraea pernyi* and *Antheraea mylitta* silkworm cocoons. *Mater. Sci. Eng. C* **33**, 3206–3213. https://doi.org/10.1016/j.msec.2013.03.051 (2013).
6. Senthil Kumar, B. & Ramachandran, T. Influence of knitting process parameters on the thermal comfort properties of eri silk knitted fabrics. *Fibres Text. East. Eur.* **26**, 47–53 (2018).
7. Silva, S. S., Kundu, B., Lu, S., Reis, R. L. & Kundu, S. C. Chinese oak tasar silkworm *Antheraea pernyi* silk proteins: Current strategies and future perspectives for biomedical applications. *Macromol. Biosci.* **19**, 1800252. https://doi.org/10.1002/mabi.201800252 (2019).
8. Yang, J. *et al.* The complete mitochondrial genome of *Antheraea proylei* strain In981 (Lepidoptera: Saturniidae). *Mitochondrial DNA Part B* **4**, 2264–2265. https://doi.org/10.1080/23802359.2019.1627944 (2019).
9. Li, Q. *et al.* Nutrient composition of Chinese oak silkworm, *Antheraea pernyi*, a traditional edible insect in China: a review. *J. Insects Food Feed* **6**, 355–369. https://doi.org/10.3920/JIFF2019.0059 (2020).
10. Li, W., Zhang, Z., Lin, L. & Terenius, O. *Antheraea pernyi* (Lepidoptera: Saturniidae) and its importance in sericulture, food consumption, and traditional Chinese medicine. *J. Econ. Entomol.* **110**, 1404–1411. https://doi.org/10.1093/jee/tox140 (2017).
11. Liu, Y., Li, Y., Li, X. & Qin, L. The origin and dispersal of the domesticated Chinese oak silkworm, *Antheraea pernyi*, in China: A reconstruction based on ancient texts. *J. Insect Sci.* **10**, 180. https://doi.org/10.1673/031.010.14140 (2010).
12. Peigler, R. S. Wild silks of the world. *Am. Entomol.* **39**, 151–162. https://doi.org/10.1093/ae/39.3.151 (1993).
13. Guo, K. *et al.* Identification and characterization of sericin5 reveals non-cocoon silk sericin components with high β-sheet content and adhesive strength. *Acta Biomater.* **150**, 96–110. https://doi.org/10.1016/j.actbio.2022.07.021 (2022).

14. Cao, T.-T. & Zhang, Y.-Q. Processing and characterization of silk sericin from *Bombyx mori* and its application in biomaterials and biomedicines. *Mater. Sci. Eng. C* **61**, 940–952. https://doi.org/10.1016/j.msec.2015.12.082 (2016).
15. Dong, Z. *et al.* Identification of *Bombyx mori* sericin 4 protein as a new biological adhesive. *Int. J. Biol. Macromol.* **132**, 1121–1130. https://doi.org/10.1016/j.ijbiomac.2019.03.166 (2019).
16. Biswal, B. *et al.* Extraction of silk fibroin with several sericin removal processes and its importance in tissue engineering: A review. *J. Polym. Environ.* **30**, 2222–2253. https://doi.org/10.1007/s10924-022-02381-w (2022).
17. Li, G., Liu, H., Li, T. & Wang, J. Surface modification and functionalization of silk fibroin fibers/fabric toward high performance applications. *Mater. Sci. Eng. C* **32**, 627–636. https://doi.org/10.1016/j.msec.2011.12.013 (2012).
18. Gupta, D., Agrawal, A. & Rangi, A. Extraction and characterization of silk sericin. *Indian J. Fibre Text. Res.* **39**, 364–372 (2014).
19. Mondal, M., Trivedy, K. & Irmal Kumar, S. The silk proteins, sericin and fibroin in silkworm, *Bombyx mori* Linn., a review. *Casp. J. Environ. Sci.* **5**, 63–76 (2007).
20. Hao, Z. *et al.* New insight into the mechanism of in vivo fibroin self-assembly and secretion in the silkworm. *Bombyx mori. Int. J. Biol. Macromol.* **169**, 473–479. https://doi.org/10.1016/j.ijbiomac.2020.12.132 (2021).
21. Malay, A. D. *et al.* Relationships between physical properties and sequence in silkworm silks. *Sci. Rep.* **6**, 27573. https://doi.org/10.1038/srep27573 (2016).
22. Kmet, P. *et al.* Identification of silk components in the bombycoid moth *Andraca theae* (Endromidae) reveals three fibroin subunits resembling those of Bombycidae and Sphingidae. *J. Insect Physiol.* **147**, 104523. https://doi.org/10.1016/j.jinsphys.2023.104523 (2023).
23. Freddi, G., Gotoh, Y., Mori, T., Tsutsui, I. & Tsukada, M. Chemical structure and physical properties of *Antheraea assama* silk. *J. Appl. Polym. Sci.* **52**, 775–781. https://doi.org/10.1002/app.1994.070520608 (1994).
24. You, Q. *et al.* Discerning silk produced by *Bombyx mori* from those produced by wild species using an enzyme-linked immunosorbent assay combined with conventional methods. *J. Agric. Food Chem.* **65**, 7805–7812. https://doi.org/10.1021/acs.jafc.7b02789 (2017).
25. Sen, K. & Babu, K. M. Studies on Indian silk. I. macrocharacterization and analysis of amino acid composition. *J. Appl. Polym. Sci.* **92**, 1080–1097. https://doi.org/10.1002/app.13609 (2004).
26. Boulet-Audet, M., Vollrath, F. & Holland, C. Identification and classification of silks using infrared spectroscopy. *J. Exp. Biol.* **218**, 3138–3149. https://doi.org/10.1242/jeb.128306 (2015).
27. Mhuka, V., Dube, S. & Nindi, M. M. Chemical, structural and thermal properties of *Gonometa postica* silk fibroin, a potential biomaterial. *Int. J. Biol. Macromol.* **52**, 305–311. https://doi.org/10.1016/j.ijbiomac.2012.09.010 (2013).
28. Reddy, N., Zhao, Y. & Yang, Y. Structure and properties of cocoons and silk fibers produced by *Attacus atlas*. *J. Polym. Environ.* **21**, 16–23. https://doi.org/10.1007/s10924-012-0549-8 (2013).
29. Ling, S., Qi, Z., Knight, D. P., Shao, Z. & Chen, X. Synchrotron FTIR microspectroscopy of single natural silk fibers. *Biomacromolecules* **12**, 3344–3349. https://doi.org/10.1021/bm2006032 (2011).
30. Peng, Z. *et al.* Structural and mechanical properties of silk from different instars of *Bombyx mori*. *Biomacromolecules* **20**, 1203–1216. https://doi.org/10.1021/acs.biomac.8b01576 (2019).
31. Zhang, X. *et al.* Identification and functional study of fhx-L1, a major silk component in *Bombyx mori*. *Int. J. Biol. Macromol.* **232**, 123371. https://doi.org/10.1016/j.ijbiomac.2023.123371 (2023).
32. Wang, F. & Zhang, Y.-Q. Effects of alkyl polyglycoside (APG) on *Bombyx mori* silk degumming and the mechanical properties of silk fibroin fibre. *Mater. Sci. Eng. C* **74**, 152–158. https://doi.org/10.1016/j.msec.2017.02.015 (2017).
33. Premalatha, S. *et al.* Pineapple: Potential source of proteolytic enzymes for degumming of raw silk. *Mod. Concep. Dev. Agrono.* **4**, 417–424. https://doi.org/10.31031/MCDA.2019.04.000585 (2019).
34. Feng, Y. *et al.* High molecular weight silk fibroin prepared by papain degumming. *Polymers* **12**, 2105 (2020).
35. Vilaplana, F., Nilsson, J., Sommer, D. V. P. & Karlsson, S. Analytical markers for silk degradation: Comparing historic silk and silk artificially aged in different environments. *Anal. Bioanal. Chem.* **407**, 1433–1449. https://doi.org/10.1007/s00216-014-8361-z (2015).
36. Dettmer, K., Stevens, A. P., Fagerer, S. R., Kaspar, H. & Oefner, P. J. in *Amino Acid Analysis: Methods and Protocols* (eds Michail A. Alterman & Peter Hunziker) 165-181 (Humana Press, 2012).
37. Kromidas, S. *Handbuch Validierung in der Analytik* (Wiley, 2011).
38. Puchalla, N. *Bachelor Thesis*, Martin-Luther-Universität Halle-Wittenberg, (2022).
39. Zhao, Z.-L., Li, W.-W., Wang, F. & Zhang, Y.-Q. Using of hydrated lime water as a novel degumming agent of silk and sericin recycling from wastewater. *J. Clean. Prod.* **172**, 2090–2096. https://doi.org/10.1016/j.jclepro.2017.11.213 (2018).
40. Zhang, X. & Wyeth, P. Using FTIR spectroscopy to detect sericin on historic silk. *Sci. China Chem.* **53**, 626–631. https://doi.org/10.1007/s11426-010-0050-y (2010).
41. Dou, H. & Zuo, B. Effect of sodium carbonate concentrations on the degumming and regeneration process of silk fibroin. *J. Text. Inst.* **106**, 311–319. https://doi.org/10.1080/00405000.2014.919065 (2015).
42. Dash, R., Ghosh, S. K., Kaplan, D. L. & Kundu, S. C. Purification and biochemical characterization of a 70 kDa sericin from tropical tasar silkworm, *Antheraea mylitta*. *Biochem. Mol. Biol.* **147**, 129–134. https://doi.org/10.1016/j.cbpb.2007.01.009 (2007).
43. Yun, H. *et al.* Extraction conditions of *Antheraea mylitta* sericin with high yields and minimum molecular weight degradation. *Int. J. Biol. Macromol.* **52**, 59–65. https://doi.org/10.1016/j.ijbiomac.2012.09.017 (2013).
44. Reddy, N. & Yang, Y. Investigation of the structure and properties of silk fibers produced by *Actias lunas*. *J. Polym. Environ.* **20**, 659–664. https://doi.org/10.1007/s10924-012-0482-x (2012).
45. Guerra, P. A., Lawson, L. P., Gatto, L. J., Albright, M. E. & Smith, S. J. Architectural evolution in cocoons spun by *Hyalophora* (Lepidoptera; Saturniidae) silk moth species. *Sci. Rep.* **10**, 5615. https://doi.org/10.1038/s41598-020-62547-1 (2020).
46. de Palaminy, L., Daher, C. & Moulherat, C. Development of a non-destructive methodology using ATR-FTIR and chemometrics to discriminate wild silk species in heritage collections. *Spectrochim. Acta A Mol. Biomol. Spectrosc.* **270**, 120788. https://doi.org/10.1016/j.saa.2021.120788 (2022).
47. Guo, C. *et al.* Structural comparison of various silkworm silks: an Insight into the structure-property relationship. *Biomacromolecules* **19**, 906–917. https://doi.org/10.1021/acs.biomac.7b01687 (2018).
48. Hušek, P. Chloroformates in gas chromatography as general purpose derivatizing agents. *J. Chromatogr. B* **717**, 57–91. https://doi.org/10.1016/S0378-4347(98)00136-4 (1998).
49. Lucas, F., Shaw, J. T. B. & Smith, S. G. Comparative studies of fibroins: I. The amino acid composition of various fibroins and its significance in relation to their crystal structure and taxonomy. *J. Mol. Biol.* **2**, 339–349. https://doi.org/10.1016/S0022-2836(60)80045-9 (1960).
50. Moini, M., Klauenberg, K. & Ballard, M. Dating silk by capillary electrophoresis mass spectrometry. *Anal. Chem.* **83**, 7577–7581. https://doi.org/10.1021/ac201746u (2011).
51. Rutherfurd, S. M. & Gilani, G. S. Amino acid analysis. *Curr. Protoc. Protein Sci.* https://doi.org/10.1002/0471140864.ps1109s58 (2009).

Acknowledgements
This work was supported by the German Research Foundation (DFG, project number 425225219). The authors are grateful to MSc. Niels Heise for photographing the cocoons. We also thank Jenny Werner and Maximilian Schneider (Martin-Luther-Universität Halle-Wittenberg) for their valuable help in the laboratory and the butterfly house of Jonsdorf (Germany) for providing hatched cocoons. We acknowledge the financial support of the Open Access Publication Fund of the Martin-Luther-University Halle-Wittenberg.

Author contributions
Conceptualization: A.E.K. (lead); Methodology: A.E.K. (equal), TS (equal); Formal analysis and investigation: T.S. (lead), NP (supporting), M.S. (supporting), A.E.K. (supporting); Writing—original draft preparation: A.E.K. (lead); Writing—review and editing: T.S. (lead); Funding acquisition: A.E.K. (lead); Supervision: A.E.K. (equal), T.S. (equal).

Funding
Open Access funding enabled and organized by Projekt DEAL.

Competing interests
The authors declare no competing interests.

Additional information
Supplementary Information The online version contains supplementary material available at https://doi.org/10.1038/s41598-023-46474-5.

Correspondence and requests for materials should be addressed to A.E.K.

Reprints and permissions information is available at www.nature.com/reprints.

Publisher's note Springer Nature remains neutral with regard to jurisdictional claims in published maps and institutional affiliations.

Degumming and Characterization of *Bombyx mori* and Non-mulberry Silks from Saturniidae Silkworms

Theresa Schmidt[1], Nils Puchalla[1], Marcel Schendzielorz[1] & Annemarie E. Kramell[1,*]

[1] Department of Organic Chemistry, Martin-Luther-University Halle-Wittenberg, Kurt-Mothes-Straße 2, 06120 Halle, Germany

corresponding author: annemarie.kramell@chemie.uni-halle.de

Abbreviations – species:

AcL - *Actias luna* L.

AcS - *Actias selene* Hübner

AM - *Antheraea mylitta* Drury

APe - *Antheraea pernyi* Guérin-Méneville

APo - *Antheraea polyphemus* Cramer

ArM - *Argema mimosa* Boisduval

AtA - *Attacus atlas* L.

BM - *Bombyx mori* L.

CC - *Caligula cachara* Moore

CaP - *Callosamia promethea* Drury

CrT - *Cricula trifenestrata* Helfer

EB - *Epiphora bauhiniae* Guerin-Meneville

HC - *Hyalophora cecropia* L.

HG - *Hyalophora gloveri* Strecker

LK - *Loepa katinka* Westwood

SCa - *Samia canningii* Hutton

SCy ricini - *Samia cynthia ricini* Boisduval

SaPa - *Saturnia pavonia* L.

SaPy - *Saturnia pyri* Denis & Schiffermüller

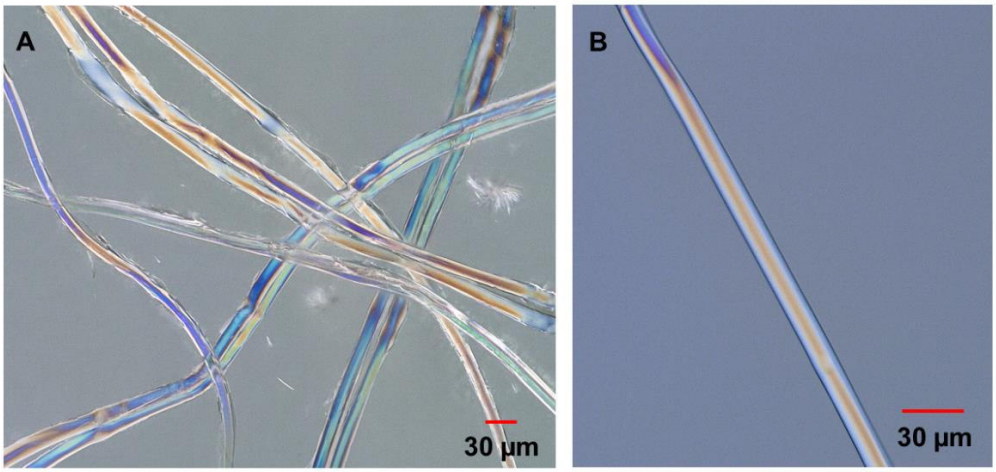

Fig. S1 Morphologies of BM silk filamtens degummed with (a) 0.1 % citric acid for 120 min at 95 °C (sample ID: BM 5-1; D_r 9 %).; (b) Periquest APG and Perlavin LMO for 60 min at 95 °C (sample ID: BM 7-1; D_r 34 %), see Table S2 for the assignment of the sample ID.

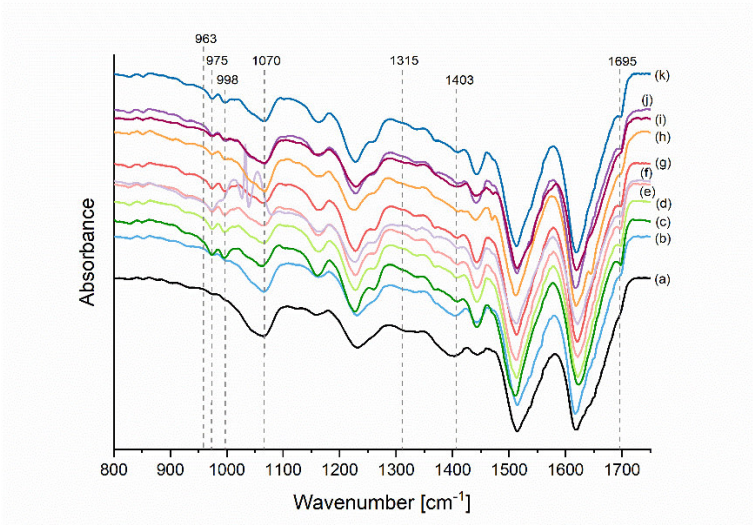

Fig. S2 ATR-FTIR spectra of untreated BM cocoons: (a) outside surface of cocoons, (b) inside surface of cocoons and BM silk degummed with different degumming agents: (c) BM 4-2, (d) BM 1-2, (e) BM 3-1, (f) BM 7-1, (g) BM 2-2, (h) BM 5-2, (i) BM 6-1, (j) BM 9-2, (k) BM 8-1, see Table S2 for the assignment of the sample ID.

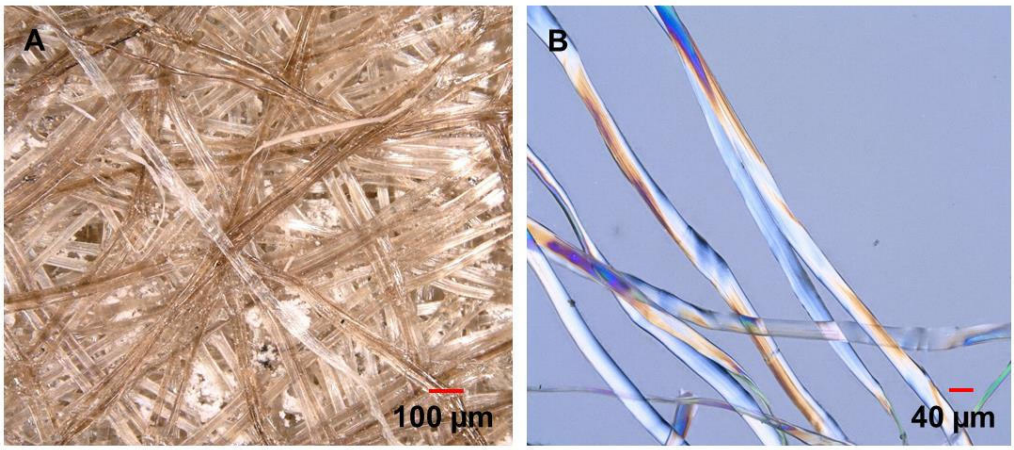

Fig. S3 Morphologies of AM silk filamtens degummed with (a) Periquest APG and Perlavin LMO for 60 min at 95 °C (sample ID: AM 7-1; D_r 11 %) and (b) a mixture of 2.5 % ethylenediamine and 0.1 % Na_2CO_3 for 90 min at 95 °C (sample ID: AM 4-3; D_r 24 %), see Table S3 for the assignment of the sample ID.

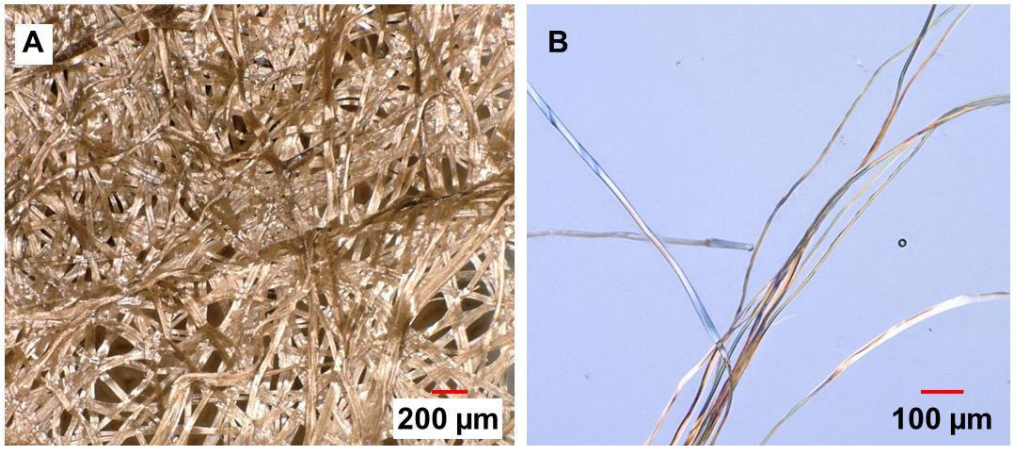

Fig. S4 Morphologies of AtA silk filamtens degummed with (a) Periquest APG and Perlavin LMO for 60 min at 95 °C (sample ID: AtA 7-2; D_r 18 %) and (b) a mixture of 2.5 % ethylenediamine and 0.1 % Na_2CO_3 for 120 min at 95 °C (sample ID: AtA 4-4; D_r 22 %), see Table S4 for the assignment of the sample ID.

Table S1 Retention time, LOD, LOQ, repeatability (peak area reproducibility at two concentration levels), method precision expressed by RSD % and recovery rates (at three concentration levels) of AAs examined (n.s. … not separated; n.d. … not determined*)*.

AA	Retention time [min]	LOD [pmol]	LOQ [pmol]	Repeatability RSD [%]		Method precision RSD [%]	Recovery [%]		
				concentration level		10 mg BM fibroin	concentration level		
				low	high		low	medium	high
Ala	3.60	170	703	0.9	0.6	2.2	92	97	94
Gly	3.81	88	397	0.6	0.6	2.1	99	74	120
Val	4.15	83	357	0.4	0.1	9.9	74	113	92
Leu	4.53	19	90	0.1	0.2	5.9	107	121	85
Ile	4.61	47	195	0.3	0.7	6.8	97	102	75
Thr	5.02	93	332	0.4	0.1	4.2	79	89	82
Ser	5.11	69	318	0.3	1.0	8.4	108	114	75
Pro	5.14	80	304	0.1	0.1	n.s.	-	-	-
Asp	6.19	50	207	0.2	0.2	3.9[a)]	73	69	74
Met	6.28	33	141	0.2	0.2	< LOD	89	103	108
Glu	6.74	65	286	0.4	0.5	4.5[a)]	100	73	72
Phe	6.86	40	176	0.1	0.03	7.5	76	70	71
Cys	7.43	88	315	0.6	2.2	< LOQ	82	97	81
Lys	8.82	131	513	0.5	0.6	7.4	72	80	78
His	9.15	31	140	1.0	2.5	7.3	88	107	78
Tyr	9.59	47	198	0.8	2.1	6.7	105	115	116
Trp	10.13	47	94	0.5	0.6	< LOD	-	-	-
Arg	n.d. (see [1,2])[b)]								

[a)] Acid hydrolysis converts Asn to Asp and Gln to Glu; [b)] As already described by Hušek, alkoxycarbonyl alkyl esters of Arg are not amenable to GC analysis

Table S2 AA composition of commercially purchased sericin from BM (family Bombycidae) and BM silks degummed with different degumming agents, expressed as the percentage of the total AA amount.

Degumming method	**Alkaline**													**Acidic**			**Detergent-based**					**Enzyme-based**				**Silk**[b]	**Sericin**
	Na_2CO_3			**$NaHCO_3$**		**Ethylenediamine**					**Na_2CO_3 and ethylenediamine**			**Citric acid**			**Marseille soap**		**Periquest APG and Perlavin LMO**			**Papain**		**Pineapple juice**			
Concentration degumming agent	1 g L^{-1}			0.5 %	1 %	2.5 %				10 %	1 g L^{-1} (Na_2CO_3), 2.5 % (ethylenediamine)			1 g L^{-1}		2 g L^{-1}	1 g L^{-1}	2 g L^{-1}	1 g L^{-1} (Periquest APG), 5 g L^{-1} (Perlavin LMO)			1 g L^{-1}		-			
Treatment time [min]	30	60	90	120	120	30	60	90	120	120	30	60	90	120	240	120	120	120	60	90	120	120	240	120	240		
Sample ID	BM 1-1	BM 1-2	BM 1-3	BM 2-1	BM 2-2	BM 3-1	BM 3-2	BM 3-3	BM 3-4	BM 3-5	BM 4-1	BM 4-2	BM 4-3	BM 5-1	BM 5-2	BM 5-3	BM 6-1	BM 6-2	BM 7-1	BM 7-2	BM 7-3	BM 8-1	BM 8-2	BM 9-1	BM 9-2		
AA composition [mol%]																											
Ala	29.3	29.4	27.7	32.8	32.3	28.3	28.3	28.4	28.2	30.3	29.5	29.5	29.7	26.6	25.7	26.8	26.0	26.6	28.6	29.0	27.7	27.4	29.6	26.9	26.1	28.0	6.5
Gly	49.0	49.4	48.6	49.4	47.3	49.7	50.7	50.3	48.6	46.4	51.7	50.7	52.1	47.3	44.8	45.5	42.9	46.0	49.6	49.0	49.1	43.4	48.1	44.9	45.6	49.2	14.3
Val	2.5	2.7	2.5	2.2	1.6	2.8	2.1	2.0	2.2	3.0	2.5	2.3	2.9	3.0	2.2	3.4	2.8	3.0	2.4	2.4	2.7	3.1	3.9	3.0	3.4	2.2	2.6
Leu	0.8	0.7	0.8	0.9	0.8	0.7	0.7	0.7	0.7	1.0	0.6	0.6	0.6	1.0	1.3	1.3	1.4	1.0	0.7	0.8	0.8	1.2	1.1	1.2	1.3	0.7	1.6
Ser	4.9	4.4	6.1	3.1	3.1	4.9	4.7	4.7	5.3	5.8	4.1	4.2	4.0	9.8	10.5	9.6	9.8	7.7	5.2	5.4	5.5	9.6	6.0	11.1	10.2	5.5	35.8
Asx (Asp+Asn)	0.7	0.6	0.9	1.3	1.6	0.8	0.8	0.8	0.9	0.8	0.7	0.8	0.5	0.8	0.9	0.9	1.0	1.0	0.8	0.8	0.9	0.9	0.5	0.8	0.8	0.9	2.0
Glx (Glu+Gln)	4.5	4.9	4.5	2.4	3.9	4.5	4.5	4.5	4.9	4.7	3.8	4.0	3.3	4.3	5.2	5.0	6.2	5.3	4.2	4.6	4.6	5.2	4.9	4.3	4.9	5.0	4.3
Phe	0.3[a]	0.2[a]	0.4[a]	<LOQ	0.1[a]	0.2[a]	0.3[a]	0.4	0.4	0.3[a]	0.2[a]	0.3[a]	0.2[a]	0.3[a]	0.3[a]	0.4[a]	0.5	0.6	0.3[a]	0.3[a]	0.3[a]	0.3[a]	0.1[a]	0.2[a]	0.2[a]	0.3[a]	0.5[a]
Cys	0.3[a]	0.3[a]	0.3[a]	0.3[a]	0.4[a]	0.3[a]	0.3[a]	0.3[a]	0.3[a]	0.3[a]	0.2[a]	0.3[a]	0.2[a]	0.3[a]	0.4[a]	0.3[a]	0.4[a]	0.4[a]	0.3[a]	0.3[a]	0.3[a]	0.3[a]	0.2[a]	0.3[a]	0.3[a]	0.3[a]	1.2[a]
Lys	1.5	1.8	1.6	1.5	1.7	1.6	1.5	1.5	1.6	1.0	1.3	1.4	1.4	1.1	1.4	0.9	1.4	1.3	1.4	1.4	1.6	1.1	0.7	1.6	0.8	1.4	6.9
His	0.7	0.7	0.7	0.6	0.7	0.7	0.7	0.7	0.8	0.4	0.6	0.6	0.6	0.4	0.5	0.4	0.6	0.5	0.6	0.7	0.7	0.4	0.3	0.4	0.4	0.7	3.5
Tyr	3.9	3.2	4.5	2.9	3.9	3.6	4.3	4.6	4.9	3.2	3.2	4.0	2.6	2.5	2.8	2.8	4.2	3.9	4.3	3.7	4.2	3.3	1.1	2.3	2.0	4.4	11.2
Ile	0.7	1.1	0.6	1.3	1.0	0.8	0.5	0.5	0.5	1.4	0.6	0.5	0.9	0.9	1.5	1.3	1.2	1.4	0.6	0.7	0.6	1.5	2.2	1.2	1.5	0.6	1.1
Met	< LOD																										2.1
Thr	0.9	0.7	1.0	0.8	0.9	1.1	0.7	0.8	0.8	1.3	1.0	0.9	1.0	1.6	2.6	1.5	1.6	1.5	0.9	1.0	1.0	2.3	1.3	1.9	2.5	0.8	5.7
Trp	< LOD																										

[a] Above LOD but just below the LOQ; [b] Commercially purchased degummed silk filaments of BM (without indication of the degumming method)

Table S3 AA composition of AM (family Saturniidae, tribe *Saturniini*) silks degummed with different degumming agents, expressed as the percentage of the total AA amount.

Degumming method	**Alkaline**					**Detergent-based**	
	Ethylenediamine		**Na_2CO_3 and ethylenediamine**			**Periquest APG and Perlavin LMO**	
Concentration degumming agent	2.5 %		1 g L^{-1} (Na_2CO_3), 2.5 % (ethylenediamine)			1 g L^{-1} (Periquest APG), 5 g L^{-1} (Perlavin LMO)	
Treatment time [min]	60	90	30	60	90	60	90
Sample ID	AM 3-2	AM 3-3	AM 4-1	AM 4-2	AM 4-3	AM 7-1	AM 7-2
AA composition [mol%]							
Ala	43.0	42.7	43.8	42.4	44.2	40.9	42.1
Gly	33.3	34.6	34.0	34.0	33.2	31.7	33.2
Val	1.4	1.6	1.4	1.5	1.5	1.9	1.6
Leu	0.5	0.5	0.5	0.5	0.4	0.8	0.6
Ser+Pro	6.4	6.1	5.4	6.0	5.9	5.7	5.5
Asx (Asp+Asn)	1.4	1.3	1.5	1.5	1.3	1.5	1.4
Glx (Glu+Gln)	2.3	2.2	2.3	2.3	2.2	2.6	2.1
Phe	0.5	0.3[a)]	0.4[a)]	0.5	0.5	0.6	0.5
Cys	0.4[a)]	0.4[a)]	0.4[a)]	0.4[a)]	0.4[a)]	0.4[a)]	0.4[a)]
Lys	2.2	2.2	2.2	2.3	2.2	3.5	3.1
His	1.0	0.9	1.1	1.1	1.0	1.3	1.1
Tyr	6.5	5.3	5.9	6.2	5.6	7.5	7.0
Ile	0.4[a)]	0.6	0.5[a)]	0.5	0.5[a)]	0.6	0.5
Met	< LOD	< LOD	0.1[a)]	< LOD	< LOD	0.4[a)]	0.4[a)]
Thr	0.8	1.2	0.6[a)]	1.0	1.1	0.7	0.6[a)]
Trp	< LOD						

[a)] Above LOD but just below the LOQ

Table S4 AA composition of AtA (family Saturniidae, tribe *Attacini*) silks degummed with different degumming agents, expressed as the percentage of the total AA amount.

Degumming method	**Alkaline**					**Detergent-based**	
	Ethylenediamine		**Na_2CO_3 and ethylenediamine**			**Periquest APG and Perlavin LMO**	
Concentration degumming agent	2.5 %		1 g L^{-1} (Na_2CO_3), 2.5 % (ethylenediamine)			1 g L^{-1} (Periquest APG), 5 g L^{-1} (Perlavin LMO)	
Treatment time [min]	60	90	60	90	120	60	90
Sample ID	AtA 3-2	AtA 3-3	AtA 4-2	AtA 4-3	AtA 4-4	AtA 7-1	AtA 7-2
D_r [%]	19	19	16	17	22	16	18
AA composition [mol%]							
Ala	39.9	48.7	47.3	47.2	48.7	47.2	49.2
Gly	33.6	33.2	33.3	32.0	34.9	31.4	31.9
Val	1.4	1.2	1.2	1.2	1.1	2.5	2.8
Leu	0.3	0.4	0.4	0.2	0.4	0.9	0.8
Ser+Pro	6.4	3.7	3.8	4.0	3.0	3.1	2.8
Asx (Asp+Asn)	2.5	1.7	1.7	1.8	1.6	1.6	1.4
Glx (Glu+Gln)	2.2	1.4	1.6	1.7	1.3	2.0	1.4
Phe	0.5[a)]	0.3[a)]	0.3[a)]	0.5[a)]	0.4[a)]	0.3[a)]	0.3[a)]
Cys	0.6[a)]	0.4[a)]	0.4[a)]	0.4[a)]	0.4[a)]	0.5[a)]	0.5[a)]
Lys	2.8	1.8	1.9	1.6	1.7	2.4	1.9
His	1.4	1.0	1.2	1.2	1.0	1.2	1.0
Tyr	6.1	4.8	5.2	5.8	4.3	4.6	4.0
Ile	0.6[a)]	0.7	0.5[a)]	0.7	0.4[a)]	1.0	0.9
Met	< LOD	< LOD	< LOD	< LOD	< LOD	0.5	0.5[a)]
Thr	1.7	0.8	1.2	1.5	0.9	0.9	0.8
Trp	< LOD						

[a)] Above LOD but just below the LOQ

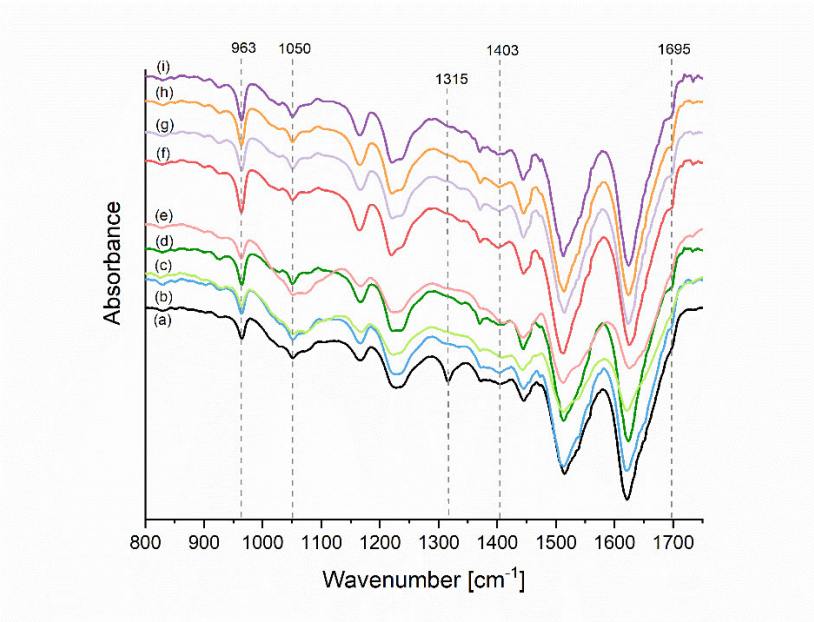

Fig. S5 ATR-FTIR spectra of untreated AtA cocoons: (a) outside surface of cocoon, (b) inside surface of cocoon and AtA silk degummed with different degumming agents: (c) AtA 7-1, (d) AtA 7-2, (e) AtA 4-4, (f) AtA 4-2, (g) AtA 4-3, (h) AtA 3-2, (i) AtA 3-3, see Table S4 for the assignment of the sample ID.

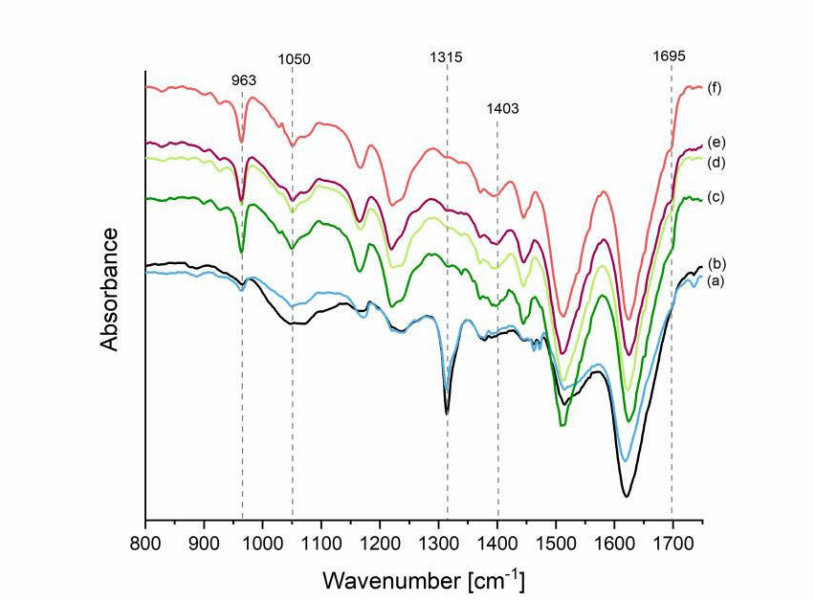

Fig. S6 ATR-FTIR spectra of untreated AM cocoons: (a) inside surface of cocoon, (b) outside surface of cocoon and AM silk degummed with different degumming agents: (c) AM 4-2, (d) AM 4-3, (e) AM 4-1, (f) AM 7-1, see Table S3 for the assignment of the sample ID.

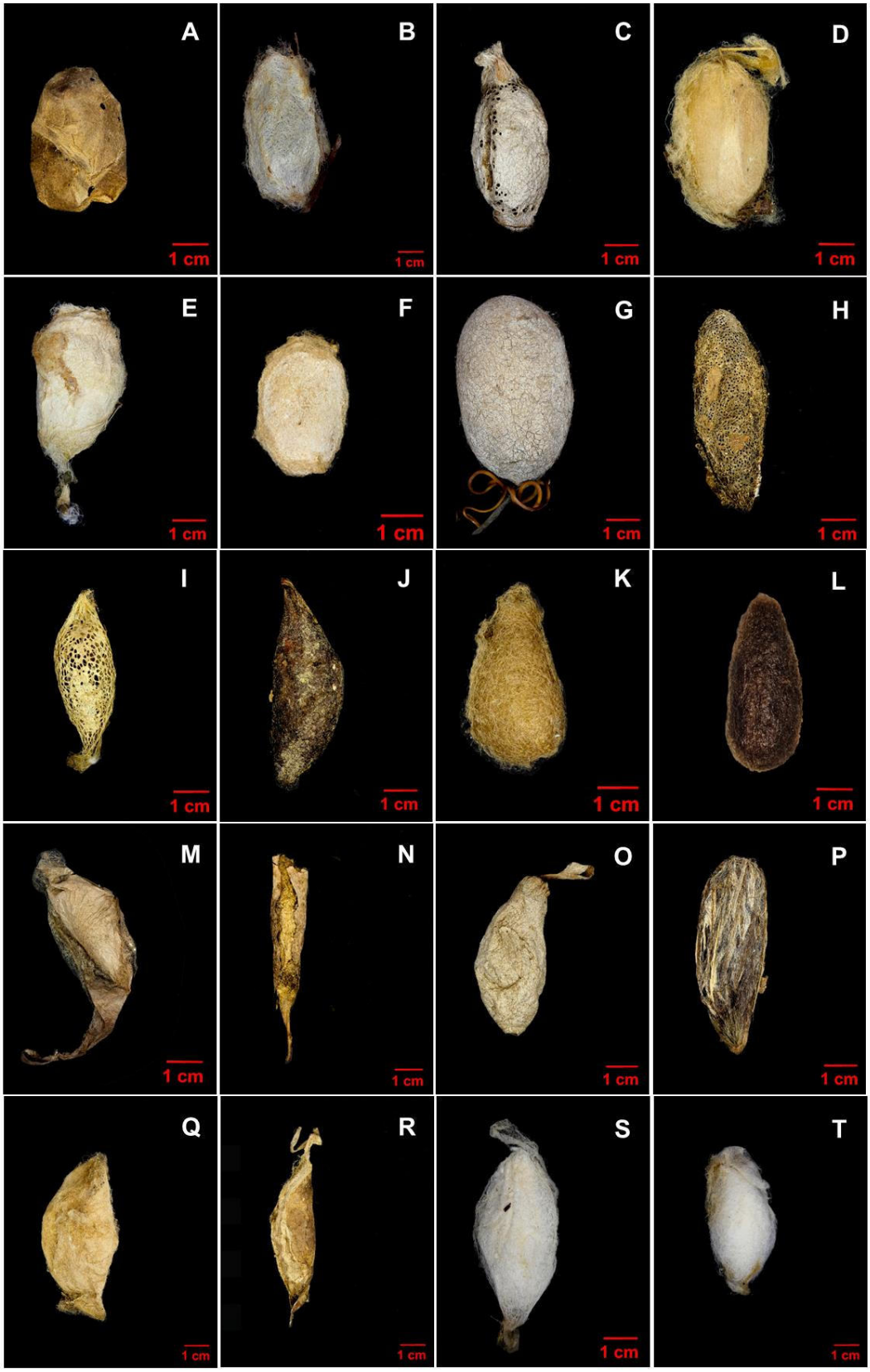

Fig. S7 (a) AcL, (b), AcS, (c) ArM, (d) APe from China, (e) APe from North Korea, (f) APo, (g) AM, (h) CC, (i) CrT; (j) LK, (k) SaPa and (l) SaPy cocoons from *Saturniini* tribe; (m) AtA, (n) CaP, (o) EB, (p) HG, (q) HC, (r) SCa, (s) Scy ricini and (t) eri silk moth cocoons from *Attacini* tribe.

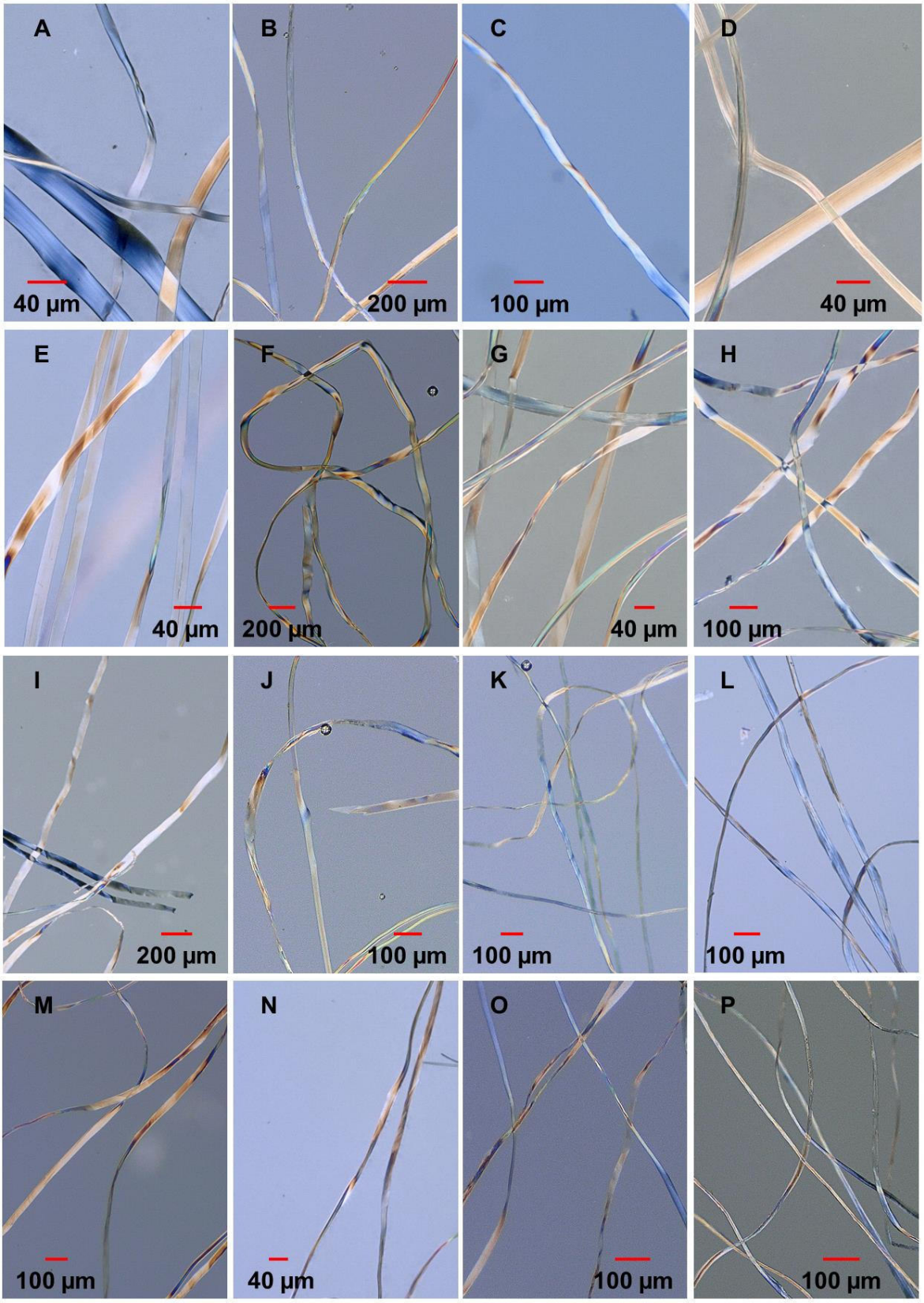

Fig. S8 Morphologies of silk filamtens degummed with a mixture of 2.5 % ethylenediamine and 0.1 % Na_2CO_3 at 95 °C: (a) AcL, (b) AcS, (c) ArM, (d) APe, (e) APo, (f) CC, (g) CrT, (h) LK, (i) SaPa and (j) SaPy from *Saturniini* tribe; (k) CaP, (l) EB, (m) HG, (n) HC, (o) SCa and (p) SCy ricini from *Attacini* tribe.

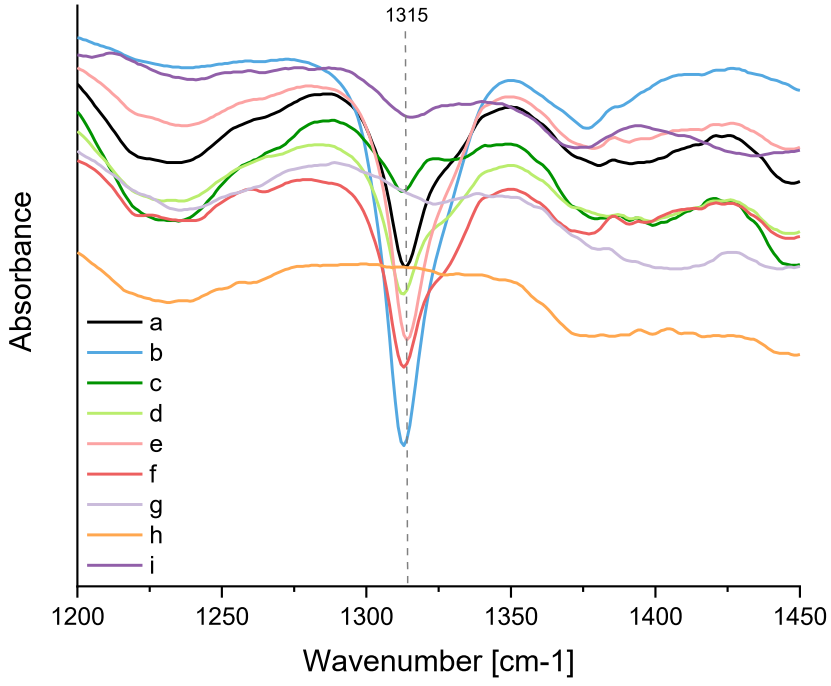

Fig. S9 ATR-FTIR spectra of untreated cocoons in the range 1200-1450 cm^{-1}: (a) APo - inside surface, (b) APo - outside surface, (c) APe - inside surface, (d) APe - outside surface, (e) AM - outside surface, (f) AM - inside surface, (g) ArM - outside surface, (h) CC - outside surface, (i) LK - outside surface.

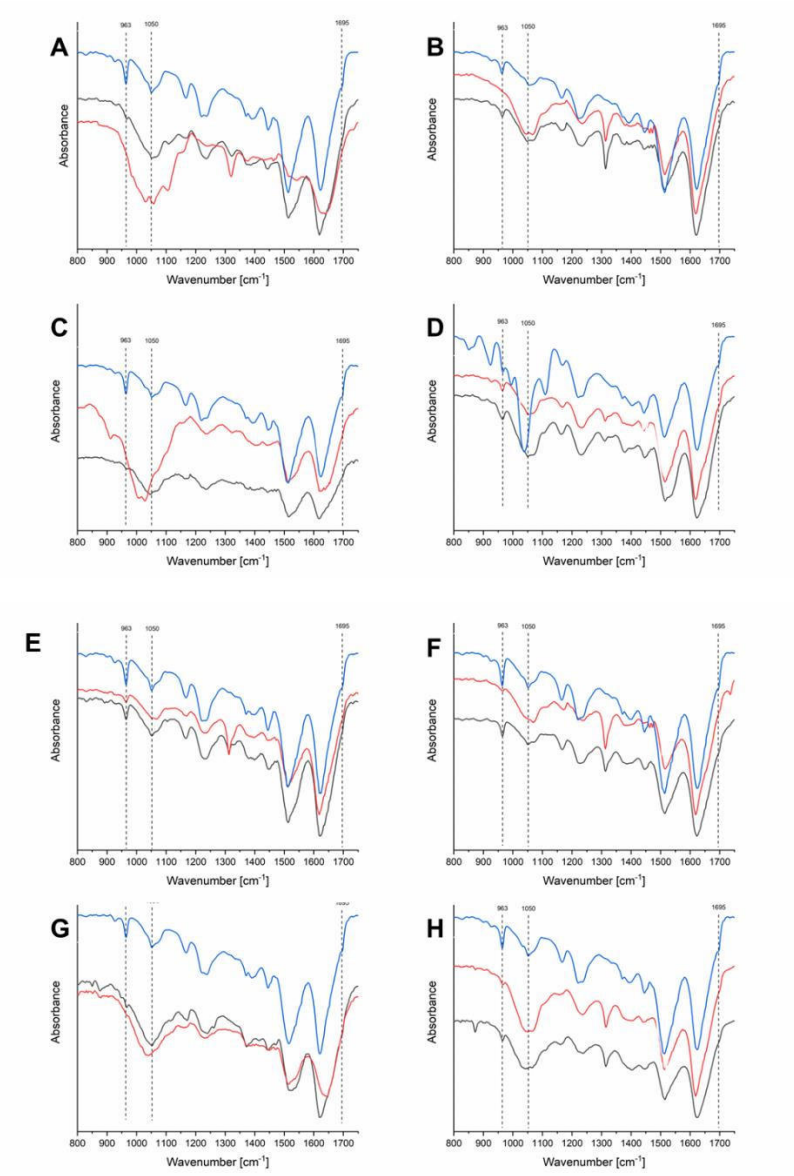

Fig. S10 ATR-FTIR spectra of untreated cocoons (black graph - inside surface, red graph - outside surface) and degummed silks (blue graph) in the range 800-1750 cm^{-1}: (a) AcL, (b) AcS, (c) ArM, (d) APe from China, (e) APe from North Korea, (f) APo, (g) CC and (h) CrT, *Saturniini* tribe.

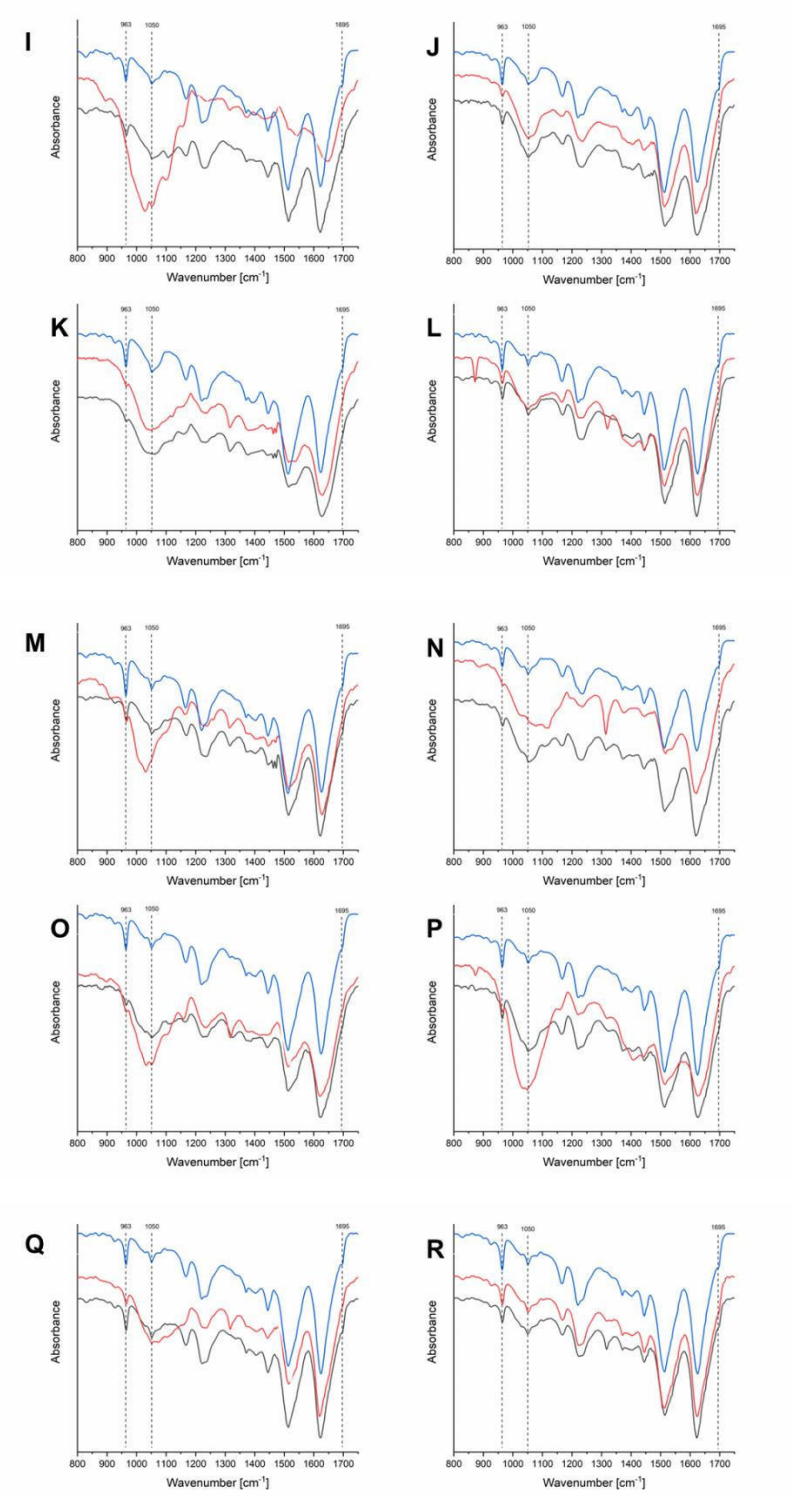

Fig. S11 ATR-FTIR spectra of untreated cocoons (black graph - inside surface, red graph - outside surface) and degummed silks (blue graph) in the range 800-1750 cm^{-1}: (i) LK, (j) SaPa and (k) SaPy, *Saturniini* tribe; (l) CaP, (m) EB, (n) HG, (o) HC, (p) SCa, (q) SCy ricini and (r) eri silk moth, *Attacini* tribe.

Table S5 Degumming ratio and treatment time of non-mulberry silkworm cocoons of the family Saturniidae and BM cocoons treated with Na_2CO_3 (1 g L^{-1}) and ethylenediamine (2.5 %) at 95 °C as well as AA composition of the degummed silks.

Tribe	Species	Description (Supplier)	Sample ID	Treatment time [min]	D_r [%]	AA composition [mol%]														
						Ala	Gly	Val	Leu	Ser+Pro	Asx (Asp+Asn)	Glx (Glu+Gln)	Phe	Cys	Lys	His	Tyr	Ile	Met	Thr	Trp
Saturniini	*Actias luna*	America	AcL	90	44	36.9	27.9	3.1	7.5	7.2	1.0	2.3	0.2[a)]	0.5[a)]	2.5	1.1	6.1	1.5	0.5	1.8	
	Actias selene	Thailand	AcS	60	64	32.3	30.6	1.8	1.4	15	1.6	1.6	0.4[a)]	0.8[a)]	2.4	1	7.9	1.4	0.8	1.0	
	Argema mimosae	Kenya	ArM	90	19	30.2	28.5	0.9	6	5.5	2.0	1.8	5.8	0.9	4.3	2.8	8.6	1.1	0.8	1.0	
	Antheraea pernyi	China	APe-1	60	29	43.4	32.3	3.8	0.7	2.7	1.8	2.9	0.4[a)]	0.5[a)]	2.5	1.3	6.2	0.8	0.3[a)]	0.5[a)]	
		North Korea	APe-2	90	21	45.6	34.0	2	0.8	1.8	1.6	3.4	0.3[a)]	0.5[a)]	2.5	1.2	4.9	0.9	0.2[a)]	0.5[a)]	
	Antheraea polyphemus	North USA	APo-1	60	39	42.7	31.9	1.9	1.7	3.7	1.8	3.1	0.3[a)]	0.6[a)]	2.7	1.2	7.0	0.7	0.3[a)]	0.6[a)]	
		North America	APo-2	60	31	43.2	32.5	1.9	1.6	3.1	1.6	2.6	0.3[a)]	0.6[a)]	2.8	1.3	7.2	0.6	0.3[a)]	0.6[a)]	
	Antheraea mylitta	-	AM-1	90	24	44.2	33.2	1.5	0.4	5.9	1.3	2.2	0.5	0.4[a)]	2.2	1.0	5.6	0.5[a)]	<LOD	1.1	
		-	AM-2	90	17	44.5	33.1	2.1	0.7	3.1	1.6	2.9	0.5	0.5[a)]	2.5	1.1	5.4	0.9	0.4[a)]	0.7[a)]	
		Tussar silk moth	AM-3	90	19	44.8	33.2	1.9	0.7	2.4	1.6	2.3	0.5	0.5[a)]	2.7	1.3	6.8	0.7	0.3[a)]	0.5[a)]	
	Caligula cachara	India	CC	240	28	40.1	26.6	1.3	7.5	6.8	1.8	1.5	0.5[a)]	0.8[a)]	3.7	1.7	4.8	1.2	0.7	1.0	
	Cricula trifenestrata	India	CrT	60	27	36.1	32.2	1.7	3	6.2	1.6	1.0	1.8	0.9	3.5	1.8	7.8	1.1	0.5	0.9	
	Loepa katinka	India	LK	90	22	40.2	29.8	3.0	2.2	2.3	1.7	1.7	0.4[a)]	0.6[a)]	4.1	2.0	10.6	0.7	0.3[a)]	0.5[a)]	
	Saturnia pavonia	Europe	SaPa-1	300	21	35.0	33.1	1.5	6.8	5.5	1.5	1.8	0.5	1.0	3.9	1.4	4.9	1.3	0.7	1.1	
		England	SaPa-2	210	20	31.9	31.7	2.0	6.5	6.5	1.2	4.7	0.4[a)]	0.7[a)]	4.0	1.5	6.1	1.4	0.6	1.0	
	Saturnia pyri	France	SaPy-1	270	33	34.6	28.7	1.9	6.5	6.9	1.3	5.3	0.4[a)]	0.7	3.5	1.4	6.0	1.2	0.5	1.1	
		Europe	SaPy-2	240	28	34.5	28.2	2.3	6.5	7.8	1.5	5.1	0.4[a)]	0.8[a)]	3.4	1.3	4.7	1.7	<LOD	1.9	<LOD
Attacini	*Attacus atlas*	Jonsdorf (butterfly house)	AtA	120	22	48.7	34.9	1.1	0.4	3.0	1.6	1.3	0.4[a)]	0.4[a)]	1.7	1.0	4.3	0.4[a)]	<LOD	0.9	
	Callosamia promethea	North America	CaP	90	26	42.2	34.5	3.1	0.7	1.5	1.8	1.7	0.4[a)]	0.6[a)]	3.3	1.5	7.7	0.6	0.2[a)]	0.5[a)]	
	Epiphora bauhiniae	Kenya	EB	120	19	44.7	33.8	2.4	0.7	2.1	1.3	2.6	0.5	0.4[a)]	2.9	1.5	5.7	0.8	<LOD	0.6[a)]	
	Hyalophora gloveri	America	HG	180	24	44.2	32.8	3.5	0.8	2.2	1.4	3.0	0.3[a)]	0.5[a)]	2.6	1.1	5.9	1.0	<LOD	0.8	
	Hyalophora cecropia	America	HC	60	22	43.6	31.6	1.9	0.6	1.6	1.8	4.4	0.4[a)]	0.5[a)]	2.8	1.4	8.1	0.6	0.2	0.5[a)]	
	Samia canningii (wild eri silk moth)	India	SCa	210	22	46	31.1	1.7	0.6	1.4	1.7	1.8	0.4[a)]	0.5[a)]	3.0	1.7	8.7	0.6	0.3[a)]	0.6[a)]	
	Samia cynthia ricini	Thailand	SCy ricini	120	26	43.5	34.6	3.3	0.9	1.5	1.7	1.3	0.3[a)]	0.6[a)]	3.0	1.5	6.5	0.8	0.2[a)]	0.5[a)]	
	Eri silk moth	-	S-1	120	16	41.1	37.0	4.3	0.8	1.6	1.7	1.8	0.3[a)]	0.5[a)]	2.6	1.3	5.1	1.0	0.3[a)]	0.6[a)]	
		India	S-2	120	23	44.3	35.0	2.4	0.7	0.9	1.6	1.4	0.3[a)]	0.5[a)]	3.4	1.5	6.8	0.7	0.2[a)]	0.4[a)]	
	Bombyx mori	Chinese web store	BM-1	60	31	29.5	50.7	2.3	0.6	4.2	0.8	4.0	0.3[a)]	0.3[a)]	1.4	0.6	4.0	0.5	<LOD	0.9	
		Halle (Saale)	BM-2	60	29	29.5	48.4	2.4	1.6	2.9	1.0	2.9	0.6	0.4[a)]	2.4	1.0	4.8	1.1	<LOD	1.0	
		China	BM-3	60	29	29.4	47.1	1.8	1.6	1.8	1.1	4.0	0.6	0.4[a)]	4.5	1.0	4.6	1.0	<LOD	0.9	

[a)] Above LOD but just below the LOQ

Table S6 Secondary structural characteristics of degummed silks treated with Na_2CO_3 (1 g L^{-1}) and ethylenediamine (2.5 %) at 95 °C.

Tribe	Species	Sample ID	β-sheet [%][a)]	β-turn [%][a)]	α-helix/random coil [%][a)]
Saturniini	*Actias luna*	AcL	56.5 ± 1.1	11.3 ± 0.5	32.1 ± 0.5
	Actias selene	AcS	57.2 ± 1.3	11.3 ± 0.9	31.6 ± 0.4
	Argema mimosae	ArM	56.6 ± 2.6	11.7 ± 1.2	31.6 ± 1.5
	Antheraea pernyi	APe-1	62.9 ± 2.3	9.4 ± 0.1	27.6 ± 2.1
		APe-2	64.1 ± 5.6	9.3 ± 0.8	26.6 ± 4.8
	Antheraea polyphemus	APo-2	60.2 ± 0.4	9.8 ± 0.2	30.0 ± 0.4
	Antheraea mylitta	AM-1	56.7 ± 1.9	11.6 ± 0.8	31.7 ± 1.1
		AM-3	56.6 ± 2.2	11.9 ± 1.4	31.5 ± 0.8
	Caligula cachara	CC	57.2 ± 1.1	11.3 ± 0.7	31.5 ± 0.5
	Cricula trifenestrata	CrT	59.2 ± 2.8	10.3 ± 1.0	30.5 ± 1.8
	Loepa katinka	LK	56.4 ± 1.2	11.4 ± 0.6	32.2 ± 0.6
	Saturnia pavonia	SaPa-2	58.6 ± 0.9	10.4 ± 0.4	31.0 ± 0.6
	Saturnia pyri	SaPy-2	56.7 ± 2.2	11.4 ± 1.3	31.9 ± 1.0
Attacini	*Attacus atlas*	AtA	66.9 ± 6.1	8.8 ± 0.9	24.2 ± 5.2
	Callosamia promethea	CaP	60.3 ± 0.8	10.1 ± 0.4	29.6 ± 0.3
	Epiphora bauhiniae	EB	62.1 ± 1.3	9.5 ± 0.7	28.3 ± 0.8
	Hyalophora gloveri	HG	57.6 ± 0.7	10.3 ± 0.2	32.1 ± 0.6
	Hyalophora cecropia	HC	60.1 ± 2.4	9.8 ± 1.0	30.1 ± 1.7
	Samia canningii (wild eri silk moth)	SCa	64.6 ± 3.3	9.2 ± 0.5	26.3 ± 3.6
	Samia cynthia ricini	SCy ricini	60.9 ±0.8	9.5 ± 0.4	29.7 ± 0.5
	Bombyx mori	BM-1	62.3 ± 0.9	8.7 ± 0.5	28.9 ± 0.5
		BM-3	66.4 ± 2.8	6.9 ± 1.5	a.7 ±1.4

[a)] Deconvolution results of amide I band in ATR-FTIR spectra (n = 3-4)

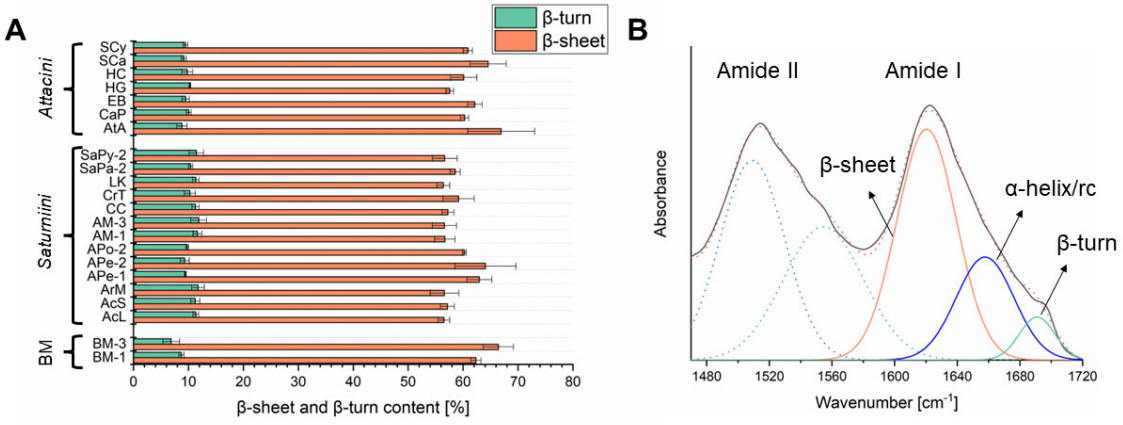

Fig. S12 (a) β-sheet and β-turn content of degummed silks treated with Na_2CO_3 (1 g L^{-1}) and ethylenediamine (2.5 %) at 95 °C. (b) Deconvolution result of amide I band of degummed APe silk: deconvoluted peaks with centers at 1620 cm^{-1} (β-sheet conformation), 1658 cm^{-1} (random coil/helical conformation) and 1691 cm^{-1} (β-turn); black solid curve, original spectrum; red dashed curve, simulated spectrum from summed peaks.

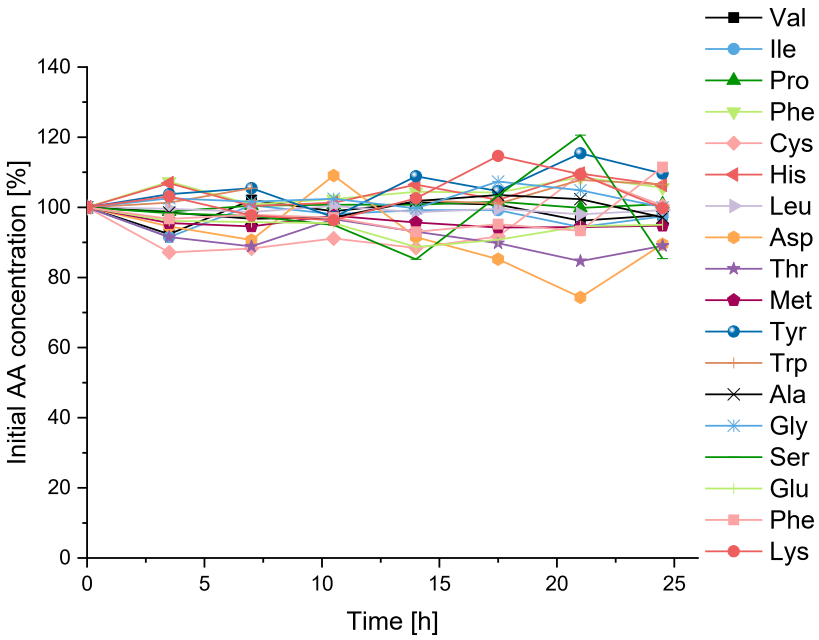

Fig. S13 Variation of AA derivatives concentration stored at room temperature over a 24 hour period.

References

1 Hušek, P. Rapid derivatization and gas chromatographic determination of amino acids. *J. Chromatogr. A* **552**, 289-299, doi:https://doi.org/10.1016/S0021-9673(01)95945-X (1991).

2 Hušek, P. Chloroformates in gas chromatography as general purpose derivatizing agents. *J. Chromatogr. B* **717**, 57-91, doi:https://doi.org/10.1016/S0378-4347(98)00136-4 (1998).

P5

JOURNAL OF NATURAL FIBERS
2024, VOL. 21, NO. 1, 2361312
https://doi.org/10.1080/15440478.2024.2361312

Taylor & Francis
Taylor & Francis Group

Characterization of Recent and Historical Silks: Effects of Silk Processing on Chemical Composition and Amino Acid Racemization

Theresa Schmidt, Jacqueline Koch, Nils Puchalla, and Annemarie E. Kramell

Department of Organic Chemistry, Martin-Luther-University Halle-Wittenberg, Halle, Germany

ABSTRACT

In this work, the influence of dyeing, mordanting and degumming techniques on the amino acid (AA) composition and the AA racemization (AAR) of (non-)mulberry silks is studied by a chiral GC-MS method. The tested dyeing and mordanting procedures as well as a pre-treatment of the silk filaments with EDTA-DMF, which enables a parallel dyestuff analysis by HPLC-DAD, do not cause any significant change in the AA composition. However, an increased proportion of e.g. (D)-Asx can be observed for some of the mordanted BM silks. Increased D/L Asx ratios can also be observed in indigo dyed silks and after an alkaline treatment at 110°C (pH > 9). Furthermore, the GC-MS method was used for the characterization of historical silk samples from finding sites in the Tarim Basin (China). The analysis of these silk fabrics reveals the presence of degraded *Bombyx* silk with significantly increased D/L Val, D/L Glx and D/L Asx ratios. Including microscopic and spectroscopic investigations, the results of this multi-analytical approach offer insights into the silk processing techniques and raw materials used.

摘要

采用手性气相色谱-质谱联用技术研究了染色、媒染和脱胶工艺对（非）桑蚕丝氨基酸（AA）组成和AA外消旋（AAR）的影响. 所测试的染色和媒染程序以及用EDTA-DMF对丝线进行预处理，这使得能够通过HPLC-DAD进行平行染料分析，不会导致AA组成的任何显著变化. 然而，对于一些媒染的BM丝，可以观察到例如（D）-Asx的比例增加. 在靛蓝染色的丝绸中以及在110°C（pH > 9）的碱性处理后，也可以观察到D/L Asx比率的增加. 此外，采用气相色谱-质谱联用技术对塔里木盆地发现地的历史丝绸样品进行了表征. 对这些丝绸织物的分析揭示了降解的家蚕丝绸的存在，其D/L-Val、D/L-Glx和D/L-Asx比率显著增加. 包括显微镜和光谱研究在内，这种多分析方法的结果为丝绸加工技术和所用原材料提供了见解.

KEYWORDS

Silk; *Bombyx mori*; silk processing; amino acid racemization; chiral GC-MS; historical textiles

关键词

丝; 家蚕; 丝绸加工; 氨基酸外消旋化; 手性GC-MS; 历史纺织品

Introduction

Silk is an exclusive material with unique properties that has been used for thousands of years in the production of textiles. Various silk producers have been used throughout history, but the most important is the domesticated silkworm *Bombyx mori* L. (BM), which feeds exclusively on mulberry leaves of the genus *Morus* and is descended from the Chinese wild silkworm *Bombyx mandarina* Moore (Arunkumar, Metta, and Nagaraju 2006; Xia et al. 2009). Studies on the genetic diversity of *Bombyx* silkworm strains indicate that silkworms were initially domesticated in China and then subjected to independent spreads along the Silk Road that gave rise to the development of most local strains (Xiang et al. 2018). The transfer of the sericulture from China westwards to the kingdoms of the Tarim Basin must have taken place between the second-century BCE and the third-century CE,

CONTACT Annemarie E. Kramell annemarie.kramell@chemie.uni-halle.de Department of Organic Chemistry, Martin-Luther-University Halle-Wittenberg, Kurt-Mothes-Straße 2, Halle 06120, Germany

Supplemental data for this article can be accessed online at https://doi.org/10.1080/15440478.2024.2361312

which correlates with China's Han Dynasty (202 BCE–220 CE) and the Three Kingdoms period (220–80) (Wu 2024). In the following centuries, sericulture spread further westwards to Byzantium and Europe, probably reaching Byzantium in the mid-sixth century (Wu 2024).

Cocoons are a multi-layered composite material consisting of two proteins, namely the water-insoluble fibroin and the water-soluble, glue-like sericin, which coats the fibroin filaments and binds them together to form an intact cocoon. The production of silk fabrics from cocoons is very complex and involves a large number of steps. To prevent the butterfly from hatching and thus destroying the cocoon, cocoons are first treated with steam or in a vacuum at 65–75°C (Veit 2022). After removing the outer, loose cocoon layer, softening the sericin in hot water and searching for the outer end of the filament with a brush, cocoons can be unwound, whereby an approximately 700–2000 m long thread can be unreeled from a single cocoon (Veit 2022). To obtain soft, smooth and glossy silk fabrics, the reeled raw silk is degummed. Enzymes, organic acids, alkaline degumming agents and/or surfactants such as sodium carbonate (Na_2CO_3) or Marseille soap are often used to remove the sericin coating (Biswal et al. 2022). In order to compensate for the weight loss during degumming, which would lower the selling price, metal salts, vegetable or synthetic substances can be incorporated into the fibroin filament in a process known as weighting (Garside, Wyeth, and Zhang 2010). Damaged or hatched cocoons and non-reeling parts of the cocoons can be used to produce spun silk yarns, which are known as Bourette, Schappe or floret silk (for a further distinction see (Veit 2022)). In the manufacture of textiles, silk is also frequently bleached, printed or dyed, whereby the dyeing can take place in the piece, i.e. as a fabric, or in strand form. In the latter case, dyed yarns are processed on various looms, e.g. treadle looms, to create colorful and luxurious fabrics.

Expensive silk fabrics, which have been a symbol of wealth and luxury for many centuries, especially in Europe, are common in museum collections. Interdisciplinary studies of these textile testimonials help to understand and reconstruct ancient technologies, trade routes and cultural exchanges. In addition to the examination of, for example, weaving patterns, fiber and dyestuff analyses are a key issue of these interdisciplinary studies (Gao et al. 2024; Ge et al. 2023; Karadag and Oraltay 2022; Kramell et al. 2014). For instance, microscopic and Fourier-transform infrared (FTIR) or Raman spectroscopic investigations can reveal the degradation state of the fibroin filaments or the presence of a sericin coating (Deveoglu et al. 2019; Koperska et al. 2014; Vilaplana et al. 2015). These methods can also be used to obtain initial indications of the presence of BM or non-mulberry silk, e.g. from *Antheraea mylitta* Drury (AM) (Boulet-Audet, Vollrath, and Holland 2015; de Palaminy, Daher, and Moulherat 2022; Gao et al. 2024). Since the amino acid (AA) sequence and composition of silk fibroin from non-mulberry silkworms differs from BM, AA analyses as well as proteomic approaches can provide further information with regard to the silk producer (Ge et al. 2023; Kmet et al. 2023; Li et al. 2015; Reddy, Zhao, and Yang 2013; Zheng et al. 2021). Nano-flow liquid chromatography tandem mass spectrometry (nanoLC-MS/MS) in combination with a calcium nitrate solubilization and a suitable enzyme digestion enables, for example, the determination of AA sequences and thus the identification of species-specific fibroin proteins. Corresponding analyses of silk fabrics from the archaeological site of Palmyra revealed the use of wild silks derived from AM (Lee et al. 2022). Lee et al. thus provide the first biochemical evidence for long-standing archaeological speculation about the production of Indian wild silk in antiquity and international trade between ancient Palmyra and the Indian subcontinent (Lee et al. 2022). Information on the structure of silk can also be obtained by ^{13}C CP-MAS NMR spectroscopy (Deveoglu et al. 2019). In addition, Deveoglu et al. use ^{27}Al MAS NMR spectra to characterize silk fabrics mordanted with alum and dyed with different flavonoids (Deveoglu et al. 2019).

Furthermore, AA racemization (AAR) rates can be used to characterize historical silks. Moini et al. introduced capillary electrophoresis MS (CE-MS) for age estimation of silk textiles based on the racemization rate of asparagine (Asn) and aspartic acid (Asp) (Moini and Rollman 2017; Moini, Klauenberg, and Ballard 2011; Shimada et al. 2023). This technique is suitable for dating BM silks from museum collections, ranging in age from the present to ~2500 years ago. At approximately 100 µg (or less), the amount of sample used is significantly less than the amount required for accelerator mass

spectrometry (AMS) dating (^{14}C dating) (Moini, Klauenberg, and Ballard 2011). In addition, the costs of authenticating silk using AMS dating are relatively high and the presence of dyestuffs or other difficult-to-remove contaminants such as humic substances can falsify the ^{14}C age (Boudin et al. 2013). In contrast, AAR is affected by environmental factors such as pH value, temperature, humidity, UV radiation, impurities and the presence of metal ions (Bada 1985; Bright and Kaufman 2011; Goodfriend 1992; Kaufman 2006; Smith, Williams, and Wonnacott 1978). The influence of factors such as UV radiation, pH value and humidity on the D/L ratio of AAs and thus on the age determination can be minimized if archaeological remains are protected, e.g. by an inorganic template. When examining silks, it should be noted that silk processing, e.g. degumming or dyeing, can accelerate AAR. Initial studies by Moini et al. and Shimada et al. have already shown that treatment of BM silk with alkaline solutions at elevated temperatures can have a significant effect on the racemization rate of Asp, Asn, phenylalanine (Phe) and tyrosine (Tyr) (Moini and Rollman 2017; Shimada et al. 2023). These studies also showed that CE-MS measurements enable the identification of artificially aged silk, obtained by a chemical treatment with a base at elevated temperatures, and thus silk forgery (Moini and Rollman 2017). Furthermore, Moini et al. investigated the effect of UV exposure on (L) to (D) conversion of silk proteins (Moini, Klauenberg, and Ballard 2011). However, systematic studies on the influence of degumming, mordanting and dyeing techniques on AAR rates are still pending. The influence of mordants is of particular interest as it is known that the presence of metal ions such as Cu^{2+}, Cd^{2+} and Fe^{2+}, which are typically used for mordanting (Cardon 2007; Schweppe 1992), can a) catalyze degradation reactions of AAs or proteins and b) affect AAR rates by stabilizing the carbanion intermediate (Johnson and Pratt 2010; Smith, Williams, and Wonnacott 1978). Fe^{2+} in particular leads to powerfully oxidizing hydroxide radicals in a so-called Fenton's reaction. Furthermore, when examining proteinaceous materials by GC or LC, it should be noted that metal ions and polyvalent cations such as Ca^{2+} can reduce the efficiency of AA derivatization by forming strong cation ion-AA complexes (Bonaduce, Cito, and Colombini 2009; Colombini and Modugno 2004). These complexes can selectively subtract some AAs from the analysis and thus prevent the identification of the proteins (Bonaduce, Cito, and Colombini 2009). The effect of polyvalent cations on the identification of proteinaceous binders in paintings has already been investigated, including the development of analytical procedures with purification steps to remove inorganic components (Bonaduce, Cito, and Colombini 2009; Lluveras et al. 2010). However, the authors are not aware of any corresponding studies on silk. In addition to the use of metal salts such as copper(II) sulfate or stannic chloride for mordanting or weighting, the conditions of use, storage or conservation may also result in a higher content of metal ions in historical silk samples. A high content of metal ions is to be expected, especially in archaeological samples with soil contact.

In this study, we investigate the influence of different dyeing and mordanting techniques on the AA composition of mulberry and non-mulberry silks. The investigations were carried out on BM, AM and *Attacus atlas* L. (AtA) silk samples, which differ in terms of their morphology, chemical composition and physical structure. In addition, the AAR rates of mordanted and dyed samples were determined, whereby the effect of the degumming method was also considered. In this context, a gas chromatography-MS (GC-MS) method for the identification and quantification of 11 enantiomeric AA pairs in silk fibroin was developed and validated. In the course of method development, clean-up steps using organic-aqueous systems and the chelating agent EDTA were tested, which enable the extraction of natural dyes and thus a parallel dyestuff analysis by high-performance liquid chromatography-diode array detection (HPLC-DAD). Furthermore, the influence of the derivatization and hydrolysis procedure on the racemization of AAs was studied. The developed and validated GC-MS method was used to characterize historical silk samples from finding sites in the Tarim Basin, covering a period from the first millennium BC to third century AD. Furthermore, these samples were analyzed by optical microscopy (OM), scanning electron microscopy (SEM), SEM in combination with energy-dispersive X-ray spectroscopy (SEM-EDX), FTIR spectroscopy in attenuated total reflection mode (ATR-FTIR spectroscopy), HPLC-DAD and liquid chromatography-electrospray ionization-MS/MS (LC-ESI-MS/MS). On the one hand, the aim was to evaluate the influence of silk processing on the AA

composition and the AAR of recent silks. On the other hand, a multi-analytical technique-based approach was established, which enables a comprehensive characterization of historical silk samples and thus provides information on ancient silk processing techniques and processed raw materials, especially on colorants and silk used. In addition, degradation processes are characterized on a molecular level.

Material and methods

Chemicals and materials

L-Alanine (L-Ala; 99%), L-isoleucine (L-Ile; 99%), L-proline (L-Pro; 99%), L-cysteine (L-Cys; >98%), L-lysine (L-Lys; 98%) and L-norleucine (L-Nle; 99%) were obtained from Alfa Aesar. D-Alanine (D-Ala, 99%), D-aspartic acid (D-Asp, 99%), D-cysteine (D-Cys, 98%), D-isoleucine (D-Ile, >98%), D-methionine (D-Met, 99%), D-norleucine (D-Nle, 99%), D-phenylalanine (D-Phe, 99%), D-threonine (D-Thr, 99%), D-tyrosine (D-Tyr, 99%), D-tryptophane (D-Trp, 99%) and chloroform (HPLC grade) were purchased from Thermo Fisher GmbH; glycine (Gly; ≥99%) and D-histidine (D-His; >99%) from TCI (Tokyo Chemical Industry); L-leucine (L-Leu; ≥99%), L-valine (L-Val; ≥99%), D- and L-glutamic acid (Glu; ≥99%), L-aspartic acid (L-Asp; ≥99%), L-threonine (L-Thr; ≥99%), L-phenylalanine (L-Phe; ≥99%), L-methionine (L-Met; ≥99%), D-serine (D-Ser; >99%), D-leucine (D-Leu; >99%), calcium oxalate (≥98%) and iron(II) sulfate heptahydrate ($Fe(II)SO_4 \cdot 7\,H_2O$, ≥99%, p.a.) from Carl Roth GmbH + Co. KG; L-serine (L-Ser; >99%), L-histidine (L-His; ≥99%), D-lysine (D-Lys, >98%), sodium carbonate (Na_2CO_3; anhydrous), pyridine (≥99.0%), ethylene diamine (≥99%), phenol (≥96%), ethylenediaminetetraacetic acid (EDTA, 99.4–100.6%), 3,3′-dithiodipropionic acid (DTDPA, 99%) and indigo (95%) from Sigma-Aldrich; L-tryptophane (L-Trp; 99%) and D-proline (p-Pro, >99%) from Acros Organics; D-valine (D-Val, >99%) from MP Biomedicals LLC.; isooctane from VWR Chemicals [ACS (American Chemical Society), Reag. Ph. Eur. (*Pharmacopoea Europaea*)] and Supelco (for liquid chromatography; ACS reagent, ≥99.0%); *N,N*-dimethylformamide (DMF, 99.5%), isopropanol (for HPLC), concentrated hydrochloric acid (HCl; 37%) and sodium hydroxide (NaOH, 98%, reinst, pellets) from Fisher Scientific; methanol (MeOH, HPLC gradient grade) and acetonitrile (ACN, HPLC super gradient grade) from VWR Chemicals; ethylene diamine (≥99.5%; GC), potassium hydrogen tartrate and sodium dithionite from Merck KGaA; potassium aluminum sulfate dodecahydrate ($KAl(SO_4)_2 \cdot 12\,H_2O$, 99.0–100.5%) from Riedel-de Haën; copper(II) sulfate pentahydrate ($Cu(II)SO_4 \cdot 5\,H_2O$, >99%, p.a.) from Fluka. 2,2,3,3,4,4,4-Heptafluorobutyl chloroformate (HFBCF) was brought from Apollo Scientific Ltd (97%, Cheshire, United Kingdom) and Carbolution Chemicals GmbH (95%, St. Ingbert, Germany). Dried and ground madder roots (*Rubia tinctorum* L.) were bought from Kremer Pigmente GmbH & Co KG (Aichstetten, Germany).

Cocoons, recent silk and wool samples

BM cocoons were obtained from the World of Butterflies & Moths (Lincolnshire, England), the Francke Foundations (Halle/Saale, Germany) and a Chinese web store. Degummed BM silk and cocoons of AM (Indian tasar silkmoth) were purchased from Seidentraum (organic peace silk, Sternenfels, Germany), a sheep wool fleece (100% merino wool) from Galerie Smend (Köln, Germany). Cocoons of AtA were obtained from the butterfly house of Jonsdorf (Germany); *Antheraea pernyi* Guérin-Méneville (APe) silkworm cocoons from the World of Butterflies & Moths (Lincolnshire, England).

Historical textile samples

Silk and wool samples from archaeological sites of Niya, Yanghai and Wupu in the Xinjiang Uyghur Autonomous Region (Tarim Basin, China) were taken within the framework of an interdisciplinary

Chinese-German research project (for a further description of the samples and finding sites, see Beck et al. 2014; Kramell et al. 2014; Kramell et al. 2016; Wertmann et al. 2020).

Degumming of cocoons (Schmidt et al. 2023)

Before degumming, pupae, plant parts and coarse impurities were removed with tweezers. Cocoons were degummed at 95°C for 60–120 min (reaction time for BM cocoons: 30–90 min; reaction time for AM and APe cocoons: 90 min, reaction time for AtA cocoons: 120 min) in an aqueous solution containing Na_2CO_3 (1 g/L) and ethylenediamine (2.5% w/w). After degumming, the fibers were immediately rinsed thoroughly with distilled water until a neutral pH value was achieved and dried at 100°C until constant weight was reached. All experiments were repeated three times. The efficiency of the degumming process was monitored by microscopic and ATR-FTIR spectroscopic studies, as well as by determining the degumming ratio D_r (%), as reported by (Schmidt et al. 2023).

To investigate the influence of alkaline degumming procedures, BM cocoons were treated with aqueous solution containing Na_2CO_3 (1 g/L or 2.5 g/L) at 95°C for 30–120 min. Furthermore, BM cocoons were degummed with ethylenediamine (2.5% w/w) at 95°C for 120 min as described by (Schmidt et al. 2023).

Treatment of silk with Na_2CO_3 solutions (modified according to (Moini and Rollman 2017))

To simulate the artificial aging described by Moini and Rollman (Moini and Rollman 2017), degummed BM silk samples and cocoons (200 mg) were treated in sealed tubes with aqueous Na_2CO_3 solutions (3 mL, pH 9, 11 and 13) at 110°C for 60–120 min. The pH of the solutions was measured using a digital pH meter and adjusted to a pH of 9, 11 and 13 with HCl (6 M) or NaOH (1 M). After alkaline treatment, the filaments were then rinsed with MeOH and distilled water and dried at room temperature. Dried silk samples were hydrolyzed and then analyzed by GC-MS as described below.

Sample treatment with calcium oxalate

In order to determine the influence of a possible residue of calcium oxalate, which is found on some wild silk cocoons, BM, AtA and AM silk samples were treated with calcium oxalate. For this purpose, degummed silk (200 mg) was moistened with water and treated with an aqueous calcium oxalate suspension (100 mL; 15% based on the dry weight of the silk) for 60 min at 40°C. Subsequently, the silk fibers were rinsed two times with water and dried at room temperature.

Dyeing and mordanting procedure (modified according to (Cardon 2007) and (Schweppe 1992))

In the course of the mordanting procedure, degummed silk (200 mg) was first moistened with water to ensure uniform and complete wetting with the metal salt solution. During the mordanting and dyeing process, the silk is turned occasionally.

All experiments were repeated three times with degummed silk of BM, AtA and AM.

Mordanting procedure with potassium alum

The mordant bath was prepared by adding $KAl(SO_4)_2 \cdot 12\,H_2O$ (15% - based on the dry weight of the silk) in water (100 mL) at 40°C. Degummed and moistened silk was immersed into the bath, which was then heated to 60°C and left at this temperature for 60 min. After the mordant bath had cooled to room temperature, the silk was removed, rinsed several times with water, and dried at room temperature or used while still wet for the subsequent madder dyeing process.

Mordanting procedure with potassium alum and potassium hydrogen tartrate

Mordanting procedure described above was carried out in the presence of $KAl(SO_4)_2 \cdot 12\ H_2O$ (15% - based on the dry weight of the silk) and potassium hydrogen tartrate (4% - based on the dry weight of the silk).

Mordanting procedure with copper(II) sulfate or iron(II) sulfate

The mordant bath was prepared by adding $Cu(II)SO_4 \cdot 5\ H_2O$ (6% based on the dry weight of the silk) or $Fe(II)SO_4 \cdot 7\ H_2O$ (3% based on the dry weight of the silk) in water (100 mL) at 40°C. Afterward, degummed and moistened silk was immersed into the bath and was treated for 60 min at 60°C with this solution. After the mordant bath had cooled to room temperature, the silk was removed, rinsed several times with water, and dried at room temperature.

Mordant dyeing with madder (Rubia tinctorum *L.*)

Preparation of the dye bath: A filter containing dried and ground madder roots (10 g) was soaked in water (200 mL) overnight. The extract was then heated slowly within 60 min until reflux began, and the temperature was kept constant for a further 10 min. After removing the heat source, water (100 mL) was added and the plant material was removed. Degummed and moistened silk mordanted with potassium alum or potassium alum and potassium hydrogen tartrate was added to the dye bath. The dye bath was heated to 60°C and left at this temperature for 30 min. Afterward, the dye bath was cooled to room temperature, the silk was removed, rinsed several times with water until the wash water appeared clear and dried at room temperature.

Vat dyeing with indigo

For a suspension of synthetic indigo (2 g, powder) in water (8 mL), an aqueous NaOH solution (7%, m/v) was added and the suspension was heated to 60°C. Then sodium dithionite was added until the solution began to turn yellow. Degummed silk (200 mg) was moistened with water and immersed into the dye bath at 55°C for 2–3 min. The silk was then removed, squeezed vigorously and air-dried. After drying, the silk was thoroughly rinsed with water and dried at room temperature. If necessary, the dyeing process can be repeated so that deeper shades can be achieved.

Sample pre-treatment with an EDTA solution

Sample preparation with EDTA-ACN-MeOH (modified according to (Manhita et al. 2011; Zhang and Laursen 2005))

For some silk samples, an additional purification step was performed prior to the hydrolysis (see Conventional hydrolysis of silk samples) to eliminate interfering components such as metal ions or organic impurities. For this purpose, silk samples (20 mg) were treated with an EDTA solution [4 mL, H_2EDTA (aqueous, 0.1%)/ACN/MeOH, 2:10:88, v/v/v] for 30 or 60 min at 60°C. Subsequently, the sample material was rinsed with MeOH (2 × 4 or 10 mL) and dried at room temperature. In the course of method development, the procedure was tested on recent BM, AM and AtA silk samples (non-mordanted/undyed and mordanted/dyed samples).

Sample preparation with EDTA-DMF (modified according to (Manhita et al. 2011))

For some dyed silk samples, an additional extraction step was performed prior to the hydrolysis to allow parallel dyestuff analyses. For this purpose, red and blue dyed samples (recent and historical materials, 20 mg) were extracted with an EDTA solution (4 mL, 0.1%, aqueous-organic system consisting of water and DMF, 1:1 v/v) for 30 and 60 min at 95°C. The fibers were then rinsed with MeOH (2 × 4 or 10 mL) and dried at room temperature. Dried silk samples were hydrolyzed and then analyzed by GC-MS as described below. EDTA-DMF extracts were analyzed for dyestuffs by HPLC-DAD as described in previous studies (Kramell et al. 2014; Kramell et al. 2016). In the course of method development, the procedure was tested on BM, AM and AtA silk, dyed with indigo or madder.

AA analysis by GC-FID

AA analyses using GC-FID were performed as reported by (Schmidt et al. 2023).

AA analysis by GC-MS

Samples were analyzed with a Shimadzu gas chromatograph Nexis GC-2030, equipped with an AOC-20i injector (injection volume: 0.5 µL, splitless mode), an AOC-20s autosampler and a mass spectrometer (MS; GCMS-QP2020 NX, ion source temperature: 210°C, mass range: *m/z* 60–650, full scan mode, voltage conversion dynode: 70 eV). Chromatographic separation was performed on a CP-ChiraSil-L-Val column (25 m × 0.25 mm × 0.12 µm, Agilent). The chromatogram was recorded in the retention time range from 4 to 54 min. The injection port was held at 230°C, and the interface between the column and the detector source was set at 200°C. The column oven temperature was initially set to 92°C, held for 1 min and then ramped with 2.5°C min^{-1} to 200°C, held for 10 min; the carrier gas was hydrogen at a constant column flow of 1.20 mL/min (linear velocity: 66.0 cm/sec). All analyses were performed in triplicate. After use, the autosampler syringe should be rinsed with isopropanol followed by chloroform and isooctane to prevent corrosion of the plunger.

Preparation of standard solutions

Stock solutions (5, 10, 20 and 50 mM) of (L-)AAs and (D)-AAs were individually prepared in aqueous hydrochloric acid (0.1 M). (L)-Nle and (D)-Nle (20 mM) were used as internal standards.

Conventional hydrolysis of silk samples (modified according to (Vilaplana et al. 2015))

Hydrolysis of the silk samples (1–8 mg) was performed with HCl (1000 µL, 6 M) at 110°C for 24 h. As stabilization reagents and chelating agents, phenol in water (50 µL, 1%), DTDPA (50 µL, 1%) in an aqueous solution of sodium hydroxide (0.2 M) and EDTA (100 µL, 0.1%) in an aqueous solution of NaOH (pH 9) were added to all samples. The hydrolyzate was concentrated to dryness at 90°C using a nitrogen stream, and the residue was dissolved in HCl (200 µL, 0.1 M). Aliquotes (25–200 µL) were used for AA derivatization.

Hydrolysis with HCl assisted by microwave (modified according to (Colombini et al. 1998))

Various proteins (e.g. lupine flour protein, bovine serum albumin, ovalbumin, fibroin) and working solutions of (L)-Ala and (L)-Asp (14 µL, 50 mM) were treated with HCl (2000 µL, 6 or 7 M) at 150°C or 160°C for 10–180 min in a sealed tube using an Anton Paar Monowave 300 microwave system (max. power: 250 W, stirring speed: 600 rpm). The hydrolyzate was concentrated to dryness at 90°C using a nitrogen stream and the residue was dissolved in HCl (200 µL, 0.1 M). Aliquotes (50 µL) were used for AA derivatization.

AA derivatization with HFCBF (modified according to (Zahradníčková, Hušek, and Šimek 2009))

Aliquotes of AA stock solutions or hydrolyzates (25–200 µL) were diluted with distilled water (100 µL), a NaOH-Na_2CO_3 solution was added (50 µL, 1 M NaOH/0.5 M Na_2CO_3, 4:1 v/v), and this solution was mixed with a vortex for 20 sec. Then, the derivatization reagent solution (85 µL, HFCBF/isooctane, 1:3 v/v) was added and it was mixed again for 20 sec. Subsequently, the catalyst solution (50 µL, 50 mM Na_2CO_3/pyridine, 3:1 v/v) was added, the solution was thoroughly vortexed for 20 sec, and then remained at room temperature for about 5 min. Finally, isooctane (165 µL) was added and the solution was mixed for several minutes until the upper organic phase remained clear after mixing and showed no turbidity. An aliquot of the organic phase (0.5 µL) was injected into the gas chromatograph.

AA analysis by GC-MS – validation experiments

Specificity

To determine the specificity of the method, a mixture of all studied (L)- and (D)-AAs was measured by GC-MS after derivatization with HFBCF [for retention times see Table S1, Supplementary Material (SM)]. Furthermore, hydrolyzates of degummed BM and AM silks as well as blank samples (without AA or protein addition) were analyzed by GC-MS.

Linearity, limit of detection (LOD) and limit of quantification (LOQ)

For the calibration, solutions were prepared with different mixtures of (L)- and (D)-AAs [AAs: in the range of min 0.4 to max 50 mM with (L)- and (D)-Nle as internal standards (22 µL, 20 mM)]. Each calibration solution was measured three times, and analyses were executed with average peak area ratios of the respective (L)- or (D)-AA and (L)- or (D)-Nle. The linearity of each calibration function was tested with the Mandel's test. LOD and LOQ were determined by means of a calibration curve method according to DIN 32645 (Kromidas 2011). These validation data are shown in Table S1, SM.

Precision

To determine the repeatability, six replicate measurements were carried out for two different concentrations (Table S1, SM). For this purpose, working solutions containing respective (L)- or (D)-AAs as well as the internal standard [(L)- or (D)-Nle] were prepared, derivatized and analyzed with GC-MS. (L)-Ala and Gly were analyzed separately from the other AAs due to the high concentration differences. For the interpretation of the repeatability, the relative standard deviation (RSD) of the respective AA concentration was used. For determining the method precision, six BM as well as six AM cocoons were degummed with Na_2CO_3 (1 g/L) and ethylenediamine (2.5% w/w) at 95°C for 60 (BM cocoons) or 90 min (AM cocoons) as described above, degummed and dried BM and AM silk samples (max 6.5 mg) were treated with an EDTA-ACN-MeOH solution (see Sample preparation with EDTA-ACN-MeOH), hydrolyzed with HCl at 110°C for 24 h and independently derivatized with HFCBF in the presence of the internal standards (L)- and (D)-Nle. Aliquots (0.5 µL) of the organic phases were analyzed by GC-MS. For the interpretation of the method precision, the RSD of the AA concentrations was used (Table S1, SM). Furthermore, Dixon's Q test and Neumann trend test were applied for the identification of outliers or trends.

Recovery

The calculation of the recovery rate for each AA was performed for three concentration levels with a number of three replicates (Table S1, SM). For this purpose, degummed silken filaments of BM [max 6.5 mg, degumming method: Na_2CO_3 (1 g/L) and ethylenediamine (2.5% w/w), 95°C, 60 min] were spiked with defined (L)- or (D)-AA concentrations [(L)- and (D)-AAs were studied separately], hydrolyzed with HCl at 110°C for 24 h and derivatized with HFCBF as described above. Hydrolysis, derivatization and GC-MS analysis of the spiked silk samples were performed independently of each other on different days. The calculated AA concentrations were compared with the target concentrations, and the recovery rate was determined. The average AA concentrations of degummed silken filaments of BM, determined in the course of the method precision, were used for the calculation of the target concentrations.

Results and discussion

The subjects of the studies were degummed BM (family Bombycidae) filaments as well as non-mulberry silks of the species AM (family Saturniidae, tribe *Saturniini*) and AtA (family Saturniidae, tribe *Attacini*). In the course of the investigations, degummed silks were mordanted according to historical recipes with copper(II) sulfate, iron(II) sulfate, potassium alum as well as potassium alum and potassium hydrogen tartrate. Madder (*R. tinctorum* L.) roots and the blue vat dye indigo were

used for dyeing. Both colorants were used in various regions of the world by different cultures to produce red, purple or blue colored textiles (Cardon 2007; Hofenk de Graaff 2004; Schweppe 1992). Madder, for example, was cultivated in various regions of Europe and Anatolia and was among the most demanded products in the Ottoman Empire (Ozdemir and Karadag 2023b). Since the second half of the 19th century, synthetic dyes were increasingly used in the textile industry. Today, a return to natural colorants can be observed. Interest in textile products dyed with natural dyes has increased in recent years, particularly among environmentally sensitive and conscious consumers (Karadag 2023). In this context, the economic and scientific interest is also growing in textiles dyed with natural indigo or madder and mordanted with natural, nontoxic metal salts such as potassium alum or plant-based mordants such as acorns (*Quercus* species) (Deveoglu et al. 2012; Ozdemir and Karadag 2023a, 2023b).

In addition to the recent samples mentioned above, textile samples from archaeological sites in the Tarim Basin (Xinjiang Uyghur Autonomous Region, Eastern Central Asia) – covering a period from the first millennium BC to third century AD (see Examination of historical samples) – were analyzed.

Effect of dyeing and mordanting procedures on the determined AA composition of recent silks

To investigate the effect of the mordanting and dyeing process on the AA composition, mordanted, dyed and untreated (i.e. degummed, undyed and non-mordanted) BM, AM and AtA silk samples were analyzed by GC-FID as described in a study of (Schmidt et al. 2023) and the determined AA composition was compared. BM silk was also treated with calcium oxalate to investigate the influence of Ca^{2+} ions, which are detectable on the surface of some wild silks in the form of calcium oxalate (Boulet-Audet, Vollrath, and Holland 2015). The dyeing and mordanting procedures as well as the presence of Ca^{2+} ions do not cause any significant change in the AA composition under the selected conditions (Figures S1–S3 and Tables S2–S4, SM). Consequently, no significant changes can be observed for structural indices such as the Gly/Ala or the long chain/short chain ratio (100LC/SC), which can be used to characterize silk fibroins (see (Freddi et al. 1994; Schmidt et al. 2023)). For instance, the 100LC/SC ratio of BM fibroin is 21–29, regardless of the mordanting and dyeing conditions (Table S2, SM). However, as already described by Ahmed and Darwish (Ahmed and Darwish 2012), some of the treated silks are characterized by a slight increase of the acidic AAs. For example, BM and AtA silks mordanted with alum and dyed with madder show a slightly higher Glx content (BM-Al/madder: 5.4 mol%; AtA-Al/madder: 2.3 mol%) compared to the untreated BM (3.5 mol%) and AtA samples (1.3 mol%, Figures S1B and S3B, for the assignment of the sample ID, see Tables S2–4, SM).

In addition to AA analysis, bluish and reddish silk samples were also examined for the colorants used. Since only a small sample amount is usually available, especially for precious historical samples, the following procedure is used: The silk samples are extracted, the extracts are examined for the presence of dyestuffs by HPLC-DAD and the remaining silk filaments are then analyzed for their AA composition. In this context, different extraction methods and their effects on the AA composition were tested (see next section).

Sample pre-treatment with an EDTA solution: clean-up step and dyestuff analyses

Dyed silk samples were treated with an aqueous EDTA-DMF or EDTA-ACN-MeOH solution prior to AA analysis by GC-FID, and the extracts were analyzed for the presence of organic dyestuffs by HPLC-DAD (see (Kramell et al. 2014; Kramell et al. 2016)). Alizarin and purpurin, dyes of the anthraquinone type, were detected, for example, in EDTA-DMF extracts of recent silk samples mordanted with potassium aluminum sulfate and dyed with madder. The EDTA-DMF extraction step is also suitable for the detection of vat dyes such as indigo. A slight discoloration was observed for dyed silk samples after treatment with the aqueous EDTA-ACN-MeOH solution. However, as already described by (Manhita et al. 2011), this milder method does not allow efficient extraction of anthraquinones and vat dyes such as indigo.

GC-FID studies on dyed and undyed BM, AM and AtA silks show that sample pre-treatment with EDTA-ACN-MeOH or EDTA-DMF does not cause any significant change in the AA composition and the resulting structural indices of indigo and madder dyed silks (Figures S4-S6 and Tables S2–S4, SM). However, an increased Glx content, comparable to that of dyed samples (see previous section), can be observed for undyed and non-mordanted AM and AtA silk samples after treatment with EDTA-ACN-MeOH or EDTA-DMF (AM: 2.2 mol%, AM EDTA-ACN-MeOH: 3.5 mol%, AM EDTA-DMF: 3.5 mol%, AM-Al/tartrate/madder EDTA-DMF: 3.6 mol%, AtA: 1.3 mol%, AtA EDTA-ACN-MeOH: 2.6 mol%, AtA EDTA-DMF: 2.9 mol%, AtA- Al/tartrate/madder EDTA-DMF: 2.8 mol%, for the assignment of the sample ID see Tables S2–S4, SM). Consequently, sample pre-treatment with EDTA-ACN-MeOH or EDTA-DMF of undyed and non-mordanted silks also leads to an enrichment of the acidic AA Glu in hydrolyzed samples (see previous section).

In summary, pre-treatment of dyed silk samples with EDTA-DMF enables the analysis of e.g. indigoid- and anthraquinone-type dyes without significantly changing the AA composition of the silk. Since sample material from historical textiles is usually only available to a very limited extent, a parallel dyestuff analysis is aimed for the characterization of these materials. In addition, interfering organic components and metal ions, especially from historical samples, can be removed by EDTA-ACN-MeOH or EDTA-DMF pre-treatment (see Introduction).

Chiral AA analyses on recent silks using GC-MS

In addition to the AA composition, D/L ratios of silk fibroin AAs were used to characterize silks.

For chiral analysis of AAs by GC-MS, degummed silk samples were hydrolyzed with 6 N HCl, then the free AAs were derivatized with HFBCF and enantiomeric AA pairs were separated on a Chirasil-Val capillary column. Eleven (DL)-AA pairs were identified and quantified in hydrolyzates of degummed silks, namely (DL)-Ala, (DL)-Val, (DL)-Leu, (DL)-Asx (Asp + Asn), (DL)-Met, (DL)-Ser, (DL)-Phe, (DL)-Glx (Glu + Gln), (DL)-His, (DL)-Lys and (DL)-Tyr.

Effect of hydrolysis, derivatization and treatment with an EDTA solution on the racemization rate

To investigate the influence of the derivatization procedure on AA racemization (AAR), stock solutions of (L)-AAs and (D)-AAs were derivatized with HFBCF at room temperature. The content of (D)- or (L)-AA derivatives after reaction of (L)- or (D)-AAs with HFBCF was below the detection limit (Table S1, SM). Thus, the derivatization procedure has no significant influence on the D/L ratio. Subsequently, the influence of silk fibroin digestion and sample pre-treatment was investigated. For this purpose, recent degummed BM and AM silk samples, treated with an aqueous EDTA-ACN-MeOH solution at 60°C for 30–60 min, were digested without microwave irradiation with 6 N HCl at 110°C for 24 h. HFBCF was also added to the hydrolyzates at room temperature. As shown in Figure 1 and Tables S5–S6 (SM), only the content of five (D)-enantiomers – namely (D)-Ala, (D)-Val, (D)-Ser, (D)-Glx and (D)-Asx – was above the LOQ. (L)-Ala and the achiral AA Gly are predominant in BM and AM fibroin and account for approximately between 70 and 80 mol% of the total AA content (for comparison see Tables S2–3). Under the above conditions, the conversion of (L)- to (D)-Ala is less than 1% (D/L Ala: 0.3–0.7%). D/L ratios between 5% and 12% were determined for the AAs Ser (BM: 12.0%, AM: 10.3%), Val (BM: 7.7%, AM: < LOQ), Glx (BM: 5.0%, AM: 8.5%) and Asx (BM: D-Asx < LOQ, AM: 7.4%), which occur with a significantly lower proportion in BM and AM fibroin. A comparison of BM silk before and after treatment with EDTA-ACN-MeOH shows no significant changes in the AAR rates (Figure 1). Thus, digestion and sample pre-treatment are suitable for a D/L analysis of silk.

In this context, different hydrolysis procedures using HCl with microwave irradiation were tested on stock solutions of (L)-AAs and various proteins. As expected, the hydrolysis time can be significantly reduced by microwave irradiation (for comparison see (Andreotti et al. 2006; Bonaduce, Cito, and Colombini 2009)). However, the use of microwave-assisted hydrolysis leads to greatly increased levels of (D)-AAs. For example, D/L AA ratios of almost 100%, i.e. racemic mixtures, were observed

for the stock solutions of Ala and Asp after 40 min of hydrolysis in the microwave (Koch 2022; Puchalla 2022). The effect of digestion time on Asx racemization using 6 N HCl at 110°C without microwave irradiation was already investigated on BM silk by Moini et al. (Moini, Klauenberg, and Ballard 2011) The (L) to (D) conversion by heating was found to be about 1% after 2 h and 4% after 24 h, reaching a plateau after 24 h. Since we cannot observe complete hydrolysis for all silk samples after 2 h, all further experiments were carried out without microwave irradiation for 24 h with a 6 N HCl at 110°C.

Effect of dyeing and mordanting procedures on AAR

As described above, racemization rates and/or degradation reactions of AAs can be affected by the presence of metal ions. Since metal salts such as iron(II) sulfate, copper(II) sulfate and potassium alum are frequently used as mordants, the influence of dyeing and mordanting procedures on (L) to (D) conversion of silk fibroin AAs was investigated. For this purpose, degummed BM silk samples treated with various metal salts and colorants were prepared according to the procedure described above (see previous section and Tables S5–S6, SM). In this context, dyed and mordanted silks were examined before and after treatment with EDTA-ACN-MeOH or EDTA-DMF (see sample pre-treatment with an EDTA solution). Furthermore, calcium oxalate was treated in BM silks and thus the effect of divalent Ca^{2+} ions on AAR rates was analyzed. In most cases, the (D)-AA proportions as well as D/L ratios determined for dyed and/or mordanted silks are comparable to those of the undyed and unmordanted silk filaments (Figure 1 and Table S6, SM). However, a D/L Met ratio of 67% was determined for sample BM-Cu EDTA-ACN-MeOH. For all other dyed and/or mordanted BM

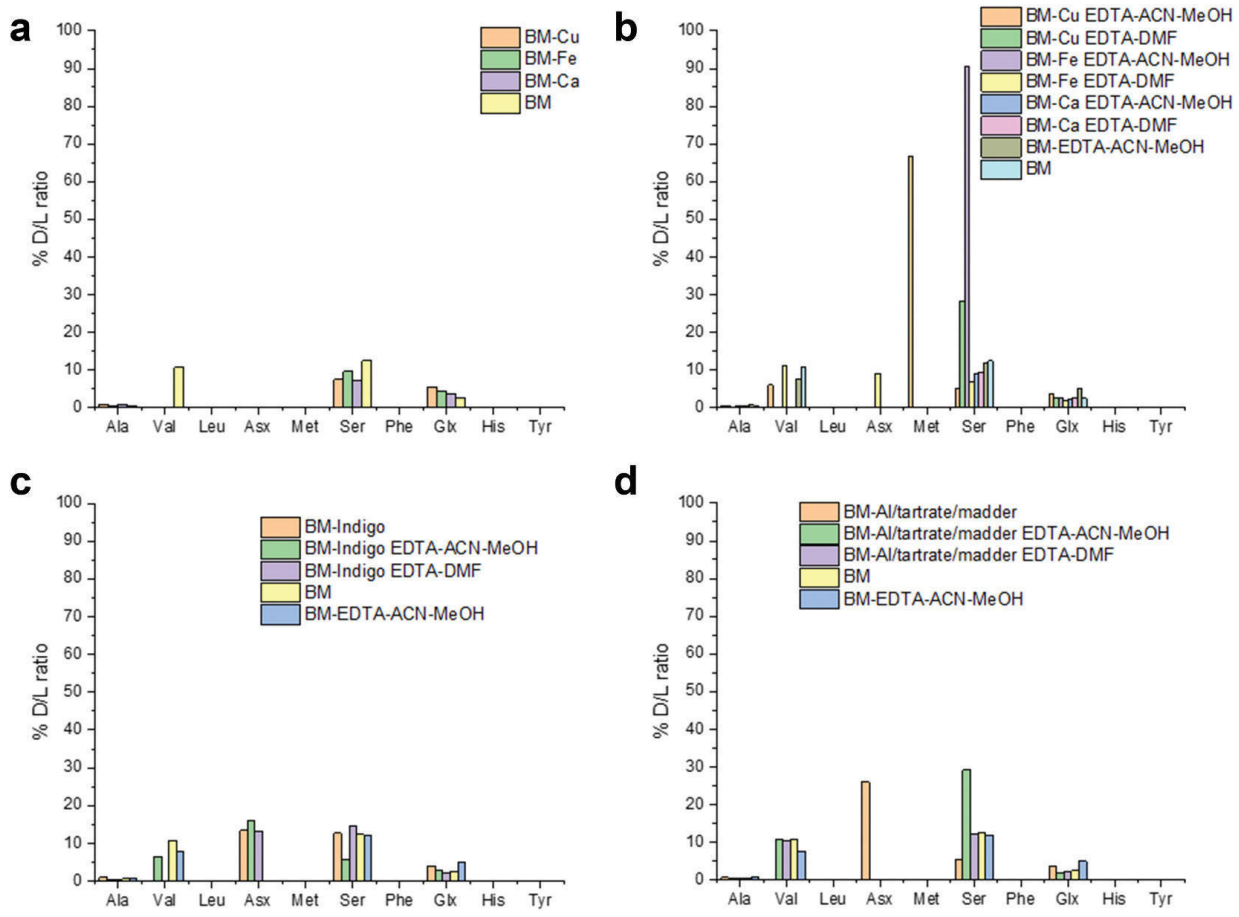

Figure 1. D/L ratios for (a–b) mordanted and calcium oxalate treated BM silks, (c) indigo dyed BM silks and (d) madder dyed BM silks before and after treatment with EDTA-ACN-MeOH or EDTA-DMF (degumming procedure: 0.1% Na_2CO_3 and 2.5% ethylenediamine, 95°C, 60 min, see Table S5 for assignment of the sample ID).

samples, the (D)- and/or (L)-Met content was below the LOQ. This is not surprising due to the low Met content in BM silk and the sensitivity of Met to oxidation. It is well known that Met can be oxidized to methionine sulfoxide and methionine sulfone when proteins are digested with 6 N HCl (Rutherfurd and Gilani 2009). The D/L ratio of Ser varies greatly between the samples tested, ranging from 5% to 90%. For instance, BM silk that has been mordanted with iron(II) sulfate and treated with EDTA-ACN-MeOH shows a D/L Ser ratio of 90.48%. In contrast, D/L Ser ratios of 6.80% and 28.35% were determined for BM silk mordanted with iron(II) sulfate or copper(II) sulfate and treated with EDTA-DMF. In addition, an increased (D)-Asx content was detected for the sample BM-Al/tartrate/madder (D/L Asx: 26.04%). However, the proportion of (D)-Asx in alum/tartrate-mordanted and madder-dyed samples treated with EDTA-DMF or EDTA-ACN-MeOH prior to hydrolysis is below the LOQ. In summary, an increased proportion of (D)-AAs can be observed for some mordanted samples, with thermodynamically unstable AAs such as Ser racemizing more readily than other AAs (see (Reischl and Lindner 2015) for studies on the mechanisms of Ser racemization) (Bada 1985). In addition, it should be noted that AAs such as Ser, Asn and Asp occur more frequently in amorphous fibroin regions, which are more susceptible to chiral rearrangements than crystalline fibroin regions (Shimada et al. 2023).

A (D)-Asx content of 0.1–0.2 ± 0.0005–0.02 mol% and thus D/L Asx ratios between 13% and 16% were found for BM samples dyed with indigo (Figure 1c). Since no metal salts were used for the preparation of these samples, the slightly increased (D)-Asx content is probably due to the alkaline conditions during the indigo dyeing process. In the present study, NaOH was added to the dye bath (pH 8–9) and silk dyeing was carried out for 2–3 min at 55°C, repeating the dyeing process several times to obtain a deep blue color. As described by Moini and Rollman, such alkaline conditions lead to an increased proportion of (D)-Asx (Moini and Rollman 2017). For instance, a previous study by Moini and Rollman shows that treatment of BM silk at pH 9.07 and a temperature of 110°C results in a 12% increase in D/L Asx after 120 min. However, the temperature of the dye bath and the previously used degumming process also appear to be important for changes in the D/L Asx ratio during the dyeing process. A study by Shimada et al. shows, for example, that indigo dyeing at 21°C and a pH of 10.5 does not change the D/L Asx ratio of a silk sample previously degummed at 85–90°C and a pH of 11–12 (Shimada et al. 2023). A D/L Asx ratio of approximately 17% was found for this alkaline degummed silk sample before and after indigo dyeing. Using the calibration curve of Moini et al., this value corresponds to an age of 500–600 years (Moini, Klauenberg, and Ballard 2011; Shimada et al. 2023).

Since the AAR rate is affected by the pH and temperature, various alkaline degumming methods are considered in the next step.

Effect of degumming procedures and artificial aging with Na_2CO_3 solutions on AAR

Studies by Shimada et al. show that the D/L Asx ratio of alkaline degummed silk is significantly higher than that of an untreated cocoon (Shimada et al. 2023). In comparison, Shimada et al. found that the D/L Asx ratio for enzymatically degummed silks did not change greatly. Consequently, the degumming conditions are crucial for the racemization of Asx.

To investigate the influence of alkaline degumming procedures in more detail, BM cocoons were treated with 0.1–0.25% Na_2CO_3 and/or 2.5% ethylenediamine at 95°C for 30–120 min (pH 8–10), using microscopic studies and the average degumming ratio D_r to evaluate the degumming efficiency. As already described in a previous study, under these conditions the degumming ratio of BM cocoons is about 30–35% (Table 1), indicating high degumming efficiency without destruction of the filaments (Schmidt et al. 2023). Harsher conditions, i.e. long treatment time and/or high concentration of the degumming agent, lead to partial degradation of fibroin fibers and a degumming ratio >35%. In order to induce a partial loss of silk fibroin, BM cocoons were treated with 10% ethylenediamine at 95°C for 120 min (sample ID: BM-4 120 min). This sample shows brittle fibers with a degumming ratio of 38%. However, as described by (Schmidt et al. 2023), the above-mentioned degumming conditions do not

Table 1. D/L ratios of the recent, undyed and non-mordanted BM silk degummed with alkaline-degumming agents and subsequently digested with 6 N HCl at 110°C for 24 h (derivatization with HFCBF).

			% D/L ratio									
Sample ID	Degumming procedure	Degumming ratio D_r[a]	Ala	Val	Leu	Asx	Met	Ser	Phe	Glx	His	Tyr
BM-1 30 min	Na_2CO_3 (1 g L^{-1}) and ethylenediamine (2.5%), 30 min, 95°C, pH 9–10	32	0.5	10.6	[c]	[c]	[c]	13.7	[c]	2.6	[b]	[c]
BM-1 60 min (BM)	Na_2CO_3 (1 g L^{-1}) and ethylenediamine (2.5%), 60 min, 95°C, pH 9–10	31	0.6	10.7	[c]	[c]	[c]	12.4	[b]	2.4	[b]	[c]
BM-1 90 min	Na_2CO_3 (1 g L^{-1}) and ethylenediamine (2.5%), 90 min, 95°C, pH 9–10	31	0.5	7.2	[c]	12.2	[c]	13.6	[c]	1.2	[b]	[c]
BM-2 30 min	Na_2CO_3 (1 g L^{-1}), 30 min, 95°C, pH 8–9	34	0.8	8.6	[c]	[c]	[c]	3.7	[c]	2.2	[b]	[c]
BM-2 60 min	Na_2CO_3 (1 g L^{-1}), 60 min, 95°C, pH 8–9	31	0.6	6.9	[c]	10.2	[c]	3.3	[c]	[b]	[b]	[c]
BM-2 90 min	Na_2CO_3 (1 g L^{-1}), 90 min, 95°C, pH 8–9	28	0.5	8.2	[c]	[c]	[b]	8.8	[c]	[b]	[b]	[c]
BM-2 120 min	Na_2CO_3 (1 g L^{-1}), 120 min, 95°C, pH 8–9	32	0.9	16.8	35.4	[b]	[b]	[b]	[c]	[b]	[b]	[b]
BM-3 120 min	Na_2CO_3 (2.5 g L^{-1}), 120 min, 95°C, pH 10	30	1.0	6.3	30.5	[b]	[b]	[b]	[c]	[b]	[b]	[b]
BM-4 120 min	Ethylenediamine (10%), 120 min, 95°C, pH 12–14	38	0.5	4.2	[c]	[b]	[b]	1.9	[c]	[b]	[b]	[c]

[a](Schmidt et al. 2023); [b](D)-enantiomer concentration is below the LOD; [c](D)-enantiomer concentration is below the LOQ.

lead to a significant change in AA composition. The effects of the degumming procedure on the D/L ratios are considered below.

As shown in Table 1, D/L ratios are comparable to those of the undyed and unmordanted fibroin filaments (degumming method: 0.1% Na_2CO_3 and 2.5% ethylenediamine, 95°C, 60 min), with D/L Ala < 1%, D/L Val < 17%, D/L Ser < 14% and D/L Glx < 3% (Figure 2a). With the exception of the samples BM-1 90 min (0.1% Na_2CO_3 and 2.5% ethylenediamine, 95°C, 90 min, pH 9–10) and BM-2 60 min (0.1% Na_2CO_3, 95°C, 60 min, pH 8–9), the (D)-Asx concentration is below the LOQ or LOD. A D/L Asx ratio of 10–12% was determined for BM-1 90 min and BM-2 60 min, which is comparable to that of the indigo dyed samples (see previous section). For sample BM-4 120 min (degumming method: 10% ethylenediamine, 95°C, 120 min, pH 12–14), which shows brittle fibers due to the harsh degumming conditions, the (D)-Asx and (L)-Asx content was below the LOD. However, a treatment with 0.1% or 0.25% Na_2CO_3 for 120 min leads to an increased (D)-Leu content and thus to D/L Leu ratios of 31–35%.

To simulate the artificial aging as well as the alkaline processing described by Moini and Rollman (Moini and Rollman 2017), degummed BM silk samples and BM cocoons were treated with Na_2CO_3 solutions at pH 9, 11 and 13 at 110°C for 60–120 min. At pH 9 and 11, similar D/L ratios for Ala, Val, Ser and Glx were obtained as with the alkaline degumming procedures described above (Table 2 and Figure 2b). In this context, treatment times of 90–120 min also lead to increased D/L Leu ratios (26–28%). In agreement with the studies by Moini and Rollman (Moini and Rollman 2017), increased (D)-Asx formation is observed with increasing pH. As shown in Figure 2b–d, the D/L Asx ratio increases from 12% to 13% at pH 9 to 44–67% at pH 11, with the proportion of (D)-Asx at pH 11 increasing with increasing treatment time. In addition, a (D)-Tyr concentration above the LOQ was detected at pH 11 and thus a D/L Tyr ratio of 5.6% was determined. At pH 13, silk samples are almost completely dissolved and a further increase in the D/L Asx ratios to 85–100% can be observed. Furthermore,

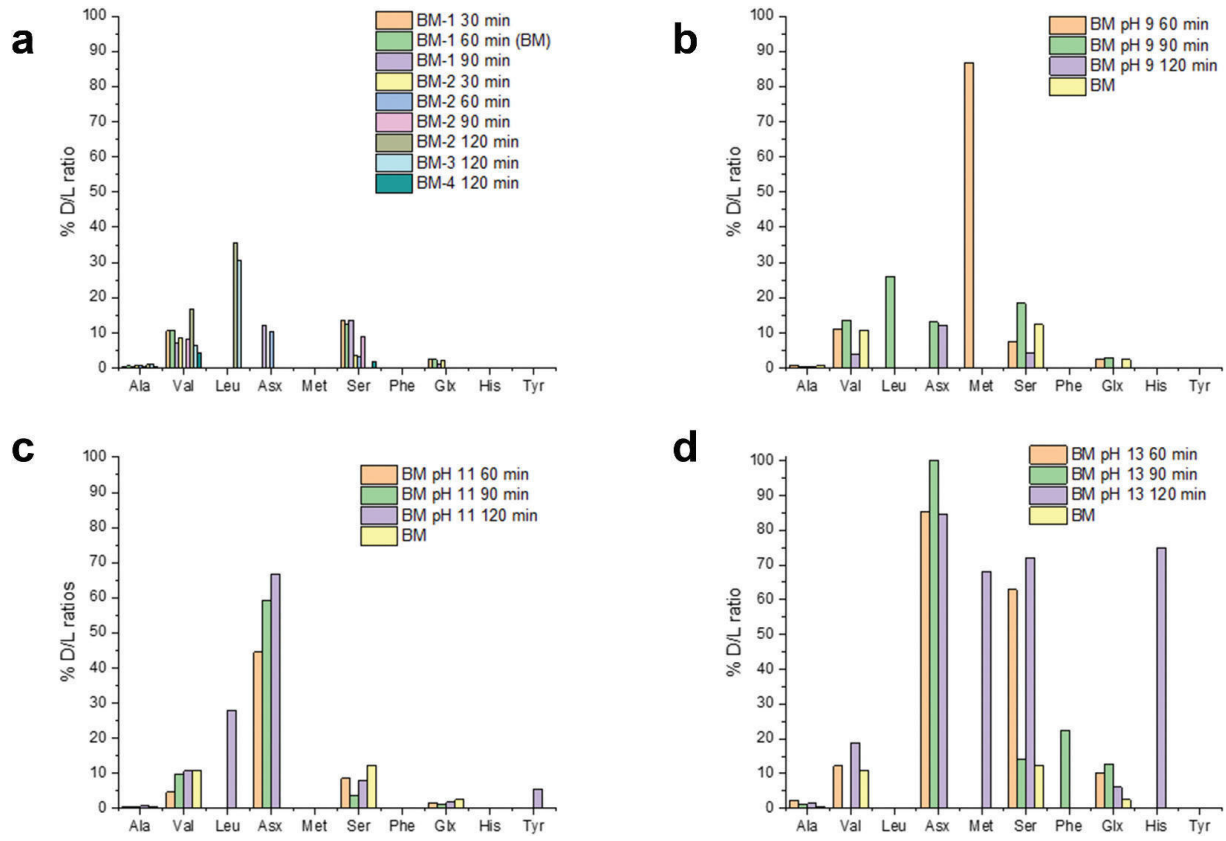

Figure 2. D/L ratios for (a) BM silks degummed with various degumming agents and (b–d) BM silks after treatment with Na_2CO_3 solutions at pH 9, 11 and 13 at 110°C (see Tables 1–2 for assignment of the sample ID).

Table 2. D/L ratios of the recent, undyed and non-mordanted BM silk degummed with alkaline degumming agents and subsequently digested with 6 N HCl at 110°C for 24 h (derivatization with HFCBF).

		% D/L ratio									
Sample ID	Alkaline treatment	Ala	Val	Leu	Asx	Met	Ser	Phe	Glx	His	Tyr
BM pH 9 60 min	Na_2CO_3, pH 9, 60 min, 110°C	0.9	11.1	[b]	[b]	86.7	7.4	[b]	2.5	[a]	[b]
BM pH 9 90 min	Na_2CO_3, pH 9, 90 min, 110°C	0.5	13.6	26.1	13.0	[b]	18.4	[a]	2.9	[a]	[a]
BM pH 9 120 min	Na_2CO_3, pH 9, 120 min, 110°C	0.3	4.1	[a]	12.1	[b]	4.4	[b]	0.8	[b]	[b]
BM pH 11 60 min	Na_2CO_3, pH 11, 60 min, 110°C	0.5	4.6	[b]	44.4	[b]	8.5	[b]	1.5	[a]	[b]
BM pH 11 90 min	Na_2CO_3, pH 11, 90 min, 110°C	0.4	9.7	[b]	59.3	[b]	3.7	[b]	1.2	[a]	[b]
BM pH 11 120 min	Na_2CO_3, pH 11, 120 min, 110°C	0.6	10.7	27.9	66.7	[b]	8.0	[b]	1.8	[a]	5.6
BM pH 13 60 min	Na_2CO_3, pH 13, 60 min, 110°C	2.3	12.1	[b]	85.2	[b]	62.9	[b]	10.2	[a]	[b]
BM pH 13 90 min	Na_2CO_3, pH 13, 90 min, 110°C	1.2	[b]	[b]	100	[b]	14.2	22.5	12.7	[a]	[b]
BM pH 13 120 min	Na_2CO_3, pH 13, 120 min, 110°C	1.4	18.9	[b]	84.7	68.2	72.2	[b]	6.1	[b]	[b]

[a](D)-enantiomer concentration is below the LOD; [b](D)-enantiomer concentration is below the LOQ.

increasing the pH to 13 also results in increased D/L Ala (1.2–2.3%), Ser (14–72%) and Glx (6–13%) ratios as well as a (D)-Phe and (D)-His content above the LOQ after a treatment period of 90–120 min (D/L Phe: 22.5%, D/L His: 75.0%). In summary, alkaline treatment at 110°C leads to increased D/L ratios, with the D/L Asx ratio being particularly affected. Consequently, not only the pH value but also the temperature is a decisive factor for the AAR pattern in alkaline treatments.

Chiral AA analyses by GC-MS - validation experiments

The results of the validation study for AA analyses using GC-MS are summarized in Table S1, SM. Retention times of derivatized AAs were determined using (L)- and (D)-AA standard solutions. Fifteen enantiomeric (DL)-AA pairs were separated on a Chirasil-Val capillary column under gradient temperature conditions. However, coelution was observed for (D-) and (L)-Pro derivatives, as already described by Zahradníčková et al., the content is therefore given as the sum of (D)- and (L)-Pro (Zahradníčková, Hušek, and Šimek 2009). Chromatograms of hydrolyzed silk samples of non-mulberry and mulberry silkworms as well as blank samples were free from interference. Calibration plots [concentration of (D)- or (L)-AA versus peak area ratio of (D)- or (L)-AA and (D)- or (L)-Nle as internal standards] are linear in the respective selected range (Ala and Gly: min 1.6 mM, max 11.8 mM; other AAs: min 0.3 mM, max 2.6 mM). For all AAs considered, an R^2 value >0.978 was obtained, and both LODs and LOQs were considered adequate for the purposes of the present study. The repeatability, expressed by relative standard deviations (RSD), ranged from 2.6% for (D)-Met and (D)-Leu to 28% for (D)-Lys. To determine the method precision, hydrolysis of degummed BM or AM silk, treated with an EDTA solution, was performed six times, and RSDs of AA concentrations were calculated. The RSD values range from 2.7% for (D)-Glx [(D)-Glu + (D)-Gln] to 23.7% for (L)-Ile. The (D/L)-Cys, (D/L)-Pro, (D)-Ile, (D)-Leu, (D)-Thr, (D)-Phe, (D)-His, (D)-Tyr, (D)-Lys and (D)-Met concentrations of the hydrolyzates are below the LOQ and LOD, respectively. Thus, no values for method precision are given for these AAs. Trp, a low abundance AA of BM silk (Moini, Klauenberg, and Ballard 2011), is decomposed during treatment with HCl (Rutherfurd and Gilani 2009) and cannot be determined using this method. In addition, it should be noted that Asn and Gln are deaminated during acid hydrolysis to Asp and Glu (Rutherfurd and Gilani 2009). Thus, after hydrolysis with 6 N HCl, values for (D/L)-Asp and (D/L)-Glu are reported as the sum of the acid and amide derivatives [(D/L)-Asx or (D/L)-Glx]. Recovery tests were carried out on spiking decummed BM silks with defined concentrations of (D)- and (L)-AAs, whereby (D)- and (L)-AAs were analyzed separately. The recovery rate of the different AAs after hydrolysis and derivatization ranged from 57% for (D)-Cys to 120% for Gly with an average recovery rate of 89% at the low, 84% at the medium and 82% at the high concentration level. (L)-Ile and (L)-Thr, AAs with two chiral carbon centers, which are only present in small amounts in silk fibroin, are converted into (D)-*allo*-Ile and (D)-*allo*-Thr by epimerization. The content of these diastereomers is below the LOD for all silk samples, and therefore these AAs are not included in the AAR studies described above. The studies on AAR rates focused on 11 (DL)-AA pairs that were identified and quantified in hydrolyzates of degummed BM and AM silks (see chiral AA analyses on recent silks using GC-MS). The developed and validated chiral GC-MS method was successfully used for the analysis of recent (see chiral AA analyses on recent silks using GC-MS) and historical silk samples (see next section).

Examination of historical samples – case study on silk fabrics from the Tarim Basin

Silk samples from archaeological sites of Niya and Yanghai in the Xinjiang Uyghur Autonomous Region (China) were analyzed using OM, SEM, SEM-EDX and ATR-FTIR spectroscopy as reported by (Kramell et al. 2014, 2016). In addition, dyestuff analyses were performed using HPLC-DAD and LC-ESI-MS/MS. As already described by Kramell et al., no dyestuffs were detected in these silk fragments (Table 3) (Kramell et al. 2014, 2016).

As shown in Figure 3, warps and wefts of the tabby weave fragments from grave M5 of the Niya site, which can be dated to the Han dynasty (206 BC –220 AD (Kramell et al. 2016)), are not twisted. These

Table 3. D/L ratios of historical silk and wool samples treated with EDTA-ACN-MeOH before hydrolysis with 6 N HCl at 110°C for 24 h (derivatization with HFCBF).

						% D/L ratio										
Archaeological graveyard sites	Object/object ID	Sample ID	Description of the sample[d]	Material	Detected dyestuffs[d]	Ala	Val	Leu	Asx	Met	Ser	Phe	Glx	His	Lys	Tyr
Niya (objects originate from grave M5), Han dynasty (206 BC −220 AD)[d]	Robe 95MNIM5–15	95MNIM5-15D	Fabric fragment (tabby weave) with beige/non-pigmented warps and wefts	Silk	-	0.6	51.8	[a]	76.5[b]	[c]	8.7	[a]	57.1	[a]	[b]	[b]
		95MNIM5-15G	Fabric fragment (tabby weave) with brownish warps and wefts,	Silk	No dyes detected	0.5	50.0	[b]	80	[c]	21.1	[a]	23.7	[c]	[b]	[b]
	Skirt 95MNIM5–18	95MNIM5-18A	Fabric fragment (tabby weave) with brownish warps and wefts	Silk	Traces of unknown UV active compounds (λ_{max} = 350 nm)	0.4	51.4	[b]	86.2	[c]	16.1	[b]	25.0	[a]	[b]	[b]
	Shirt 95MNIM5–43	95MNIM5-43A	Fabric fragment (tabby weave) with brownish warps and wefts	Silk	No dyes detected	0.3	59.3	[b]	66.7	[c]	17.8	[a]	19.4	[c]	[b]	[b]
Yanghai, Zone III, probable period of use: 7th-4th centuries BCE	Skirt 03SAYM376:13 (IIIM376:13)	03SAYM376:13-1	Fabric fragment with twisted beige/non-pigmented warps and wefts	Silk	-	0.5	50.0	[b]	59.5	[b]	25.9	[a]	55.2	[b]	[b]	[b]
Wupu, calibrated AMS radiocarbon date (95.4% probability) of the robe: 760–682 cal. BC[e]	Robe 86HWMNN–1 (no number)	86HWMNN-1D	Fabric fragment (twill) with twisted brownish warps and wefts	Wool	Traces of rubiadin and indigotin	[b]	10.8	[b]	47.7[b]	[c]	[b]	[b]	[c]	[c]	[b)]	[b]
Yanghai, calibrated AMS radiocarbon date (95.4% probability) of the textile fabric: 839–601 cal. BC[d,f]	Surface find without assignment to specific graves	20110615/OF11-B	Fabric fragment (twill) with blue warps and wefts (single yarn, Z-twist), 2:2 float	Wool	Indigo and indirubin	[b]	10.3	[b]	37.3[b]	[b]	100	[b]	54.2	[c]	[b]	[b]

[a](D)-enantiomer concentration is below the LOD; [b](D)-enantiomer concentration is below the LOQ; [c](L)- and (D)-enantiomer concentration is below the LOQ; [d](Kramell et al. 2014; Kramell et al. 2016); [e]A blue wool thread from the robe of tomb 86HWMNN–1 was radiocarbon dated by (Schröder et al. 2016). The wool fabric 20,110,615/OF11-B was radiocarbon dated by (A. Kramell et al. 2014). A recent merino wool sample was also analyzed by GC-MS (Tables S6 and S7, SM).

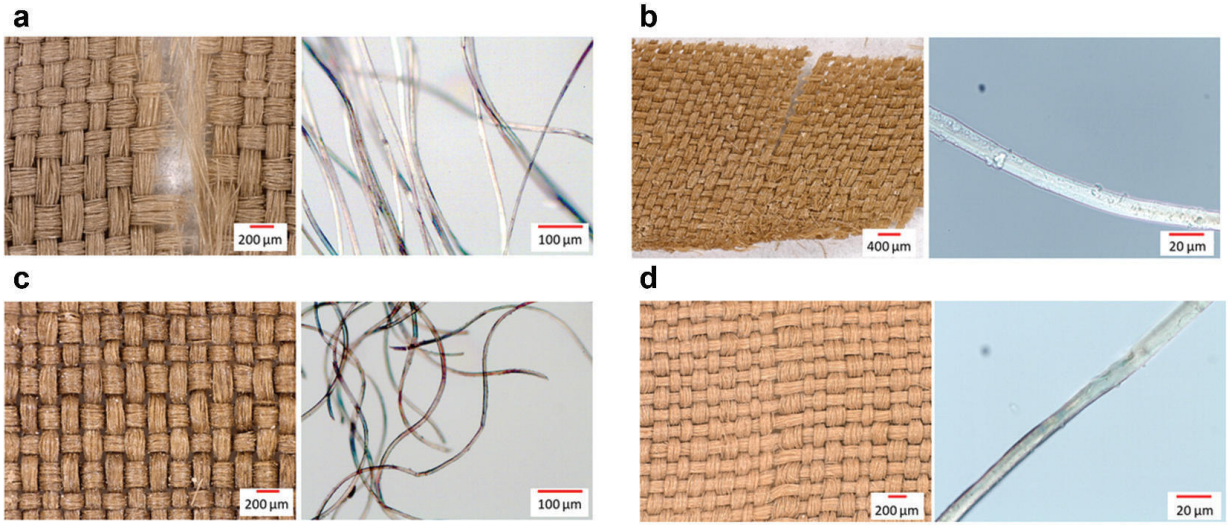

Figure 3. Tabby weave fragments from the Niya site and morphologies of the silk filaments; sample ID: (a) 95MNIM5-15D, (b) 95MNIM5-15G (c), 95MNIM5-18A (d) 95MNIM5-43A.

textile fragments consist of long silk filaments, revealing the use of reel silk and thus of intact cocoons for textile production. Long continuous silk filaments can be obtained by killing the pupae with boiling water or steam before hatching and unwinding the cocoon as a continuous thread. In contrast, the fabric fragment 03SAYM376:13-1 from a tomb of the Yanghai burial ground consists of twisted warps and wefts, whereby the diameter of the yarns varies greatly (Figure 4). Microscopic studies show that silk filaments from the Niya and the Yanghai site have a triangular cross-sectional shape typical of BM silk, with a filament cross-section of around 8–15 µm (Figure S7, SM). Compared to the silk fabrics from the Niya site, however, shorter silk filaments were used to produce textile fragment 03SAYM376:13-1. This indicates that this textile fragment was made of hatched and thus non-reelable cocoons. Another interpretation approach is the use of the so-called Bourette silk, produced from the waste of silk extraction or from damaged cocoons (see (Veit 2022)).

SEM-EDX studies on silk filaments and adhering particles reveal the presence of ubiquitous elements such as N, O, Si, Na, K, Al, Cl, Mg, Ca and Fe (Figure S8, SM), which can often be detected in samples with soil contact. ATR-FTIR spectra of silk samples from the finding sites of Niya and Yanghai show characteristic bands in the range 1600–1700, 1480–1560 and 1210–1270 cm^{-1} which are assigned to the amide I, amide II and amide III bands of silk fibroin (Figure S9, SM). Previous studies have shown that degummed BM silk has characteristic bands at 975 and 998 cm^{-1}, corresponding to

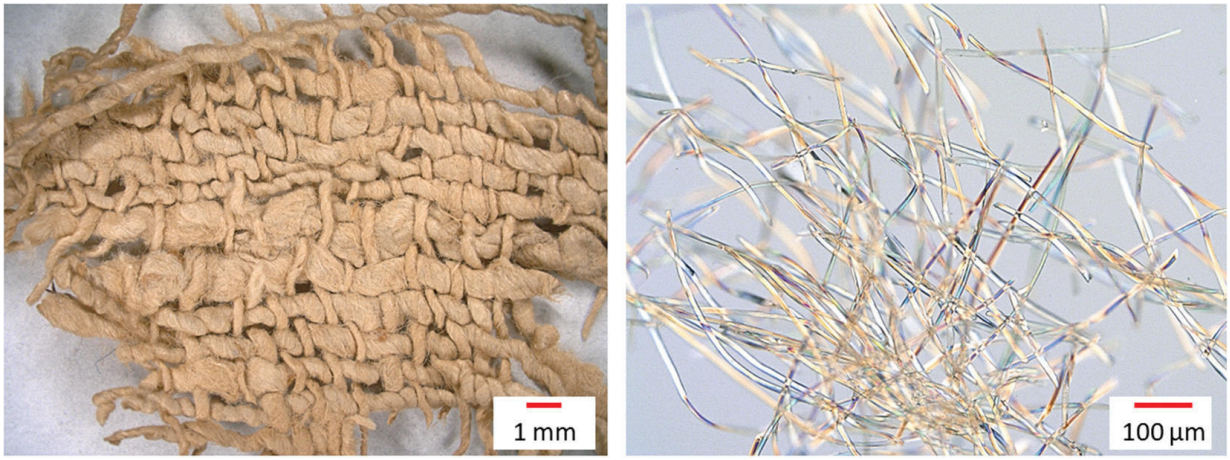

Figure 4. Textile fragment from the Yanghai site and morphologies of the silk filaments (sample ID: 03SAYM376:13-1).

the β-sheet conformation of polyalanineglycine $(AG)_n$ (Boulet-Audet, Vollrath, and Holland 2015; Koperska et al. 2014; Schmidt et al. 2023). In contrast, a prominent peak at 963 cm^{-1} can be observed for non-mulberry silks, e.g. from Saturniidae silk moths, which are assigned to polyalanine $(A)_n$ β-sheets (Boulet-Audet, Vollrath, and Holland 2015; Schmidt et al. 2023). These characteristic bands are masked in the historical samples by the presence of a broad and intense band in the range 940–1090 cm^{-1} displaying submaxima at 1000 and 1033 cm^{-1}, which are probably ascribed to vibrations of adhesions such as silicate minerals. In samples 03SAYM376:13-1 and 95MNIM5-43A, however, the peaks at 975 and 998 cm^{-1} characteristic of BM silk are detectable as submaxima. Another characteristic band for BM silk is a shoulder at 1260 cm^{-1}, corresponding to the β-sheet conformation in the amide III band (de Palaminy, Daher, and Moulherat 2022). This band can be detected in all historical samples, which indicates the presence of *Bombyx* silk. Distinct signature peaks for sericin (Aguayo et al. 2014) at around 1400 cm^{-1} and 1070 cm^{-1} cannot be observed in the historical samples, with the exception of sample 03SAYM376:13-1. ATR-FTIR spectra of sample 03SAYM376:13-1 show a characteristic band for sericin at 1403 cm^{-1} with an intensity comparable to recent degummed BM samples (Figure S9, SM). Differences in sericin content may be due to different storage conditions or different degumming methods. Due to the good water solubility of sericin, a low sericin content in historical silk samples with soil contact is not surprising. However, in the case of sample 03SAYM376:13-1, the increased sericin content may also indicate the presence of Bourette silk (see above), which usually has a high sericin content.

For further characterization, historical samples were analyzed for their AA composition and AAR rates using GC-MS (Tables 3–4). Ala and Gly are predominant in all historical silk samples and account for between 81 and 92 mol% of the total AA content. The Gly content of samples 95MNIM5-18A, 95MNIM5-43A and 03SAYM376:13-1 is between 47 and 54 mol%, which is higher than the Ala content of 38–43 mol%. Thus, the Gly/Ala ratio is >1, which is characteristic for BM fibroin. A Gly/Ala ratio of 1 was determined for samples 95MNIM5-15D and 95MNIM5-15 G, with a Gly content of 40–45 mol% and an Ala content of 41–47 mol%. Furthermore, all historical samples have a 100LC/SC ratio between 6 and 9. Thus, these samples have a lower 100LC/SC ratio than recent BM or non-mulberry silk, suggesting a higher structural regularity compared to recent silk (100LC/SC of BM fibroin: 17–26, 100LC/SC of Saturniidae fibroin: 14–53 (Schmidt et al. 2023)). This is not surprising, since poorly ordered and loose amorphous regions, containing a high proportion of bulky side groups, are degraded faster than ordered and compactly stacked crystalline regions. Since the crystalline regions of BM fibroin consist of Ala- and Gly-rich repetitive motifs, the degradation of amorphous regions also leads to an increased Ala and Gly proportion, which can be observed in particular for samples 95MNIM5-15 G, 95MNIM5-18A and 95MNIM5-43A (Gly+Ala: 91–92 mol%) (Li et al. 2013). At the same time, these historical samples have a very low amount of polar AAs as well as lower Tyr/Ala and Tyr/Gly ratios compared to recent fibroin (Tables 4 and S2, SM). The ratios of Tyr/Ala and Tyr/Gly are markers for oxidative changes in the silk fibroin structure, as Tyr is sensitive to degradation and oxidation reactions and can be transformed into Ala by loss of the phenol group (Vilaplana et al. 2015). Consequently, a decrease in the Tyr content is also observed for all historical silk samples examined (Table S7, SM). Compared to the recent BM samples, the historical silk samples show a lower Val and Glx content, with D/L Glx ratios of 19–57% and D/L Val ratios of 50–59% (Table S7, SM). Thus, the D/L Val ratio in particular is significantly increased compared to the recent samples, regardless of the silk processing. At 0.3–0.7 mol%, the Asx content of the historical samples is also slightly decreased than that of recent BM silk, which contains 1 mol% Asx. The Asx racemization ratio for these samples is between 60% and 86%, with D/L Asx ratios of 67–86% for the Niya samples from tomb 5. A D/L Asx ratio of 60% was determined for sample 03SAYM376:13-1 from the Yanghai site. Using the calibration curve of (Moini, Klauenberg, and Ballard 2011), which spans in time from the present to ~2500 years ago, these D/L Asx ratios result in AAR dates of over 2500 years (Moini, Klauenberg, and Ballard 2011). However, it should be noted that, Moini et al. used silk samples from museum collections, which were stored with extraordinary care, to create the calibration curve. Thus, many of the environmental factors that affect racemization rates remain fairly constant. The silk samples examined from the Niya and Yanghai sites were stored in tombs for a large part of the time and

Table 4. AA composition of historical silk and wool samples treated with EDTA-ACN-MeOH before hydrolysis with 6 N HCl at 110°C for 24 h (derivatization with HFCBF).

		Comparative AA composition									
Sample ID	Material	Ala+Gly [mol%]	Gly/Ala	100LC/SC[a]	P [mol%][b]	NP [mol%][c]	Ser+Pro+Thr+Tyr [mol%][d]	A [mol%][e]	B [mol%][f]	Tyr/Ala	Tyr/Gly
95MNIM5-15D	Silk	81	1.0	8	13	87	16	1	1	0.10	0.10
95MNIM5-15G	Silk	91	1.0	7	4	96	5	1	0	0.06	0.06
95MNIM5-18A	Silk	92	1.1	6	3	97	5	1	0	0.07	0.06
95MNIM5-43A	Silk	92	1.4	8	2	98	4	1	0	0.06	0.04
03SAYM376:13-1[g]	Silk	86	1.2	9	8	92	9	1	1	0.08	0.06
86HWMNN-1D	Wool		31	0.8	212	3	97	17	1	0.19	0.24
20110615/OF11-B	Wool		26	0.6	273	4	96	15	2	0.19	0.31

[a]Ratio between long chain (LC: other AAs) and short chain (SC: Ala, Gly, Ser, Thr) AAs; [b]Polar AAs: acidic, basic and hydroxyl AAs; [c]Non-polar AAs: other AAs; [d]AAs with hydroxyl groups: Ser, Thr, Tyr; [e] Basic AAs: Lys, His; [f]Acidic AAs: Asx, Glx; [g]Sample 03SAYM376:13-1 was also analyzed by GC-FID without treatment with EDTA-ACN-MeOH, yielding similar AA compositions (Ala+Gly: 85 mol%, Gly/Ala: 1.5, 100LC/SC: 11, P: 9 mol%, NP: 91 mol%, Ser+Pro+Thr+Tyr: 8 mol%, A: 2 mol%, B: 1 mol%, Tyr/Ala: 0.08, Tyr/Gly: 0.05, for GC-FID method see (Schmidt et al. 2023).

were therefore exposed to various environmental influences, which can affect the Asx racemization rate. It is difficult to estimate the influence of environmental factors such as pH, temperature or metal ion chelation on the D/L Asx ratio of archaeological silk samples. The authors advise against determining the age of these silk samples solely on the basis of the Asx racemization rate. The ages given in Table 3 are based on ^{14}C dating and/or the archaeological context.

In summary, the textile fragments from archaeological sites of Niya and Yanghai were most likely made of silk produced by a moth of the genus *Bombyx*. At this point, it should be noted that silk of the Chinese wild silkworm *Bombyx mandarina* Moore has a similar AA composition to BM silk filaments, with a Gly content higher than that of Ala (Deng et al. 2021). This phenomenon, i.e. fibroin filaments with a Gly/Ala ratio of >1, is only presented in a few species worldwide, e.g. *Bombyx* species or *Pseudoips prasinana* L. (originally belonging to the genus of Bena, Nolidae family) (Boulet-Audet, Vollrath, and Holland 2015; Lucas, Shaw, and Smith 1960; Rindos et al. 2021). The latter is native to the Palearctic region, and its filaments of the main cocoon have a triangular cross-section, whereby *P. prasinana* filaments are a little thinner than BM silk (Rindos et al. 2021). The use of this species in the course of ancient textile production is not known to the authors.

For comparison, the AA composition of historical wool samples from the ninth to seventh century BC was determined. As expected, the silk and wool samples show significant differences in their AA composition and can therefore be easily distinguished (Tables 4, S7 and Figure S10, SM). In addition, the treatment with EDTA-DMF described above (see Sample pre-treatment with an EDTA solution) was successfully used to detect indigoid dyes in the blue sample 20,110,615/OF11-B (Table 3). As shown in Table 3, the D/L Asx ratios of the wool samples are 37% and 48%, respectively, and are thus increased in comparison to an undyed recent wool sample (D/L Asx: 5.2%, Table S6). Environmental influences could also have affected the D/L Asx ratio in these cases. Furthermore, AAR rates also depend on the AA composition, bond strengths and thus on the protein type (e.g. (Bright and Kaufman 2011)). Thus, investigations on AA racemization in wool samples are the subject of future studies.

Conclusion

Mulberry and non-mulberry silk samples, mordanted and dyed according to historical recipes, were analyzed for their AA composition using GC-FID and structural indices such as the 100LC/SC ratio were compared. With the exception of a slight increase in Glx, no significant differences were found in the mordanted and dyed samples compared to untreated silk. For dyeing and mordanting, madder roots and indigo as well as various metal salts were used, which – with the exception of copper(II) sulfate – are natural, eco-friendly and sustainable raw materials that have been used for centuries. Pre-treatment of the dyed samples with EDTA-ACN-MeOH or EDTA-DMF, which enables parallel detection of mordant and vat dyes and thus comprehensive characterization of the sample material, also does not cause any significant changes in the AA composition. To investigate the influence of silk processing on AA racemization, a chiral GC-MS method was developed and validated that allows the identification and quantification of 11 enantiomeric AA pairs in fibroin hydrolyzates. In the course of the method development, various hydrolysis procedures were tested. Since microwave-assisted hydrolysis leads to significantly reduced hydrolysis times but to greatly increased levels of (D)-AAs, the hydrolysis was carried out without microwave irradiation using 6 N HCl. Studies on mordanted BM silk samples, before and after treatment with EDTA-ACN-MeOH or EDTA-DMF, show that an increased proportion of (D)-Ser, (D)-Met and (D)-Asx can be observed for some of these samples. Furthermore, indigo dyeing carried out under basic conditions (pH 8–9) at 55°C led to a slightly increased (D)-Asx content and thus to D/L Asx ratios of 13–16%. In the next step, the effect of alkaline degumming procedures, using 0.1–0.25% Na_2CO_3 and/or 2.5% ethylenediamine at 95°C for 30–120 min as well as 10% ethylenediamine at 95°C for 120 min, was investigated. However, only two samples were found to contain (D)-Asx above the LOQ, with D/L Asx ratios of 10–12%. In addition, a treatment

with 0.1% or 0.25% Na_2CO_3 for 120 min at 95°C led to an increase in the (D)-Leu content and thus to D/L Leu ratios of 31–35%. Harsh conditions, i.e. temperatures of 110°C and pH values >9, lead to a significant increase in the D/L Asx ratio to 44–67%, with the (D)-Asx content increasing with treatment time. At pH 13 and a temperature of 110°C, the silk filaments are almost completely dissolved and D/L Asx ratios of up to 100% can be observed, with increased (D)-Ala, (D)-Ser, (D)-Glx, (D)-Phe and (D)-His ratios also being observed.

The study of silk fabrics from the archaeological sites of Niya and Yanghai in the Tarim Basin (China) using the described GC-MS method as well as microscopic and spectroscopic techniques reveals the presence of degraded *Bombyx* silk with a low proportion of AAs with bulky side groups. A low sericin content was found in silk fabrics from the Niya site, which are dated to the Han dynasty (206 BC –220 AD) and consist of long silk filaments, indicating the use of intact cocoons for textile production. A silk fabric from the Yanghai site contains a higher sericin content than the samples from Niya and was made from spun warp and weft threads. D/L Asx ratios of 60–86% as well as significantly increased D/L Val and D/L Glx ratios were determined for the silk fabrics from both sites. The influence of environmental factors such as metal chelation or pH on the AA racemization of archaeological silk samples is difficult to estimate. The AA composition of a wool sample from the Yanghai site differs significantly from the silk samples. With the aid of EDTA-DMF extraction procedure, indigoid dyestuffs were detected in this sample. The presented multi-analytical technique-based approach enables the analysis of dyestuffs and silk filaments and thus a comprehensive characterization of historical silk textiles.

Highligths

- The influence of dyeing, mordanting and alkaline degumming techniques on the amino acid (AA) composition and the AA racemization of silks was studied.
- A chiral GC-MS method for the identification and quantification of 11 enantiomeric AA pairs in silk fibroin hydrolyzates was developed and validated.
- Sample pre-treatment with EDTA-DMF enables parallel dyestuff analysis using HPLC-DAD and thus a comprehensive characterization of dyed silks.
- Studies on historical silk fabrics from sites in the Tarim Basin show the presence of degraded *Bombyx* silk with significantly increased D/L Val, D/L Glx and D/L Asx ratios.

Acknowledgments

This work was funded by the Deutsche Forschungsgemeinschaft (DFG, German Research Foundation, project number 425225219). Samples from the finding sites of Niya and Yanghai (Xinjiang Uyghur Autonomous Region, China) were taken within the framework of an interdisciplinary Chinese-German research project entitled “Silk Road Fashion – Clothes as a means of communication in the 1st millennium BC in Eastern Central Asia.” The authors are grateful to the Archaeological Institute in Urumqi and the Turpan Museum in Turfan, and especially to Prof. Dr M. Wagner, Dr P. Wertmann (Deutsches Archaeologisches Institut) and Prof. Dr. P. E. Tarasov (Freie Universität Berlin) for continuing support. The authors would like to thank Prof. R. Csuk (Martin-Luther-Universität Halle-Wittenberg) for continuous support, N. Quandt (working group of Prof. Ebbinghaus, Martin-Luther-Universitat Halle-Wittenberg) and U. Schwarzer (Landeskriminalamt in Magdeburg) for providing SEM- and SEM-EDX spectra. We also thank J. Werner and M. Schneider (Martin-Luther-Universität Halle-Wittenberg) for their valuable help in the laboratory and C. Jägern (Pflanzgarten School Garden, Francke Foundations, Halle) as well as the butterfly house of Jonsdorf (Germany) for providing hatched cocoons. We acknowledge the financial support of the Open Access Publication Fund of the Martin-Luther-University Halle-Wittenberg.

Disclosure statement

No potential conflict of interest was reported by the author(s).

Funding

The work was supported by the Deutsche Forschungsgemeinschaft [425225219]; Open Access Publication Fund of the Martin-Luther-University Halle-Wittenberg .

ORCID

Annemarie E. Kramell http://orcid.org/0000-0002-2417-6372

References

Aguayo, T., C. Araya, M. Icaza, and M. M. Campos-Vallette. 2014. "A Vibrational Approach for the Study of Historical Weighted and Dyed Silks." *Journal of Molecular Structure* 1075:471–478. https://doi.org/10.1016/j.molstruc.2014.07.016.

Ahmed, H. E., and S. S. Darwish. 2012. "Effect of Museum Conditions on Historical Dyed Silk Fabric with Madder Dye." *Journal of Polymers and the Environment* 20 (2): 596–606. https://doi.org/10.1007/s10924-012-0421-x.

Andreotti, A., I. Bonaduce, M. P. Colombini, G. Gautier, F. Modugno, and E. Ribechini. 2006. "Combined GC/MS Analytical Procedure for the Characterization of Glycerolipid, Waxy, Resinous, and Proteinaceous Materials in a Unique Paint Microsample." *Analytical Chemistry* 78 (13): 4490–4500. https://doi.org/10.1021/ac0519615.

Arunkumar, K. P., M. Metta, and J. Nagaraju. 2006. "Molecular Phylogeny of Silkmoths Reveals the Origin of Domesticated Silkmoth, *Bombyx Mori* from Chinese *Bombyx Mandarina* and Paternal Inheritance of *Antheraea Proylei* Mitochondrial DNA." *Molecular Phylogenetics and Evolution* 40 (2): 419–427. https://doi.org/10.1016/j.ympev.2006.02.023.

Bada, J. L. 1985. "Racemization of Amino Acids." In *Chemistry and Biochemistry of the Amino Acids*, edited by G. C. Barrett, 399–414. Dordrecht: Springer Netherlands.

Beck, U., M. Wagner, X. Li, D. Durkin-Meisterernst, and P. E. Tarasov. 2014. "The Invention of Trousers and Its Likely Affiliation with Horseback Riding and Mobility: A Case Study of Late 2nd Millennium BC Finds from Turfan in Eastern Central Asia." *Quaternary International* 348:224–235. https://doi.org/10.1016/j.quaint.2014.04.056.

Biswal, B., A. K. Dan, A. Sengupta, M. Das, B. K. Bindhani, D. Das, and P. K. Parhi. 2022. "Extraction of Silk Fibroin with Several Sericin Removal Processes and its Importance in Tissue Engineering: A Review." *Journal of Polymers and the Environment* 30 (6): 2222–2253. https://doi.org/10.1007/s10924-022-02381-w.

Bonaduce, I., M. Cito, and M. P. Colombini. 2009. "The Development of a Gas Chromatographic–Mass Spectrometric Analytical Procedure for the Determination of Lipids, Proteins and Resins in the Same Paint Micro-Sample Avoiding Interferences from Inorganic Media." *Journal of Chromatography A* 1216 (32): 5931–5939. https://doi.org/10.1016/j.chroma.2009.06.033.

Boudin, M., P. Boeckx, P. Vandenabeele, and M. Van Strydonck. 2013. "Improved Radiocarbon Dating for Contaminated Archaeological Bone Collagen, Silk, Wool and Hair Samples via Cross-Flow Nanofiltrated Amino Acids." *Rapid Communications in Mass Spectrometry: RCM* 27 (18): 2039–2050. https://doi.org/10.1002/rcm.6652.

Boulet-Audet, M., F. Vollrath, and C. Holland. 2015. "Identification and Classification of Silks Using Infrared Spectroscopy." *The Journal of Experimental Biology* 218 (19): 3138–3149. https://doi.org/10.1242/jeb.128306.

Bright, J., and D. S. Kaufman. 2011. "Amino Acids in Lacustrine Ostracodes, Part III: Effects of pH and Taxonomy on Racemization and Leaching." *Quaternary Geochronology* 6 (6): 574–597. https://doi.org/10.1016/j.quageo.2011.08.002.

Cardon, D. 2007. *Natural Dyes: Sources, Tradition, Technology and Science*. London: Archetype Publications Ltd.

Colombini, M. P., R. Fuoco, A. Giacomelli, and B. Muscatello. 1998. "Characterization of Proteinaceous Binders in Wall Painting Samples by Microwave-Assisted Acid Hydrolysis and GC-MS Determination of Amino Acids." *Studies in Conservation* 43 (1): 33–41. https://doi.org/10.1179/sic.1998.43.1.33.

Colombini, M. P., and F. Modugno. 2004. "Characterisation of Proteinaceous Binders in Artistic Paintings by Chromatographic Techniques." *Journal of Separation Science* 27 (3): 147–160. https://doi.org/10.1002/jssc.200301625.

Deng, T., L. Cheng, Y. Peng, X. Tong, N. Guo, Z. Li, T. Zhao, and F. Dai. 2021. "Structure and Properties of *Bombyx Mandarina* Silk Fiber and Hybrid Silk Fiber." *Journal of Natural Fibers* 18 (3): 330–342. https://doi.org/10.1080/15440478.2019.1623743.

de Palaminy, L., C. Daher, and C. Moulherat. 2022. "Development of a Non-Destructive Methodology Using ATR-FTIR and Chemometrics to Discriminate Wild Silk Species in Heritage Collections." *Spectrochimica Acta Part A, Molecular and Biomolecular Spectroscopy* 270:120788. https://doi.org/10.1016/j.saa.2021.120788.

Deveoglu, O., R. Karadag, A. Spinella, and E. T. Guzel. 2019. "Examination of Dyeing Properties on Silk of Some Flavonoids by Spectroscopic Techniques." *Journal of Natural Fibers* 18 (2): 238–249. https://doi.org/10.1080/15440478.2019.1616650.

Deveoglu, O., B. Y. Sahinbaskan, E. Torgan, and R. Karadag. 2012. "Investigation on Colour, Fastness Properties and HPLC-DAD Analysis of Silk Fibres Dyed with *Rubia Tinctorium* L. and *Quercus Ithaburensis* Decaisne." *Coloration Technology* 128 (5): 364–370. https://doi.org/10.1111/j.1478-4408.2012.00389.x.

Freddi, G., Y. Gotoh, T. Mori, I. Tsutsui, and M. Tsukada. 1994. "Chemical Structure and Physical Properties of *Antheraea Assama* Silk." *Journal of Applied Polymer Science* 52 (6): 775–781. https://doi.org/10.1002/app.1994.070520608.

Gao, S., M. Yao, Narenggaowa, D. Guo, Y. Li, K. L. Do, J. Liu, and F. Zhao. 2024. "Identification of Fibers and Dyes in Archaeological Textiles from Bazhou, Xinjiang (220-420 CE), and Their Silk Road Origins." *Journal of Archaeological Science: Reports* 164:105941. https://doi.org/10.1016/j.jas.2024.105941.

Garside, P., P. Wyeth, and X. Zhang. 2010. "Understanding the Ageing Behaviour of Nineteenth and Twentieth Century Tin-Weighted Silks." *Journal of the Institute of Conservation* 33 (2): 179–193. https://doi.org/10.1080/19455224.2010.501293.

Ge, R., L. Cong, Y. Fu, B. Wang, G. Shen, B. Xu, M. Hu, H. Yu, J. Zhou, and L. Yang. 2023. "Multi-Faceted Analysis Reveals the Characteristics of Silk Fabrics on a Liao Dynasty DieXie Belt." *Heritage Science* 11 (1): 217. https://doi.org/10.1186/s40494-023-01064-6.

Goodfriend, G. A. 1992. "Rapid Racemization of Aspartic Acid in Mollusc Shells and Potential for Dating Over Recent Centuries." *Nature* 357 (6377): 399–401. https://doi.org/10.1038/357399a0.

Hofenk de Graaff, J. H. 2004. *The Colourful Past: Origins, Chemistry and Identification of Natural Dyestuffs*. London: Abegg-Stiftung and Archetype Publications Ltd.

Johnson, A. P., and L. M. Pratt. 2010. "Metal-Catalyzed Degradation and Racemization of Amino Acids in Iron Sulfate Brines Under Simulated Martian Surface Conditions." *Icarus* 207 (1): 124–132. https://doi.org/10.1016/j.icarus.2009.11.028.

Karadag, R. 2023. "Establishing a New International Standard for Natural Dyed Textile Goods [Natural Organic Dye Standard (NODS)]." *Journal of Natural Fibers* 20 (1): 2162187. https://doi.org/10.1080/15440478.2022.2162187.

Karadag, R., and R. G. Oraltay. 2022. "Application of a New SEM–EDX Technique Associated with HPLC/DAD: Manufacturing Methods of Historical Textiles." *Archaeological and Anthropological Sciences* 15 (1): 8. https://doi.org/10.1007/s12520-022-01702-3.

Kaufman, D. S. 2006. "Temperature Sensitivity of Aspartic and Glutamic Acid Racemization in the Foraminifera *Pulleniatina*." *Quaternary Geochronology* 1 (3): 188–207. https://doi.org/10.1016/j.quageo.2006.06.008.

Kmet, P., L. Kucerova, H. Sehadova, B. Chia-Hsiang Wu, Y.-L. Wu, and M. Zurovec. 2023. "Identification of Silk Components in the Bombycoid Moth *Andraca Theae* (Endromidae) Reveals Three Fibroin Subunits Resembling Those of Bombycidae and Sphingidae." *Journal of Insect Physiology* 147:104523. https://doi.org/10.1016/j.jinsphys.2023.104523.

Koch, J. 2022. *Martin-Luther-Universität Halle-Wittenberg*.

Koperska, M. A., D. Pawcenis, J. Bagniuk, M. M. Zaitz, M. Missori, T. Łojewski, and J. Łojewska. 2014. "Degradation Markers of Fibroin in Silk Through Infrared Spectroscopy." *Polymer Degradation and Stability* 105:185–196. https://doi.org/10.1016/j.polymdegradstab.2014.04.008.

Kramell, A., X. Li, R. Csuk, M. Wagner, T. Goslar, P. E. Tarasov, N. Kreusel, R. Kluge, and C.-H. Wunderlich. 2014. "Dyes of Late Bronze Age Textile Clothes and Accessories from the Yanghai Archaeological Site, Turfan, China: Determination of the Fibers, Color Analysis and Dating." *Quaternary International* 348:214–223. https://doi.org/10.1016/j.quaint.2014.05.012.

Kramell, A. E., P. Wertmann, D. Hosner, R. Kluge, F. Oehler, C.-H. Wunderlich, P. E. Tarasov, M. Wagner, and R. Csuk. 2016. "A Multi-Analytical Techniques Based Approach to Study the Colorful Clothes and Accessories from Mummies of Eastern Central Asia." *Journal of Archaeological Science: Reports* 10:464–473. https://doi.org/10.1016/j.jasrep.2016.11.021.

Kromidas, S. 2011. *Handbuch Validierung in der Analytik*. Weinheim: John Wiley & Sons.

Lee, B., E. Pires, A. M. Pollard, and J. S. O. McCullagh. 2022. "Species Identification of Silks by Protein Mass Spectrometry Reveals Evidence of Wild Silk Use in Antiquity." *Scientific Reports* 12 (1): 4579. https://doi.org/10.1038/s41598-022-08167-3.

Li, L., Y. Gong, H. Yin, D. Gong, and F. Zhou. 2015. "Different Types of Peptide Detected by Mass Spectrometry Among Fresh Silk and Archaeological Silk Remains for Distinguishing Modern Contamination." *PLoS One* 10 (7): e0132827–e0132827. https://doi.org/10.1371/journal.pone.0132827.

Li, M.-Y., Y. Zhao, T. Tong, X.-H. Hou, B.-S. Fang, S.-Q. Wu, X.-Y. Shen, and H. Tong. 2013. "Study of the Degradation Mechanism of Chinese Historic Silk (Bombyx Mori) for the Purpose of Conservation." *Polymer Degradation and Stability* 98 (3): 727–735. https://doi.org/10.1016/j.polymdegradstab.2012.12.021.

Lluveras, A., I. Bonaduce, A. Andreotti, and M. P. Colombini. 2010. "GC/MS Analytical Procedure for the Characterization of Glycerolipids, Natural Waxes, Terpenoid Resins, Proteinaceous and Polysaccharide Materials in the Same Paint Microsample Avoiding Interferences from Inorganic Media." *Analytical Chemistry* 82 (1): 376–386. https://doi.org/10.1021/ac902141m.

Lucas, F., J. T. B. Shaw, and S. G. Smith. 1960. "Comparative Studies of Fibroins: I. the Amino Acid Composition of Various Fibroins and Its Significance in Relation to Their Crystal Structure and Taxonomy." *Journal of Molecular Biology* 2 (6): 339–349. https://doi.org/10.1016/S0022-2836(60)80045-9.

Manhita, A., T. Ferreira, A. Candeias, and C. Barrocas Dias. 2011. "Extracting Natural Dyes from Wool—An Evaluation of Extraction Methods." *Analytical & Bioanalytical Chemistry* 400 (5): 1501–1514. https://doi.org/10.1007/s00216-011-4858-x.

Moini, M., K. Klauenberg, and M. Ballard. 2011. "Dating Silk by Capillary Electrophoresis Mass Spectrometry." *Analytical Chemistry* 83 (19): 7577–7581. https://doi.org/10.1021/ac201746u.

Moini, M., and C. M. Rollman. 2017. "Buyid Silk and the Tale of Bibi Shahrbanu: Identification of Biomarkers of Artificial Aging (Forgery) of Silk." *Analytical Chemistry* 89 (19): 10158–10161. https://doi.org/10.1021/acs.analchem.7b02854.

Ozdemir, M. B., and R. Karadag. 2023a. "Anatolian Acorn Oak's Economic Potential in the Application to the Textile and Leather Industries." *Textile & Leather Review* 6:320–332. https://doi.org/10.31881/TLR.2023.044.

Ozdemir, M. B., and R. Karadag. 2023b. "Madder (*Rubia Tinctorum* L.) as an Economic Factor Under Sustainability Goals in the Textile Dyeing." *Journal of Natural Fibers* 20 (1): 2128968. https://doi.org/10.1080/15440478.2022.2128968.

Puchalla, N. 2022. Bachelor Thesis, Halle (Saale): Martin-Luther-Universität Halle-Wittenberg.

Reddy, N., Y. Zhao, and Y. Yang. 2013. "Structure and Properties of Cocoons and Silk Fibers Produced by *Attacus Atlas*." *Journal of Polymers and the Environment* 21 (1): 16–23. https://doi.org/10.1007/s10924-012-0549-8.

Reischl, R. J., and W. Lindner. 2015. "The Stereoselective Separation of Serine Containing Peptides by Zwitterionic Ion Exchanger Type Chiral Stationary Phases and the Study of Serine Racemization Mechanisms by Isotope Exchange and Tandem Mass Spectrometry." *Journal of Pharmaceutical & Biomedical Analysis* 116:123–130. https://doi.org/10.1016/j.jpba.2015.02.014.

Rindos, M., L. Kucerova, L. Rouhova, H. Sehadova, M. Sery, M. Hradilova, P. Konik, and M. Zurovec. 2021. "Comparison of Silks from *Pseudoips Prasinana* and *Bombyx Mori* Shows Molecular Convergence in Fibroin Heavy Chains but Large Differences in Other Silk Components." *International Journal of Molecular Sciences* 22 (15): 8246. https://doi.org/10.3390/ijms22158246.

Rutherfurd, S. M., and G. S. Gilani. 2009. "Amino Acid Analysis." *Current Protocols in Protein Science*, 58 (1): 11–9. https://doi.org/10.1002/0471140864.ps1109s58.

Schmidt, T., N. Puchalla, M. Schendzielorz, and A. E. Kramell. 2023. "Degumming and Characterization of *Bombyx Mori* and Non-Mulberry Silks from Saturniidae Silkworms." *Scientific Reports* 13 (1): 19504. https://doi.org/10.1038/s41598-023-46474-5.

Schröder, O., M. Wagner, S. Wutke, Y. Zhang, Y. Ma, D. Xu, T. Goslar, R. Neef, P. E. Tarasov, and A. Ludwig. 2016. "Ancient DNA Identification of Domestic Animals Used for Leather Objects in Central Asia During the Bronze Age." *The Holocene* 26 (10): 1722–1729. https://doi.org/10.1177/0959683616641741.

Schweppe, H. 1992. *Handbuch der Naturfarbstoffe: Vorkommen, Verwendung, Nachweis*. Landsberg/Lech: ecomed.

Shimada, C. M., B. McCarthy, C. M. Rollman, A. Hare, J. Ueda, and M. Moini. 2023. "More Reliable Dating of Japanese Silk Mounting Textiles for Conservation Decisions: Effects of Silk Processing on Silk Surface Morphology and Aspartic Acid Racemization." *Studies in Conservation*: 1–16. https://doi.org/10.1080/00393630.2023.2289720.

Smith, G. G., K. Williams, and D. Wonnacott. 1978. "Factors Affecting the Rate of Racemization of Amino Acids and Their Significance to Geochronology." *The Journal of Organic Chemistry* 43 (1): 1–5. https://doi.org/10.1021/jo00395a001.

Veit, D. 2022. "Silk." In *Fibers: History, Production, Properties, Market*, edited by D. Veit, 351–380. Cham: Springer International Publishing.

Vilaplana, F., J. Nilsson, D. V. P. Sommer, and S. Karlsson. 2015. "Analytical Markers for Silk Degradation: Comparing Historic Silk and Silk Artificially Aged in Different Environments." *Analytical & Bioanalytical Chemistry* 407 (5): 1433–1449. https://doi.org/10.1007/s00216-014-8361-z.

Wertmann, P., X. Chen, X. Li, D. Xu, P. E. Tarasov, and M. Wagner. 2020. "New Evidence for Ball Games in Eurasia from Ca. 3000-Year-Old Yanghai Tombs in the Turfan Depression of Northwest China." *Journal of Archaeological Science: Reports* 34:102576. https://doi.org/10.1016/j.jasrep.2020.102576.

Wu, G. 2024. "Mapping Byzantine Sericulture in the Global Transfer of Technology." *Journal of Global History* 19 (1): 1–17. https://doi.org/10.1017/S1740022823000050.

Xia, Q., Y. Guo, Z. Zhang, D. Li, Z. Xuan, Z. Li, F. Dai, et al. 2009. "Complete Resequencing of 40 Genomes Reveals Domestication Events and Genes in Silkworm (*Bombyx*)." *Science* 326 (5951): 433–436. https://doi.org/10.1126/science.1176620.

Xiang, H., X. Liu, M. Li, Y. N. Zhu, L. Wang, Y. Cui, L. Liu, et al. 2018. "The Evolutionary Road from Wild Moth to Domestic Silkworm." *Nature Ecology & Evolution* 2 (8): 1268–1279. https://doi.org/10.1038/s41559-018-0593-4.

Zahradníčková, H., P. Hušek, and P. Šimek. 2009. "GC Separation of Amino Acid Enantiomers via Derivatization with Heptafluorobutyl Chloroformate and Chirasil-L-Val Column." *Journal of Separation Science* 32 (22): 3919–3924. https://doi.org/10.1002/jssc.200900400.

Zhang, X., and R. A. Laursen. 2005. "Development of Mild Extraction Methods for the Analysis of Natural Dyes in Textiles of Historical Interest Using LC-Diode Array Detector-MS." *Analytical Chemistry* 77 (7): 2022–2025. https://doi.org/10.1021/ac048380k.

Zheng, H., H. Yang, Y. Zhou, T. Li, Q. Ma, B. Wang, Q. Fang, and H. Chen. 2021. "Rapid Enrichment and Detection of Silk Residues from Tombs by Double-Antibody Sandwich ELISA Based on Immunomagnetic Beads." *Analytical Chemistry* 93 (43): 14440–14447. https://doi.org/10.1021/acs.analchem.1c02556.

Supplemental Material

Characterization of recent and historical silks: Effects of silk processing on chemical composition and amino acid racemization

Theresa Schmidt[a], Jacqueline Koch[a], Nils Puchalla[a], and Annemarie E. Kramell[a,*]

[a]Department of Organic Chemistry, Martin-Luther-University Halle-Wittenberg, Halle, Germany

corresponding author: Annemarie Elisabeth Kramell, annemarie.kramell@chemie.uni-halle.de, Department of Organic Chemistry, Martin-Luther-University Halle-Wittenberg, Kurt-Mothes-Straße 2, 06120 Halle, Germany

Abbreviations – species:

AM - *Antheraea mylitta* Drury

APe - *Antheraea pernyi* Guérin-Méneville

AtA - *Attacus atlas* L.

BM - *Bombyx mori* L.

Table S1. Chiral GC-MS method: retention time, LOD, LOQ, repeatability (peak area reproducibility at two concentration levels), method precision expressed by RSD % and recovery rates (at three concentration levels) of AAs examined (n.d. … not determined, n.s. … not separated).

AA	Retention time [min]	Diagnostic ions[a]			LOD [pmol]	LOQ [pmol]	Repeatability RSD [%]		Method precision RSD [%]		Recovery [%] BM fibroin		
		m/z					Concentration level		BM fibroin	AM fibroin	Concentration level		
		q1	q2	q2			Low	High			Low	Medium	High
D-Ala	5.31	270	70	113	49	209	11.6	7.3	16,9	13.9	82	112	90
L-Ala	5.83	270	113	70	45	195	8.9	9.2	19,4	23.8	90	105	90
D/L-Pro n.s.[b]	5.53	296	69	297	44	189	3.8	7.0	< LOD	< LOD	106	88	82
Gly	6.65	256	113	81	101	379	5.7	5.4	22,5	23.3	78	92	76
D-Val	7.52	298	98	283	53	223	5.8	9.1	1.6	< LOQ	99	79	70
L-Val	7.75	298	98	283	54	226	3.2	3.8	22.1	7.9	78	87	86
D-Ile	7.78	312	69	283	18	85	5.4	3.1	< LOD	< LOD	100	85	73
L-Ile	8.83	283	312	256	36	160	4.9	3.1	21.0	23.7	82	102	98
D-Leu	10.14	256	312	112	37	163	4.6	2.6	< LOD	< LOD	75	68	63
L-Leu	10.95	312	256	112	45	197	3.3	5.4	7.0	6.0	96	94	85
D-Thr[c]	13.68 (-OR) 19.94 (-OH)	113 283	282 100	227 83	47	203	16.2	6.3	< LOQ	< LOQ	83	65	67
L-Thr[c]	14.41 (-OR) 20.13 (-OH)	282 283	113 100	227 83	41	177	11.5	20.7	16.3	17.3	73	88	73
D-Asp[d]	15.51	496	254	96	64	255	9.9	5.4	< LOQ	19.1	110	111	98
L-Asp[d]	15.99	496	254	296	63	256	8.0	12.6	19.9	4.4	106	87	106
D-Ser[c]	17.94 (-OR) 22.08 (-OH)	268 283	113 86	69 69	49	208	10.7	10.3	22.4	22.4	84	80	72
L-Ser[c]	18.67 (-OR) 22.42 (-OH)	268 283	113 86	69 69	56	233	13.4	11.8	16.1	7.2	116	77	93
D-Met	19.91	61	75	283	47	201	2.6	4.7	< LOQ	< LOQ	76	78	89
L-Met	20.53	61	75	283	41	178	3.2	6.4	< LOQ	9.0	85	65	72
D-Phe	20.82	91	330	92	37	161	5.1	5.1	< LOD	< LOD	82	77	69
D-Glu[c]	20.86	282	82	310	41	176	17.0	13.4	2.7	3.6	91	98	65
L-Phe	21.41	91	330	146	35	157	6.3	5.4	16.7	9.1	78	77	79
L-Glu[c]	21.67	282	82	310	38	169	14.5	14.0	22.2	11.7	108	69	85
D-Cys	23.05	113	285	300	31	139	19.1	8.0	< LOD	< LOD	82	57	88
L-Cys	23.37	113	285	69	74	148	6.3	9.5	< LOQ	< LOQ	63	73	80
D-His	30.84	307	81	113	63	252	13.5	16.1	< LOD	< LOD	82	68	81
L-His	31.14	307	113	81	38	167	20.5	20.2	23.0	21.6	83	88	89
D-Lys	37.47	310	256	82	57	233	28.3	15.9	< LOQ	< LOQ	93	70	71
L-Lys	37.73	310	256	113	59	248	7.3	11.9	3.8	8.2	85	85	84
D-Tyr	37.22	333	289	107	81	297	3.0	11.5	< LOQ	< LOQ	85	95	76
L-Tyr	37.65	333	289	107	64	256	5.9	22.6	18.4	16.9	122	100	105
D/L-Trp	n.d. (see (Rutherfurd and Gilani 2009))												
D/L-Arg	n.d. (see (Zahradníčková et al. 2009; Hušek 1991))[e]												

[a] q1, q2 … Diagnostic (quantitation and qualifier) fragment ions used for the GC-MS analysis. [b] As already described by (Zahradníčková et al. 2009), (DL)-Pro HFBCF derivatives are not separated on a Chirasil-Val phase. [c] During the treatment of Ser and Thr with HFBCF, 2 derivatives are formed (-OR: alkylated on the side chain; -OH: free hydroxyl group). [d] Acid hydrolysis converts Asn to Asp and Gln to Glu; [e] As already described by Zahradníčková *et al.* and Hušek, the guanidino group of Arg is not effectively derivatized in the presence of HFCBF or other alkyl chloroformates.

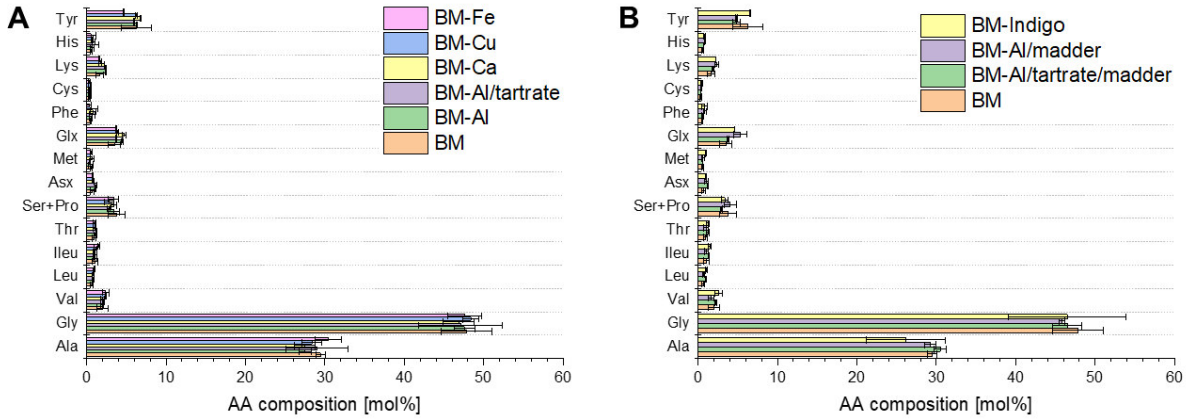

Figure S1 AA composition of (A) degummed BM silk treated with iron(II) sulfate, copper(II) sulfate, calcium oxalate, potassium alum or potassium alum and potassium hydrogen tartrate; (B) degummed BM silk dyed with synthetic indigo and mordanted BM silk dyed with madder. The AA composition of untreated BM silk (sample ID: BM) is shown for comparison; see Table S1 for the assignment of the sample ID.

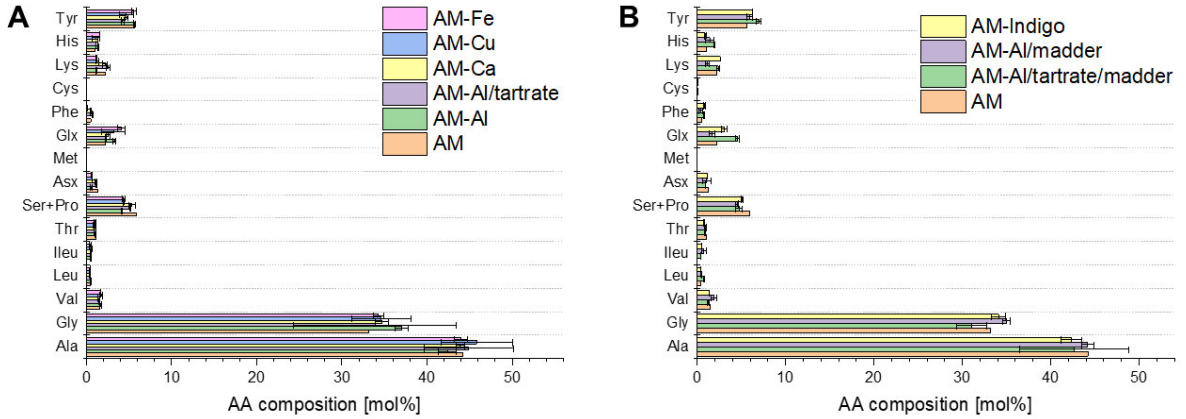

Figure S2 AA composition of (A) degummed AM silk treated with iron(II) sulfate, copper(II) sulfate, calcium oxalate, potassium alum or potassium alum and potassium hydrogen tartrate; (B) degummed AM silk dyed with synthetic indigo and mordanted AM silk dyed with madder. The AA composition of untreated AM silk (sample ID: AM) is shown for comparison; see Table S2 for the assignment of the sample ID.

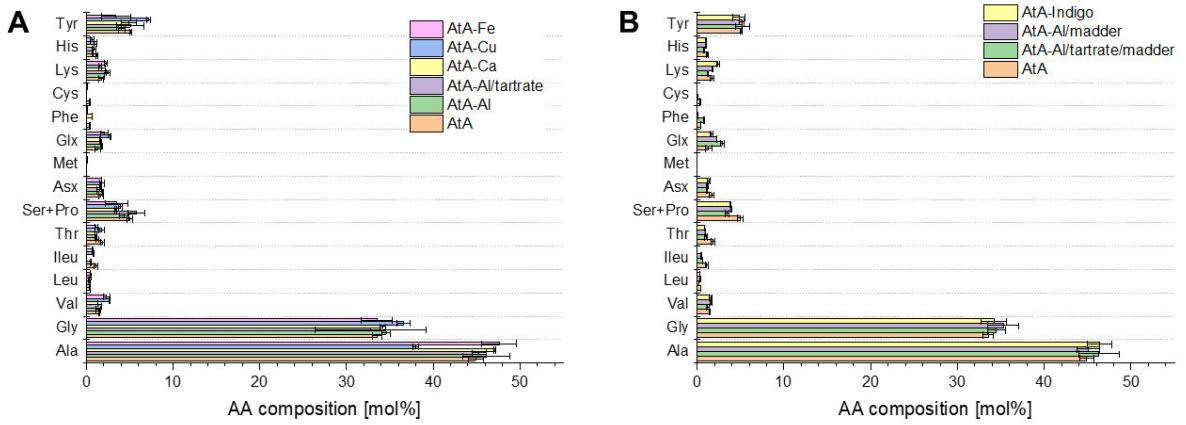

Figure S3 AA composition of (A) degummed AtA silk treated with iron(II) sulfate, copper(II) sulfate, calcium oxalate, potassium alum or potassium alum and potassium hydrogen tartrate; (B) degummed AtA silk dyed with synthetic indigo and mordanted AtA silk dyed with madder. The AA composition of untreated AtA silk (sample ID: AtA) is shown for comparison; see Table S3 for the assignment of the sample ID.

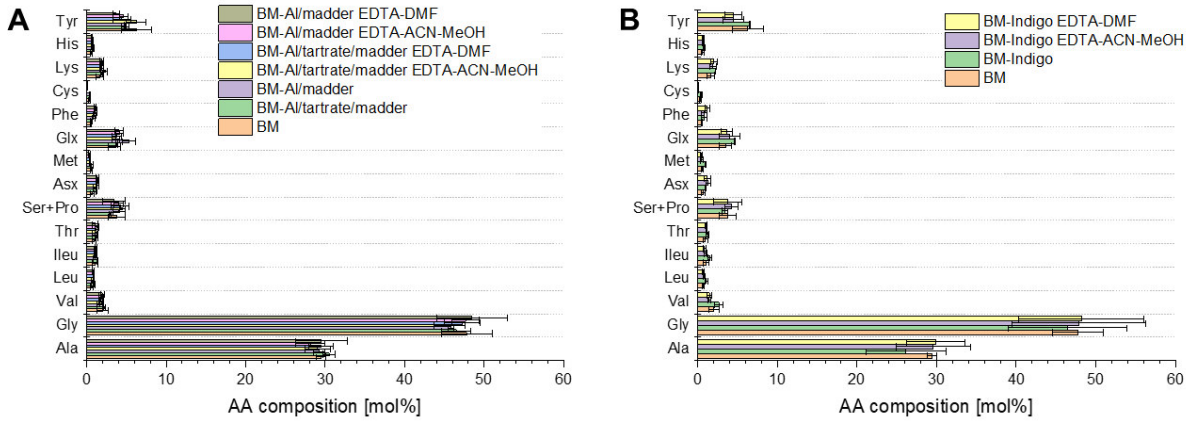

Figure S4 AA composition of (A) mordanted BM silk dyed with madder and (B) BM silk dyed with synthetic indigo before and after treatment with an aqueous EDTA-DMF or an aqueous EDTA-ACN-MeOH solution. The AA composition of untreated BM silk (sample ID: BM) is shown for comparison; see Table S1 for the assignment of the sample ID.

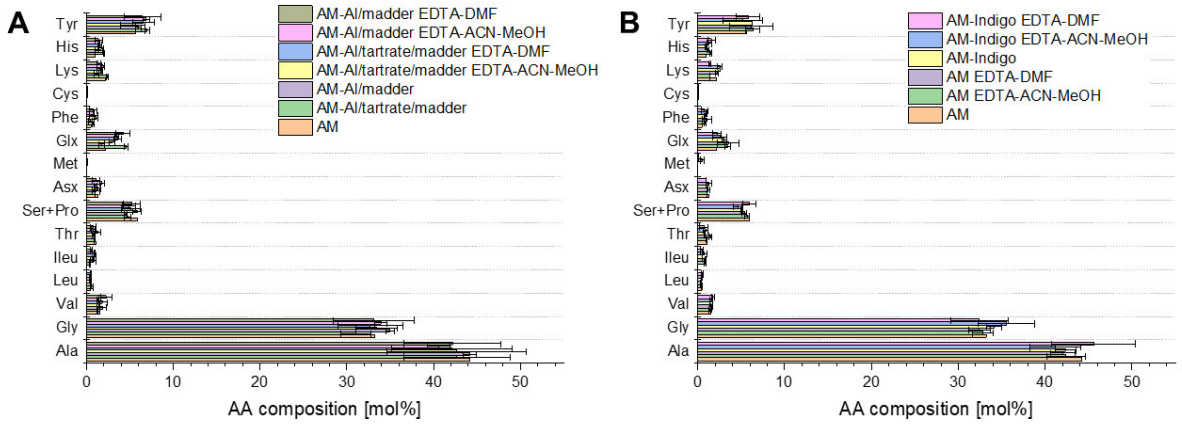

Figure S5 AA composition of (A) mordanted AM silk dyed with madder and (B) AM silk dyed with synthetic indigo as well as undyed and not mordanted AM silk before and after treatment with an aqueous EDTA-DMF or an aqueous EDTA-ACN-MeOH solution. The AA composition of untreated AM silk (sample ID: AM) is shown for comparison; see Table S2 for the assignment of the sample ID.

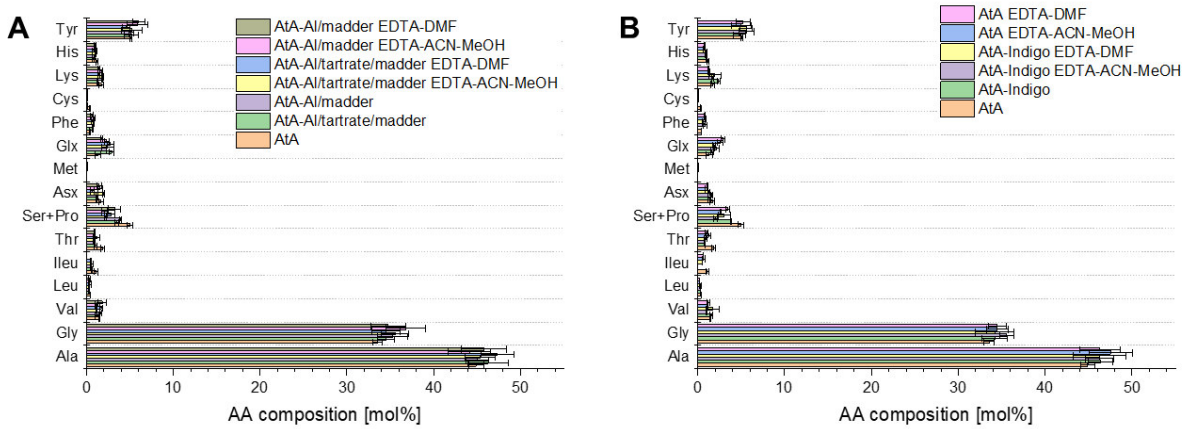

Figure S6 AA composition of (A) mordanted AtA silk dyed with madder and (B) AtA silk dyed with synthetic indigo as well as undyed and not mordanted AtA silk before and after treatment with an aqueous EDTA-DMF or an aqueous EDTA-ACN-MeOH solution. The AA composition of untreated AtA silk (sample ID: AtA) is shown for comparison; see Table S3 for the assignment of the sample ID.

Table S2. AA composition of untreated, mordanted and dyed BM silks as well as BM silks treated with an aqueous EDTA-DMF or an aqueous EDTA-ACN-MeOH solution prior to hydrolysis.

Species	Sample ID	Sample treatment				Comparative AA composition[a]									
		Degumming method	Mordanting agent/calcium salt	Colorant	Extracting agent	Ala+Gly [mol%]	Gly/Ala	100LC/SC[b]	P [mol%][c]	NP [mol%][d]	Ser+Pro+Thr+Tyr [mol%][e]	A [mol%][f]	B [mol%][g]	Tyr/Ala	Tyr/Gly
Bombyx mori L.	BM	Na_2CO_3 (1 g/L) and ethylenediamine (2.5 %), 60 min, 95 °C	-	-	-	77	1.6	22	12	88	11	4	2	0.21	0.13
	BM-Al		Potassium alum	-	-	75	1.7	26	14	86	11	6	3	0.23	0.13
	BM-Al/tartrate		Potassium alum+potassium hydrogen tartrate	-	-	76	1.6	25	13	87	10	5	3	0.20	0.13
	BM-Ca		Calcium oxalate[h]	-	-	74	1.7	27	14	86	11	6	3	0.25	0.14
	BM-Cu		Copper(II) sulfate	-	-	77	1.7	24	12	88	10	5	2	0.22	0.13
	BM-Fe		Iron(II) sulfate	-	-	78	1.6	21	11	89	9	5	2	0.15	0.10
	BM-Al/madder		Potassium alum	Madder roots	-	77	1.5	23	12	88	9	5	3	0.17	0.11
	BM-Al/tartrate/madder		Potassium alum+potassium hydrogen tartrate	Madder roots	-	75	1.6	25	15	85	10	6	3	0.16	0.10
	BM-Indigo		-	Synthetic indigo	-	73	1.8	29	14	86	11	6	3	0.25	0.14
	BM-Al/madder EDTA-DMF		Potassium alum	Madder roots	EDTA-DMF[i]	75	1.6	24	13	86	12	5	3	0.13	0.08
	BM-Al/madder EDTA-ACN-MeOH		Potassium alum	Madder roots	EDTA-ACN-MeOH[i]	77	1.6	21	13	86	10	5	3	0.17	0.10
	BM-Al/tartrate/madder EDTA-DMF		Potassium alum+potassium hydrogen tartrate	Madder roots	EDTA-DMF[i]	76	1.7	23	14	86	10	6	3	0.15	0.09
	BM-Al/tartrate/madder EDTA-ACN-MeOH		Potassium alum+potassium hydrogen tartrate	Madder roots	EDTA-ACN-MeOH[i]	78	1.6	21	12	87	8	5	3	0.22	0.14
	BM-Indigo EDTA-DMF		-	Synthetic indigo	EDTA-DMF[i]	77	1.6	20	13	86	10	5	3	0.15	0.09
	BM-Indigo EDTA-ACN-MeOH		-	Synthetic indigo	EDTA-ACN-MeOH[i]	78	1.6	20	12	87	9	5	3	0.15	0.09

[a)] The analyses were carried out using GC-FID as previously reported (see(Schmidt et al. 2023)). [b)] Ratio between long chain (LC: other AAs) and short chain (SC: Ala, Gly, Ser, Thr) AAs; [c)] Polar AAs: acidic, basic and hydroxyl AAs; [d)] Non-polar AAs: other AAs; [e)] AAs with hydroxyl groups: Ser, Thr, Tyr; [f)] Basic AAs: Lys, His; [g)] Acidic AAs: Asx, Glx. [h)] In addition to mordants, the influence of calcium oxalate treatment was investigated. [i)] Silk samples were treated with an aqueous EDTA-DMF or an aqueous EDTA-ACN-MeOH solution prior to hydrolysis.

Table S3. AA composition of untreated, mordanted and dyed AM silks as well as AM silks treated with an aqueous EDTA-DMF or an aqueous EDTA-ACN-MeOH solution prior to hydrolysis.

Species	Sample ID	Sample treatment				Comparative AA composition[a]									
		Degumming method	Mordanting agent/calcium salt	Colorant	Extracting agent	Ala+Gly [mol%]	Gly/Ala	100LC/SC[b]	P [mol%][c]	NP [mol%][d]	Ser+Pro+Thr+Tyr [mol%][e]	A [mol%][f]	B [mol%][g]	Tyr/Ala	Tyr/Gly
Antheraea mylitta Drury	AM	Na_2CO_3 (1 g/L) and ethylenediamine (2.5 %), 90 min, 95 °C	-	-	-	77	0.8	17	14	85	13	4	3	0.13	0.17
	AM-Al		Potassium alum	-	-	79	0.9	17	11	88	11	4	2	0.13	0.15
	AM-Al/tartrate		Potassium alum+potassium hydrogen tartrate	-	-	79	0.8	17	13	86	10	3	4	0.09	0.13
	AM-Ca		Calcium oxalate[h]	-	-	79	0.8	17	14	86	11	4	4	0.11	0.14
	AM-Cu		Copper(II) sulfate	-	-	80	0.8	16	11	88	10	4	2	0.10	0.14
	AM-Fe		Iron(II) sulfate	-	-	78	0.8	19	13	86	11	5	3	0.13	0.16
	AM-Al/madder		Potassium alum	Madder roots	-	74	0.7	25	16	84	13	6	4	0.13	0.17
	AM-Al/tartrate/madder		Potassium alum+potassium hydrogen tartrate	Madder roots	-	79	0.8	18	11	89	11	3	3	0.16	0.23
	AM-Indigo		-	Synthetic indigo	-	76	0.8	21	14	86	12	4	4	0.15	0.18
	AM EDTA-DMF		-	-	EDTA-DMF[i]	75	0.8	21	14	85	13	5	3	0.15	0.19
	AM EDTA-ACN-MeOH		-	-	EDTA-ACN-MeOH[i]	74	0.8	22	15	84	13	5	3	0.15	0.19
	AM-Al/madder EDTA-DMF		Potassium alum	Madder roots	EDTA-DMF[i]	76	0.8	20	14	85	12	4	3	0.15	0.20
	AM-Al/madder EDTA-ACN-MeOH		Potassium alum	Madder roots	EDTA-ACN-MeOH[i]	75	0.8	22	14	85	13	5	3	0.17	0.20
	AM-Al/tartrate/madder EDTA-DMF		Potassium alum+potassium hydrogen tartrate	Madder roots	EDTA-DMF[i]	75	0.8	24	14	85	13	5	3	0.16	0.20
	AM-Al/tartrate/madder EDTA-ACN-MeOH		Potassium alum+potassium hydrogen tartrate	Madder roots	EDTA-ACN-MeOH[i]	75	0.8	23	14	86	12	5	3	0.13	0.16
	AM-Indigo EDTA-DMF		-	Synthetic indigo	EDTA-DMF[i]	77	0.9	21	13	86	11	4	4	0.13	0.18
	AM-Indigo EDTA-ACN-MeOH		-	Synthetic indigo	EDTA-ACN-MeOH[i]	78	0.7	18	13	87	12	3	3	0.13	0.15

[a)] The analyses were carried out using GC-FID as previously reported (see(Schmidt et al. 2023)). [b)] Ratio between long chain (LC: other AAs) and short chain (SC: Ala, Gly, Ser, Thr) AAs; [c)] Polar AAs: acidic, basic and hydroxyl AAs; [d)] Non-polar AAs: other AAs; [e)] AAs with hydroxyl groups: Ser, Thr, Tyr; [f)] Basic AAs: Lys, His; [g)] Acidic AAs: Asx, Glx. [h)] In addition to mordants, the influence of calcium oxalate treatment was investigated. [i)] Silk samples were treated with an aqueous EDTA-DMF or an aqueous EDTA-ACN-MeOH solution prior to hydrolysis.

Table S4. AA composition of untreated, mordanted and dyed AtA silks as well as AtA silks treated with an aqueous EDTA-DMF or an aqueous EDTA-ACN-MeOH solution prior to hydrolysis.

Species	Sample ID	Sample treatment				Comparative AA composition[a]									
		Degumming method	Mordanting agent/calcium salt	Colorant	Extracting agent	Ala+Gly [mol%]	Gly/Ala	100LC/SC[b]	P [mol%][c]	NP [mol%][d]	Ser+Pro+Thr+Tyr [mol%][e]	A [mol%][f]	B [mol%][g]	Tyr/Ala	Tyr/Gly
Attacus atlas L.	AtA	Na_2CO_3 (1 g/L) and ethylenediamine (2.5 %), 120 min, 95 °C	-	-	-	78	0.7	17	13	87	12	3	3	0.09	0.12
	AtA-Al		Potassium alum	-	-	81	0.7	15	12	87	10	4	3	0.09	0.12
	AtA-Al/tartrate		Potassium alum+potassium hydrogen tartrate	-	-	78	0.7	16	13	85	12	3	3	0.11	0.15
	AtA-Ca		Calcium oxalate[h]	-	-	81	0.7	16	11	88	9	3	3	0.10	0.14
	AtA-Cu		Copper(II) sulfate	-	-	75	1.0	23	13	86	13	5	3	0.19	0.20
	AtA-Fe		Iron(II) sulfate	-	-	81	0.7	16	11	88	8	4	3	0.07	0.10
	AtA-Al/madder		Potassium alum	Madder roots	-	81	0.7	16	11	89	10	4	2	0.11	0.15
	AtA-Al/tartrate/madder		Potassium alum+potassium hydrogen tartrate	Madder roots	-	80	0.8	16	11	88	10	3	3	0.11	0.15
	AtA-Indigo		-	Synthetic indigo	-	81	0.7	15	11	87	9	3	3	0.10	0.14
	AtA EDTA-DMF		-	-	EDTA-DMF[i]	82	0.7	16	9	90	9	3	2	0.11	0.15
	AtA EDTA-ACN-MeOH		-	-	EDTA-ACN-MeOH[i]	81	0.7	16	11	89	10	4	2	0.11	0.14
	AtA-Al/madder EDTA-DMF		Potassium alum	Madder roots	EDTA-DMF[i]	81	0.8	18	10	89	8	4	3	0.13	0.17
	AtA-Al/madder EDTA-ACN-MeOH		Potassium alum	Madder roots	EDTA-ACN-MeOH[i]	82	0.7	16	10	90	9	3	2	0.13	0.16
	AtA-Al/tartrate/madder EDTA-DMF		Potassium alum+potassium hydrogen tartrate	Madder roots	EDTA-DMF[i]	81	0.8	18	10	89	9	4	3	0.10	0.13
	AtA-Al/tartrate/madder EDTA-ACN-MeOH		Potassium alum+potassium hydrogen tartrate	Madder roots	EDTA-ACN-MeOH[i]	81	0.8	17	10	89	10	3	2	0.12	0.15
	AtA-Indigo EDTA-DMF		-	Synthetic indigo	EDTA-DMF[i]	82	0.8	17	9	90	8	4	3	0.12	0.15
	AtA-Indigo EDTA-ACN-MeOH		-	Synthetic indigo	EDTA-ACN-MeOH[i]	80	0.7	18	10	89	10	3	3	0.12	0.16

[a)] The analyses were carried out using GC-FID as previously reported (see(Schmidt et al. 2023)). [b)] Ratio between long chain (LC: other AAs) and short chain (SC: Ala, Gly, Ser, Thr) AAs; [c)] Polar AAs: acidic, basic and hydroxyl AAs; [d)] Non-polar AAs: other AAs; [e)] AAs with hydroxyl groups: Ser, Thr, Tyr; [f)] Basic AAs: Lys, His; [g)] Acidic AAs: Asx, Glx. [h)] In addition to mordants, the influence of calcium oxalate treatment was investigated. [i)] Silk samples were treated with an aqueous EDTA-DMF or an aqueous EDTA-ACN-MeOH solution prior to hydrolysis.

Table S5. Recent silk samples, a wool sample and AA stock solutions: overview of treatment steps (degumming procedure for BM and AM cocoons: 0.1 % Na_2CO_3 and 2.5 % ethylenediamine, 95°C, 60 min; hydrolysis: 6 N HCl at 110 °C for 24 h).

Sample	**Sample treatment**	**Dyeing and mordanting procedure**	**Sample ID**
Stock solutions of (L)-AAs	Derivatization with HFCBF	-	.
Stock solutions of (D)-AAs	Derivatization with HFCBF		-
Degummed BM silk	Treatment with an EDTA-ACN-MeOH solution, hydrolysis, derivatization with HFCBF	-	BM EDTA-ACN-MeOH
Degummed AM silk	Treatment with an EDTA-ACN-MeOH solution, hydrolysis, derivatization with HFCBF	-	AM EDTA-ACN-MeOH
Degummed BM silk, teated with calcium oxalate	Hydrolysis, derivatization with HFCBF	-	BM-Ca
Degummed, mordanted and/or dyed BM silk	Hydrolysis, derivatization with HFCBF	Metal salt: $CuSO_4$	BM-Cu
		Metal salt: $FeSO_4$	BM-Fe
	Hydrolysis, derivatization with HFCBF	Dye source: indigo	BM-Indigo
		Dye source: madder Metal salt: $KAl(SO_4)_2 \cdot 12H_2O$/potassium hydrogen tartrate	BM-Al/tartrate/madder
	Treatment with an EDTA-ACN-MeOH solution, hydrolysis, derivatization with HFCBF	Metal salt: $CuSO_4$	BM-Cu EDTA-ACN-MeOH
		Metal salt: $FeSO_4$	BM-Fe EDTA-ACN-MeOH
	Treatment with EDTA-DMF, hydrolysis, derivatization with HFCBF	Metal salt: $CuSO_4$	BM-Cu EDTA-DMF
		Metal salt: $FeSO_4$	BM-Fe EDTA-DMF
	Treatment with an EDTA-ACN-MeOH solution, hydrolysis, derivatization with HFCBF	Dye source: indigo	BM-Indigo EDTA-ACN-MeOH
		Dye source: madder Metal salt: $KAl(SO_4)_2 \cdot 12H_2O$/potassium hydrogen tartrate	BM-Al/tartrate/madder EDTA-ACN-MeOH
	Treatment with EDTA-DMF, hydrolysis, derivatization with HFCBF	Dye source: indigo	BM-Indigo EDTA-DMF
		Dye source: madder Metal salt: $KAl(SO_4)_2 \cdot 12H_2O$/potassium hydrogen tartrate	BM-Al/tartrate/madder EDTA-DMF
Merino wool	Treatment with an EDTA-ACN-MeOH solution, hydrolysis, derivatization with HFCBF	-	Wool (merino) EDTA-ACN-MeOH

Table S6. D/L ratios of AA stock solutions, degummed BM and AM silk as well as a recent wool sample after various treatment steps [degumming procedure: 0.1 % Na_2CO_3 and 2.5 % ethylenediamine, 95°C, 60 min (BM), 90 min (AM); hydrolysis: 6 N HCl at 110 °C for 24 h, see Table S5 for a detailed sample description].

Sample	Sample ID	% D/L ratio									
		Ala	Val	Leu	Asx	Met	Ser	Phe	Glx	His	Tyr
Stock solutions of (L)-AAs	-	[b]									
Stock solutions of (D)-AAs	-	(L)-enantiomer concentration is below the LOQ									
Degummed BM silk	BM EDTA-ACN-MeOH	0.7	7.7	[a]	[b]	[c]	12.0	[a]	5.0	[a]	[b]
Degummed AM silk	AM EDTA-ACN-MeOH	0.3	[b]	[a]	7.4	[b]	10.3	[a]	8.5	[a]	[b]
Degummed BM silk, teated with calcium oxalate – before and after treatment with EDTA-ACN-MeOH or EDTA-DMF	BM-Ca	0.8	[b]	[b]	[b]	[c]	7.3	[b]	3.7	[a]	[b]
	BM-Ca EDTA-ACN-MeOH										
	BM-Ca EDTA-DMF										
Degummed, mordanted and/or dyed BM silk with or without EDTA-ACN-MeOH or EDTA-DMF treatment	BM-Cu	0.8	[b]	[b]	[b]	[b]	7.4	[b]	5.5	[a]	[b]
	BM-Fe	0.6	[b]	[b]	[b]	[b]	9.6	[b]	4.5	[a]	[b]
	BM-Indigo	0.9	[b]	[b]	13.4	[b]	12.7	[b]	4.0	[a]	[b]
	BM-Al/tartrate/madder	0.6	[b]	[b]	26.0	[b]	5.4	[b]	3.7	[a]	[b]
	BM-Cu EDTA-ACN-MeOH	0.5	6.0	[b]	[b]	66.7	5.0	[a]	3.5	[a]	[b]
	BM-Fe EDTA-ACN-MeOH	0.3	12.1	[b]	[b]	[c]	90.5	[b]	2.4	[a]	[b]
	BM-Cu EDTA-DMF	0.4	[b]	[b]	[b]	[b]	28.4	[a]	2.5	[a]	[b]
	BM-Fe EDTA-DMF	0.3	11.3	[b]	9.1	[b]	6.8	[b]	1.7	[c]	[b]
	BM-Indigo EDTA-ACN-MeOH	0.4	6.5	[b]	15.9	[b]	5.6	[a]	3.0	[a]	[b]
	BM-Al/tartrate/madder EDTA-ACN-MeOH	0.5	10.8	[b]	[b]	[b]	29.2	[b]	1.9	[a]	[b]
	BM-Indigo EDTA-DMF	0.4	6.2	[b]	13.2	[c]	14.4	[b]	2.3	[a]	[b]
	BM-Al/tartrate/madder EDTA-DMF	0.4	10.5	[b]	[b]	[c]	12.3	[b]	2.3	[c]	[b]
Merino wool treated with EDTA-ACN-MeOH	Wool (merino) EDTA-ACN-MeOH	[b]	[b]	[b]	5.2	[b]	9.8	[b]	12.0	[a]	[b]

[a] (D)-enantiomer concentration is below the LOD; [b] (D)-enantiomer concentration is below the LOQ; [c] (L)- and (D)-enantiomer concentration is below the LOQ.

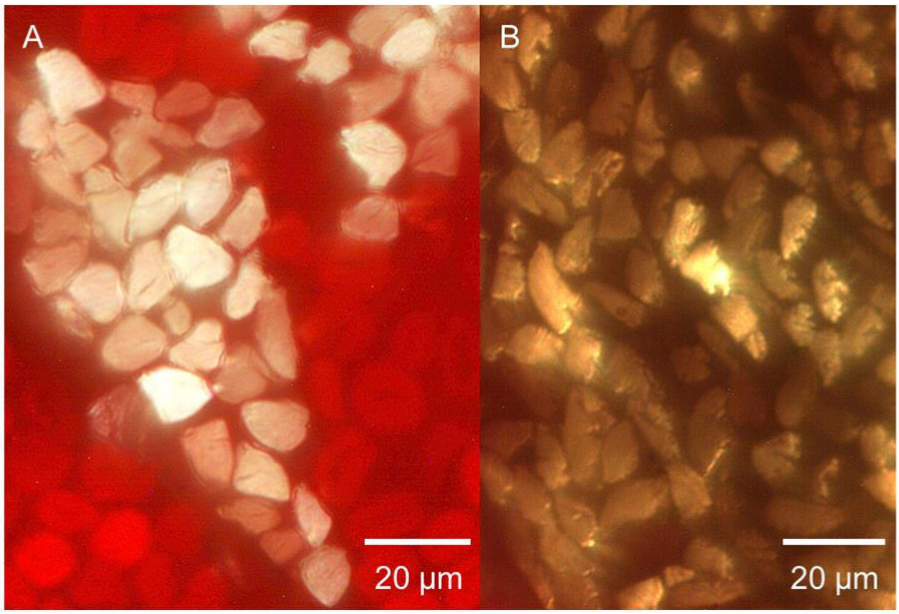

Figure S7 Cross-sections (bright-field microscopy) of silk filaments: (A) recent BM silk embedded in red woolen fibers, (B) historical silk sample from Niya site (sample ID: 95MNIM5-18C, object skirt 95MNIM5-18).

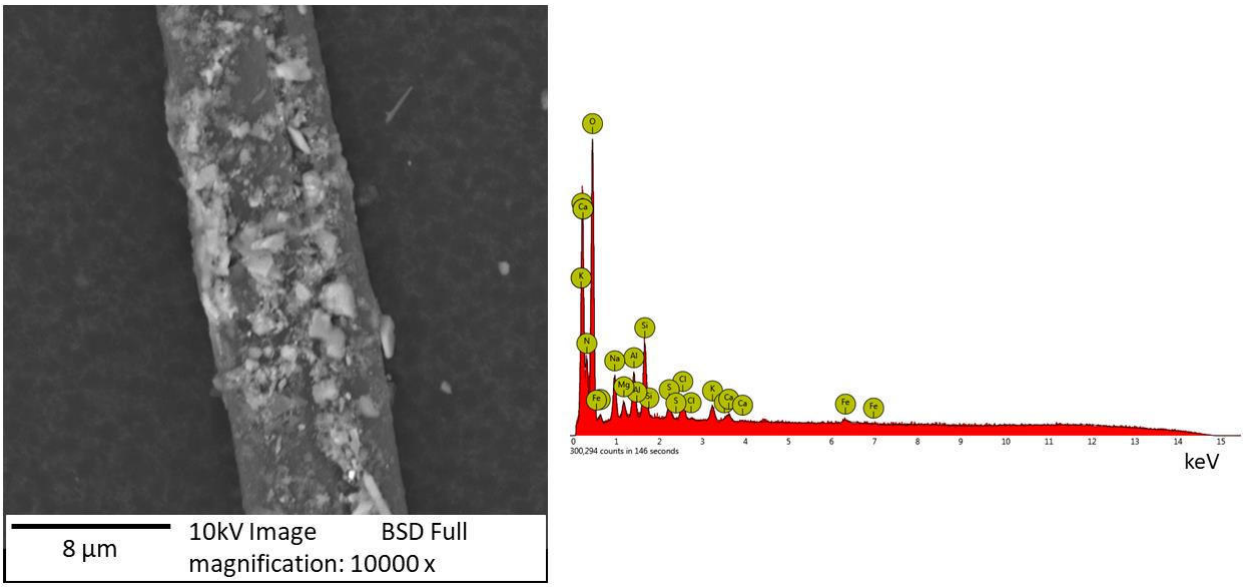

Figure S8 SEM image and corresponding SEM-EDX spectrum of a silk sample from Niya site (sample ID: 95MNIM5-15D).

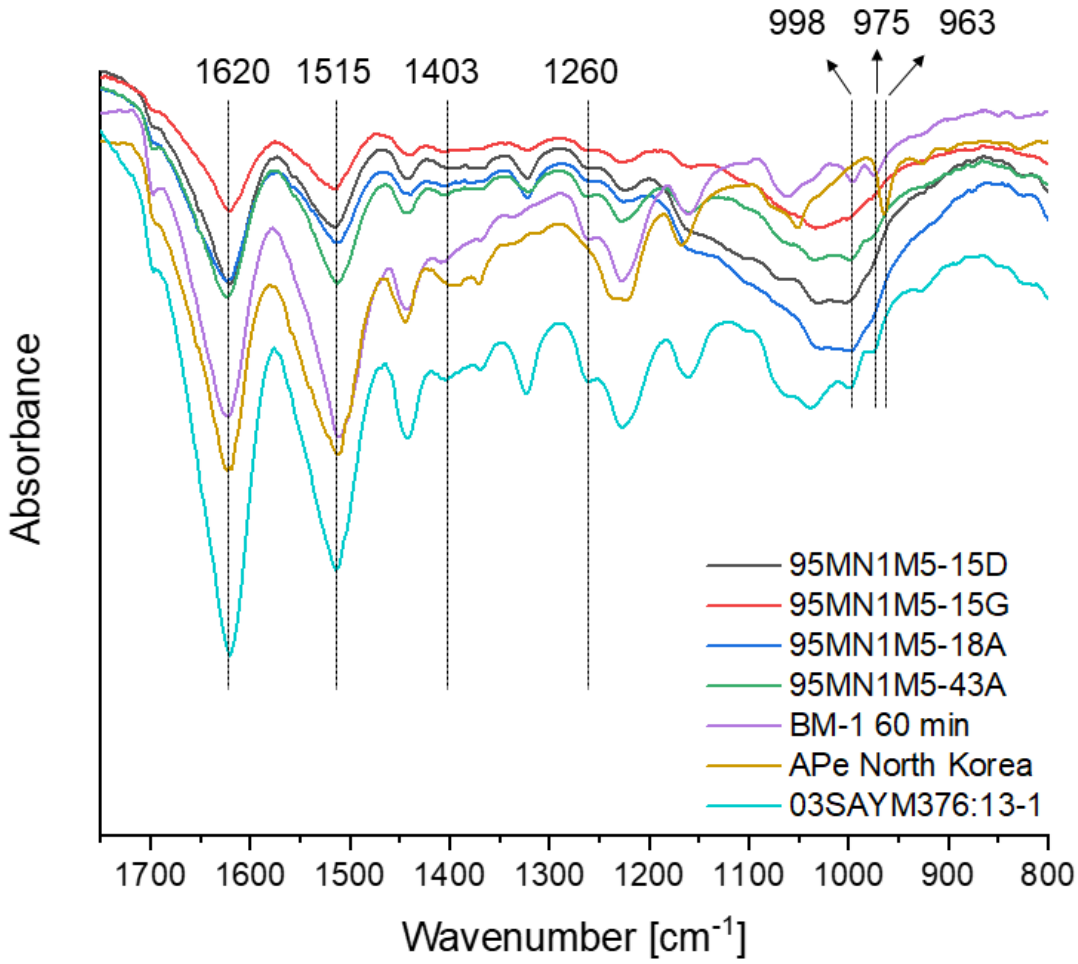

Figure S9 ATR-FTIR spectra of historical silk samples from Niya and Yanghai site (sample ID: 95MNIM5-15D, 95MNIM5-15G, 95MNIM5-18A, 95MNIM5-43A, 03SAYM376:13-1; see Table 3 in the main manuscript for further information) and recent BM and *Antheraea pernyi* Guérin-Méneville silk, degummed with Na_2CO_3 (1 g L^{-1}) and ethylenediamine (2.5 %) (sample ID: BM-1 60 min and APe North Korea), in the range 800-1750 cm^{-1}.

Figure S10 (A) Twill fragment from the Wupu site and (B) magnification of a wool fiber; sample ID: 86HWMNN-1D. (C) Twill fragment from the Yanghai site; sample ID: 20110615/OF11-B (Surface finds without assignment to specific graves).

Table S7. AA composition of historical silk and wool samples as well as recent BM silk, AM silk and merino wool treated with EDTA-ACN-MeOH before hydrolysis with 6 N HCl at 110 °C for 24 h (derivatization with HFCBF), expressed as the percentage of the total AA amount.

Sample ID	Material	AA composition [mol%][a]															
		Ala	Pro	Gly	Val	Ileu	Leu	Ser	Asx (Asp+Asn)	Thr	Phe	Glx (Glu+Gln)	Met	Cys	His	Lys	Tyr
		Historical samples															
95MNIM5-15D	Silk	41.3	0.4	39.6	0.9	0.3	0.2	9.5	0.3	2.0	0.4	0.4	0.1[b]	0.1[b]	0.2	0.4	4.0
95MNIM5-15G	Silk	46.6	0.4	44.6	0.8	0.2	0.3	2.0	0.5	0.3	0.5	0.7	0.1[b]	0.0[b]	0.1[b]	0.3	2.6
95MNIM5-18A	Silk	43.0	0.4	49.4	0.6	0.2	0.2	1.5	0.5	0.3	0.3	0.4	0.1[b]	0.0[b]	0.1	0.2	3.0
95MNIM5-43A	Silk	37.7	0.3	53.8	0.4	1.1	1.7	1.3	0.3	0.2	0.3	0.4	0.1[b]	0.0[b]	0.1[b]	0.1	2.4
03SAYM376:13-1	Silk	38.3	0.5	47.4	0.7	0.2	0.4	5.0	0.7	0.9	1.1	0.5	0.3	0.2	0.5	0.3	3.0
86HWMNN-1D	Wool	17.5	12.8	13.6	4.4	4.1	40.0	0.6	0.7	0.3[b]	1.3	0.4[b]	0.2[b]	0.1[b]	0.2[b]	0.5	3.3
20110615/OF11-B	Wool	15.9	10.7	9.8	5.1	6.5	35.3	0.7	1.0	0.3[b]	9.3	0.9	0.4	0.1	0.2[b]	0.6	3.0
		Recent silk samples															
BM EDTA-ACN-MeOH	Silk	34.0	[c]	47.2	2.1	0.4	0.6	3.4	1.0	1.1	1.2	3.2	0.2[b]	[c]	0.4	1.2	4.2
AM EDTA-ACN-MeOH	Silk	48.2	[c]	36.1	1.5	0.2	0.3	3.0	2.3	0.5	0.3	1.3	0.1[b]	[c]	0.8	0.8	4.7
Wool (merino) EDTA-ACN-MeOH	Wool	20.7	5.2	20.6	2.7	4.8	13.2	3.8	6.5	4.6	5.9	2.7	1.1	0.14[b]	1.1	1.6	5.6

[a] AA proportion is given as the sum of both enantiomers (L- + D-enantiomer) and was determined by GC-MS. [b] above LOD but just below the LOQ, [c] below the LOD

References

Hušek, P. 1991. Rapid derivatization and gas chromatographic determination of amino acids. *J. Chromatogr. A* 552:289-299. https://doi.org/10.1016/S0021-9673(01)95945-X.

Rutherfurd, S. M., and G. S. Gilani. 2009. Amino acid analysis. *Curr. Protoc. Protein Sci.* 58 (1):11.19.11-11.19.37. https://doi.org/10.1002/0471140864.ps1109s58.

Schmidt, T., N. Puchalla, M. Schendzielorz, and A. E. Kramell. 2023. Degumming and characterization of *Bombyx mori* and non-mulberry silks from Saturniidae silkworms. *Sci. Rep.* 13 (1):19504. https://doi.org/10.1038/s41598-023-46474-5.

Zahradníčková, H., P. Hušek, and P. Šimek. 2009. GC separation of amino acid enantiomers via derivatization with heptafluorobutyl chloroformate and Chirasil-L-Val column. *J. Sep. Sci.* 32 (22):3919-3924. https://doi.org/10.1002/jssc.200900400.